TRACKING MAGMATIC PROCESSES THROUGH Zr/Hf RATIOS IN ROCKS AND Hf AND Ti ZONING IN ZIRCONS: AN EXAMPLE FROM THE SPIRIT MOUNTAIN BATHOLITH, NEVADA

By

Lily Lowery Claiborne

Thesis

Submitted to the Faculty of the

Graduate School of Vanderbilt University

in partial fulfillment of the requirements

for the degree of

MASTER OF SCIENCE

in

Geology

August, 2006

Nashville, Tennessee

Approved:	Date:
Calvin F. Miller	7/26/06
John E. Ayers	7/26/06

DEDICATION

To Dr. Bran Potter and Dr. Steve Shaver, who taught me not only geology,
but also about the kind of person and teacher I want to be.
I am here because I want to share with others the kind of experience they shared with me.

and

To my mother, who has finally managed to convince me that I can do anything,
and who is an unfailing guide and companion in all things.

ACKNOWLEDGEMENTS

I owe a great deal of gratitude to Dr. Calvin Miller, who is not only a respected, admirable, knowledgeable, and innovative geologist, but an advisor of the highest caliber. Without his patience, compassion, humor, enthusiasm, encouragement, faith, and total support, I would not have completed this project. He is a constant guide and mentor for all his students, and I am honored to work with him and to know him.

The work represented in the body of this thesis is a collaborative effort with Dr. Miller, BJ Walker, Joe Wooden, Frank Mazdab, and Fernando Bea, with financial support from the National Science Foundation. I also want to thank Dan Perrault, Nick Lang, Rick Hazlett, Nichole Knepprath, Scott Crombie, and Margia Lowery for their assistance in the field, for sharing their thoughts, and for their moral support throughout this process. Bruce Watson was very helpful in application of the Ti-in-zircon thermometer. Lab assistance was provided by Chris Fisher, Kirsten Hodge, and Greg Rhodes. Dr. John Ayers, Dr. David Furbish, and Dr. Brendan Bream lent their expertise in things both geologic and technical, and I thank them.

Finally, I give many thanks to my eternally patient and supportive husband, Andrew Claiborne. He holds down the home-front while I am off gallivanting in the desert, the mountains, and even foreign climes. He answers the phone in the middle of the night when animals are trying to get into my tent, and does his best to help. He makes dinner and waits up when I am working late. He is always absolutely sure that I will get it done and do it well, even when I am convinced it is impossible. Thank you.

TABLE OF CONTENTS

LIST OF TABLES

LIST OF FIGURES

CHAPTER I

INTRODUCTION

Zircon and Zr/Hf Ratios

Zirconium (Zr) and hafnium (Hf), with identical charges of +4 and very similar radii of 0.84 and 0.83 Å (8-fold coordination), respectively (Shannon, 1976; Jia, 1991), behave nearly identically in most systems on Earth. Therefore, most materials have near chondritic Zr/Hf ratios of ~35-40 (Ahrens and Erlank, 1969; Hoskin and Schaltegger, 2003). Although Zr and Hf may be fractionated from each other to some extent by minerals such as amphibole, clinopyroxene, garnet, and sphene (titanite), especially where coexisting melts are strongly polymerized (Linnen and Keppler, 2002; David et al., 2000; Bea et al., in press), their relatively low abundances and/or K_Ds generally render these phases inefficient at affecting whole-rock Zr/Hf ratios. By contrast, zircon, which is by far the dominant reservoir for both Zr and Hf in Earth's crust (Bea and Montero, 1999; Bea et al., in press) and is ubiquitous in all but the most mafic magma systems in continental and arc crust, has the potential to significantly affect Zr/Hf (cf. Linnen and Keppler, 2002; Bea et al., in press).

Among all rocks, only the most felsic granites and rhyolites commonly deviate appreciably from near-chondritic Zr/Hf ratios, with values ranging from 15-30 being reasonably common (e.g., Ahrens and Erlank, 1969, and data presented here). These rocks have relatively low concentrations of both Zr and Hf, but Zr is especially depleted. We contend that this reduction in Zr, Hf, and Zr/Hf reflects crystallization and removal of

zircon. Thus, modest zircon fractionation has the potential to profoundly affect Zr/Hf ratios. Concentration of Zr in melt falls with temperature once saturation is reached (e.g. Watson and Harrison, 1983; Miller et al., 2003). "Zircon" is in fact a zircon-hafnon solid solution ($ZrSiO_4$-$HfSiO_4$; Figure 1); the relatively low hafnon content of most natural zircons is simply a consequence of the high Zr/Hf in nature - HfO_2 content in almost all natural zircons falls between ~0.5 and 5 wt%, and in a majority it lies between 1 and 2 wt % (Ahrens and Erlank, 1969; Heaman et al., 1990; Belousova et al., 2002; Hoskin and Schaltegger, 2003). Because of zircon's preference for Zr over Hf, the solid solution is enriched in the zircon end member over coexisting melt.

We argue that low whole-rock Zr/Hf indicates effective extraction of evolved melt after extensive crystallization of zircon (Miller et al., 2005). The near ubiquity of this signature in highly felsic rocks, particularly high-silica rhyolites, thus suggests that formation of such rocks requires melt segregation from a zircon-bearing crystal assemblage.

Zr and Hf: A Potential Tracer of Thermal and Compositional Evolution of Felsic Magmatic Systems

Many lines of evidence have recently been cited from both plutonic and volcanic rocks to suggest that felsic magma systems have protracted histories, on the order of several hundred thousand to several million years, and that these histories require frequent replenishment (e.g., Wiebe and Hawkins, 2004; Davies et al., 1994; Reid et al., 1997; Brown & Fletcher, 1999; Schmitt et al., 2003; Vazquez & Reid, 2002; Charlier et al., 2005; Miller and Wooden, 2004; Glazner et al., 2004; Coleman et al., 2004). Such

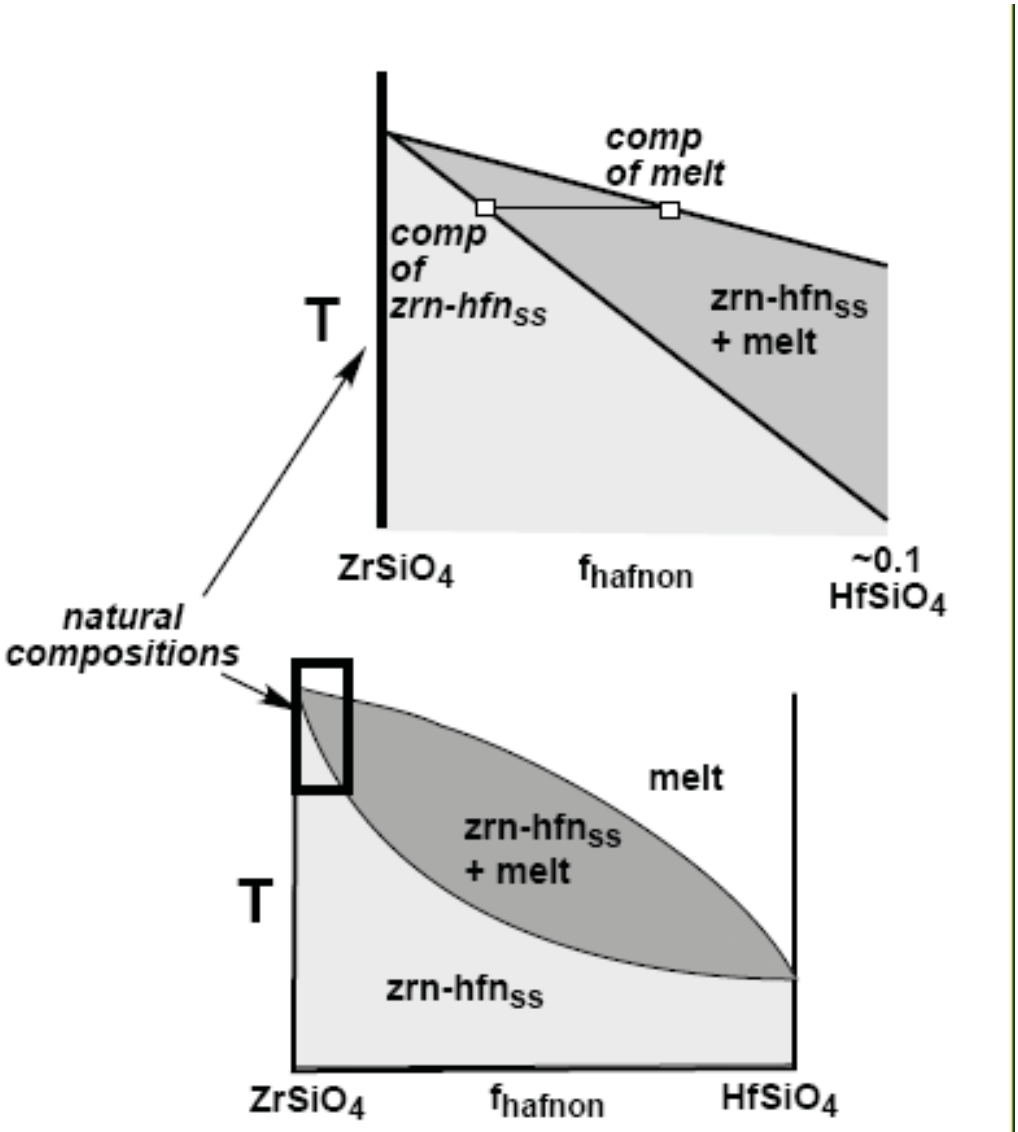

Figure 1: Schematic phase diagram showing crystallization of zircon-hafnon solid solution. Note that as zircon crystallizes, Zr/Hf in the remaining melt decreases.

histories imply the possibility that temperature and quantity and composition of melt fluctuate in time and space (e.g. Vazquez & Reid, 2002; Harper et al., 2004), but elucidating the time-composition path has proven difficult. Combined analysis of elemental and U,Th-Pb system isotopes in individual crystals of allanite is promising (Vazquez and Reid, 2004), but allanite is relatively restricted in its distribution and at present cannot be used in thermometry. In contrast, zircon is a very common constituent of intermediate to felsic igneous rocks that can be dated by microanalytical methods using either U-series disequilibria (young volcanic rocks) or U-Pb. We propose that Hf content of zircon effectively monitors evolution of coexisting melt (cf. Pupin, 2000). Combining Hf measurements with *in situ* dating and Ti analysis (Ti-in-zircon thermometry; Watson and Harrison, 2005; Watson et al., 2006) can thus provide an absolute chronological record of changing melt composition and temperature.

Elemental Zoning in Zircon

Elemental zoning in zircon is spectacularly revealed by cathodoluminescence (CL) and backscattered electron imaging (e.g., Hanchar and Miller, 1993; Corfu et al., 2003). *Patterns of zoning* can distinguish pre-magmatic inherited cores, metamorphic overgrowths, and hydrothermal replacement zones. For purposes of this study, key features reflect magmatic processes and include fine-scale (~μm) oscillatory bands and sector zoning and resorption surfaces, as well as simple euhedral, concentric growth zones. *Elemental concentrations that define zones* in zircon crystallizing in a magma depend on concentrations in the medium from which they grow (generally melt, potentially from fluid phase as well) and partitioning behavior. In a simple scenario

where zircon crystallizes in equilibrium with a substantial melt pool and partition coefficients remain constant, there is a straightforward relationship between zone composition and melt composition. However, partition coefficients for various elements may change appreciably as temperature, melt composition (including concentrations of halogens and water), and oxygen fugacity evolve (e.g., Hoskin and Schaltegger, 2003). Furthermore, effects of crystal/melt interface kinetics, including those that promote disequilibrium and supersaturation of slowly diffusing elements around growing crystals, will result in mineral compositions that may not reflect general melt compositions (Hoskin, 2000; Hoskin and Schaltegger, 2003; Fowler et al., 2001; Shore and Fowler, 1996; Putnis et al., 1992). Oscillatory bands and sector zoning (Watson and Liang, 1995) probably reflect these kinetic effects. Diffusivities of most elements in zircon, and all that we discuss in this paper, are extraordinarily low as long as crystals remain intact (refs: Cherniak; Watson et al., 2006). As a consequence, elements are immobile on a scale of (or less than) microns and zoning survives unless a grain experiences either recrystallization or significant radiation damage.

Spirit Mountain Batholith, Nevada: Case Study of Evolving Zr/Hf Preserved in Rocks and Zircons

The Spirit Mountain batholith provides an excellent opportunity to evaluate the hypotheses presented above. It includes granitoids ranging from quartz monzonites (interpreted as cumulates) to high-silica leucogranites (interpreted as solidified, highly fractionated melt), and zircon crystallization spans an interval of two million years (Walker et al., 2005, and in press). The leucogranites – equivalent in composition to

high-silica rhyolites – are abundant and widespread. In this paper, we discuss the petrology, geochemistry, field relations, and geochronology of the leucogranites, compare them to the less evolved granitoids, and present data on the elemental zoning of zircons from leucogranites and granites.

CHAPTER II

METHODS

We initiated this study by compiling data from 12 studies of volcanic sequences that included high-silica rhyolite and that presented analytical data for Zr and Hf (in addition to other routine elements). Patterns for these data were compared with Zr-Hf data from studies of four plutons by Miller, Bea, and their collaborators. This led to detailed study of highly silicic granites and the zircons they contain from the Spirit Mountain batholith, which builds on and complements a broad-based investigation that includes mapping and extensive U-Pb age dating of zircons by SHRIMP-RG (sensitive high-resolution ion microprobe-reverse geometry) and whole-rock elemental analysis (Walker et al., in press; methods for SHRIMP and elemental analyses presented therein).

For the Walker et al. (in press) study, we obtained cathodoluminescence images of zoning patterns in close to 1000 zircon grains from 15 dated samples. U and Th concentrations were determined for all of the ~282 dated spots from the 15 samples, and Hf concentrations were determined for analyzed spots from 6 of the samples. Zircons from two dated SHRIMP samples were selected for detailed trace element analysis (see sample descriptions in "Zr/Hf and Zircon Zoning in Spirit Mountain Batholith" section).

The basic operating parameters of the SHRIMP-RG (primary beam current, spot size, mass resolution) were the same for both the standard U-Pb analyses and the more comprehensive trace element analyses. Hafnium (measured as $^{180}Hf^{16}O^{+}$) was included as part of the standard U-Pb age determinations for 4 samples. The more extensive trace

element routine included $^{31}P^{+}$, $^{40}Ca^{+}$, $^{49}Ti^{+}$, $^{56}Fe^{+}$, $^{89}Y^{+}$, $^{172}Yb^{16}O^{+}$, $^{180}Hf^{16}O^{+}$, $^{232}Th^{16}O^{+}$ and $^{238}U^{16}O^{+}$, in addition to $^{30}Si^{+}$, $^{96}Zr^{+}$ and $^{90}Zr_2{}^{16}O^{+}$ reference peaks. $^{49}Ti^{+}$ was selected over more abundant $^{48}Ti^{+}$ to avoid interference from $^{96}Zr^{++}$. For Yb, Hf, Th and U, the oxide peaks rather than the element peaks were used due to their greater ion production during sputtering. Each measurement consisted of one block of three cycles. Each cycle peak stepped sequentially through all of the masses. Data reduction involved averaging raw counts for the three cycles and then normalizing to the average $^{30}Si^{+}$ count rate. This normalization minimizes variations caused both by drift in the primary current and by time-dependent ionization phenomena related to sputtering. Normalized count rates from the unknowns were compared to comparable measurements of standard zircons from the Mud Tank carbonatite, Australia (Hoskin and Ireland, 2000), Samé, Tanzania, and synthetic Ti-bearing zircon (Watson et al., 2006) to determine absolute elemental concentrations.

Temperature estimates are derived from Ti concentrations using the equation of Watson and Harrison (2005). The thermometer is calibrated under rutile-saturated conditions ($a_{TiO2} = 1$); rutile saturation in magmas is exceedingly rare, but a_{TiO2} is approximately fixed at values >0.5 in most felsic magmas by saturation in other Ti phases (see discussion in Watson et al., 2006; E.B. Watson, personal communication, 2006). We therefore adjust the ideal equation of Watson and Harrison (2005) to reflect a_{TiO2} ~0.7, appropriate for sphene and titanomagnetite saturation, as follows:

$T(^{\circ}C) = \frac{5080}{6.01 - LOG((10/7) \times ppmTi)} - 273$. Uncertainty in true a_{TiO2} introduces tens of ºC uncertainty in absolute temperature, but because a_{TiO2} remains close to constant as

long as melt is saturated in a Ti phase, errors will be systematic and the relative temperature differences indicated by the thermometer will be real. Calcium and iron were monitored to assess any possible contamination by infiltration along cracks during metamictization or alteration, as well as indicating unseen inclusions that would yield erroneously high apparent Ti concentrations in zircon.

SHRIMP spatial resolution (in this case, 30-40 μm spot diameter) does not allow analysis of single oscillatory bands, which are of the order of only a few microns thick. We refer to a continuous region of oscillatory bands as an 'oscillatory zone;' such zones are commonly broad enough to be readily analyzable. Although an individual oscillatory *band* may represent only short term and very local fluctuations due to feedback mechanisms resulting in local disequilibrium at the crystal/melt interface (e.g., Hoskin, 2000; Fowler et al., 2001; Putnis et al., 1992), in our view an entire oscillatory *zone* reflects more closely the mean composition of host melt during growth.

CHAPTER III

BACKGROUND RESEARCH

Patterns of Zr/Hf Variability in Felsic Igneous Rocks, with Implications for Zircon/Melt Segregation

In Figures 2, 3 and 4, we present compilations of Zr/Hf data for selected igneous suites, both plutonic and volcanic, that include high-silica rocks. Figure 2 shows the ratio plotted against SiO_2, in Figure 3 we plot Zr/Hf vs. Sr, and Figure 4 shows Zr/Hf vs. Rb/Sr (conventional monitors of fractionation). General trends in both pairs of diagrams are clear. Zr/Hf hovers in the chondritic range with little systematic change at SiO_2 up to 73-75 wt%, and then there is a sharp decrease to values as low as 15. Strontium correlates directly with Zr/Hf and Rb/Sr inversely, but Sr falls and Rb/Sr rises considerably after Zr/Hf begins its dramatic drop.

Not all of the compositional range exhibited by the sequences can be attributed to fractional crystallization alone, but it is likely that the strong decreases in both Zr/Hf and Sr at relatively high SiO_2 are primarily a consequence of fractionation. Continuing Sr depletion throughout crystallization of intermediate to felsic magmas is anticipated because of feldspar growth, and it is evident in these plots, but the delay in the sharp decrease in Zr/Hf until very high SiO_2 might not be expected. Most magmas are probably not this silicic when they reach saturation in zircon - note the common occurrence of zircon in dacites and peak Zr and zircon abundances in granodiorites – and thus the plots imply a delayed effect of zircon fractionation. This could be a consequence

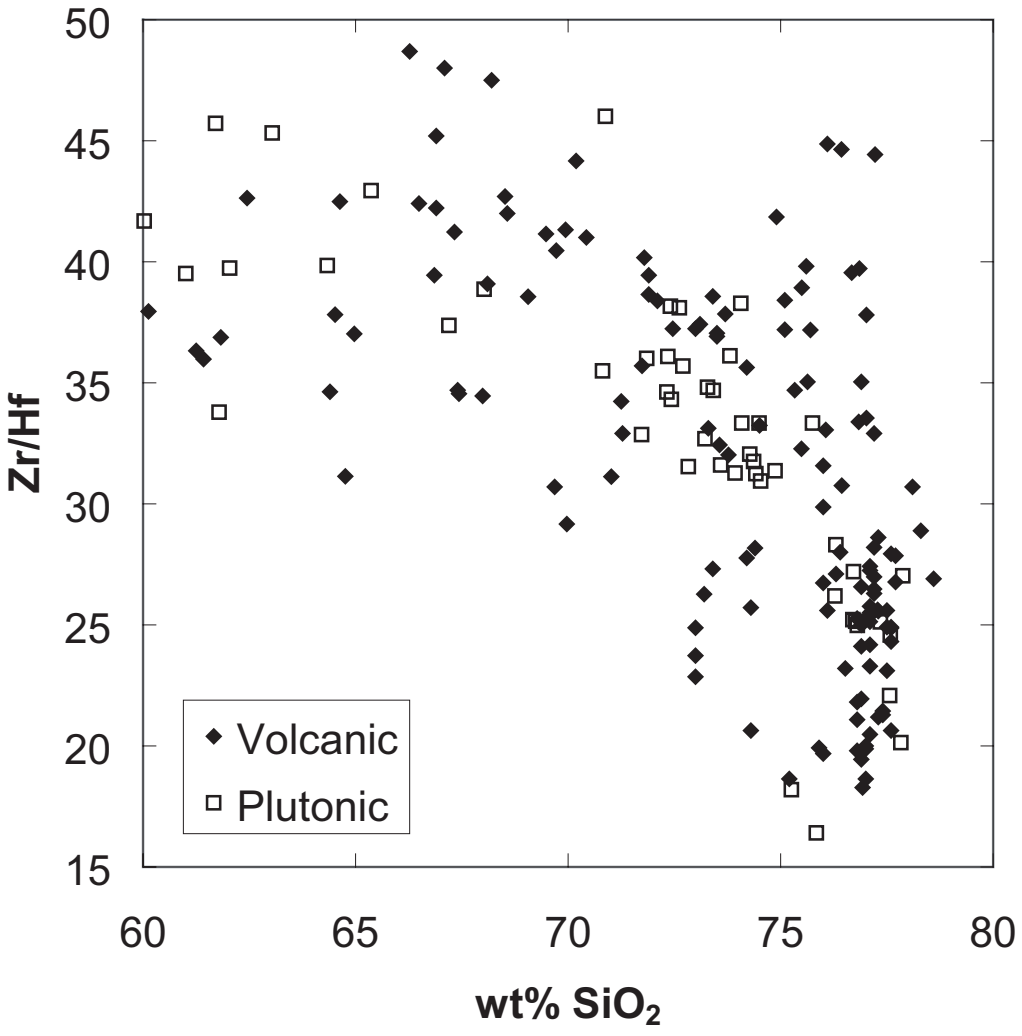

Figure 2: Zr/Hf vs. SiO2 for twelve volcanic sequences that include highly silicic rocks (Anderson, et al., 2000; Bachl, 1997; Briggs, et al., 1993; Heumann and Davies, 1997; Johnson and Grunder, 2000; Mahood, 1981; Metz and Mahood 1991; Reagan, et al., 2003; Stix, et al., 1988; Stix and Gorton, 1990; White and Urbanczyk, 2001) and plutonic data from the Sweetwater Wash pluton, CA (Wark and Miller, 1993), the Searchlight pluton, NV, the Aztec Wash pluton, NV and the Stepninsk pluton, Russia. Note similarly sharp drop in Zr/Hf at ~73 wt% SiO2.

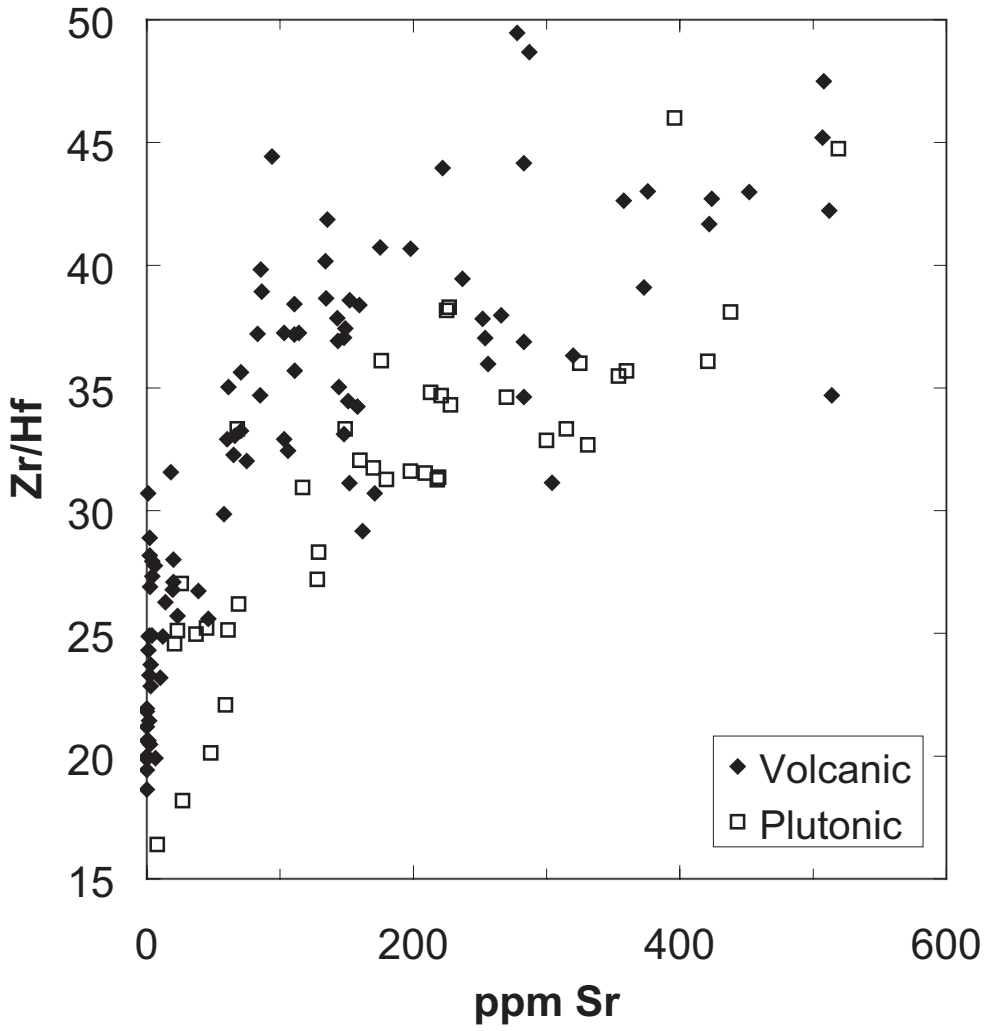

Figure 3: Zr/Hf vs. Sr for twelve volcanic sequences that include highly silicic rocks (Anderson, et al., 2000; Bachl, 1997; Briggs, et al., 1993; Heumann and Davies, 1997; Johnson and Grunder, 2000; Mahood, 1981; Metz and Mahood 1991; Reagan, et al., 2003; Stix, et al., 1988; Stix and Gorton, 1990; White and Urbanczyk, 2001) and plutonic data from the Sweetwater Wash pluton, CA (Wark and Miller, 1993), the Searchlight pluton, NV, the Aztec Wash pluton, NV and the Stepninsk pluton, Russia. Note the strong correlation between Sr and Zr/Hf, although Sr begins its decline before Zr/Hf shows much change.

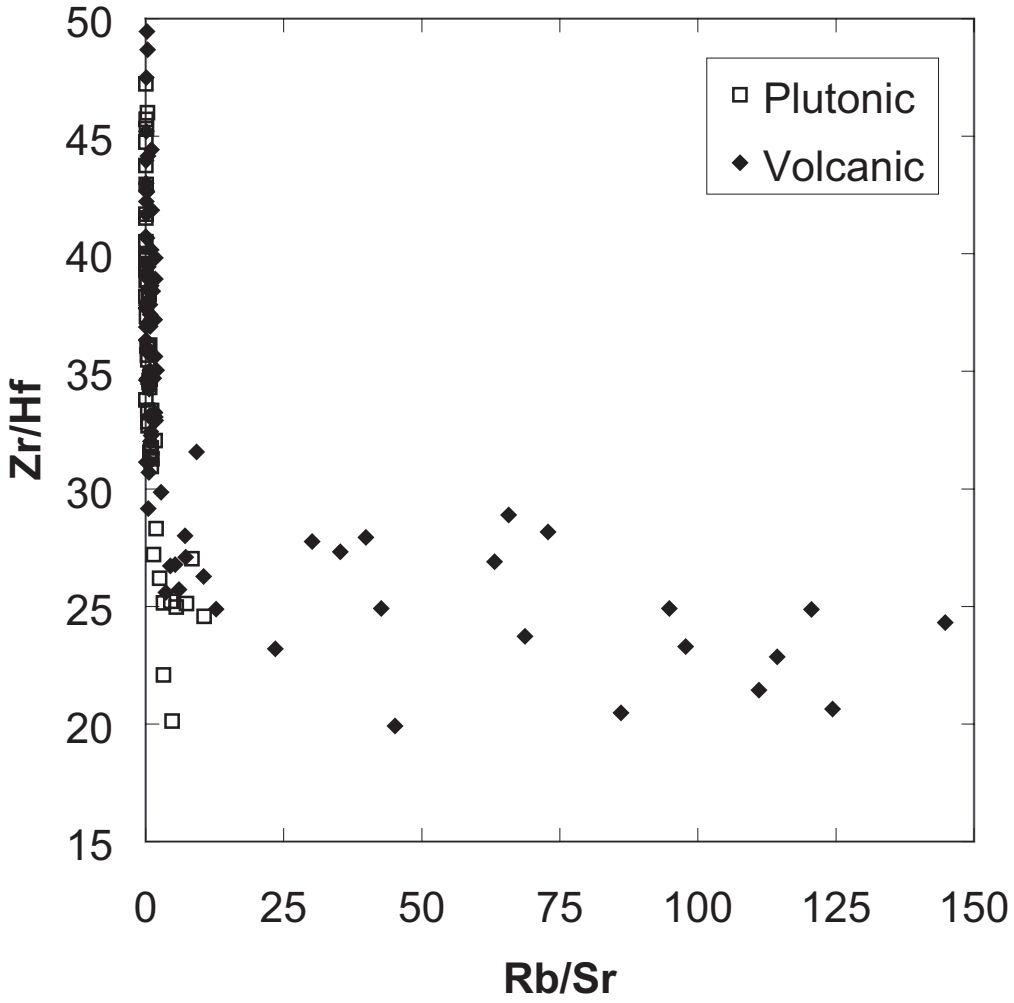

Figure 4: Zr/Hf vs. Rb/ Sr for twelve volcanic sequences that include highly silicic rocks (Anderson, et al., 2000; Bachl, 1997; Briggs, et al., 1993; Heumann and Davies, 1997; Johnson and Grunder, 2000; Mahood, 1981; Metz and Mahood 1991; Reagan, et al., 2003; Stix, et al., 1988; Stix and Gorton, 1990; White and Urbanczyk, 2001) and plutonic data from the Sweetwater Wash pluton, CA (Wark and Miller, 1993), the Searchlight pluton, NV, the Aztec Wash pluton, NV and the Stepninsk pluton, Russia. Note abrupt rise in Rb/Sr with drop in Zr/Hf.

of either the modest Zr/Hf fractionation of zircon (perhaps prolonged growth of zircon is required before Zr/Hf in the melt is substantially reduced) or of delayed extraction of zircon grains from melt. In order for whole rock compositions to reflect the reduction in Zr/Hf, the zircon must be removed from the melt (or melt must be segregated from crystallizing zircon). Physical segregation of zircon must be difficult because of its small size. Therefore, successful fractionation of zircon likely requires separation of any other minerals present as well, and it is plausible that coexisting minerals are removed before zircon because of their larger size or even influence the motion of the zircons themseleves. However, we note that Zr concentration begins to drop at lower SiO_2 and higher Sr than the abrupt drop in Zr/Hf, so it is likely that rapid decline in Zr/Hf marks the onset of extreme fractionation (removal of zoned zircon in equilibrium with melt that has evolved well beyond the onset of zircon fractionation).

As zircon saturation temperatures are relatively low for most magmas, generally ranging from ~750 to <900°C (Miller et al., 2003), zircon-induced modification of Zr/Hf ratios must be a relatively low-temperature process. The fact that reduction of Zr/Hf appears to be restricted to high-silica rhyolites and granites indicates that this zircon signature is an even lower T phenomenon, probably in general below 800°C (see discussion of Spirit Mountain batholith that follows).

Spirit Mountain Batholith: Monitoring and Interpreting Zr/Hf in a Complexly Evolving Felsic System

The Spirit Mountain batholith (SMB) is a complex, "patchwork" batholith of Miocene age, assembled over a period of two million years and capped by an extensive

roof zone composed of high-silica leucogranite. The leucogranite roof zone, according to U-Pb ages of zircons (Walker et al., in press), amassed over a period of about one million years as pulses of magma differentiated and the buoyant, fractionated magma migrated upward and was trapped beneath the roof. In addition to investigating the petrology of this roof zone, we examined zoned zircons from both the leucogranite and the underlying accumulated granite for internal Zr/Hf variation using SHRIMP-RG and tied the measured Hf of those zones to temperatures and specific ages using Ti-in-zircon thermometry (Watson and Harrison, 2005) and U-Pb geochronology, respectively, to unravel a protracted history of repeated fractionation for the Spirit Mountain batholith.

CHAPTER IV

THE SPIRIT MOUNTAIN BATHOLITH

Geologic Setting

The SMB underlies a large portion of the Newberry Mountains, Nevada, in the northern Colorado River Extensional Corridor (Figure 5) (Howard and John, 1987; Faulds et al., 1990). Magmatism swept northward through the northern part of the corridor in the early to middle Miocene, followed closely by and generally outlasting extension related-faulting (Faulds et al., 1995; Gans and Bohrson, 1998; Howard et al., 1996). At this latitude, magmatic activity spanned the interval 18 to 5 Ma (Gans and Bohrson, 1998; Faulds et al., 2001), but exposed plutons were all emplaced between ~17.5 and 15.5 Ma (Faulds et al., 1995; Cates et al., 2003; Miller et al., 2004). Paleomagnetic data indicate that the fault block containing the SMB was tilted 40 to 50° to the west (Faulds et al., 1992), exposing a cross-section at least 9 km thick, from the roof in the west to deep levels in the east (Figure 6) (Hopson et al., 1994; Walker et al., in press).

Petrology and Field Relations of the Batholith

The SMB is exposed over an area of about ~250 km^2 (Figure 6). Much of it appears relatively homogeneous, but close examination of field relations reveals that it varies subtly throughout and dramatically in some areas. With the cross sectional view afforded by westward tilting, it is apparent that much of the batholith has a fairly

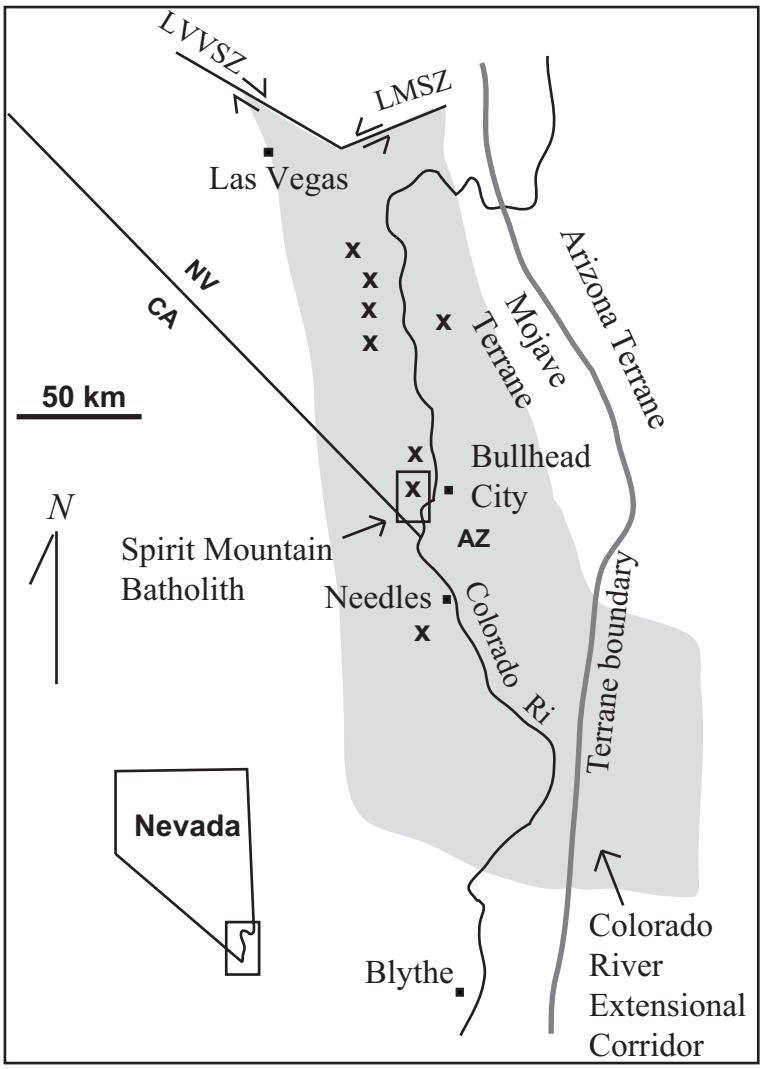

Figure 5: Map of the Colorado River Extensional Corridor (shaded) showing the location of the Spirit Mountain batholith (from Walker et al.., in press). LVVSV is the Las Vegas Valley Shear Zone and LMSZ is the Lake Mead Shear Zone. The x's represent Miocene-aged plutons.

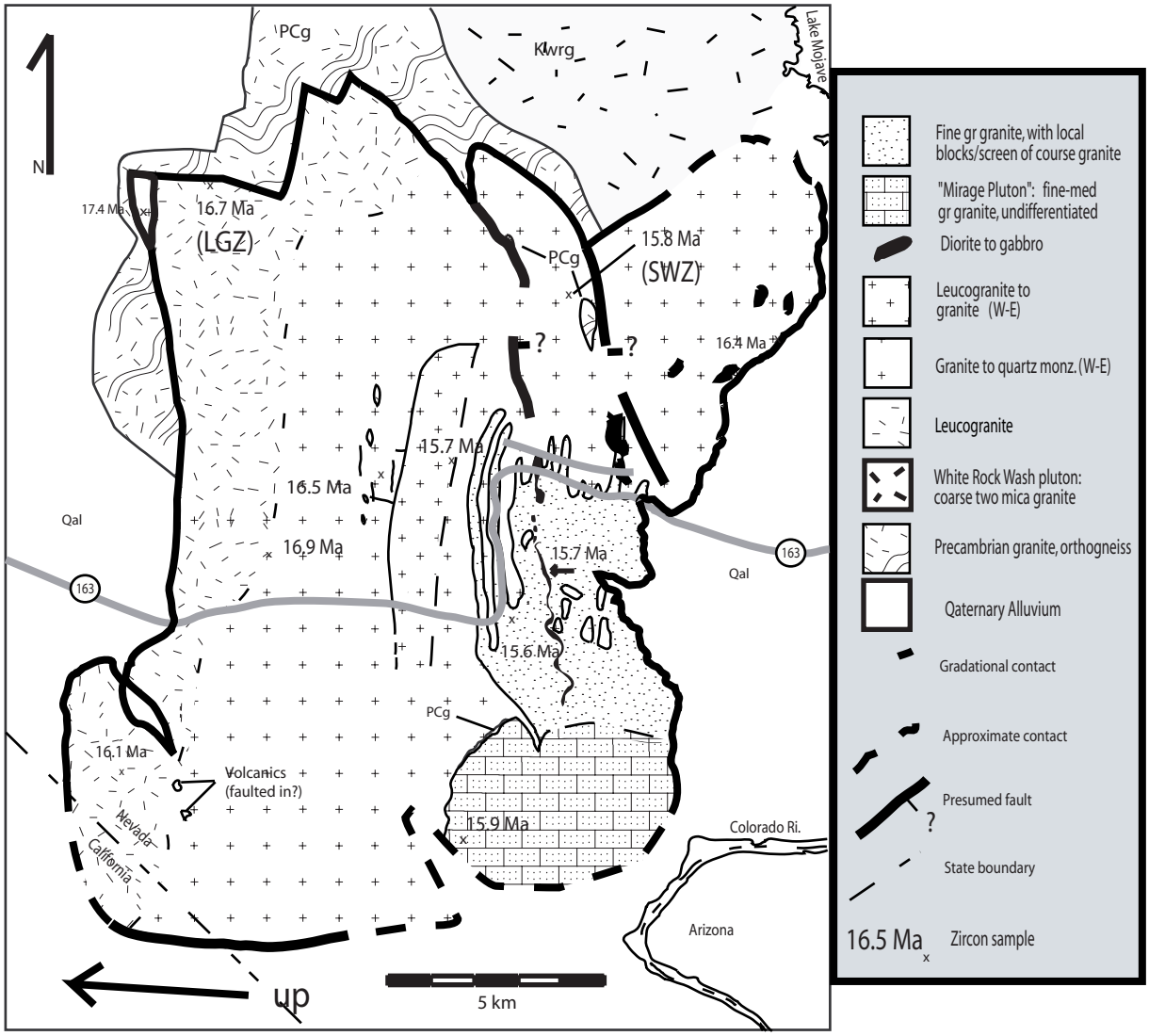

Figure 6: Geologic map of the Spirit Mountain batholith, showing locations of samples LGZ and SWZ. Ages shown represent U-Pb zircon SHRIMP ages (modified from Walker et al., in press). Note that the map view also represents a near cross-section of the batholith, with up in the west direction.

consistent textural and compositional stratigraphy from west to east (top to bottom) that is laterally continuous from north to south. This stratigraphy is interrupted in several places by younger intrusions of the batholith. The entire SMB, including later intrusions and more poorly exposed portions, consists mostly of granitic rock with a uniform mineral assemblage of alkali feldspar + plagioclase + quartz + biotite + accessory sphene, zircon, apatite, oxides, and allanite or chevkinite (fluorite is also present in some leucogranites). Dioritic to basaltic dikes, sills and pods are present, but they are volumetrically minor in comparison to the granites; the sills and pods are restricted to the lower 1/3 of the batholith, and the dikes are part of a distinct late swarm that marks termination of the intrusive history.

Walker et al. (in press) divide the batholith into six units that are distinct in texture, field relations (Figure 6), and in some cases compositions. These include a small exposure of the moderately felsic *roof unit* at one corner of the western margin the batholith; the *Spirit Mountain granite*, by far the most extensive unit and the one upon which we focus in this paper; *Mirage granite*, which forms a discrete pluton; *diorite sheets* that are locally abundant; *fine-grained granite* that cuts most other units as thin to thick sheets; and the mafic to felsic *Newberry dike swarm*, the latest intrusions into the batholithic system. The batholith as a whole ranges in age from 15.3 ± 0.3 to 17.4 ± 0.2 Ma (all uncertainties stated at $\pm 1\sigma$) (Walker et al., in press).

The Spirit Mountain granite comprises a sequence that ranges from west to east (top to bottom), for the most part gradationally, from high-silica leucogranite into foliated quartz monzonite (cf. Volborth, 1973; Howard et al., 1994; Hopson et al., 1994; Haapala et al., 1996; Haapala et al., 2005; Walker et al., in press). This sequence ranges from 61-

79 wt% SiO_2 and in age from 15.7 ± 0.2 to 16.8 ± 0.2 Ma. Except for the small roof unit, the oldest part of the batholith (17.4 ± 0.2 Ma), the remainder of the units that comprise the batholith (the Mirage granite, diorite sheets, fine-grained granite, and the Newberry dike swarm) are coeval with or slightly younger than the youngest part of the Spirit Mountain granite and were emplaced after most of it was largely to entirely solid (Walker et al., in press). Previous work (Hopson et al., 1994) suggested that the leucogranite melt segregated during fractional crystallization of the batholith, and that the coarser grained granites to the east represent the residual cumulates from the segregation events. Our work (Walker et al., in press) generally supports this interpretation, but ranges of ages in both the leucogranite and the cumulate granite suggest that the Spirit Mountain granite represents a patchwork accumulation of multiple intrusions that differentiated repeatedly, sending the fractionated high-silica magma toward the roof, leaving cumulate granites below. The leucogranite in the roof zone, therefore, amassed over much of the lifetime of the batholith, as a series of pulses of magma were injected, differentiated, and the buoyant, fractionated melt migrated upward, leaving melt-depleted cumulate behind.

Leucogranites in the Spirit Mountain granite

This study focuses primarily on the high-silica leucogranites of the Spirit Mountain granite. The bulk of the leucogranites form a roof zone that is exposed over an area of ~55 km^2 with an original total thickness near 2 km. This zone, which spans the north to south extent of the roof (western margin) of the batholith, varies in texture from aplitic to porphyritic to medium-grained equigranular and is locally miarolitic or pegmatitic. The internal contacts range from very sharp to gradational over several

meters and indicate that this zone comprises a collection of initially subhorizontal sheets and pods that range in size from one to tens of meters in thickness and up to hundreds of meters in length. Some contacts suggest initially vertical dikes, on the scale of one meter in thickness, of aplite and leucogranite porphyry that appear to feed into the base of the subhorizontal structures. We interpret these relations as evidence of repeated emplacement of the leucogranites - some sheets intruding a hot, melt-bearing mush, and some intruding solid rock, and this is supported by U-Pb zircon ages. Three dated samples yielded ages of 16.8 ± 0.2 Ma, 17.7 ± 0.2 Ma (age uncertain), and 16.1 ± 0.2 Ma (Walker et al., in press), suggesting that the roof zone accumulated over much of the lifetime of the batholith, and, together with field relations, that only a fraction of it was largely molten at any point in time. Similar rock is found throughout the Spirit Mountain granite in a network of interconnected pod-like structures, sills, and dikes. Parts of this network appear to feed into the leucogranite of the roof.

The leucogranites are composed of ~40-50% alkali feldspar, 30-40% quartz, 10-30% sodic plagioclase, ~1% biotite, and accessory apatite, allanite, sphene, zircon, fluorite and opaque oxides. They range in SiO_2 from 76 to 79 wt%, with very low Sr and Ba concentrations (mostly 5-50 ppm and 20-100 ppm, respectively), moderate light REE depletions and strong middle REE depletions compared to other granitoids in the batholith, and extreme negative Eu anomalies (Walker et al., in press), all of which suggest that this high-silica leucogranite is the product of fractional crystallization.

Zircon saturation temperatures (T_{zrc}) (Watson and Harrison, 1983; Hanchar and Watson, 2003; Miller et al., 2003) calculated for granitoid rocks in Spirit Mountain

batholith range from 696 to 878°C[1]. T_{zrc}s for the leucogranite are limited to 696 to 806°C, with an average of 759°C. Granites interpreted to be cumulates have an average T_{zrc} of 821°C. T_{zrc}s for cumulates are suspect, because the rocks do not likely represent melt compositions (Miller et al., 2003). The leucogranites appear to be better candidates for reliable T_{zrc} estimates of their temperatures upon extraction from residual mush because they were probably melt rich. However, our data on zoning suggest that much of the zircon grew prior to final fractionation (see below), and hence these T_{zrc} may also be overestimates.

[1] Influence of melt composition on zircon saturation (thus on calculated T_{zrc}) was incorporated into the factor "M," which takes into account silica content and peraluminosity (Watson and Harrison, 1983). Subsequent work suggests that other compositional variables, including concentrations of halogens, Fe, and Mg, and oxygen fugacity, affect zircon solubility (Baker et al., 2002; Keppler, 1993; Hanchar and Watson, 2003). However, these effects appear to limited for typical magmas and have not been sufficiently characterized to permit modification of the initial thermometer. The effect of H_2O is also not factored into the thermometer, but, as initially demonstrated by Watson and Harrison (1983), this effect is minimal where water content is >2 wt% (see also Linnen, 2005; Baker et al., 2002); the water content in Spirit Mountain granite was undoubtedly more than 2 wt% (e.g., early crystallization of biotite, absence of pyroxene). Modest uncertainties in T_{zrc} do not affect any conclusions of this paper.

CHAPTER V

RESULTS

Zr/Hf in the Spirit Mountain Batholith

Zr/Hf ratios in granitoid rocks of the Spirit Mountain batholith reflect the typical crustal Zr/Hf trend of intermediate to felsic rocks, remaining near chondritic until reaching a relatively high-silica-content (~73 wt%). The ratio falls slowly, to ~30 at ~76 wt% SiO_2, and then plummets to values as low as 18 between 76 and 79 wt% SiO_2 (Table 1; Figure 7). Zr/Hf of the leucogranite samples is ~18 to 30, while the samples interpreted as cumulate rocks, along with having lower SiO_2 contents, have Zr/Hf ~35 to 45. The whole-rock Zr/Hf trend corresponds to other geochemical indicators of fractionation processes. For example, Sr and Zr/Hf correlate very well, with the lowest Sr concentrations corresponding to the lowest Zr/Hf ratios (Figure 8), as do Rb/Sr and Zr/Hf with high Rb/Sr corresponding to the lowest Zr/Hf (Figure 9). As with SiO_2 vs. Zr/Hf, the Sr-Zr/Hf plot, though generally monotonic, is decidedly non-linear; Zr/Hf rises rapidly from 18 to 30 as Sr rises from 5 to 50 ppm, then more gradually (30 to 37 as Sr increases to ~250 ppm), and then levels off at higher Sr concentrations. The Rb/Sr-Zr-Hf plot shows a similar nonlinear trend, with very low Rb/Sr across a wide range of Zr/Hf (45 to 30), then a dramatic increase in Rb/Sr as Zr/Hf continues to drop.

Table 1: Abbreviated geochemistry of all samples from Spirit Mountain batholith. Full geochemistry available in Walker *et al.* (in press).

Sample ID	rock unit	SiO2 (wt%)	Sr (ppm)	Zr (ppm)	Hf (ppm)	Zr/Hf
SML78	Spirit Mountain granite: leucogranite	78.59	5	96	5.4	18
SML67	Spirit Mountain granite: leucogranite	78.49	5	114	5.6	20
SML71	Spirit Mountain granite: leucogranite	78.10	12	131	5.4	24
SML69	Spirit Mountain granite: leucogranite	77.96	23	68	2.9	23
SML73	Spirit Mountain granite: leucogranite	77.84	15	128	6.2	21
BW24	Spirit Mountain granite: leucogranite	77.74	83	152	4.5	34
SML132	Spirit Mountain granite: leucogranite	77.65	16	93	3.9	24
SML74	Spirit Mountain granite: leucogranite	77.55	13	111	5.2	21
SML76	Spirit Mountain granite: leucogranite	77.51	7	123	6.9	18
SML49Z	Spirit Mountain granite: leucogranite	77.37	17	99	4.2	24
SML47	Spirit Mountain granite: leucogranite	77.31	73	83	2.8	30
SML63C	Spirit Mountain granite: leucogranite	77.19	4	186	8.1	23
BW47	Spirit Mountain granite: leucogranite	77.01	11	47	2.2	21
SML52	Spirit Mountain granite: leucogranite	77.00	42	137	4.6	30
SML130	Spirit Mountain granite: leucogranite	76.96	7	92	4.4	21
LGZ	Spirit Mountain granite: leucogranite	76.80	27	83	4.1	20
SML133	Spirit Mountain granite: leucogranite	76.18	48	165	6.3	26
SML129Z	Spirit Mountain granite: leucogranite	76.07	26	116	5.1	23
BW48	Spirit Mountain granite: granite	75.58	121	153	5.1	30
SML54Z	Spirit Mountain granite: granite	75.57	89	127	4.2	30
BW43	Spirit Mountain granite: granite	74.85	210	152	4.4	34
BW40	Spirit Mountain granite: granite	74.24	224	160	4.9	33
SML120Z	Spirit Mountain granite: granite	73.84	191	202	5.4	37
BW36	Spirit Mountain granite: granite	73.59	188	125	3.9	32
BW63	Spirit Mountain granite: granite	72.98	240	180	4.9	37
BCOZ	Spirit Mountain granite: granite	72.33	311	186	5.0	38
BW11	Spirit Mountain granite: granite	72.12	268	167	4.4	38
BW62	Spirit Mountain granite: granite	71.36	332	172	4.7	37
BW33	Spirit Mountain granite: granite	70.93	315	186	5.0	37
BC101Z	Spirit Mountain granite: granite	70.84	272	229	5.8	40
101Z	Spirit Mountain granite: granite	69.93	323	322	8.2	39
BW49	Spirit Mountain granite: granite	68.88	356	312	7.7	40
BW41	Spirit Mountain granite: granite	67.55	456	204	5.6	36
BW32	Spirit Mountain granite: quartz monzonite	64.38	383	421	10.4	40
SWZ	Spirit Mountain granite: quartz monzonite	63.19	551	557	12.3	45
SML213	Spirit Mountain granite: quartz monzonite	61.39	578	586	12.5	47
BGZ	fine-grained granite	73.83	243	150	4.4	34
MI-2	Mirage granite	74.01	215	163	4.5	36
MI-1	Mirage granite	73.69	261	203	5.6	36
SML59Z	roof unit	74.41	63	199	6.6	30
BW61	diorite sheet	56.04	319	160	4.3	37
BW34	diorite sheet	54.99	368	193	4.8	40
DIORITE	diorite sheet	53.56	386	137	3.4	40

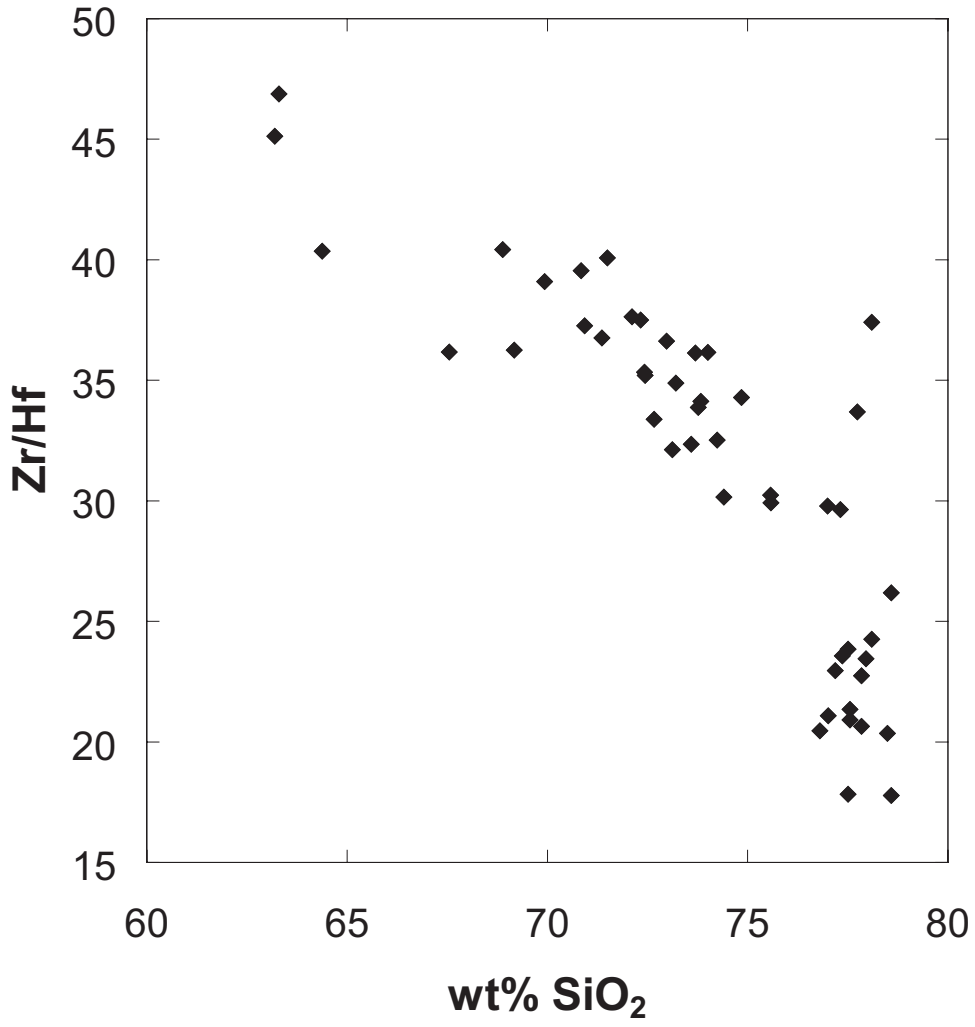

Figure 7: Zr/Hf vs. SiO2 in the Spirit Mountain batholith. Note the sharp drop in Zr/Hf at approximately 76 wt% SiO2.

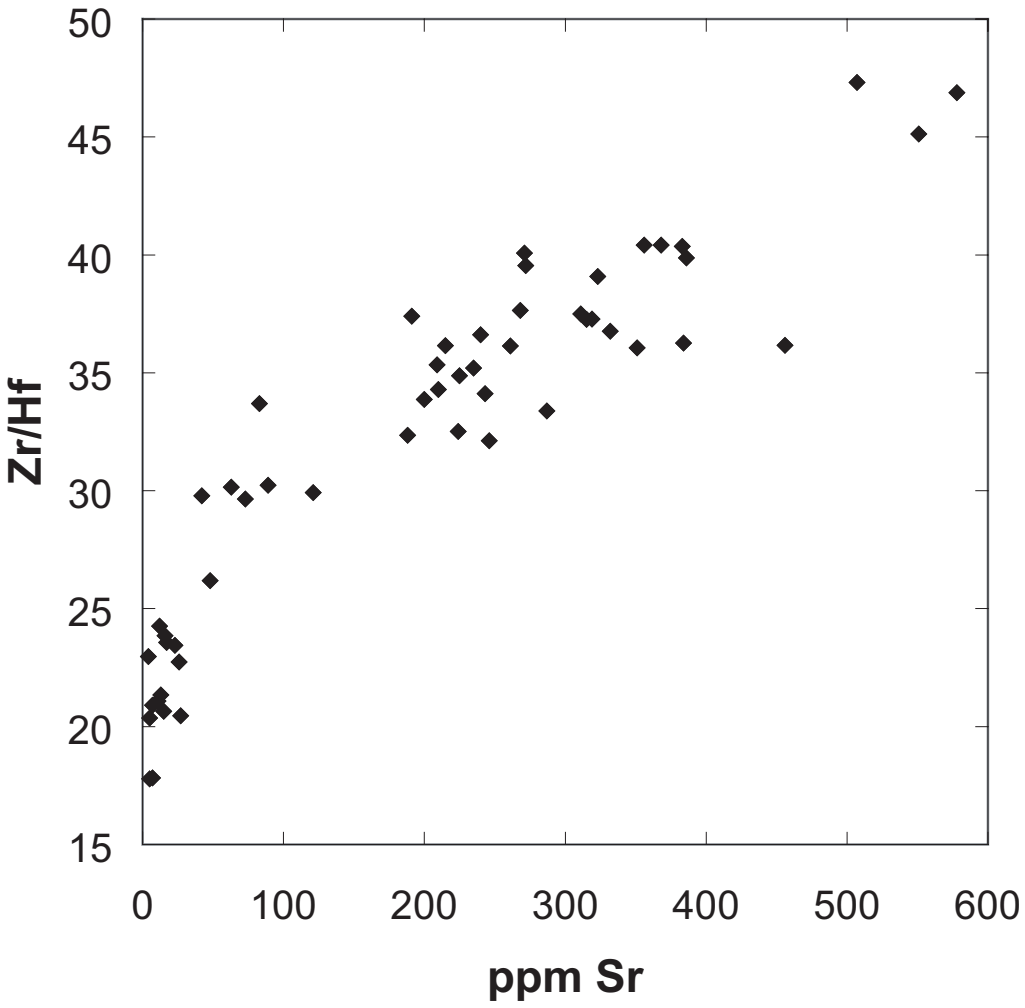

Figure 8: Zr/Hf vs. SiO2 in the Spirit Mountain batholith.

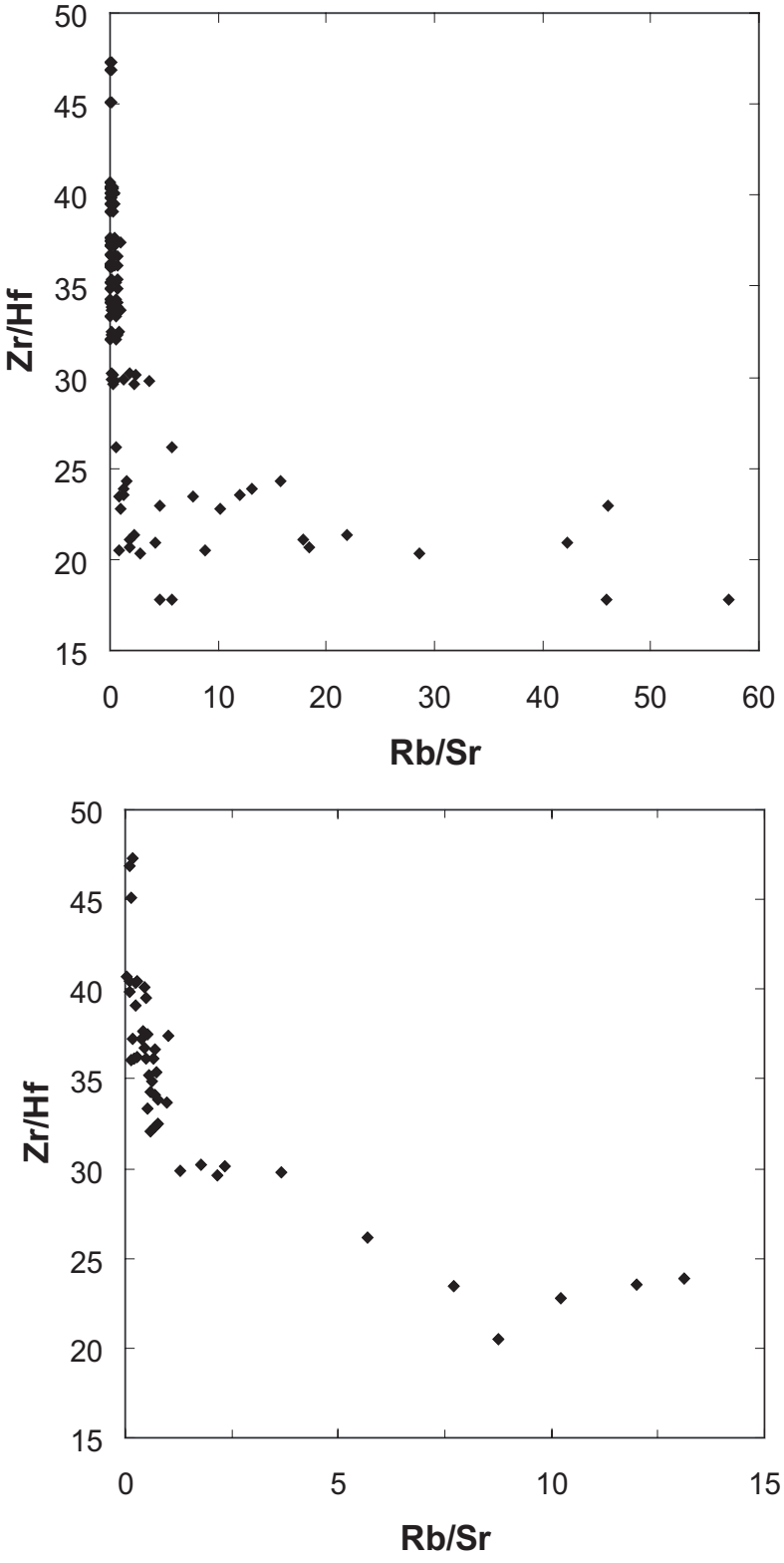

Figure 9: Zr/Hf vs. Rb/Sr for the Spirit Mountain batholith.

Elemental Zoning in Zircons from the Spirit Mountain Batholith

Zircons from two samples (see Figure 6) were selected for detailed in situ elemental analysis based upon results of the U-Pb analysis and field and petrologic considerations. One, a quartz monzonite (sample SWZ), was interpreted to represent crystal accumulation and for the most part to document growth from less fractionated melt. SWZ is composed of large, euhedral alkali feldspar, plagioclase feldspar, quartz, and biotite with accessory sphene, allanite, apatite, zircon and an opaque phase. It is relatively low in SiO_2 (63.2 wt%) and high in Zr (560 ppm; T_{zrc} 878ºC), Zr/Hf (~45), Sr (551 ppm), and Ba (1850 ppm), reflecting accumulation of feldspars and zircon (hence high T_{zrc}) along with biotite and other accessory minerals (Table 2). SHRIMP ages of zircon from SWZ yield two major age peaks, one at 16.8 ± 0.3 Ma and the other 15.8 ± 0.2 Ma. These are interpreted to represent initial accumulation and partial reactivation during subsequent recharging, respectively (Walker et al., in press). LGZ, a porphyritic leucogranite from the roof zone, is composed of alkali feldspar, quartz, plagioclase feldspar, biotite, and accessory allanite, apatite, sphene and zircon. Phenocrysts consist of rounded quartz, euhedral alkali feldspar, and less abundant small, euhedral plagioclase grains. It was selected to represent a highly fractionated magma, with high SiO_2 (76.8 wt%) and low Zr (80 ppm; T_{zrc} 734º C), Zr/Hf (20), Sr (27 ppm), and Ba (92 ppm). LGZ has a predominant age peak at 16.8 ± 0.2 Ma that is considered to represent the dominant time of melt segregation and solidification, with a small number of grains at 17.7 ± 0.1 Ma that probably were entrained from remnants of the first pulse of batholith emplacement (now represented by the small roof unit). Following Wes Hildreth (presentation at Penrose Conference, 2001), we refer to such grains as "antecrysts."

Table 2: Whole-rock geochemistry of samples SWZ and LGZ from Spirit Mountain batholith, from Walker *et al.* (in press). Oxides listed in wt %, Trace Elements in ppm.

Element	SWZ	LGZ
SiO2	63.19	76.8
Al2O3	17.64	12.65
CaO	2.73	0.67
MgO	1.35	0.10
Na2O	4.70	3.92
K2O	5.07	4.75
Fe2O3	4.10	0.92
MnO	0.09	0.05
TiO2	0.87	0.13
P2O5	0.27	0.02
Rb	83	236
Sr	551	27
Ba	1850	92
Cs	0.3	0.7
Ta	1.11	3.33
Nb	19.2	38.3
Tl	0.38	0.86
Hf	12.3	4.1
Zr	530	99
Zr	557	83
Y	26	18
V	57	5
Th	8.91	19.1
U	1.09	2.67
Ga	22	31
La	103	46.7
Ce	210	77.7
Pr	21.7	6.39
Nd	79.5	17.9
Sn	1.17	1.10
Eu	2.41	0.235
Gd	7.86	2.16
Tb	1.15	0.43
Dy	5.65	2.60
Ho	1.00	0.58
Er	3.06	2.18
Tm	0.442	0.400
Yb	2.92	2.67
Lu	0.414	0.404
Sm	12.0	2.76
Be	2	6
Ge	1.0	2.3
Bi	0.2	0.8
Zr/Hf	**45.12**	**20.46**

Zircons from the Spirit Mountain batholith are strongly zoned (see Figure 11). Most zones are euhedral and concentric, though some internal zones are truncated. Thin to medium-thick zones that enclose oscillatory dark-light bands are common. We refer to innermost identifiable zones of grains (centers) as cores, regardless of whether there is evidence that the centers are appreciably older than the outer zones (only a few cores have identifiable truncated [resorption] surfaces). 'Rims', in the context of this discussion, represent the outermost zones of the zircons, either on an edge or a tip.

Hafnium content of zircons from SWZ and LGZ ranges from 7500 ppm to 16700 ppm (Zr/Hf ~64 to 29) (Table 3 and 4). In SWZ, Hf contents of all analyzed spots (cores, rims, and intermediate zones) average approximately 10000 ppm (Zr/Hf ~50). There are, however, large fluctuations in Hf within core to rim traverses, as discussed below; Hf concentrations of individual spots range from 7500 ppm to 15000 ppm (Zr/Hf ~64 to 32). The cores of SWZ average ~10000 ppm (Zr/Hf ~49) and the rims average a similar ~9500 ppm (Zr/Hf ~50). LGZ has a higher average Hf content (12000 ppm) and Zr/Hf (39; from 29-63) and a wider range of Hf concentrations (7500-16700 ppm) than SWZ. The cores of grains in LGZ have average Hf concentrations of approximately 11000 ppm (Zr/Hf ~43) and the rims average approximately 13300 ppm Hf (Zr/Hf ~36). Fluctuations in Hf from core to rim and in zones between the cores and rims in grains from both samples are discussed in detail below.

Table 3: Composition of zircon grains from sample LGZ, determined by SHRIMP-RG analysis of grains; data arranged in groups according to grain, and spots listed in order from core (top) to rim (bottom); ages of spots determined previously using SHRIMP-RG U-Pb geochronology (Walker et al., in press); o-zone indicates oscillatory zoning.

Spot ID	Spot description	Age (Ma ± 1σ)	Ti (ppm)	T_{Tiz} (°C)	Hf (ppm)	U (ppm)	Th (ppm)	Zr/ Hf	Th/U
LGZTE-1.1C	dark unzoned core		4.8	709	13557	1230	2702	35	2.20
LGZTE-1.3T2	medium-dark zone		7.5	747	11213	69	76	43	1.10
LGZTE-1.2T	dark zoned tip		4.7	708	15630	2082	2600	31	1.25
LGZTE-2.1C	light zoned core	16.5 ± 0.7	9.4	767	10051	68	136	48	2.00
LGZTE-2.4T2	band of med-dark o-zones	17.5 ± 0.3	9.3	767	13793	401	529	35	1.32
LGZTE-2.2T	dark zoned tip		4.6	706	14762	1625	2752	32	1.69
LGZTE-3.3C	med-dark unzoned core	15.9 ± 1.2	24.6	865	7536	29	103	63	3.55
LGZTE-3.4C2	light, zoned		13.1	800	10129	117	225	47	1.92
LGZTE-3.2T2	med-dark zoned tip	16.7 ± 0.3	3.2	678	16716	1102	951	29	0.86
LGZTE-3.1T1	very dark zoned rim		5.9	726	14332	2268	3053	33	1.35
LGZTE-4.1C	med-dark unzoned core		17.9	831	7766	251	803	61	3.20
LGZTE-4.2	light, zoned		17.2	826	9156	69	132	52	1.91
LGZTE-4.3T	med-dark zoned tip		6.3	732	12930	322	385	37	1.20
LGZTE-5.1C	dark zoned core		7	741	12417	641	1218	38	1.90
LGZTE-5.2	light, zoned		8.7	761	10653	203	382	45	1.88
LGZTE-6.2	light, zoned		12.8	797	11512	532	868	41	1.63
LGZTE-6.3T	very dark zoned tip		11.7	788	13608	4823	13141	35	2.72
LGZTE-7.1C	dark zoned core		4.9	710	14884	1862	3534	32	1.90
LGZTE-7.3	light zoned tip		5.9	726	11291	108	115	42	1.06
LGZTE-8.1C	dark zoned core	17.2 ± 0.3	3.3	679	13812	756	921	35	1.22
LGZTE-8.3T2	light, zoned		10.2	776	10601	228	210	45	0.92
LGZTE-8.2T	light zoned tip		7.7	750	10979	121	161	44	1.33
	sample average		9.1	754	12151	859	1591	39	1.73
	core average		11.2	766	11078	601	1119	43	2.29
	rim/tip average		6.7	734	13362	1621	3172	36	1.51

Table 4: Composition of zircon grains from sample SWZ, determined by SHRIMP-RG analysis of grains; data arranged in groups according to grain, and spots listed in order from core (top) to rim (bottom); ages of spots determined previously using SHRIMP-RG U-Pb geochronology (Walker et al., in press); o-zone indicates oscillatory zoning.

Spot ID	Spot description	Age (Ma ± 1σ)	Ti (ppm)	T_{Tiz} (°C)	Hf (ppm)	U (ppm)	Th (ppm)	Zr/ Hf	Th/U
SWZTE-1.2C	light, unzoned core	14.9 ± 0.6	6.4	733	10890	101	110	44	1.09
SWZTE-1.1T	light, zoned tip	15.1 ± 0.6	10.6	778	9773	79	110	49	1.39
SWZTE-2.1C	med-dark, unzoned core	15.6 ± 0.3	5.3	718	10948	188	315	44	1.68
SWZTE-2.2T	very light, zoned tip		9.9	772	9582	71	110	50	1.55
SWZTE-3.2C	light, zoned core	16.6 ± 0.4	10.8	781	9021	205	646	53	3.15
SWZTE-3.3T2	light, zoned	16.5 ± 0.5	12.4	794	8837	141	265	54	1.88
SWZTE-3.1T	very light zoned tip		11.8	789	9658	52	80	49	1.54
SWZTE-4.1C	light, unzoned core		15.2	814	8168	65	175	58	2.69
SWZTE-4.6T5	light, slightly zoned		12.7	796	9978	123	203	48	1.65
SWZTE-4.5T4	dark band of o-zones		5.7	723	11448	203	233	42	1.15
SWZTE-4.7T6	same dark band of o-zones	16.8 ± 0.5	5.8	725	11496	214	220	42	1.03
SWZTE-4.4T3	light, unzoned tip		13.3	801	9165	49	80	52	1.63
SWZTE-4.1C	light unzoned core		15.2	814	8168	65	175	58	2.69
SWZTE4.3T2	very light, zoned		14.4	809	8296	70	101	58	1.44
SWZTE-4.2T1	dark zoned tip		29.6	886	10813	144	164	44	1.14
SWZTE-5.1C	dark unzoned core	16.3 ± 0.4	14.8	811	8099	242	733	59	3.03
SWZTE-5.2T	light zoned tip		13.6	803	8914	106	221	54	2.08
SWZTE-6.1C	light, unzoned core		19.4	840	8468	41	89	56	2.17
SWZTE-6.2T	med-dark zoned tip	15.4 ± 0.5	10.3	776	10003	283	640	48	2.26
SWZTE-7.1C	dark zoned core	16 ± 0.2	5.3	717	12453	925	1258	38	1.36
SWZTE-7.3T2	light, zoned		16.9	825	8464	51	90	56	1.76
SWZTE-7.2T	light zoned tip	14.3 ± 0.7	11.9	790	9390	77	137	51	1.78
SWZTE-8.1C	light, zoned core	15.8 ± 0.7	32.3	896	7472	48	162	64	3.38
SWZTE-8.3T	medium-dark zoned		25.5	869	7847	196	757	61	3.86
SWZTE-8.4T	light, zoned		14.3	808	8477	119	284	56	2.39
SWZTE-8.1T	light, zoned tip	15.7 ± 0.4	11.6	788	9507	192	468	50	2.44
SWZTE-9.1C	dark unzoned core	17 ± 0.3	5.9	726	15037	850	1081	32	1.27
SWZTE-9.3T2	med-dark, zoned		5.2	715	11609	196	269	41	1.37
SWZTE-9.2T	light zoned tip	15.6 ± 0.7	11.1	783	9084	66	104	53	1.58
SWZTE-10.1C	med-dark, unzoned core		7.2	743	10669	108	188	45	1.74
SWZTE-10.3T2	med-dark, zoned		5.1	713	11402	277	273	42	0.99
SWZTE-10.2T	light, zoned tip		7.3	744	10462	61	63	46	1.03
	sample average		12.3	783	9853	179	311	50	1.85
	core average		12.3	778	10123	277	476	49	2.16
	rim/tip average		12.8	792	9668	107	198	50	1.76

Uranium, Th, and Hf concentrations in the analyzed zircons vary directly with one another, but U and Th vary by much larger factors (Figure 10). SWZ zircons have an average U concentration of 179 ppm, ranging from 41 ppm to 925 ppm, with cores averaging 277 ppm and rims averaging 107 ppm. LGZ averages much higher U, at 859 ppm, ranging from 29 to 2268 ppm (a single outlier has U = 4823 ppm), with an average of 601 ppm in the cores and 1621 ppm in the rims. The cores of SWZ have distinctly higher U than cores of LGZ, and LGZ has distinctly higher U in rims than SWZ. The two samples overlap in Hf, U, and Th but only a few LGZ analyses plot at the low values characteristic of SWZ, and the maxima for LGZ are considerably higher than those for SWZ. U concentrations vary only slightly between 8000 and 13000 ppm Hf, and then rise rapidly for higher Hf. Almost all Th/U ratios are between about 1 and 3 and average near 2 for both samples (Figure 10e).

Titanium concentrations in the zircons, indicative of melt temperature, vary directly with Zr/Hf and inversely with Hf, U, and Th concentrations. Ti in the zircons vary by a factor of 10, from 3.2 ppm to 32.3 ppm, indicating a temperature range of ~200°C based on the thermometry equation of Watson and Harrison (2005). Adjusting the equation for $a_{TiO2} \sim 0.7$, as discussed in the Methods section, the calculated T (referred to here as T_{TiZ}) range becomes 678°C to 896°C. SWZ Ti concentrations range from 5.1 ppm to 32.3 ppm, yielding T_{TiZ} from 713°C to 896°C, with an average of 12.3 ppm (average of calculated temperatures = 783°C). Cores and rims of grains in SWZ have nearly identical average Ti concentrations of 12.3 ppm (mean core T_{TiZ} = 791°C) and 12.8 ppm (mean T_{TiZ} 792°C), respectively. Titanium concentrations in zircons from LGZ range from 3.2 ppm to 24.6 ppm, with an average of 9.1 ppm, yielding adjusted T_{TiZ}

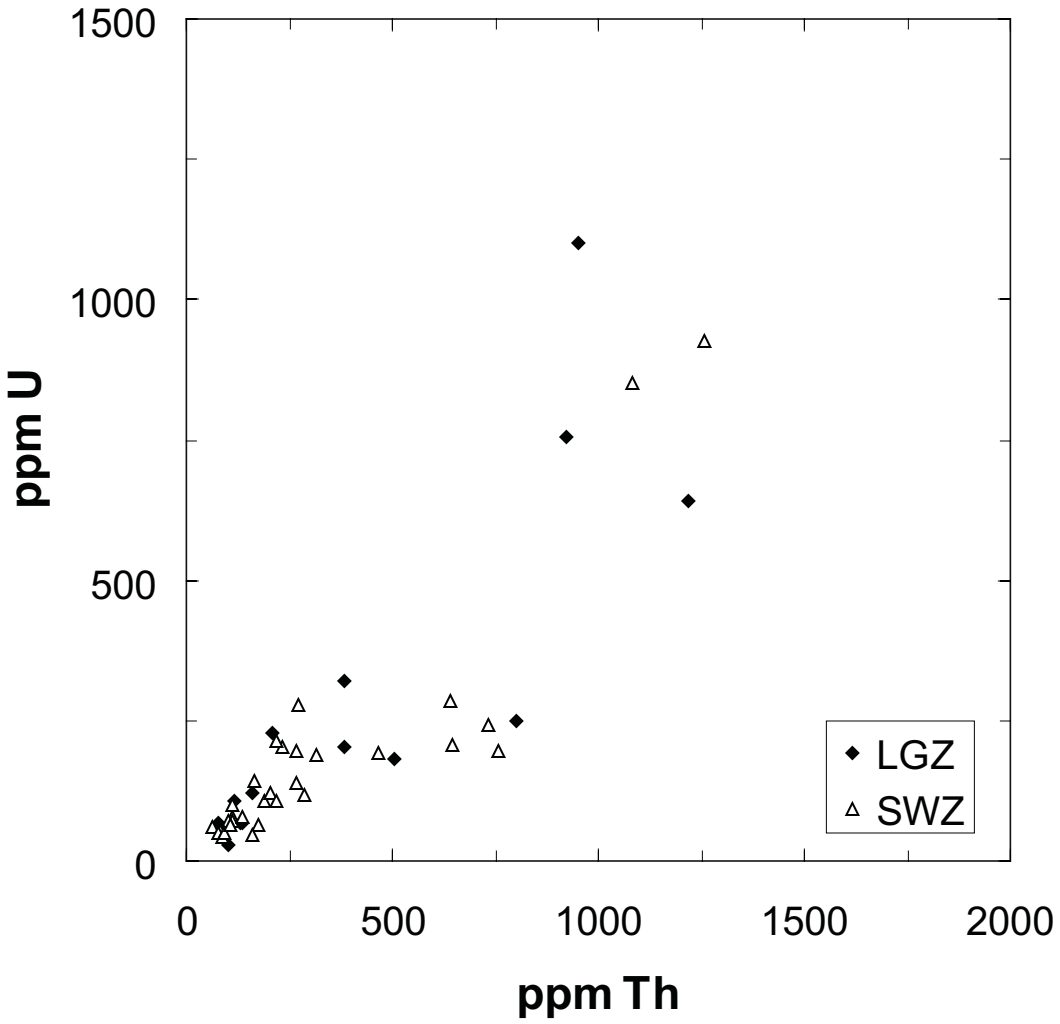

Figure 10e: U vs. Th in zircons from the Spirit Mountain batholith. LGZ represents fractionated leucogranite, and SWZ represents cumulates. Each point represents one SHRIMP spot analysis of a zircon grain.

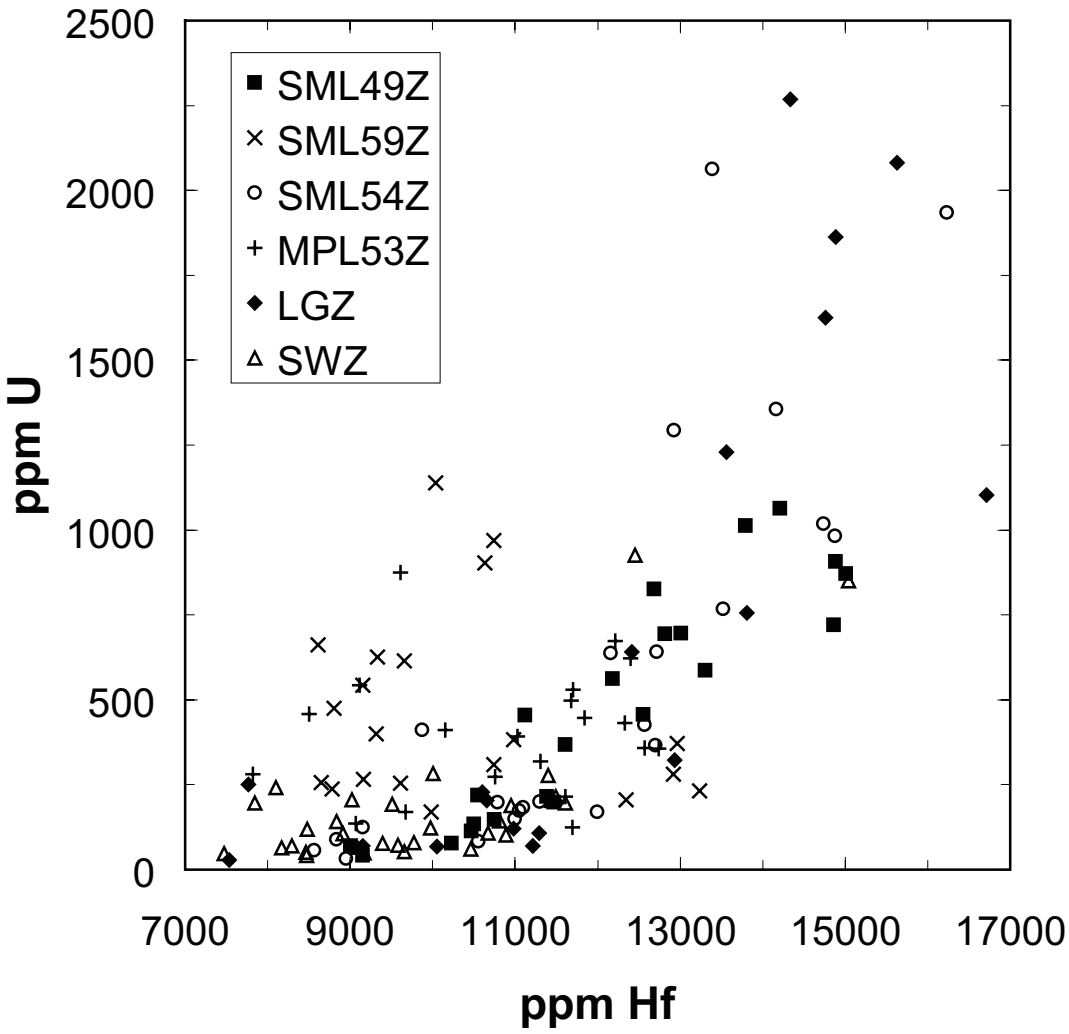

Figure 10d: U vs. Hf in zircons from six samples from the Spirit Mountain batholith. LGZ and SML49Z represent fractionated leucogranites, SWZ and SML54Z represent cumulates, SML59Z represents the older roof unit, and MPL53Z is from the Mirage Granite (see Walker et al., in press). Each point represents one SHRIMP spot analysis of a zircon grain.

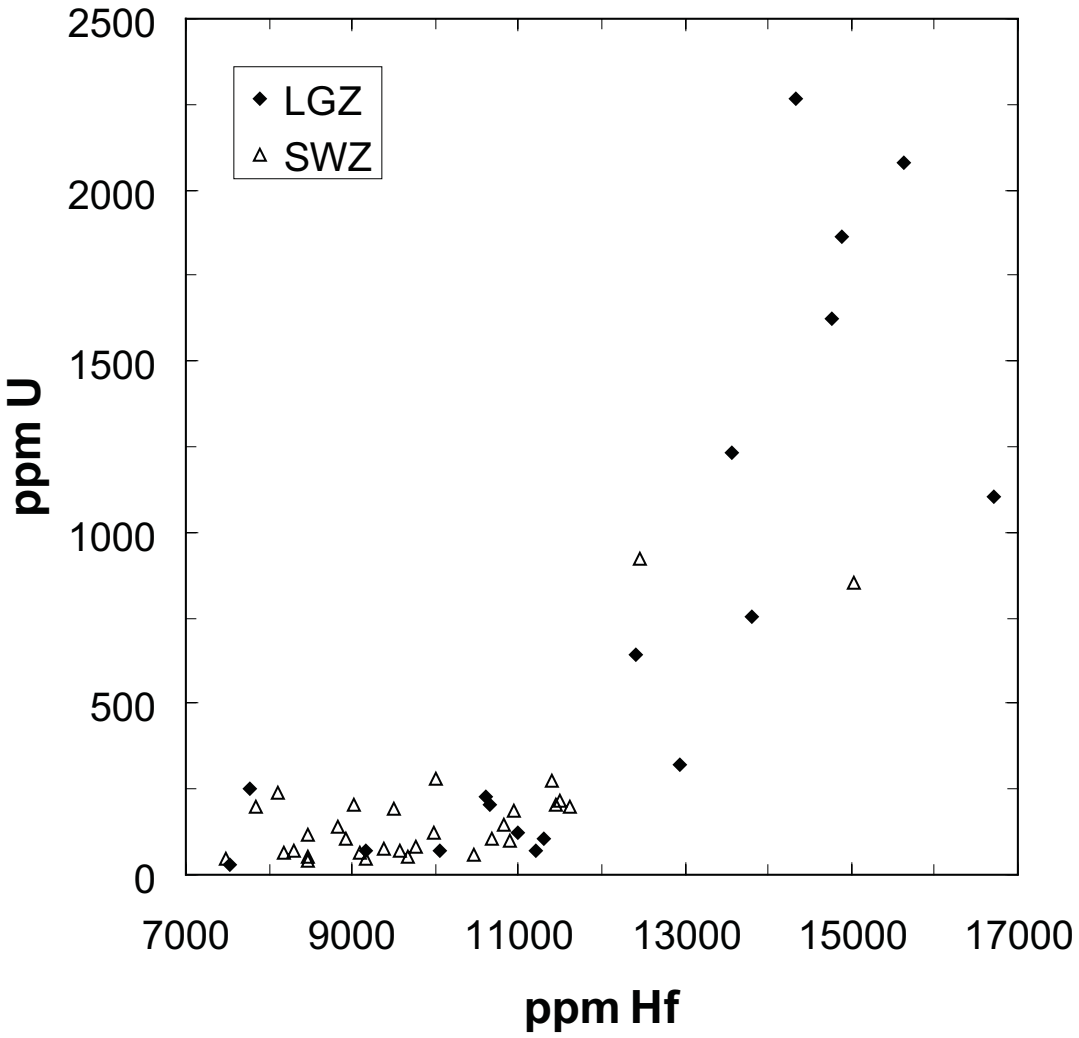

Figure 10c: U vs. Hf in zirconsfrom the Spirit Mountain batholith. LGZ represents fractionated leucogranite, and SWZ represents cumulates. Each point represents one SHRIMP spot analysis of a zircon grain.

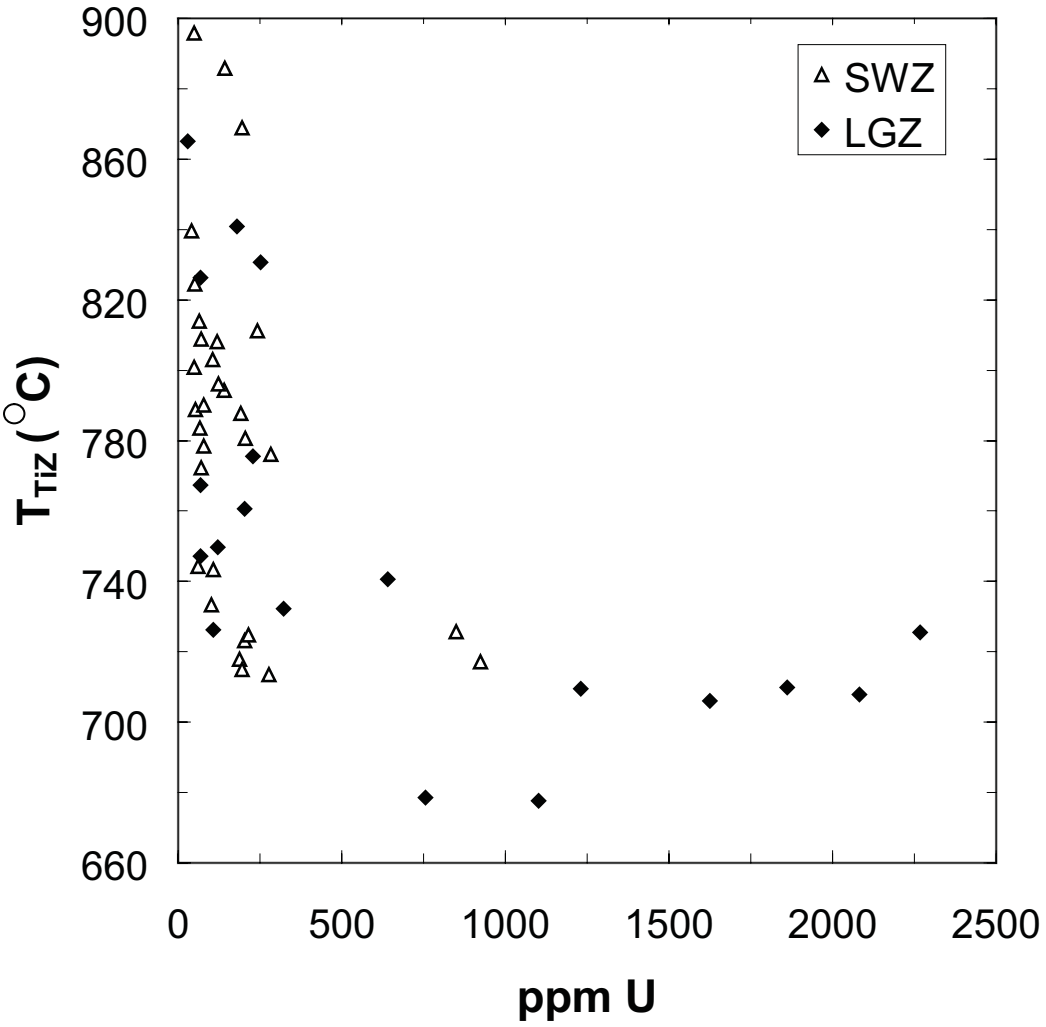

Figure 10b: Temperature estimates based on Ti concentrations vs. U in zircons from the Spirit Mountain batholith. LGZ represents fractionated leucogranite, and SWZ represents cumulates. Each point represents one SHRIMP spot analysis of a zircon grain.

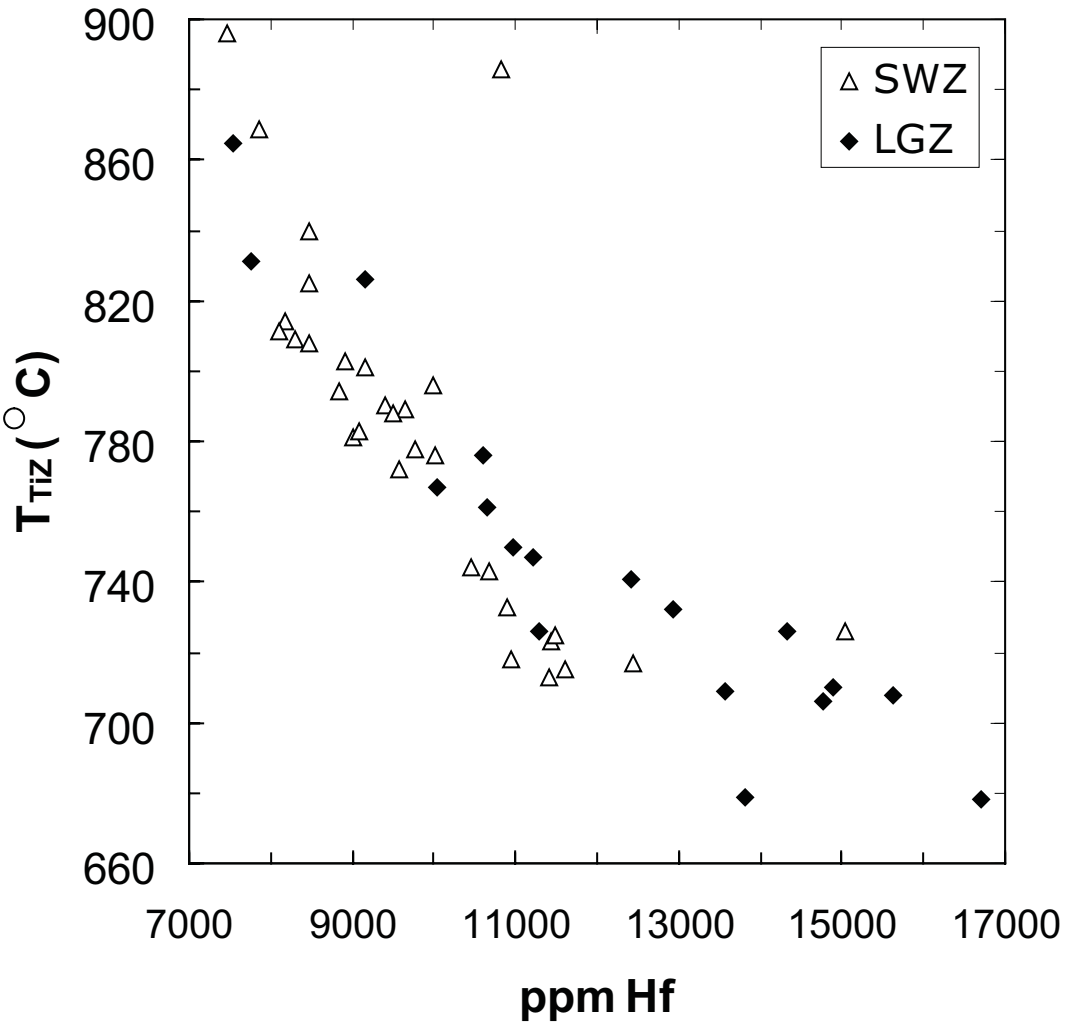

Figure 10a: Temperature estimates based on Ti concentrations vs. Hf in zircons from the Spirit Mountain batholith. LGZ represents fractionated leucogranite, and SWZ represents cumulates. Each point represents one SHRIMP spot analysis of a zircon grain.

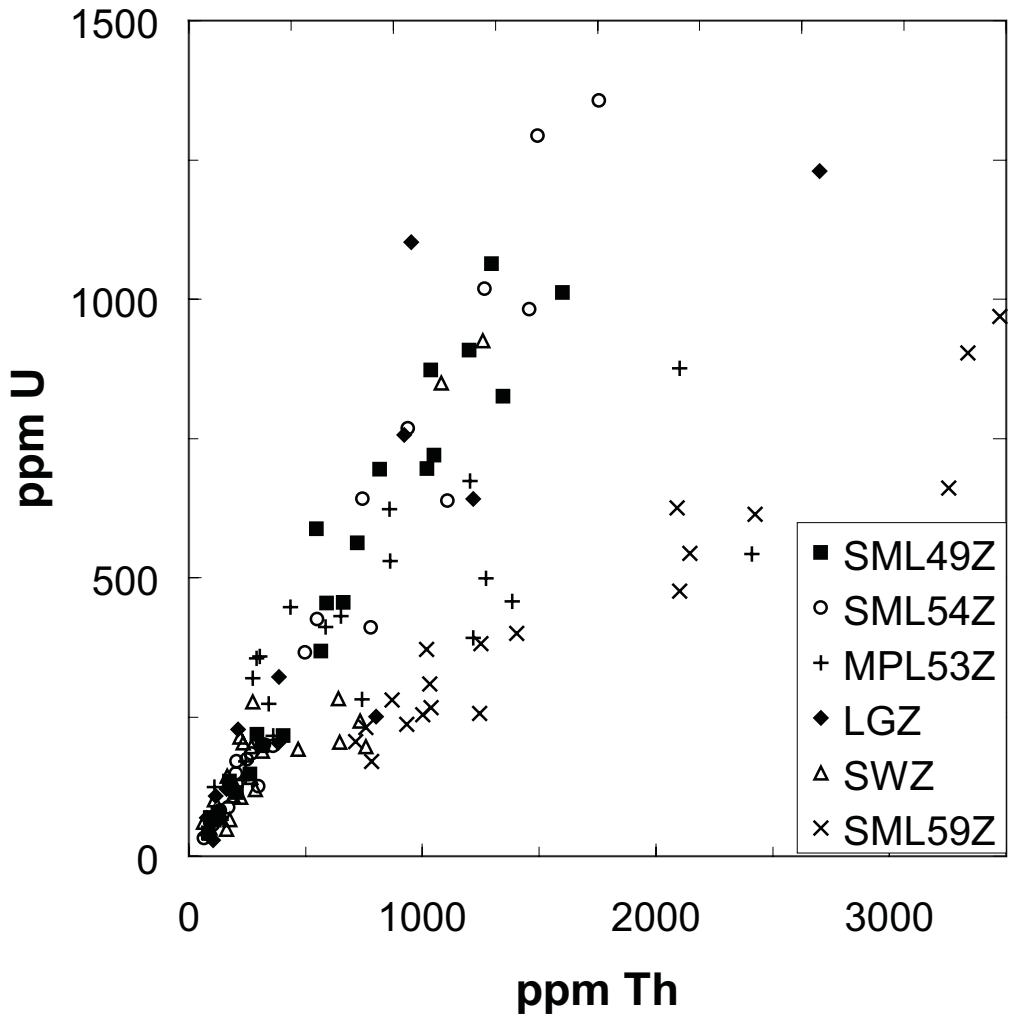

Figure 10f: U vs. Th in zircons from six samples from the Spirit Mountain batholith. LGZ and SML49Z represent fractionated leucogranites, SWZ and SML54Z represent cumulates, SML59Z represents the older roof unit, and MPL53Z is from the Mirage Granite (see Walker et al., in press). Each point represents one SHRIMP spot analysis of a zircon grain.

ranging from 678°C to 865°C and an average T_{TiZ} of 754°C. Cores and rims of grains in LGZ vary distinctly with average Ti concentrations of 11.2 ppm (mean T_{TiZ} 766°C) and 6.7 ppm (mean T_{TiZ} 734°C), respectively.

Variation in elemental concentrations correlates with variation in brightness of zones visible in CL images - bright zones are rich in Ti and poor in Hf, U, and Th, and vice versa (Figure 9). Although we do not suggest that Ti is the CL activator, the correlation is notably consistent. For this discussion, Hf, U, and T_{TiZ} will be used to track trends and fluctuations recorded in grains; Th trends correspond closely to U trends. In SWZ, three analyzed grains show "normal" zoning, with continuous increase in Hf and U and a corresponding decrease in Ti (T_{TiZ}) from core to rim (Figure 11b). Core to rim transects on six other grains demonstrate normal zoning followed by reverse zoning at the rim (decrease in Hf and U and corresponding increase T_{TiZ}), as shown in Figure 11a. Three grains contain a zone of oscillatory bands that deviates from the trend in the zones around it. For example, grain SWZTE-4 (Figure 11a) has a thin, dark, oscillatory zone of bands that has much higher Hf and U concentrations and much lower Ti (and T_{TiZ}) than the points on either side of it. Conversely, grain SWZTE-7 (Figure 11c) has a zone of oscillatory bands with higher T_{TiZ} and lower Hf than the zones around it.

In LGZ, core to rim transects demonstrate the variability of zircon histories. Two grains show normal zoning, with Hf, U, and Th increasing and T_{TiZ} decreasing continuously from core to rim. Three grains show reverse zoning at the rim, LGZTE-3 for example (Figure 11e). Two grains, including LGZTE-1 (Figure 11d), exhibit fluctuations (intervening zones that deviate from the monotonic core to rim progression). Most of the grains in LGZ have relatively high Hf and low T_{TiZ} throughout, but two

(e) LGZTE-3

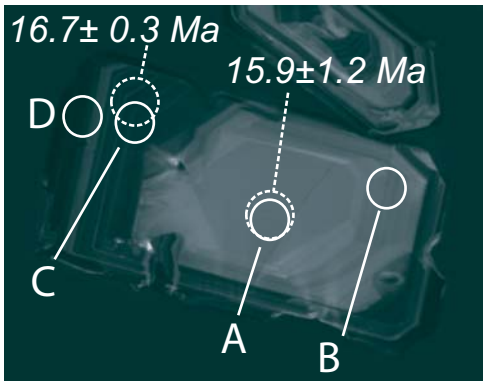

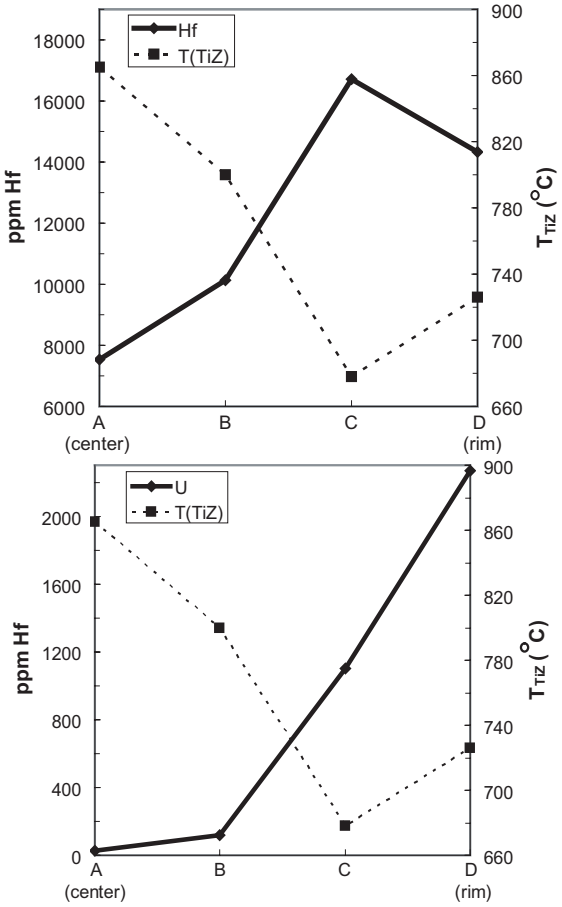

Figure 11e: CL image of zoned zircon LGZTE-3 from the Spirit Mountain batholith showing locations of SHRIMP-RG trace element analyses (solidcircles) and U-Pb analyses (dashed circles). Graphs represent Hf and T(TiZ)for each spot and U and T(TiZ) for each spot. Note the correlation between Hf and U and the inverse relationship between Hf/U and temperature. Graphs represent spot analyses, and lines between spots represent trends determined by spots, not true profiles across the grain. Grain has an antecrystic, unfractionated core, but fractionates outward, with a recharge or reheating event recorded by the rim.

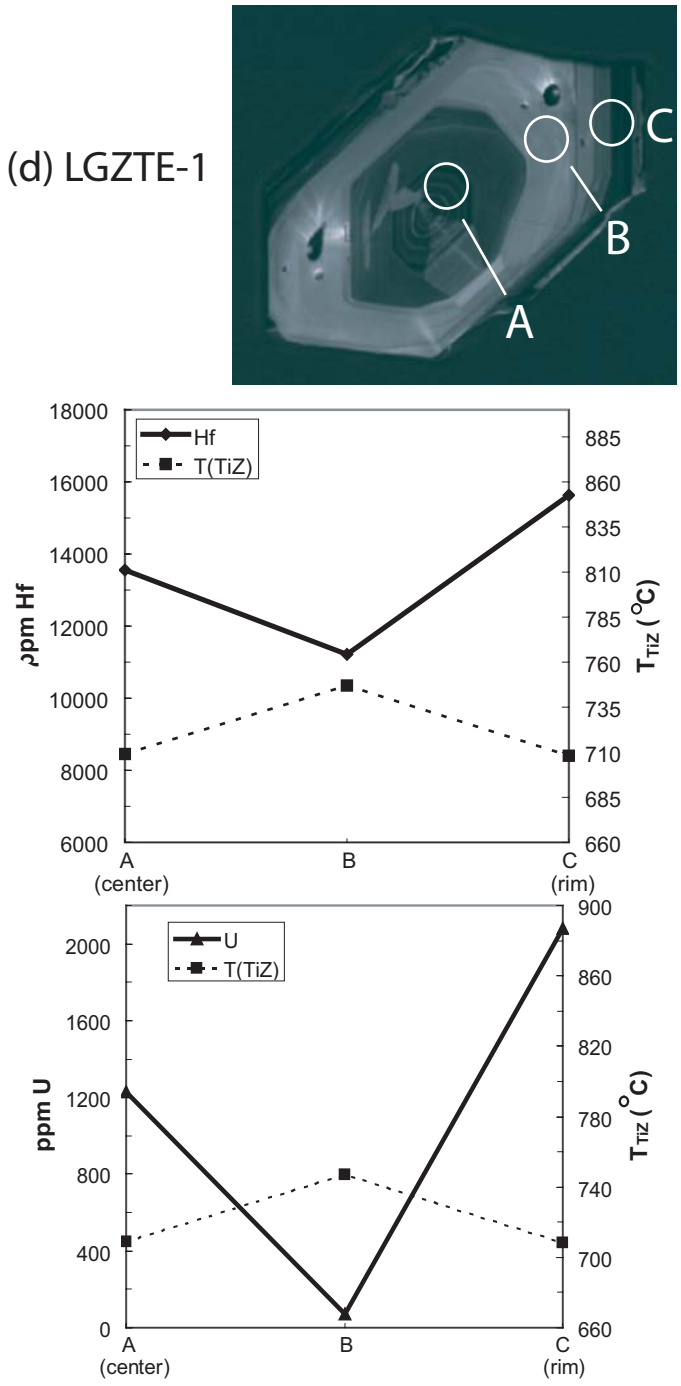

Figure 11d: CL image of zoned zircon LGZTE-1 from the Spirit Mountain batholith showing locations of SHRIMP-RG trace element analyses (solidcircles) and U-Pb analyses (dashed circles). Graphs represent Hf and T(TiZ)for each spot and U and T(TiZ) for each spot. Note the correlation between Hf and U and the inverse relationship between Hf/U and temperature. Graphs represent spot analyses, and lines between spots represent trends determined by spots, not true profiles across the grain. Grain is highly fractionated throughout, but shows a recharge event followed by continued fractionation.

(c) SWZTE-7

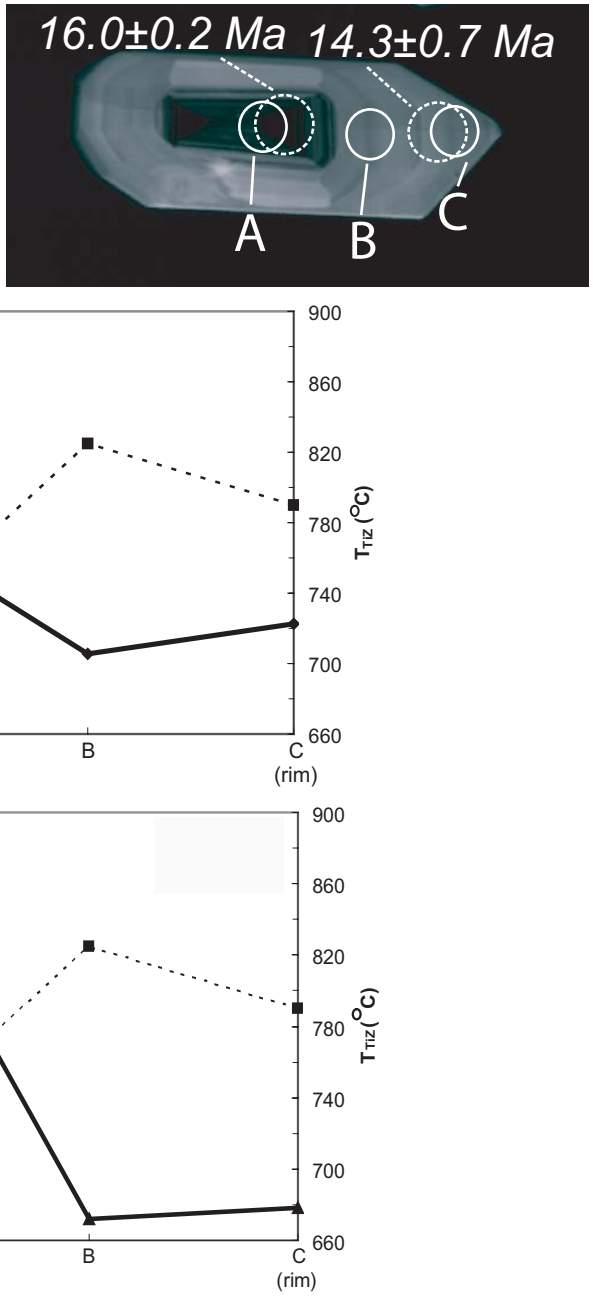

Figure 11c: CL image of zoned zircon SWZTE-7 from the Spirit Mountain batholith showing locations of SHRIMP-RG trace element analyses (solidcircles) and U-Pb analyses (dashed circles). Graphs represent Hf and T(TiZ)for each spot and U and T(TiZ) for each spot. Note the correlation between Hf and U and the inverse relationship between Hf/U and temperature. Graphs represent spot analyses, and lines between spots represent trends determined by spots, not true profiles across the grain. Zone of medium-dark oscillatory-bands represents a recharge/reheating event, followed by continued fractionation.

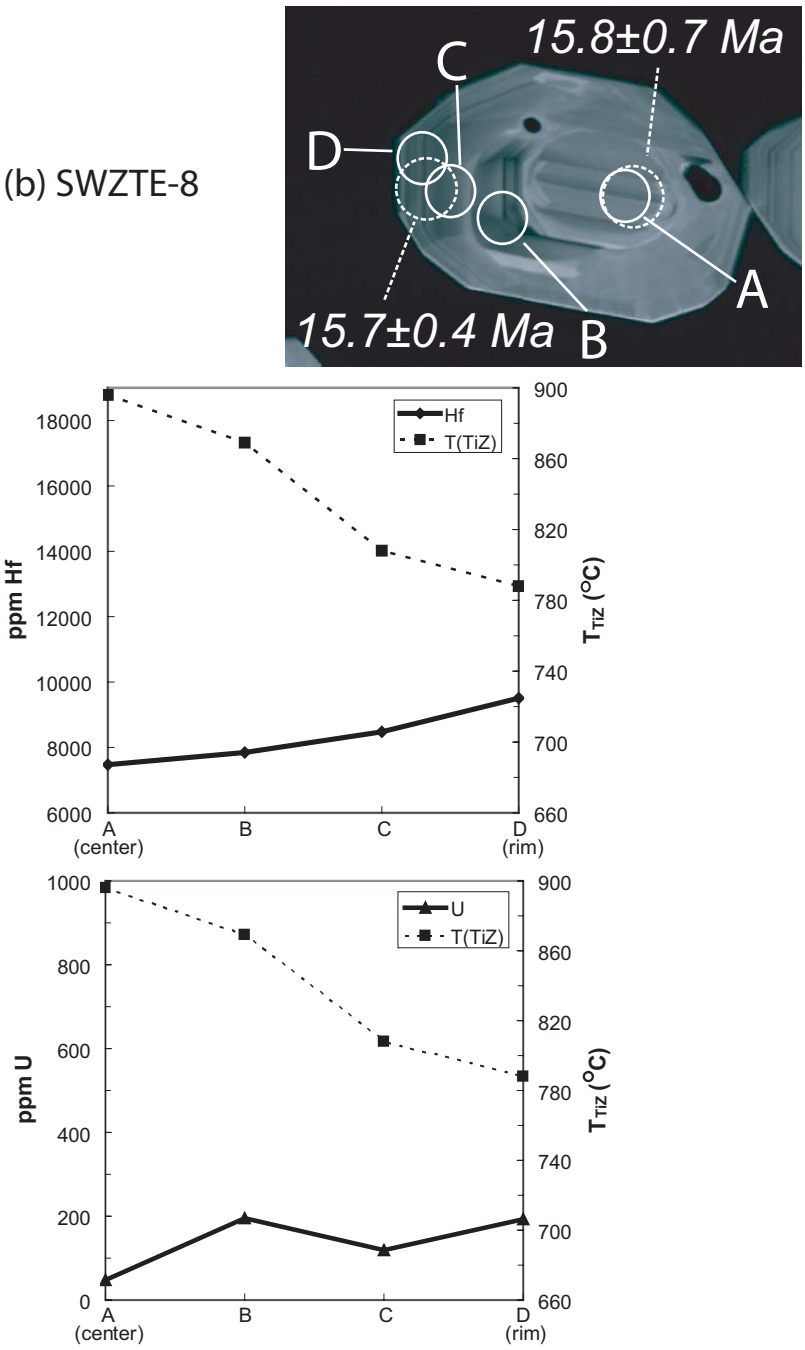

Figure 11b: CL image of zoned zircon SWZTE-8 from the Spirit Mountain batholith showing locations of SHRIMP-RG trace element analyses (solidcircles) and U-Pb analyses (dashed circles). Graphs represent Hf and T(TiZ)for each spot and U and T(TiZ) for each spot. Note the correlation between Hf and U and the inverse relationship between Hf/U and temperature. Graphs represent spot analyses, and lines between spots represent trends determined by spots, not true profiles across the grain. Note low Hf and U and high T throughout, indicating an unfractionated melt, although core to rim shows continual fractionation and cooling.

(a) SWZTE-4

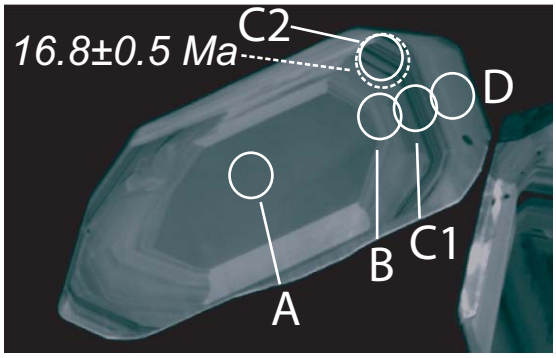

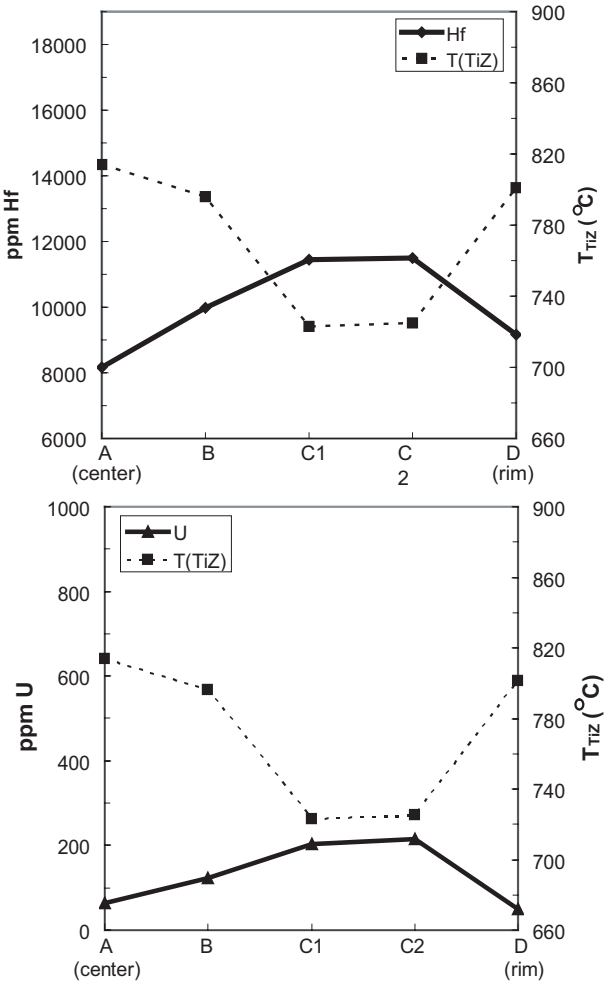

Figure 11a: CL image of zoned zircon SWZTE-4 from the Spirit Mountain batholith showing locations of SHRIMP-RG trace element analyses (solidcircles) and U-Pb analyses (dashed circles). Graphs represent Hf and T(TiZ)for each spot and U and T(TiZ) for each spot. Note the correlation between Hf and U and the inverse relationship between Hf/U and temperature. Graphs represent spot analyses, and lines between spots represent trends determined by spots, not true profiles across the grain. Note zone identified by points C1 and C2 that has high Hf and low T relative to surrounding zones, indicating a fractionation event. The rim suggests recharge or reheating.

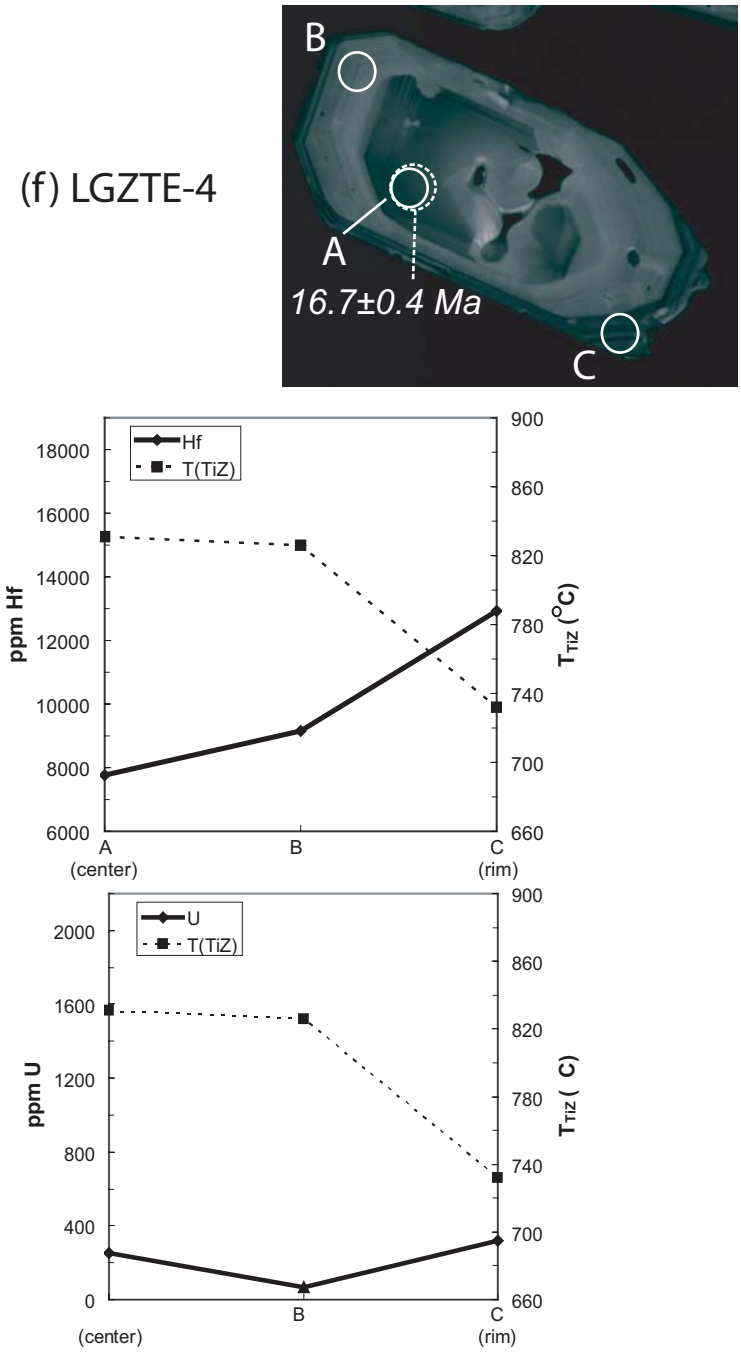

Figure 11f: CL image of zoned zircon LGZTE-4 from the Spirit Mountain batholith showing locations of SHRIMP-RG trace element analyses (solidcircles) and U-Pb analyses (dashed circles). Graphs represent Hf and T(TiZ)for each spot and U and T(TiZ) for each spot. Note the correlation between Hf and U and the inverse relationship between Hf/U and temperature. Graphs represent spot analyses, and lines between spots represent trends determined by spots, not true profiles across the grain. Grain has antecrystic, unfractionated core, but continuous fractionation from the center to the rim, and reaches relatively low temperature and high Hf.

grains (LGZTE-3 and LGZTE-4) have cores with unusually high Ti and low Hf. Most grains in LGZ have a very dark, fairly thick rim, that is absent in images of grains from SWZ. Where analyzed, this rim has extremely high Hf and U and very low T_{TiZ}, and may represent an important final episode in the zircon growth.

Plots of T_{TiZ} against both Hf and U for all zircon analyses from SWZ and LGZ (Figure 10a and b) demonstrate the positive correlations among Hf, U, and Th, and the negative correlation of these elemental concentrations with T_{TiZ}. Uranium rises slowly as T_{TiZ} drops until T_{TiZ} falls to approximately 700°C, then it increases sharply. Hafnium shows a similar but much less extreme inflection at ~700°C.

Zircons from four other samples from the SMB were analyzed for Hf, Th and U (but not Ti) during U-Pb analysis. SML49Z (16.1 ± 0.2 Ma) and SML54Z (16.8 ± 0.2 Ma) are, like SWZ and LGZ, from the main Spirit Mountain granite unit (respectively, a leucogranite similar to LGZ and a granite from just beneath the leucogranite zone, interpreted as formed in part by cumulate processes); SML59Z (17.4 ± 0.2 Ma) is from the older roof unit; and MPL53Z (15.9 ± 0.2 Ma) is Mirage granite (Walker et al.,in press). The four samples from the Spirit Mountain granite (SML49Z, SML54Z, LGZ, SWZ) cluster within very well-defined trends in plots of in Hf, Th, and U against one another (Figure 11d, f). Zircons from the two samples from other units (SML59z and MPL53z) are broadly similar but have generally higher U with low Hf and extremely higher Th with low U than the Spirit Mountain granite samples.

CHAPTER VI

DISCUSSION

Implications of Leucogranite Petrology and Zircon Zonation for Melt Fractionation and Crystal-melt Redistribution in Spirit Mountain Batholith

The leucogranites that form the roof zone of Spirit Mountain batholith are the plutonic equivalent of a high-silica rhyolite (cf. Bachmann and Bergantz 2004). Field relations and age data suggest that they amassed over much of the lifetime of the batholith, as various pulses of magma were injected, differentiated, and the buoyant, fractionated melt migrated upward, leaving cumulate granitoids behind. The sharp drop in leucogranite Zr/Hf ratios at approximately 76 wt% SiO_2 supports this interpretation, indicating that they evolved through appreciable fractional crystallization and segregation from a crystal assemblage rich in zircon.

While the whole-rock geochemistry of the Spirit Mountain batholith, notably Zr/Hf as well as compatible dispersed elements such as Sr, Ba, and middle REE, indicates that extensive fractionation occurred, the zircons reveal details of a more complex history. Generally, zircons from the cumulate sample, SWZ, record significantly higher T_{TiZ} and Zr/Hf and lower Hf, U, and Th concentrations than the fractionated sample, LGZ, as would be expected for a cumulate relative to its fractionated and segregated melt. Fluctuating zonation and reverse zoning, however, reveal a much more complex history than a simple cumulate-melt relation. Fairly common increases in T_{TiZ} toward the exterior of crystals documents reheating, probably a consequence of

recharging, and imply resorption of zircon. These increases in T_{TiZ} are invariably accompanied by decreases in Hf, U, and Th, indicating entrainment of the zircon in less fractionated melt. Zircons from both SWZ and LGZ record multiple examples of such events, as well as periods of monotonic cooling and fractionation. Grains from SWZ, in particular, record multiple reheating or recharge events throughout their history.

Most zones in most grains in leucogranite LGZ are rich in Hf, U, and Th, indicating that they grew largely or entirely from a fractionated, low Zr/Hf melt. The relatively unfractionated and high T_{TiZ} cores of some grains probably represent initial growth in unfractionated, hot, high Zr/Hf melt prior to a fractionation event, with subsequent entrainment within the segregating melt during fractionation. Only the outer portions of these zircons represent growth in the local, post-fractionation melt. These antecrystic cores lead to zircons from LGZ recording a wider range of T_{TiZ} and Hf and U concentrations than those of SWZ and to considerable overlap in compositions (Figure 10).

As T_{TiZ} approaches 700°C, the rate of increase in concentrations of U and Th with decreasing T rises dramatically. This is also evident in plots of U (or Th) vs. Hf, which show a strong inflection at this T_{TiZ}. This may be a consequence of increased rate of crystallization for a given decrease in T as the system approaches eutectic-like conditions (U and Th are dispersed elements, whereas Hf is an essential structural constituent in zircon, perhaps explaining the difference in behavior as the solidus is approached). Alternatively, the partition coefficients for U and Th may change as T drops, water content increases (and reaches saturation), and melt structure changes, or unidentified kinetic effect effects may lead to extreme local build-up of U and incorporation into

CHAPTER VII

CONCLUSIONS

Data from numerous studies of moderate to high-SiO_2 volcanic and plutonic suites, including Spirit Mountain batholith, demonstrate the distinctiveness of low Zr/Hf as a fingerprint of extreme fractional crystallization and effective melt segregation. Specifically, this fingerprint demonstrates efficient segregation of zircon, which in turn implies removal of the accompanying crystal assemblage (further supported by other geochemical characteristics). It follows that the geochemical similarities between plutonic aplites and leucogranites and high-silica rhyolites denote similar origins, representing the intrusive and extrusive manifestations of the same magmatic processes. Furthermore, granitic batholiths may represent in large part the cumulate mushes from the extraction of these highly evolved magmas (cf. Bachmann and Bergantz, 2004). As suggested by the fluctuations in zonation in zircons from the Spirit Mountain batholith, the assembly of these magmatic systems may be protracted, with repeated fractionation and reheating (through recharge) events, in order to accumulate large volumes of high-silica magma.

Zoning in zircons from the SMB, especially in Hf and Ti but also in U, Th, and other elements, not only confirms complex histories as suggested above, it also uniquely permits quantitative assessment of the timing and rates of thermal and compositional evolution. Zonation in many minerals has been cited previously as evidence for complex histories (fractionation and recharge, reheating, mixing), and zircon has been used to

record multi-stage magmatic histories (e.g., Davidson and Tepley, 1997; Wallace and Bergantz, 2002; Vazquez and Reid, 2002; Cooper and Reid 2003; Miller et al., 2004; Vazquez and Reid, 2004). The advent of the Ti-in-zircon thermometer (Watson and Harrison, 2005) and the simplicity of using Hf content to track fractionation, however, promise a refined, common, and quantifiable record of such histories. Zircons from the granitic Adui batholith in the Ural Mountains, Russia, show inverse correlations between Hf and Ti similar to those in the SMB, along with systematic zonation from core (Zr/Hf average ~50) to rim (avg ~30, as low as 22)(Bea, unpub. data). We suggest that such patterns are likely to be typical in zircons from felsic systems. Dating zones in plutonic zircons can yield very useful constraints on the rates of the processes recorded in the zoning, though currently attainable precision (on the order of a few hundred thousand years) of in-situ U-Pb analysis of zircons that are millions of years old places some limitations on the sensitivity of the plutonic record. A combination of U-series dating with Hf and Ti analysis of zones in zircons from very young volcanic rocks may provide an unprecedented high-resolution record of the complex pre-eruptive processes that occur in subjacent magma chambers.

APPENDIX A:

Petrography of the

Spirit Mountain Batholith Leucogranites

Table A1: Petrography of the Spirit Mountain Batholith

sample	date collected	latitude (35°N)	longitude (114°W)	field location	handsample description	unit	other analyses
SML3	5/05	15.363	43.801	top of Grapevine Canyon (GVC)	med - crs gr, rounded qtz phenos, <1% biotite, weak fabric, rapikivi	LG	**-------**
SML4	5/05	15.363	43.801	top of GVC	same as SML 3, but slt. finer grained	LG	-------
SML5	5/05	15.218	43.578	top of GVC - aplite dike (N80E, 63°S)	very fg, <1% biotite, see some qtz phenos	LG (aplite?)	-------
SML13	5/05	15.715	46.677	W of pluton - above main roof	very pink granite, fspar and qtz phenos	Dylan Granite	-------
SML17	5/05	-------	-------	W of pluton in "granite host"	very pink granite, mostly kspar w/ a few qtz phenos	Dlyan Granite	-------
SML47	5/05	7.917	47.551	roof zone - s. of hwy	porphyry w/ qtz, bio, fspar	LG	GC
SML49z	5/05	8.181	47.214	roof zone - s. of hwy	mglg - 30% qtz, ~1% bio,	LG	GC, Z
SML50	5/05	8.043	47.073	roof zone - s. of hwy	aplite porphyry - qtz and kspar phenos, <1% bio, plage rim on kspar, plag encl bio	LG	-------
SML51	5/05	8.099	46.949	roof zone - s. of hwy	aplite w/ a few qtz and bio phenos	-------	-------

Table A1: Petrography of the Spirit Mountain Batholith

sample	date collected	latitude (35ºN)	longitude (114ºW)	field location	handsample description	unit	other analyses
SML52	5/05	8.077	46.995	lower in roof zone - s. of hwy	crunchy LG - med to crse gr, 2-3% bio	LG	GC
SML54z	5/05	10.902	44.568	s. powerline rd - driving transect - uppermost crunchy granite	25% qtz, very pink kspars, ~5% bio	uppermost CG	GC, Z
SML57	5/05	15.27	46.392	on Radio Tower Road	very fg granite porphyry w/ sub-rounded qtz phenos	LG	-------
SML59z	5/05	15.355	46.612	W side of pluton, N of RT Road	MG/porphyry, pink granite, 3%mafic, 60%kspar, 30%plag, 7%qtz,	BD granite	GC, Z
SML61	5/05	15.764	46.558	porphyry LG E/W dike cutting Dylan	aplite porphyry	LG dike	-------
SML62a	5/05	15.775	46.921	furthest high point W of roof - porphyry cutting PC	porphyry - aplite groundmass w/ phenos of 1% bio, 5% fspar, 5% qtz	-------	-------
SML62b	5/05	15.775	46.921	furthest high point W of roof - porphyry cutting PC	porphyry - aplite groundmass w/ phenos of 1% bio, 5% fspar, 5% qtz	-------	-------
SML63a	5/05	15.538	44.798	above Christmas Tree Pass - aplite pod (S80E, 80ºN, 100m thick)	-------	LG	-------
SML63b	5/05	15.538	44.798	above Christmas Tree Pass - aplite pod (S80E, 80ºN, 100m thick)	gradation between aplite and CLG	LG	-------

Table A1: Petrography of the Spirit Mountain Batholith

sample	date collected	latitude (35°N)	longitude (114°W)	field location	handsample description	unit	other analyses
SML63c	5/05	15.538	44.798	above Christmas Tree Pass - aplite pod (S80E, 80ºN, 100m thick)	CLG	LG	GC
SML66	5/05	15.492	44.765	above Christmas Tree Pass - aplite porphyry mass in middle of aplite pod	aplite porphyry	LG	-------
SML67	5/05	15.498	44.773	above Christmas Tree Pass - aplite pod (S80E, 80ºN, 100m thick)	aplite	LG	GC
SML68	5/05	10.848	45.034	s. powerline rd - driving transect - east side of LG cap (just above 54Z) - tops ridge	very fine grained granite porphyry (not apl) - qtz phenos, <1% bio, <3% fspar phenos	LG	-------
SML69	5/05	10.775	45.134	s. powerline rd - driving transect - stratigraphically lowest unit along this transect	CLG/CG - ~20% qtz, kspars slightly pink, ~3% bio	LG/CG	GC
SML70	5/05	10.795	45.292	s. powerline rd - driving transect - moving W	MGLG - 20-25% qtz kspar barely pink, 2-3% bio	LG	-------
SML71	5/05	10.912	45.474	s. powerline rd - driving transect - moving W	MGLG - slt finer grained than SML70, 25-30% qtz, no pink, 2-3% bio	LG	GC
SML73	5/05	10.838	45.623	s. powerline rd - driving transect - moving W	MGLG - finer granied than SML71, 25% qtz, 2% bio, barely pink kspars	LG	GC
SML74	5/05	10.838	45.769	s. powerline rd - driving transect - moving W	MGLG - finer granied than SML71, 25% qtz, 2% bio, barely pink kspars	LG	GC

Table A1: Petrography of the Spirit Mountain Batholith

sample	date collected	latitude (35°N)	longitude (114°W)	field location	handsample description	unit	other analyses
SML75	5/05	10.905	45.883	s. powerline rd - driving transect - moving W	MGLG - finer granied than SML71, 25% qtz, 1-2% bio, barely pink kspars	LG	-------
SML76	5/05	10.954	46.027	s. powerline rd - driving transect - moving W	MGLG - no pink, some large qtz, 25% qtz, 1-2% bio	LG	GC
SML77	5/05	10.801	46.099	s. powerline rd - driving transect - moving W	MGLG	LG	-------
SML78	5/05	10.886	46.191	s. powerline rd - driving transect - moving W	MGLG - 30% qtz, 1% bio	LG	GC
SML80a	5/05	15.698	44.971	ridge west of Christmas tree pass - looks same as aplite above CTP	med to fine gr, qtz from GM size to euhedral 0.5cm phenos, pockets appear pegmatitic throughout, 2-3% bio in pegs, some graphic texture	LG	-------
SML80b	5/05	15.698	44.971	ridge west of Christmas tree pass - looks same as aplite above CTP	-------	LG	-------
SML81	5/05	15.659	45.007	ridge west of Christmas tree pass - looks same as aplite above CTP	aplite porphyry - qtz and fspar phenos, <1% bio	LG	-------
SML91	1/06	13.083	45.379	Juniper Mine	aplite/mglg contact gradational over ~1cm, graphic texture at contact?	LG - aplite/mglg contact	-------

Table A1: Petrography of the Spirit Mountain Batholith

sample	date collected	latitude (35°N)	longitude (114°W)	field location	handsample description	unit	other analyses
SML120Z	1/06	11.643	42.549	inside big white mass	MG-FGLG - qtz phenos, ~2% bio,	LG	GC, Z
SML129Z	1/06	12.553	44.63	lowermost LG (JM transect w/Calvin)	very white MGLG, 30% qtz, 1-2% bio, euh faspars	LG	GC, Z
SML130	1/06	-------	-------	JM transect w/Calvin - just above SML129Z	MGLG - no euh fspar, slt finer grained than 129Z, 1% bio	LG	GC
SML132	1/06	12.809	45.431	JM transect w/Calvin	MGLG - finer grained, not quite porphyritic, but qtz larger than fspars	fg/porphyr LG	GC
SML133	1/06	12.747	45.813	JM transect w/Calvin	coarser granite, slt more mafic, euhedral fspars, pinkish color	Dylan?	GC
SML151	1/06	10.775	45.134	driving transect - aplite sheet trends N/S dips moderately west	aplite porphyry w/qtz phenos and <1% bio	pod/sheet of fglg	-------
SML152	1/06	-------	-------	driving transect - next hill over - aplite sheet trends N/S dips moderately west	aplite porphyry w/qtz phenos and <1% bio	aplite	-------
SML171	1/06	15.034	46.158	W. Margin	med to fine gr porphyry w/ qtz and fspar phenos	Dylan?	-------
SML179	1/06	7.981	44.734	s. transect II	-------	dylan?	-------

Table A1: Petrography of the Spirit Mountain Batholith

sample	date collected	latitude (35°N)	longitude (114°W)	field location	handsample description	unit	other analyses
SML196	1/06	9.162	45.371	s.transect II - crossed from MGLG into CG/TLG into this	2-3% bio, pinkish	lowest LG?? BDG??	-------
SML207	1/06	8.175	47.254	roof zone - s. of hwy	crunchy granite!	cg - faulted?	-------
SML211	1/06	8.126	48.106	roof zone, s. of hwy - southwesternmost hill - past where we though batholith margin was	MGLG	outermost LG	-------
SML213	1/06	10.132	40.931	Haiko Springs	quartz monsonite	qtz monzonite	GC
MPL53z	38842	7.349	41.554	mirage granite	biotite granite	Mirage	GC, Z

Table A1: Petrography of the Spirit Mountain Batholith

sample	modal abundances (%)				accessory minerals	alteration minerals	groundmass				phenocrysts			
	kspar	quartz	plag	bio			%	minerals	size (mm)	shape	%	minerals	size (mm)	shape
SML3	40	35	23	1	1% opaques, zircon, muscovite, apatite, epidote	sericite	95	qtz kspar plag biotite	0.125 to 0.25	anhedral	5	mostly kspar qtz	<1.25	an-subhedral
SML4	30	35	34	1	muscovite, sphene, zircon	chlorite, sericite	80	qtz kspar plag biotite	0.125 to 0.5	anhedral	20	kspar plag qtz	<3.5	subhedral
SML5	35	35	30	<1	opaque (euhedral), sphene, zircon	-------	100	plag kspar qtz	0.125 to 1.25	anhedral	-------	-------	-------	-------
SML13	65	35	0	<1	apatite, zircon, sphene, opaques	-------	-------	-------	-------	-------	100	qtz kspar biotite	0.75 - 2.5 1.25 - 3.25 < .625	subhedral anhedral anhedral
SML17	65	30	0	<1	sphene, zircon, opaque, apatite	-------	60	qtz kspar plag	0.025 to 0.5	anhedral	40	qtz kspar biotite	<2.5 <3.75 0.5 - 1.25	anhedral
SML47	60	35	5	<1	sphene, zircon, opaque, apatite, chev/all, muscovite	sericite	30	kspar qtz plag biotite	0.125 to 0.75	anhedral	70	kspar qtz plag	<3.75 <5 <2.5	anhedral anhedral sub-euh laths
SML49z	40	35	25	<1	sphene, zircon, opaque, apatite, muscovite, epidote	sericite	-------	-------	-------	-------	100	kspar qtz plag biotite	<6.25 <3.75 0.125 - 1 0.5 - 2.5	anhedral anhedral subhedral subhedral
SML50	35	35	30	<1	sphene, euhedral opaques, apatite, zircon	sericite	60	qtz plag biotite	<0.5	anhedral	40	kspar qtz plag	<6.25 <2.5 <6.0	anhedral
SML51	35	35	30	<1	sphene, epidote, apatite	sericite	95	kspar qtz plag biotite	<0.375	anhedral	5	qtz biotite kspar	<1.25 1 - 1.75 <1	anhedral subhedral anhedral

Table A1: Petrography of the Spirit Mountain Batholith

sample	modal abundances (%)				accessory minerals	alteration minerals	groundmass				phenocrysts			
	kspar	quartz	plag	bio			%	minerals	size (mm)	shape	%	minerals	size (mm)	shape
SML52	40	35	25	<1	epidote, opaques, sphene, chev/all, large apatite	-------	-------	-------	-------	-------	100	kspar	<6.25	anhedral
												quartz	0.75 - 3.25	anhedral
												plagioclase	1.25 - 2	sub-euhedral
												biotite	0.5 - 2.5	sub-euhedral
SML54z	40	30	30	3	lots of euh sphene, opaque, apatite, zircon	sericite	-------	-------	-------	-------	100	qtz	0.5 - 3.75	anhedral
												kspar	0.75 - 4.25	anhedral
												plag	0.75 - 1.25	subhedral
												biotite	0.75 - 1.75	subhedral
SML57	35	35	30	<1	muscovite, isotropic (gar?), bio, opaque	-------	70	qtz	0.025 - 0.075	anhedral	30	qtz	0.75 - 2.5	subhedral
								plag				kspar	~2.5	subhedral
								kspar				plag	0.25 - 1.25	euh-subhedral
												muscovite	<1.25	subhedral
SML59z	60	30	10	<1	sphene, biotite, opaque, apatite, chev/all	sericite, chlorite	40	qtz	0.125 to 0.75	anhedral	60	kspar	1.25 - 2.5	sub-anhedral
								kspar				plag	1.25	sub-anhedral
								plag						
SML61	70	25	5	<1	bio, sphene, opaques	sericite, chlorite	70	qtz	0.125 to 0.25	anhedral	30	kspar	1.25 - 3.75	anhedral
								kspar				qtz	1.25 - 2.5	rounded
								plag						
SML62a	65	35	0	0	opaques, sphene, apatite	sericite	95	qtz	<1.25	anhedral	5	kspar	2	euhedral
								kspar	<1.25	anhedral		qtz	1.75	euh or rounded
								myrmekite	0.25 - 0.75	subhedral				
SML62b	65	35	0	0	opaques, sphene, apatite	sericite	100	qtz	0.025 - 1	anhedral	-------	-------	-------	-------
								kspar	0.025 - 1.75	anhedral				
								myrmekite	0.25 - 1.25	anhedral				
SML63a	45	35	20	<1	opaques, apt, zirc, sphene, euhedral all/chev	chlorite	100	kspar	0.125 - 1	anhedral	-------	-------	-------	-------
								qtz	0.125 - 1	anhedral				
								plag	0.125 - 0.25	subhedral				
SML63b	45	35	20	<1	opaque, sphene, apt, zircon	chlorite	100	kspar	0.25 - 1.75	anhedral	-------	-------	-------	-------
								qtz	0.25 - 2.5	anhedral				
								plag	0.25 - 1.25	subhedral				
								biotite	<1.25	subhedral				

Table A1: Petrography of the Spirit Mountain Batholith

sample	modal abundances (%)				accessory minerals	alteration minerals	groundmass				phenocrysts			
	kspar	quartz	plag	bio			%	minerals	size (mm)	shape	%	minerals	size (mm)	shape
SML63c	60	35	5	1	sphene, opaques, apt, zirc, monazite?	-------	100	kspar	1 - 3.75	anhedral	-------	-------	-------	-------
								verm. Qtz	2.5 - 3.75	graph, subhed				
								plag	0.25 - 0.75	anhedral				
								biotite	<0.5	subhedral				
SML66	45	35	20	<1	opaque, apt, epidote, sphene	sericite	70	kspar	<0.5	anhedral	30	kspar	1.25 - 5	sub-euhedral
								qtz		graph & anhed		qtz	1.25 - 6.25	sub-euhedral
								plag		subhedral		plag	1.25 - 5	sub-euhedral
												biotite	0.25 - 1.25	sub-euhedral
SML67	65	35	0	<1	opaque (mass and needles), bio, sphene, apt	-------	90	qtz	<0.5	graphic	10	qtz	-------	aggregates of anhedral med gr
								kspar	<0.5					
								biotite	<.125	blades				
SML68	39	25	35	1	opaque, sphene, apt	-------	-----	-----	-----	-----	100	kspar	0.5 - 1.25	an-subhedral
												plag		sub-euhedral
												qtz		an-subhedral
SML69	34	30	35	1	opaque, musc, zircon	chlorite, sericite	-------	-------	-------	-------	100	plag	1.25 - 3.75	euhedral
												kspar	1.25 - 5	anhedral
												qtz	1.25 - 5	subhedral
												biotite	1.25	euhedral
SML70	35	30	35	0	muscovite, opaques, zirc, all/chev	chlorite, veins	-----	-----	-----	-----	100	plag	1.25 - 3.75	euhedral
												kspar	1.25 - 5	anhedral
												qtz	1.25 - 5	subhedral
SML71	34	30	35	1	sphene, opaque, musc, zircon, all/chev	chlorite, sericite	-------	-------	-------	-------	100	kspar	1.25 - 6.25	subhedral
												plag	<2.5	sub-euhedral
												qtz	<2.5	anhedral
												biotite	<2.5	sub-euhedral
SML73	34	30	35	1	opaque, sphene, muscovite, garnet, zircon	chlorite, sericite	10	kspar	0.25 - 1.25	anhedral	90	kspar	<3.75	an-subhedral
								plag		subhedral		plag	<2.5	sub-euhedral
								qtz		anhedral		qtz	<3.75	an-subhedral
								biotite		an-subhedral		biotite	<1.75	subhedral
SML74	39	30	30	1	sphene muscovite, opaques, zircon, epidote	sericite	20	plag	0.25 to 0.75	subhedral	80	kspar	~2.5	an-subhedral
								qtz				plag		
								biotite				qtz		

Table A1: Petrography of the Spirit Mountain Batholith

sample	modal abundances (%)				accessory minerals	alteration minerals	groundmass				phenocrysts			
	kspar	quartz	plag	bio			%	minerals	size (mm)	shape	%	minerals	size (mm)	shape
SML75	39	30	30	1	epidote, opaque, muscovite, zircon, fluorite	sericite, chlorite	30	plag qtz biotite	~0.75	sub-euhedral	70	kspar qtz plag	2.5 - 5	subhedral
SML76	40	35	25	<1	opaques, muscovite, fluorite, chev/all	sericite	30	plag qtz kspar biotite	0.25 - 1.25	subhedral anhedral anhedral subhedral	70	qtz kspar	2.5 - 5 ~2.5	an-subhedral subhedral
SML77	40	35	25	<1	opaques, muscovite, fluorite, apt, biotite	sericite, chlorite	50	plag qtz kspar biotite	0.25 - 1.25	subhedral anhedral anhedral subhedral	50	kspar qtz	2.5 - 6.25 2.5 - 5	an-subhedral subhedral
SML78	40	35	25	<1	opaques, muscovite, fluorite, apt, biotite	sericite, chlorite	50	plag qtz kspar biotite	0.25 - 1.25	subhedral anhedral anhedral subhedral	50	kspar qtz	2.5 - 6.25 2.5 - 5	an-subhedral subhedral
SML80a	55	35	10	<1	sphene, biotite, opaques, biotite	sericite	80	qtz kspar plag	0.125 - 0.5	anhedral anhedral an-subhedral	20	kspar qtz	2.5 - 5 1.25 - 3.75	subhedral subhedral
SML80b	40	30	25	<1	opaques, apatite, [small, low BR, hi relief euh greenish - amphibole??]	-------	-------	-------	-------	-------	100	kspar plag qtz	<2.5 <1.25 <1.25	anhedral anhedral graphic (mostly)
SML81	45	35	20	<1	opaques, fluorite, biotite, zircon	sericite	80	qtz kspar plag biotite	<1.25	anhedral	20	qtz kspar plag biotite	0.5 & 3.25 0.5 - 1 0.5 - 1 ~1.25	an & euhedral subhedral subhedral subhedral
SML91	40	30	30	<1	opaques, sphene, zircon, muscovite	-------	80	qtz kspar plag	0.125 - 0.5	anhedral	20	kspar qtz plag	<5 ~1.25 ~1.25	euhedral euhedral euhedral

Table A1: Petrography of the Spirit Mountain Batholith

sample	modal abundances (%)				accessory minerals	alteration minerals	groundmass				phenocrysts			
	kspar	quartz	plag	bio			%	minerals	size (mm)	shape	%	minerals	size (mm)	shape
SML120Z	47	30	20	3	sphene, musc, chevkinite, opaques	sericite	60	qtz	0.5 - 1.25	anhedral	40	qtz	1.25 - 2.5	euhedral
								plag		subhedral		kspar		subhedral
								kspar		anhedral		plag		subhedral
SML129Z	39	30	30	1	opaque, fluorite, epidote, zircon	sericite	-------	-------	-------	-------	100	qtz	0.5 - 5	anhedral
												kspar	0.5 - 3.75	subhedral
												plag	0.5 - 1.25	sub-euhedral
SML130	50	30	20	<1	fluorite, muscovite, biotite, opaque, zircon, apt	chlorite, sericite	-------	-------	-------	-------	100	kspar	0.75 - 5	subhedral
												qtz	.125 - 3	anhedral
												plag	0.5 - 2.25	anhedral
SML132	50	30	20	<1	sphene, muscovite, [fiberous, brownish, hi BR, hi R mineral?]	sericite	-------	-------	-------	-------	100	kspar	0.25 - 5	anhedral
												qtz	0.25 - 3.75	anhedral
												plag	0.25 - 2	subhedral
												biotite	1	subhedral
SML133	50	28	20	2	sphene, opaques, musc, apt, epidote, fluorite	sericite	-------	-------	-------	-------	100	kspar	0.75 - 7.5	anhedral
												qtz	0.25 - 5	anhedral
												plag	0.5 - 3.75	subhedral
												biotite	<1.25	subhedral
SML151	49	35	15	1	sphene, musc, opaques, fluorite, apt, epidote	sericite	60	kspar	~0.5	anhedral	40	kspar	1.25 - 5	subhedral
								qtz		anhedral		qtz	1.25 - 3.75	subhedral
								plag		subhedral		plag	1.25 - 2.5	sub-euhedral
												biotite	<1.25	subhedral
SML152	50	35	15	<1	biotite, opaques, muscovite	sericite	100	kspar	0.125 - 1.25	anhedral	-------	-------	-------	-------
								qtz	0.125 - 1.25	anhedral				
								plag	0.125 - 0.75	anhedral				
SML171	50	35	15	<1	biotite, opaque, sphene, epidote	sericite	80	qtz	0.5 - 1	anhedral	20	kspar	1.25 - 3.75	euhedral
								plag				qtz	1.25 - 2.5	euhedral
								kspar				plag	<1.25	euhedral
SML179	45	30	25	<1	biotite, sphene, opaque, fluorite	chlorite, sericite	70	qtz	0.25 - 1.25	anhedral	30	kspar	1.25 - 5	euhedral
								kspar		anhedral		qtz	1.25 - 7	
								plag		subhedral		plag	1.25 - 3.75	

Table A1: Petrography of the Spirit Mountain Batholith

sample	modal abundances (%)				accessory minerals	alteration minerals	groundmass				phenocrysts			
	kspar	quartz	plag	bio			%	minerals	size (mm)	shape	%	minerals	size (mm)	shape
SML196	40	30	30	<1	biotite, sphene, opaque, fluorite	chlorite, asericite	-------	-------	-------	-------	100	kspar	0.75 - 7.5	subhedral
												qtz	0.75 - 5	subhedral
												plag	1.25 - 2.5	subhedral
SML207	42	20	35	3	muscovite, opaque, sphene, apatite	sericite	-------	-------	-------	-------	100	kspar	1.25 - 7.5	subhedral
												qtz	1.25 - 5	sub-euhedral
												plag	1.25 - 3.75	anhedral
												biotite	0.75 - 2..5	euhedral
SML211	30	35	35	<1	nusc, bio, opaque	sericite	-------	-------	-------	-------	100	qtz	0.5 - 5	subhedral
												kspar	0.5 - 3.75	subhedral
												plag	0.5 - 2.5	sub-euhedral
SML213	38	10	40	7	HBL - 5% sphehe, opaques	sericite	------	-------	-------	-------	100	plag	1.25 - 5	subhedral
												kspar		subhedral
												qtz		subhedral
												hbl		euhedral
												biotite		euhedral
MPL53z	30	25	40	5	sphene, opaques, zircon, chev/all	chlorite	-------	-------	-------	-------	100	kspar	0.25 - 2.5	anhedral
												plag	0.25 - 2.0	sub-euhedral
												qtz	0.25 - 2.5	anhedral
												biotite	0.25 - 1	subhedral

Table A1: Petrography of the Spirit Mountain Batholith

sample	texture	rims	zoning	alteration	description/ notes
SML3	anhedral granular porphyry w/ med-gr groundmass, myrmekite	**-------**	**-------**	sericite of plag and kspar	bio often w/ opaques, plag phenos smaller than others, epidote w/ opaques
SML4	anhedral granular porphyry with myrmekite	-------	-------	chlorite of biotite, sericite of kspar and plag	kspar poik. Enloses plag, qtz has NO inclusions, verm qtz in kspar
SML5	anhedral granular	-------	-------	-------	qtz clean, kspar w/ qtz incl., plag more subhedral than others… VERY felsic
SML13	myrmekite porphyry with qtz and kspar phenos	-------	-------	sericite of kspar	TONS of graphic qtz in kspar, sphene+opaques+bio+zirc often together, mostly large kspar phenos w/some qtz
SML17	anhedral granular porphyry	-------	-------	sericite of kspar	kspar phenos poik encl. qtz+opaques+sphene, myrmekite some verm kspar in qtz
SML47	anhedral granular porphyry w/ myrmekite	sphene on opaques	-------	sericite of kspar and plag	graphic kspar in qtz, graph qtz in kspar, kspar poik encl. plag+qtz - perthites turn into plag
SML49z	medium grained anhedral granular	sphene on opaques	-------	sericite of kspar and plag	qtz poik encl. musc, kspar poik encl. Plag+qtz+bio, epidote w/ opaques
SML50	anhedral granular porphyry w/ myrmekite	myrmekite on plag and on kspar	euhedral zone of graphic qtz in kspar	sericite of kspar and plag	kspar poik encl. plag, TONS of myrmekite
SML51	anhedral granular aplite with myrmekite	-------	-------	-------	VERY fine grained w/ few phenos, more opaques than bio, epidote w/ opaques

Table A1: Petrography of the Spirit Mountain Batholith

sample	texture	rims	zoning	alteration	description/ notes
SML52	anhedral granular	-------	-------	sericite of plag, opaque repl. Sphene	veins filled w/ qtz and musc oat edges, spherulitic biotite, opaque mass poik encl. epidote, bio, sphene and chev/all
SML54z	medium grained anhedral granular	-------	-------	sericite of plag	kspar poik encl qtz and plag, sphene, opaque and bio together, kspar w/patches of plag
SML57	very fg porphyry	qtz mantle on muscovite	spongy cellular qtz in kspar	-------	all phenos being 'intruded' by groundmass, phenos large and some phenos aggregates of med gr qtz, kspar enclosing plag
SML59z	porphyry w/ med-gr groundmass and some myrmekite	myrmekite rims on kspar	-------	sericite of plag, chlor of bio, kspar highly alt.	plag patches in kspar, more opaques than bio, mafics together, almost all phenos kspar
SML61	porphyry w/ very fine grained gm	-------	-------	sericite	biotite is sheared and often w/mafics, spongy cellular kspar w/qtz, kspar encl in qtz, kspar twinned
SML62a	medium to fine grained myrmekite porphyry	-------	-------	kspar highly altered	gm is mostly med-gr crystals of myrmekite with a few pockets of fine grained qtz/kspar
SML62b	fine to medium grained anhedral granular	-------	-------	kspar highly altered	larger grained than 62a (including myrmekite), 2 grain sizes but not a groundmass and phenos
SML63a	very fine grained (aplite)	-------	-------	chlorite of biotite	large qtz in optical cont totally enclosing/intruded by kspars and plages (graphic?), some verm qtz
SML63b	medium grained anhedral granular	-------	-------	chlorite of biotite	much coarser than 63a, lots of plag altering to kspar (patchy), some graphic qtz

Table A1: Petrography of the Spirit Mountain Batholith

sample	texture	rims	zoning	alteration	description/ notes
SML63c	med to coarse grained anhedral granular	-------	-------	-------	coarser than 63b w/ lots of grphic qtz and more biotite
SML66	myrmekite porphyry	-------	spongy cellular in kspar	sericite of plag	plag intruded by kspar, about 1/2 of gm is myrmekite (TONS of graphic qtz)
SML67	myrmekite porphyry	-------	-------	-------	bio in TINY shards, most of gm altered by graphic qtz, phenos are only aggregates of anhedral qtz
SML68	medium grained anhedral granular	-------	-------	-------	veins of very FG throughout (<0.125), qtz enclosing plag and kspar
SML69	coarse-grained subhedral granular	-------	-------	sericite of plag	a few pockets of fine-grained anhedral granular kspar filling interstitial spaces
SML70	coarse-grained subhedral granular	-------	-------	chlorite totally replaced biotite, veins filling late	lots of tiny veins thru everything filled w/isotropic and bright, patches of very fine grained anhedral granular qtz, most of kspar very large, most of plag medium grained
SML71	coarse-grained subhedral granular	-------	-------	sericite of plag, chlorite of biotite	some plag/kspar intergrowth, kspar enclosing plag laths, graphic qtz in kspar
SML73	medium grained subhedral granular	bioitite rimmed by muscovite	-------	-------	lots of muscovite, garnet encl. musc, more fg pieces than previous, kspar w/plag patches, almost a porphyry with the two sizes, but not exactly a groundmass
SML74	medium grained subhedral granular	biotite rimmed by muscovite, plag mantling kspar	-------	-------	most of the finer grained material is plag and qtz, plag filling interstitial spaces and as patches in kspar

Table A1: Petrography of the Spirit Mountain Batholith

sample	texture	rims	zoning	alteration	description/ notes
SML75	medium grained subhedral granular	-------	-------	-------	kspar cuts some euhedral medium grained plages, larger also more euhedral, finer grained began xlization with plag
SML76	medium grained subhedral granular porphyry	qtz rim on patchy (w/plag) kspar	-------	-------	large qtz phenos w/med-large kspar phenos and a medium grained groundmass, lots of kspar patchy with plag, opaques+fluorite+musc together
SML77	medium grained subhedral granular porphyry	-------	-------	-------	large qtz phenos w/med-large kspar phenos and a medium grained groundmass, lots of kspar patchy with plag, opaques+fluorite+musc together
SML78	medium grained subhedral granular porphyry	plag rimmed by kspar	-------	-------	large qtz phenos w/med-large kspar phenos and a medium grained groundmass, lots of kspar patchy with plag, opaques+fluorite+musc together
SML80a	porphyry with graphic groundmass	plag on kspar	-------	sericite	plag all im groundmass or paches in or enclosed by kspar, lots of graphic qtz in kspar, large kspars twinned
SML80b	graphic	-------	spongy cellular kspar	feldspars highly altered	tons of large graphic qtz (5mm in optical continuity), hard to tell kspar from plag due to alteration, so %s are very rough estimates
SML81	aplite porphyry	-------	-------	-------	phenos are LARGE EUHEDRAL QTZ and aggregates of kspars, some graphic qtz in groundmass
SML91	medium grained porphyry with graphic groundmass	-------	some visible zoning in plag	-------	phenos are aggregates of very large grains, kspar enclosing euhedral plag laths

Table A1: Petrography of the Spirit Mountain Batholith

sample	texture	rims	zoning	alteration	description/ notes
SML120Z	subhedral granular porphyry	-------	-------	sericite highly altered plag	phenos in aggregates, qtz encl all else, few plag phenos (mostly qtz)
SML129Z	med-coarse grained subhedral granular	-------	-------	sericite of plag	kspar has loads of plag patches and stringers, sort of two size populations, but not exactly a 'groundmass'
SML130	med-grained anhedral granular	biotite on opaque	-------	biotite replaced by chlorite, sericitization of plag	qtz is clean but appears pitted, wide range of sizes…
SML132	med-grained anhedral granular	plag on kspar	-------	ser. Of plag	more finer grained xls than sml130, ~70%fine grained and 30% larger
SML133	coarse-grained anhdedral granular	-------	spongy cellular kspar	lots of sericitization of plag	much coarser grained than previous samples, although has some FG too, mafics together, kspars are very patchy with plag
SML151	porphyry (w/ some graphic texture)	-------	-------	ser. Of plag	some graphic texture in phenos, although mostly in groundmass, kspar poik encl plag and is highly patchy with plag
SML152	fine-grained anhedral granular	plag on kspar	-------	high sericitization of plag	much coarser grained than previous althoug has some fine-grained, mafics together, kspars very patch with plag
SML171	medium grained porphyry	sphene on opaque,	-------	plag highly sercicitized	kspars poik enclosing plag, highly altered fspars, plag being repl by kspar, ground mass not significantly smaller than kspars but two are distinct, qtz veins, some graphic qtz
SML179	graphic porphyry	highly ser plag rim on kspar then rimmed in myrmekite	-------	high ser of plag, chlor repl bio	kspar encl plag, qtz encl kspar, lots of graphic in groundmass

Table A1: Petrography of the Spirit Mountain Batholith

sample	texture	rims	zoning	alteration	description/ notes
SML196	coarse grained subhedral granular	-------	-------	chlorite replacing bio, ser of plag	kspar encl plag and qtz, mafics together
SML207	very coarse subhedral granular	muscovite on biotite	-------	ser of plag	kspar encl plag, VERY COARSE GRAINED, kspars patchy with plag
SML211	medium-grained subhedral granular	biotite rim on opaques, kspar on plag	-------	ser of plag	most large phenos are subhedral qtz and aggregates of qtz
SML213	subhedral granular (coarse)	sphene on opaque	-------	sericite	graphic plag in kspar - VERY different from rest of my rocks (not a LG)
MPL53z	subhedral granular	-------	-------	high sericitization of plag	kspar poik encl small euhedral plag laths, lots of biotite compared to leucogranites

APPENDIX B:

Whole Rock Geochemistry of the

Spirit Mountain Batholith Leucogranites

	SiO2	Al2O3	Fe2O3	MnO	MgO	CaO	Na2O	K2O	TiO2	P2O5
LGZ	76.80	12.65	0.92	0.05	0.10	0.67	3.92	4.75	0.13	0.02
SWZ	63.19	17.64	4.10	0.09	1.35	2.73	4.70	5.07	0.87	0.27
SML47	77.31	12.28	0.85	0.03	0.13	0.55	3.44	5.22	0.14	0.04
SML49Z	77.37	12.46	0.68	0.05	0.09	0.43	4.08	4.69	0.12	0.04
SML52	77.00	12.50	0.99	0.06	0.13	0.48	4.04	4.62	0.16	0.02
SML54Z	75.57	13.09	1.19	0.05	0.28	0.78	3.67	5.12	0.20	0.05
SML59Z	74.41	13.82	1.11	0.06	0.15	0.42	4.34	5.45	0.21	0.03
SML63C	77.19	12.03	1.46	0.07	0.11	0.24	3.62	5.05	0.21	0.02
SML67	78.49	12.12	0.67	0.01	0.04	0.38	3.94	4.23	0.10	0.01
SML69	77.96	12.22	0.57	0.04	0.07	0.43	3.94	4.68	0.09	0.01
SML71	78.10	11.92	0.81	0.05	0.07	0.40	3.90	4.58	0.13	0.03
SML73	77.84	12.11	0.77	0.07	0.07	0.33	3.87	4.79	0.12	0.02
SML74	77.55	12.30	0.73	0.07	0.07	0.40	3.94	4.80	0.12	0.01
SML76	77.51	12.40	0.73	0.09	0.05	0.35	4.31	4.50	0.07	0.00
SML78	78.59	11.97	0.59	0.08	0.03	0.20	4.19	4.26	0.08	0.01
SML120Z	73.84	13.78	1.76	0.05	0.42	1.20	3.34	5.29	0.25	0.08
SML129Z	76.07	13.11	0.91	0.08	0.07	0.47	4.11	5.03	0.12	0.03
SML130	76.96	12.83	0.61	0.09	0.08	0.41	4.08	4.83	0.09	0.02
SML132	77.65	12.45	0.63	0.05	0.08	0.39	3.84	4.79	0.10	0.02
SML133	76.18	12.88	1.00	0.06	0.18	0.57	3.98	4.93	0.17	0.04
SML213	61.39	18.78	4.22	0.10	1.28	3.09	5.58	4.41	0.80	0.34
MPL53Z	73.77	13.82	1.86	0.04	0.54	1.56	3.39	4.72	0.24	0.07

Table B1: Whole-rock major element oxide geochemistry of the Spirit Mountain batholith
Concentrations listed in wt%.

	Ba	Sr	Y	Zr	Be	V	Ga	Ge	Rb	Nb	Sn	Cs
LGZ	92	27	18	83	6	5	31	2.3	236	38.3	1	0.7
SWZ	1850	551	26	557	2	57	22	1.0	83	19.2	1	0.3
SML47	277	73	20	83	3	7	17	1.5	159	20	< 1	1
SML49Z	37	17	19	99	3	< 5	20	1.7	204	43.8	1	0.7
SML52	120	42	27	137	4	5	20	1.6	154	30.8	2	0.7
SML54Z	326	89	16	127	2	11	18	1.4	157	23.4	1	0.8
SML59Z	252	63	26	199	3	7	19	1.4	148	31.2	< 1	0.9
SML63C	22	4	42	186	5	< 5	22	2	184	65.3	3	1.1
SML67	10	5	20	114	7	< 5	21	1.9	143	49.8	1	0.3
SML69	59	23	15	68	4	< 5	18	1.4	177	21.9	1	0.7
SML71	37	12	23	131	4	< 5	18	1.7	189	44.3	1	0.7
SML73	49	15	22	128	5	< 5	19	1.7	277	60.7	1	1.4
SML74	48	13	23	111	6	< 5	20	1.8	284	51.9	2	3.1
SML76	20	7	24	123	8	< 5	24	2.2	321	50.2	2	3.5
SML78	19	5	18	96	6	< 5	22	2.2	286	55.4	2	1.9
SML120Z	826	191	22	202	2	23	24	1.7	192	17.9	< 1	1.6
SML129Z	102	26	21	116	5	< 5	25	2.1	266	51.6	< 1	1.2
SML130	21	7	20	92	6	< 5	26	2.3	296	53.8	< 1	2.1
SML132	38	16	16	93	4	< 5	22	1.9	210	31.1	< 1	0.8
SML133	165	48	25	165	7	9	25	2.2	273	45.2	1	1.4
SML213	1811	578	26	586	1	53	29	1.4	67	20.5	< 1	0.4
MPL53Z	830	200	22	166	2	18	17	1.4	150	16.9	< 1	0.8

Table B2: Whole-rock trace element geochemistry of the Spirit Mountain batholith. Concentrations listed in ppm.

	Hf	Ta	Tl	Bi	Th	U	Cu	Zn	Sc	Pb	Zr/Hf	Rb/Sr	Nb/Ta
LGZ	4.1	3.33	0.86	0.8	19.1	2.67					20.46	8.74	
SWZ	12.3	1.11	0.38	0.2	8.91	1.09					45.12	0.15	
SML47	2.8	1.5	0.7		10.9	1.58	6	31	1.05	24	29.64	2.18	
SML49Z	4.2	3.2	0.88		20.8	2.89	11	29	1.31	31	23.57	12.00	
SML52	4.6	2.3	0.79		17	1.87	6	29	1.18	13	29.78	3.67	
SML54Z	4.2	1.5	0.82		17.1	1.34	7	44	1.97	30	30.24	1.76	
SML59Z	6.6	2	0.68		15.3	1.79	6	39	1.7	19	30.15	2.35	
SML63C	8.1	4.7	0.73		44.3	2.99	6	39	1.84	24	22.96	46.00	
SML67	5.6	3.7	0.63		38.5	4.71	27	26	2.03	20	20.36	28.60	
SML69	2.9	1.8	0.71		17.5	2.14	18	22	0.91	28	23.45	7.70	
SML71	5.4	3.1	0.92		25.3	4.01	9	31	1.18	33	24.26	15.75	
SML73	6.2	3.6	1.5		67.7	8.12	7	30	2.15	43	20.65	18.47	
SML74	5.2	3.8	1.29		29.8	3.06	8	35	1.79	28	21.35	21.85	
SML76	6.9	3.8	1.6		41.5	6.27	8	48	1.79	41	17.83	45.86	
SML78	5.4	3.7	1.49		33.6	4.88	6	31	1.6	36	17.78	57.20	
SML120Z	5.4	1.4	0.81	0.6	35.1	3.12	8	36	3.79	26	37.41	1.01	12.79
SML129Z	5.1	4.2	1.07	0.3	35.5	4.19	2	23	1.95	33	22.75	10.23	12.29
SML130	4.4	4.1	1.29	0.3	30.4	3.9	2	34	1.64	31	20.91	42.29	13.12
SML132	3.9	2.8	0.78	< 0.1	25.9	3.74	2	15	1.36	30	23.85	13.13	11.11
SML133	6.3	3.8	0.98	0.1	40.3	3.92	1	24	2.45	26	26.19	5.69	11.89
SML213	12.5	0.9	0.24	< 0.1	10.1	0.71	6	71	5.86	22	46.88	0.12	22.78
MPL53Z	4.9	1.2	0.85		15.8	2.33	7	46	4.22	33	33.88	0.75	

Table B2 (cont'd): Whole-rock trace element geochemistry of the Spirit Mountain batholith. Concentrations listed in ppm.

	La	Ce	Pr	Nd	Sm	Eu	Gd	Tb	Dy	Ho	Er	Tm	Yb	Lu
LGZ	46.7	77.7	6.39	17.9	2.76	0.235	2.16	0.43	2.60	0.58	2.18	0.400	2.67	0.404
SWZ	103	210	21.7	79.5	12.0	2.41	7.86	1.15	5.65	1.00	3.06	0.442	2.92	0.414
SML47	39.9	76	8.03	25.1	4.42	0.581	3.14	0.62	3.49	0.69	2.21	0.328	1.97	0.257
SML49Z	36	63	5.77	15.7	2.49	0.202	1.65	0.38	2.48	0.58	2.15	0.387	2.62	0.395
SML52	40.6	87.4	8.29	25.9	4.56	0.414	3.16	0.64	4.09	0.88	2.9	0.466	2.86	0.384
SML54Z	36.5	73.2	7.81	23.7	3.93	0.546	2.52	0.47	2.61	0.55	1.81	0.298	1.89	0.272
SML59Z	62	120	12.7	37.5	6.53	0.777	4.37	0.76	4.14	0.84	2.69	0.41	2.52	0.359
SML63C	60.5	123	12	35.1	5.91	0.197	4.43	0.97	6.3	1.41	4.82	0.8	5	0.684
SML67	41.8	64.8	5.48	13.6	1.84	0.09	1.08	0.28	2.05	0.51	2.01	0.404	3.02	0.493
SML69	32.7	59.9	5.64	15.8	2.66	0.229	1.69	0.36	2.32	0.51	1.74	0.294	1.89	0.268
SML71	43.9	77.3	7.01	18.8	2.84	0.203	1.84	0.4	2.72	0.65	2.43	0.445	3.09	0.481
SML73	38.9	65.3	5.6	14.6	2.2	0.157	1.49	0.34	2.43	0.61	2.43	0.455	3.35	0.544
SML74	50.6	86.1	7.38	18.8	2.76	0.174	1.59	0.38	2.55	0.64	2.4	0.448	3.18	0.507
SML76	44.6	74.2	5.81	14.1	1.94	0.103	1.17	0.31	2.32	0.6	2.39	0.475	3.73	0.588
SML78	26.7	49.6	4.41	11.9	1.79	0.076	1.33	0.28	2.1	0.51	1.96	0.37	2.66	0.421
SML120Z	55.2	104	11.7	36.7	6.51	0.93	4.75	0.7	3.82	0.76	2.27	0.361	2.37	0.36
SML129Z	36	60.2	5.58	15.2	2.42	0.19	1.79	0.38	2.51	0.59	2.19	0.451	3.29	0.51
SML130	29.7	49	4.4	11.9	1.9	0.09	1.43	0.31	2.18	0.53	2.08	0.42	3.13	0.5
SML132	29.2	48.1	4.47	12.5	1.97	0.15	1.46	0.3	2.04	0.48	1.73	0.34	2.5	0.39
SML133	45.5	79.3	7.76	22.4	3.59	0.32	2.68	0.51	3.25	0.72	2.49	0.456	3.35	0.54
SML213	106	181	20	62.8	9.96	1.98	7.18	1.02	5.16	0.96	2.75	0.38	2.41	0.35
MPL53Z	53.5	99.5	10.8	33	5.62	0.913	3.82	0.69	3.57	0.71	2.3	0.353	2.24	0.343

Table B3: Whole-rock Rare Earth Element geochemistry of the Spirit Mountain batholith. Concentrations listed in ppm

APPENDIX C:

U-Pb Geochronology and

Cathodoluminescence Images of Zircons

from the Spirit Mountain Batholith

Table C-1: Geochronology data from SHRIMP-RG analysis of zircons from the Spirit Mountain batholith

Spot Name	% comm 206	ppm U	ppm Th	232Th /238U	207corr 206Pb /238U Age	1s err	7corr 206Pbr /238U	1s err	Total 238 /206	% err	Total 207 /206	% err
SML49Z-1.1R	3.47	72	94	1.35	18.3	0.8	.0028	0.000126	340.35	4.1	.0738	16.7
SML49Z-2.1T	0.79	473	595	1.30	17.3	0.3	.0027	0.000047	368.50	1.7	.0526	8.0
SML49Z-3.1C	1.83	113	200	1.83	16.1	0.6	.0025	0.000093	393.67	3.5	.0608	17.4
SML49Z-4.1C	3.58	149	258	1.79	16.5	0.5	.0026	0.000082	375.21	3.0	.0747	11.9
SML49Z-4.2T	3.60	438	633	1.49	15.2	0.3	.0024	0.000045	407.59	1.8	.0748	7.1
SML49Z-3.2T	0.23	984	1541	1.62	16.8	0.2	.0026	0.000031	381.27	1.1	.0482	5.8
SML49Z-5.1T	1.03	369	554	1.55	16.0	0.3	.0025	0.000051	398.82	1.9	.0545	9.3
SML49Z-6.1C	9.53	42	85	2.11	15.9	1.0	.0025	0.000156	367.11	5.5	.1217	17.9
SML49Z-6.2T	0.47	707	809	1.18	16.2	0.2	.0025	0.000037	395.68	1.4	.0501	7.0
SML49Z-7.1T	3.20	221	290	1.36	16.4	0.4	.0025	0.000066	380.48	2.4	.0717	10.2
SML49Z-8.1C	3.92	202	373	1.91	15.4	0.4	.0024	0.000070	402.49	2.7	.0773	11.2
SML49Z-8.2T	0.01	588	536	0.94	16.5	0.3	.0026	0.000041	389.23	1.5	.0465	7.7
SML49Z-9.1R	1.03	714	1026	1.48	16.8	0.2	.0026	0.000037	379.90	1.3	.0545	6.4
SML49Z-10.1T	0.49	1030	1247	1.25	17.4	0.2	.0027	0.000031	368.65	1.1	.0503	5.3
SML49Z-11.1C	2.74	198	307	1.60	16.2	0.4	.0025	0.000069	387.35	2.5	.0680	11.8
SML49Z-11.2T	1.32	861	1006	1.21	16.0	0.2	.0025	0.000034	398.22	1.3	.0568	6.4
SML49Z-12.1T	0.44	883	1159	1.36	16.3	0.2	.0025	0.000032	392.07	1.2	.0499	6.1
SML49Z-13.1T	1.26	558	707	1.31	16.2	0.3	.0025	0.000040	393.29	1.5	.0563	7.1
SML49Z-14.1T	2.11	135	173	1.33	16.1	0.5	.0025	0.000080	390.68	3.0	.0630	13.0
SML49Z-15.1T	0.24	694	999	1.49	17.4	0.2	.0027	0.000038	368.22	1.3	.0483	6.6
SML49Z-16.1C	2.98	74	117	1.65	17.6	0.8	.0027	0.000119	354.18	4.1	.0699	16.7

Table C-1: Geochronology data from SHRIMP-RG analysis of zircons from the Spirit Mountain batholith

Spot Name	% comm 206	ppm U	ppm Th	232Th /238U	207corr 206Pb /238U Age	1s err	7corr 206Pbr /238U	1s err	Total 238 /206	% err	Total 207 /206	% err
SML54Z-1.1T	~~6.33~~	~~201~~	~~317~~	~~1.62~~	~~15.6~~	~~0.4~~	~~.0024~~	~~0.000069~~	~~387.82~~	~~2.6~~	~~.0964~~	~~9.2~~
SML54-2.1R	0.50	424	786	1.91	17.2	0.3	.0027	0.000047	372.48	1.7	.0503	8.1
SML54-3.1T	1.27	644	732	1.17	16.8	0.2	.0026	0.000038	378.65	1.4	.0564	6.5
SML54-4.1T	0.65	1016	1237	1.26	16.5	0.2	.0026	0.000030	388.44	1.1	.0515	5.4
SML54-5.1T	0.55	174	245	1.46	16.9	0.5	.0026	0.000074	378.46	2.7	.0507	12.8
SML54-6.1T	2.12	125	294	2.42	16.7	0.6	.0026	0.000088	376.79	3.2	.0631	15.4
SML54-7.1C	-0.13	1336	1704	1.32	17.2	0.2	.0027	0.000026	374.12	0.9	.0453	4.9
SML54-8.1T	3.03	167	199	1.23	16.4	0.5	.0025	0.000073	380.92	2.7	.0703	11.4
SML54-9.1C	~~13.84~~	~~32~~	~~63~~	~~2.03~~	~~16.9~~	~~1.3~~	~~.0026~~	~~0.000197~~	~~327.87~~	~~5.6~~	~~.1558~~	~~21.6~~
SML54-9.2T	3.53	147	197	1.39	16.5	0.5	.0026	0.000085	376.90	2.8	.0743	17.2
SML54-10.1T	0.35	424	539	1.31	17.0	0.3	.0026	0.000046	377.14	1.7	.0492	8.2
SML54-11.1C	0.53	764	917	1.24	17.0	0.2	.0026	0.000035	377.11	1.2	.0506	6.3
SML54-12.1T	0.83	185	263	1.47	17.0	0.4	.0026	0.000070	375.26	2.5	.0529	12.1
SML54-13.1T	1.16	197	353	1.85	17.5	0.5	.0027	0.000071	363.79	2.4	.0555	14.3
SML54-14.1R	0.65	357	483	1.40	16.6	0.3	.0026	0.000050	384.41	1.8	.0515	8.9
SML54-15.1T	-0.10	636	1087	1.77	17.4	0.2	.0027	0.000038	370.33	1.4	.0456	7.1
SML54-15.2C	4.27	87	165	1.95	17.8	0.7	.0028	0.000107	346.47	3.6	.0801	14.1
SML54-16.1C	2.70	83	134	1.66	16.2	0.7	.0025	0.000109	387.80	4.0	.0677	19.7
SML54-17.1T	0.05	2005	7182	3.70	17.6	0.1	.0027	0.000022	364.68	0.8	.0468	3.8
SML54-16.2T	0.01	1851	3119	1.74	17.6	0.1	.0027	0.000023	366.78	0.8	.0465	4.1
SML54-18.1C	1.60	57	102	1.86	16.2	0.8	.0025	0.000126	391.15	4.7	.0590	21.8
SML54-19.1T	0.06	1395	1524	1.13	16.8	0.2	.0026	0.000029	383.63	1.1	.0468	5.5

Table C-1: Geochronology data from SHRIMP-RG analysis of zircons from the Spirit Mountain batholith

Spot Name	% comm 206	ppm U	ppm Th	232Th /238U	207corr 206Pb /238U Age	1s err	7corr 206Pbr /238U	1s err	Total 238 /206	% err	Total 207 /206	% err
MPL53-1.1R	1.24	413	575	1.44	16.2	0.3	.0025	0.000045	393.44	1.7	.0562	8.0
MPL53-2.1T	1.19	332	275	0.85	16.7	0.3	.0026	0.000054	381.02	2.0	.0557	9.1
MPL53-2.2C	3.26	131	218	1.71	19.1	0.6	.0030	0.000092	326.83	2.9	.0722	12.2
MPL53-3.1C	1.97	170	237	1.44	18.4	0.5	.0029	0.000079	342.54	2.6	.0620	12.1
MPL53-4.1T	1.56	1917	1776	0.96	17.3	0.1	.0027	0.000023	366.50	0.8	.0587	3.7
MPL53-5.1C	1.73	278	718	2.67	15.9	0.4	.0025	0.000057	398.55	2.2	.0600	9.7
MPL53-6.1C	1.46	454	1351	3.08	15.7	0.3	.0024	0.000044	403.52	1.7	.0579	7.9
MPL53-7.1T	1.35	485	1229	2.62	15.9	0.3	.0025	0.000051	400.29	1.9	.0570	8.9
MPL53-8.1T	~~52.37~~	~~525~~	~~838~~	~~1.65~~	~~14.3~~	~~0.8~~	~~.0022~~	~~0.000124~~	~~214.23~~	~~1.4~~	~~.4602~~	~~4.1~~
MPL53-9.1C	2.14	536	2346	4.53	14.9	0.3	.0023	0.000051	423.24	2.0	.0632	10.0
MPL53-10.1	1.18	670	1176	1.81	16.3	0.3	.0025	0.000045	391.15	1.7	.0557	7.7
MPL53-11.1T	2.01	356	285	0.83	16.2	0.4	.0025	0.000062	389.60	2.3	.0622	10.3
MPL53-12.1C	0.54	886	2094	2.44	15.9	0.2	.0025	0.000037	403.09	1.4	.0506	7.2
MPL53-13.1C	2.38	125	107	0.89	15.9	0.7	.0025	0.000106	395.16	4.0	.0651	19.4
MPL53-14.1C	3.55	423	633	1.55	15.1	0.4	.0023	0.000065	410.87	2.1	.0744	18.4
MPL53-15.1T	1.10	613	834	1.41	16.1	0.3	.0025	0.000046	396.61	1.8	.0550	8.5
MPL53-16.1C	2.43	212	350	1.71	16.6	0.5	.0026	0.000080	377.76	2.9	.0656	12.5

Table C-1: Geochronology data from SHRIMP-RG analysis of zircons from the Spirit Mountain batholith

Spot Name	% comm 206	ppm U	ppm Th	232Th /238U	207corr 206Pb /238U Age	1s err	7corr 206Pbr /238U	1s err	Total 238 /206	% err	Total 207 /206	% err
SML59Z-1.1T	5.51	231	359	1.60	17.3	0.5	.0027	0.000082	351.58	2.7	.0899	11.5
SML59Z-2.1T	1.15	253	629	2.58	17.0	0.5	.0026	0.000071	374.85	2.5	.0555	12.5
SML59Z-3.1C	0.54	604	2213	3.78	17.7	0.3	.0028	0.000046	361.06	1.6	.0507	8.0
SML59Z-4.1R	0.84	367	644	1.81	17.4	0.4	.0027	0.000058	367.13	2.1	.0530	9.9
SML59Z-5.1T	7.37	171	390	2.35	16.9	0.6	.0026	0.000088	353.53	3.0	.1046	10.3
SML59Z-6.1C	2.13	478	1871	4.05	16.6	0.3	.0026	0.000052	379.83	1.9	.0632	8.4
SML59Z-7.1C	0.89	646	3124	5.00	17.6	0.3	.0027	0.000044	362.33	1.5	.0534	7.3
SML59Z-8.1T	3.20	259	914	3.65	17.3	0.5	.0027	0.000073	360.30	2.5	.0717	10.3
SML59Z-9.1C	0.77	1126	4959	4.55	17.2	0.2	.0027	0.000034	370.50	1.2	.0525	5.8
SML59Z-10.1T	4.81	381	916	2.48	16.6	0.4	.0026	0.000058	370.06	2.1	.0844	8.1
SML59Z-11.1C	3.65	883	3208	3.76	17.6	0.3	.0027	0.000049	351.79	1.5	.0752	9.7
SML59Z-12.1T	3.42	205	309	1.56	17.3	0.5	.0027	0.000080	359.45	2.7	.0734	12.0
SML59Z-13.1T	1.58	309	667	2.23	17.0	0.4	.0026	0.000064	372.24	2.3	.0588	10.5
SML59Z-13.2C	0.73	960	3391	3.65	17.4	0.2	.0027	0.000037	366.43	1.3	.0521	6.3
SML59Z-14.1C	2.92	236	552	2.41	16.0	0.5	.0025	0.000073	391.51	2.7	.0695	13.3
SML59Z-15.1C	1.73	538	1898	3.64	16.9	0.3	.0026	0.000049	374.56	1.7	.0601	7.9
SML59Z-16.1T	2.94	281	483	1.78	15.9	0.4	.0025	0.000065	393.30	2.5	.0696	10.5
SML59Z-17.1C	1.59	621	1840	3.06	17.8	0.3	.0028	0.000039	356.74	1.3	.0590	6.1
SML59Z-18.1T	0.69	263	665	2.61	17.3	0.4	.0027	0.000056	370.32	2.0	.0518	9.6
SML59Z-19.1C	1.18	401	1080	2.79	16.9	0.3	.0026	0.000046	376.40	1.7	.0557	8.0

Table C-1: Geochronology data from SHRIMP-RG analysis of zircons from the Spirit Mountain batholith

Spot Name	% comm 206	ppm U	ppm Th	232Th /238U	207corr 206Pb /238U Age	1s err	7corr 206Pbr /238U	1s err	Total 238 /206	% err	Total 207 /206	% err
SML120Z-1	2.11	60	105	1.80	14.6	0.7	.0023	0.000105	431.9276	4.4	.0630	17.5
SML120Z-2T	0.13	303	369	1.26	15.4	0.3	.0024	0.000046	416.9810	1.8	.0474	8.4
SML120Z-3.1C	0.67	57	24	0.43	82.4	1.6	.0129	0.000252	77.1868	1.9	.0530	7.8
SML120Z-3.2	0.29	465	139	0.31	56.3	0.6	.0088	0.000092	113.6208	1.0	.0494	4.5
SML120Z-4.1C	0.64	1208	22	0.02	1549.4	3.9	.2717	0.000763	3.6571	0.2	.1016	0.5
SML120Z-5.1I	-0.11	118	207	1.81	15.5	0.5	.0024	0.000082	416.0294	3.3	.0454	15.8
SML120Z-6.1I	-0.69	192	439	2.36	16.5	0.4	.0026	0.000067	393.5914	2.5	.0409	12.7
SML120Z-6.2R	0.00	386	720	1.93	15.5	0.3	.0024	0.000047	416.4686	1.9	.0463	8.9
SML120Z-7.1T	-0.20	452	698	1.60	16.6	0.3	.0026	0.000044	387.7783	1.7	.0448	7.8
SML120Z-7.2I	3.61	68	170	2.59	15.3	0.7	.0024	0.000109	405.2302	4.3	.0749	16.4
SML120Z-8.1I	-0.52	296	473	1.65	17.2	0.4	.0027	0.000056	376.5349	2.0	.0422	10.0
SML120Z-8.2R	1.49	71	151	2.18	18.5	0.8	.0029	0.000118	342.5709	3.9	.0582	16.7
SML120Z-9.1C	-0.19	3584	3503	1.01	17.4	0.1	.0027	0.000016	371.1710	0.6	.0449	2.8
SML120Z-10.1I	0.40	112	122	1.12	17.0	0.6	.0026	0.000089	376.2590	3.2	.0496	15.0
SML120Z-11.1R	1.47	128	175	1.42	16.7	0.6	.0026	0.000087	380.5328	3.2	.0580	13.5
SML120Z-11.2I	1.55	144	296	2.11	17.8	0.5	.0028	0.000081	356.6967	2.8	.0586	11.5
SML120Z-12.1I	-0.04	254	506	2.06	17.2	0.4	.0027	0.000068	375.2573	2.5	.0460	10.3
SML120Z-12.2R	6.51	104	181	1.80	15.7	0.6	.0024	0.000095	384.1062	3.5	.0978	12.9
SML120Z-13.1I	1.94	44	86	2.02	17.5	0.9	.0027	0.000147	360.2899	5.1	.0617	21.1
SML120Z-13.2R	0.99	204	264	1.34	17.8	0.5	.0028	0.000071	358.0533	2.4	.0542	13.1
SML120Z-14.1R	-0.01	254	269	1.09	18.5	0.4	.0029	0.000063	348.7892	2.1	.0463	9.9
SML120Z-15.1R	1.44	83	169	2.09	15.8	0.7	.0025	0.000101	400.8191	3.9	.0577	16.5
SML120Z-15.2C	0.26	303	523	1.78	16.3	0.3	.0025	0.000053	393.4925	2.0	.0484	9.3
SML120Z-16.1C	0.80	37	70	1.96	16.8	1.0	.0026	0.000155	380.2397	5.7	.0527	25.7
SML120Z-17.1R	0.84	106	182	1.78	16.1	0.6	.0025	0.000090	397.4870	3.4	.0530	15.0
SML120Z-18.1R	-0.18	389	512	1.36	17.6	0.3	.0027	0.000049	366.3561	1.7	.0450	8.2

Table C-1: Geochronology data from SHRIMP-RG analysis of zircons from the Spirit Mountain batholith

Spot Name	% comm 206	ppm U	ppm Th	232Th /238U	207corr 206Pb /238U Age	1s err	7corr 206Pbr /238U	1s err	Total 238 /206	% err	Total 207 /206	% err
SML129Z-1	4.29	25	64	2.62	15.3	1.2	.0024	0.000184	403.5948	7.2	.0803	26.6
SML129Z-2R	0.37	2034	1917	0.97	16.6	0.1	.0026	0.000021	385.9727	0.8	.0493	3.5
SML129Z-3C	-0.31	200	322	1.66	17.0	0.4	.0026	0.000067	380.2318	2.5	.0439	11.6
SML129Z-4I	-0.30	91	161	1.82	17.1	0.7	.0027	0.000102	376.5785	3.7	.0440	17.8
SML129Z-5T	1.54	3471	5047	1.50	17.8	0.1	.0028	0.000017	355.1807	0.6	.0585	2.3
SML129Z-6C	-0.31	1668	2392	1.48	18.2	0.2	.0028	0.000024	355.6586	0.8	.0440	4.0
SML129-7T	0.28	1958	4054	2.14	17.3	0.1	.0027	0.000022	372.0087	0.8	.0486	3.6
SML129Z-8.1C	-0.26	999	1465	1.51	17.0	0.2	.0026	0.000031	380.0493	1.1	.0443	5.9
SML129Z-8.2R	-0.27	856	854	1.03	16.8	0.2	.0026	0.000032	383.6798	1.2	.0443	5.6
SML129Z-9C	0.46	964	1172	1.26	17.1	0.2	.0027	0.000032	374.6853	1.1	.0500	5.1
SML129Z-10R	0.32	1123	1011	0.93	17.7	0.2	.0028	0.000029	361.6220	1.0	.0489	4.6
SML129Z-11.1C	-0.23	180	283	1.63	17.9	0.5	.0028	0.000072	361.0704	2.5	.0446	12.1
SML129Z-11.2R	0.25	3351	2679	0.83	17.6	0.1	.0027	0.000017	364.5022	0.6	.0483	2.7
SML129Z-12R	-0.23	306	771	2.60	17.7	0.4	.0027	0.000055	365.4108	1.9	.0446	9.1
SML129Z-13R	-0.31	300	322	1.11	17.6	0.4	.0027	0.000057	367.6149	2.0	.0439	9.5

Figure C1:
Cathodoluminsecence images of zircons from sample SML49z with spots from U-Pb SHRIMP-RG analyses marked

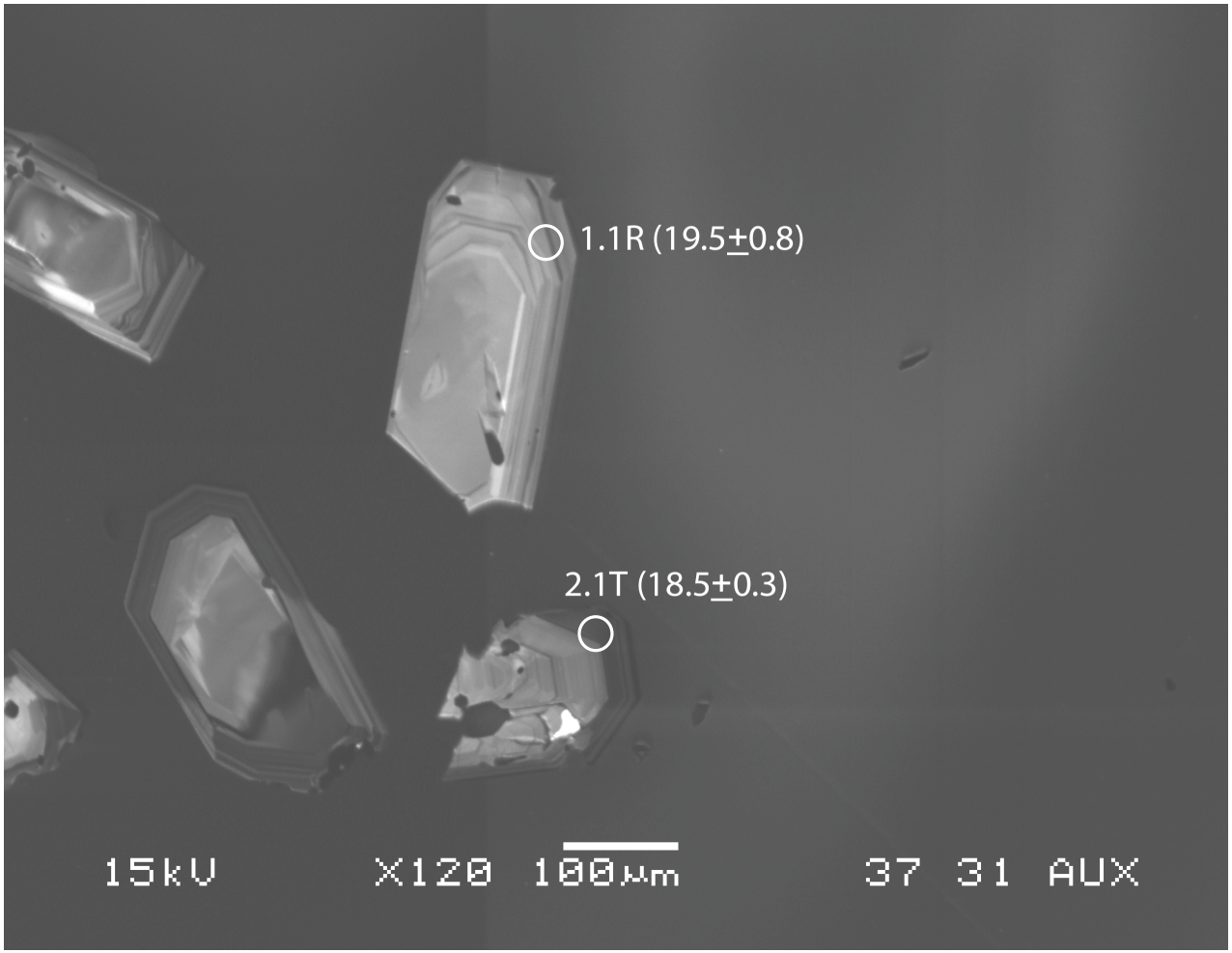
1.1R (19.5±0.8)
2.1T (18.5±0.3)
15kV
X120 100µm
37 31 AUX

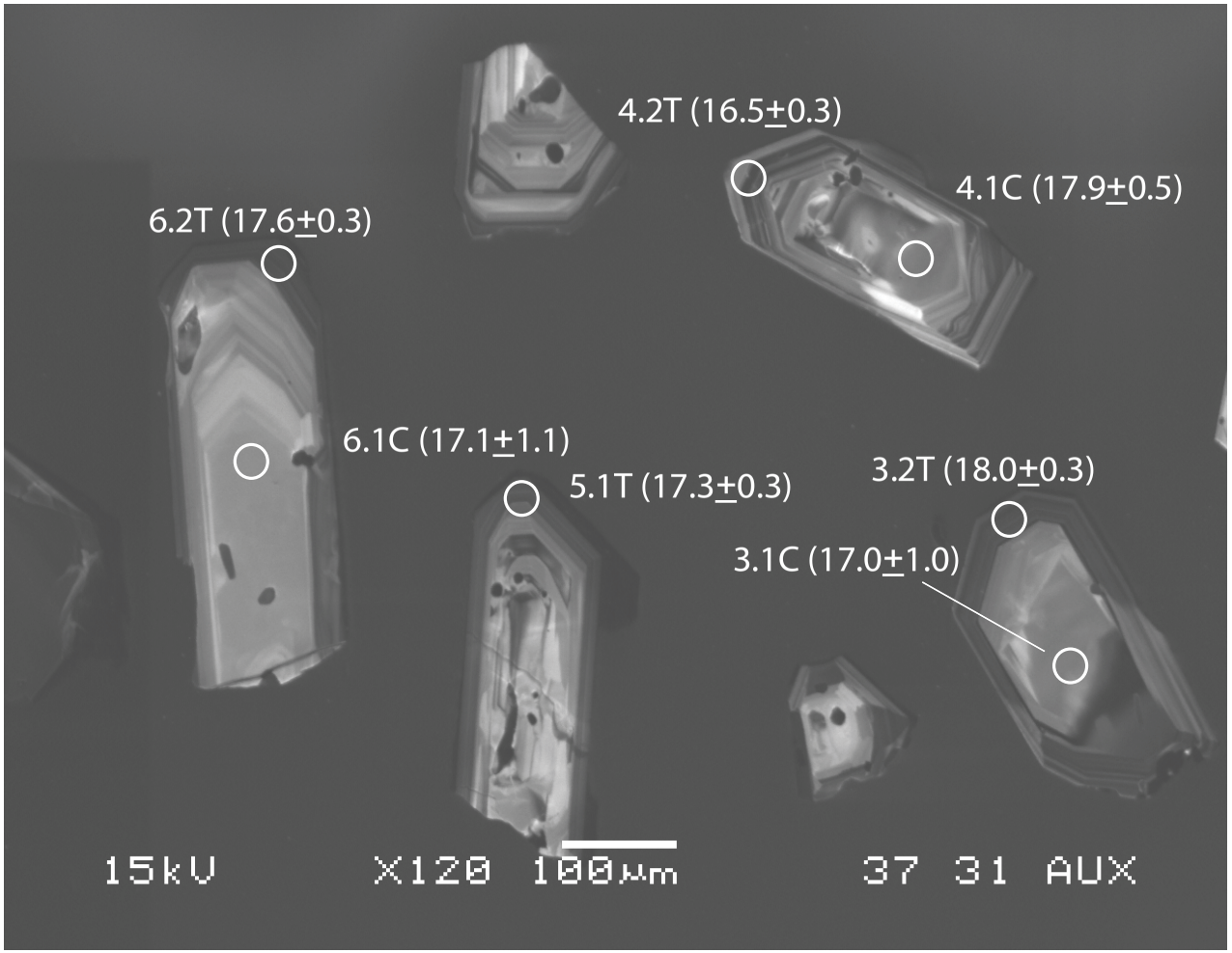
4.2T (16.5±0.3)
4.1C (17.9±0.5)
6.2T (17.6±0.3)
6.1C (17.1±1.1)
5.1T (17.3±0.3)
3.2T (18.0±0.3)
3.1C (17.0±1.0)
15kV X120 100µm 37 31 AUX

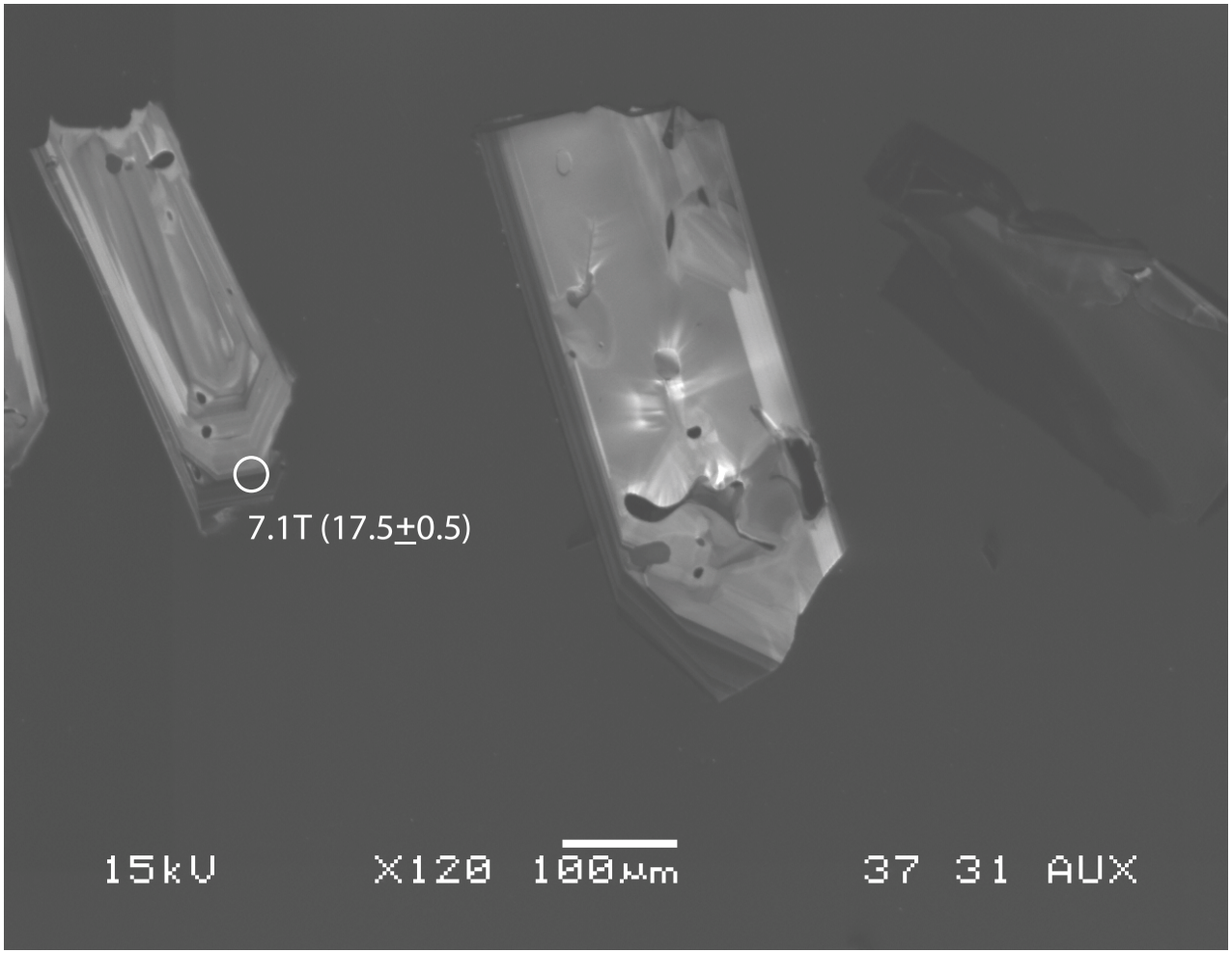
7.1T (17.5±0.5)
15kV
X120
100µm
37 31 AUX

9.1R (18.0±0.3)
8.1C (16.7±1.8)
8.2T (18.0±0.3)
10.1T (18.8±0.2)
15kV X120 100μm 37 31 AUX

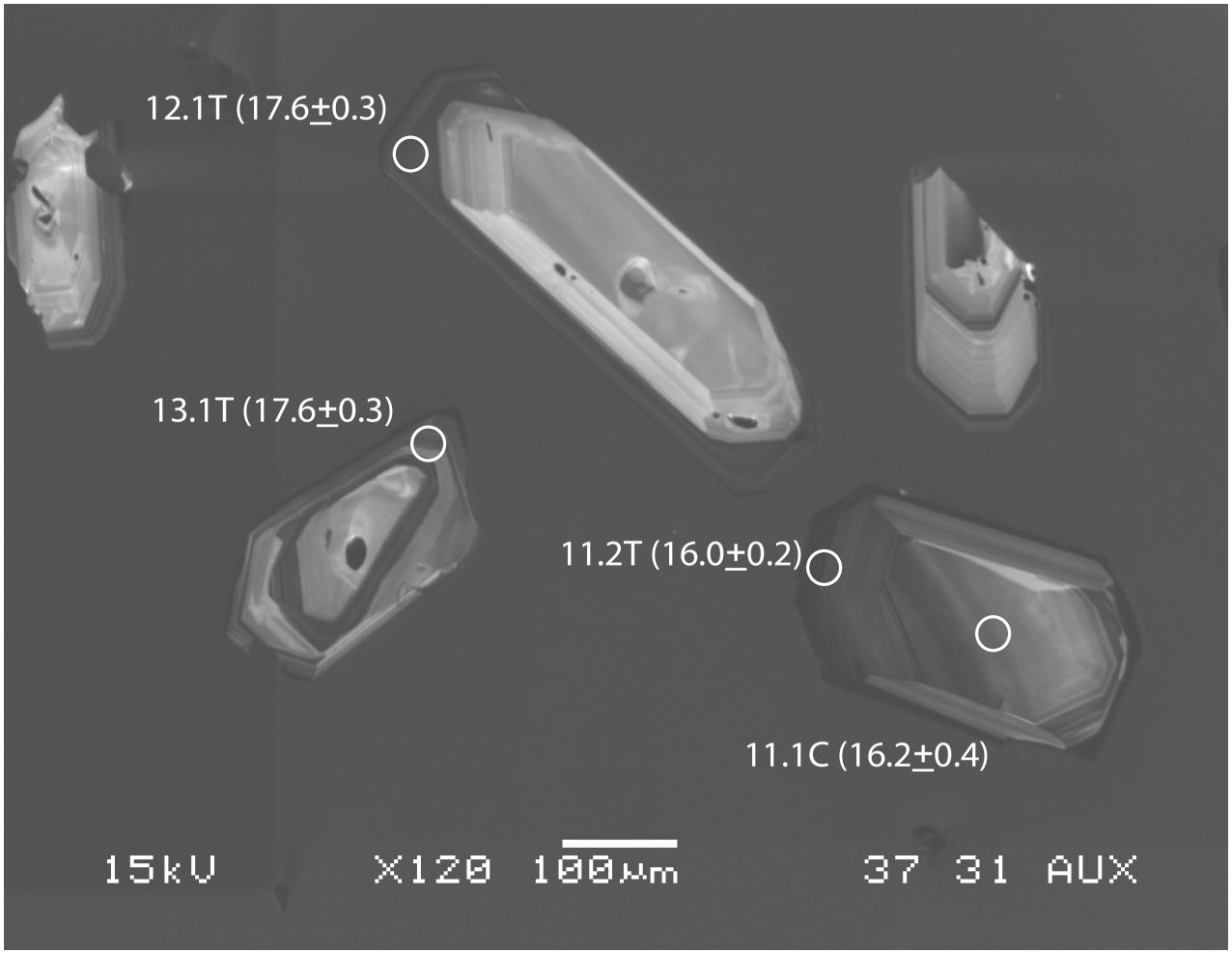
12.1T (17.6±0.3)
13.1T (17.6±0.3)
11.2T (16.0±0.2)
11.1C (16.2±0.4)
15kV X120 100µm 37 31 AUX

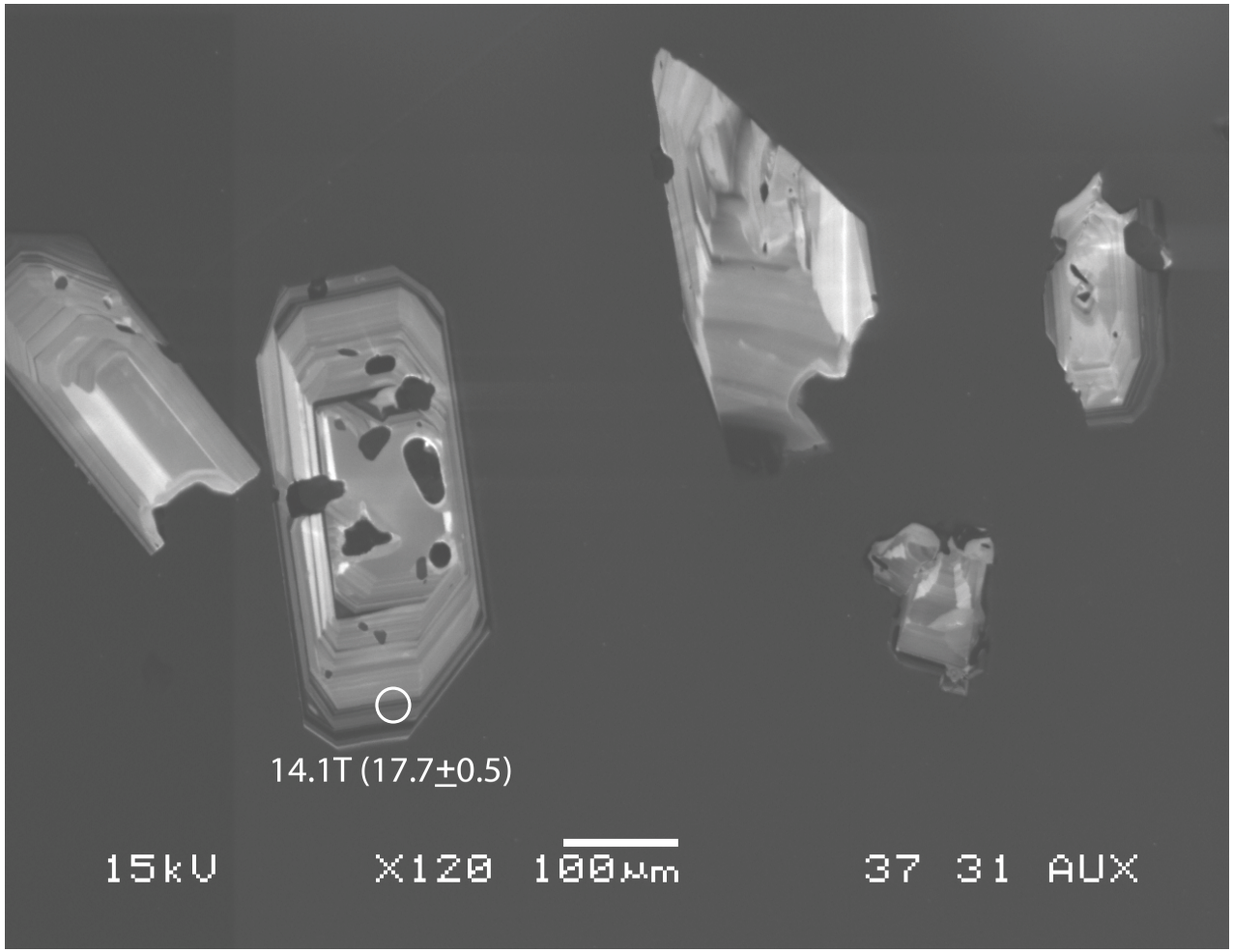
14.1T (17.7±0.5)
15kV
X120 100µm
37 31 AUX

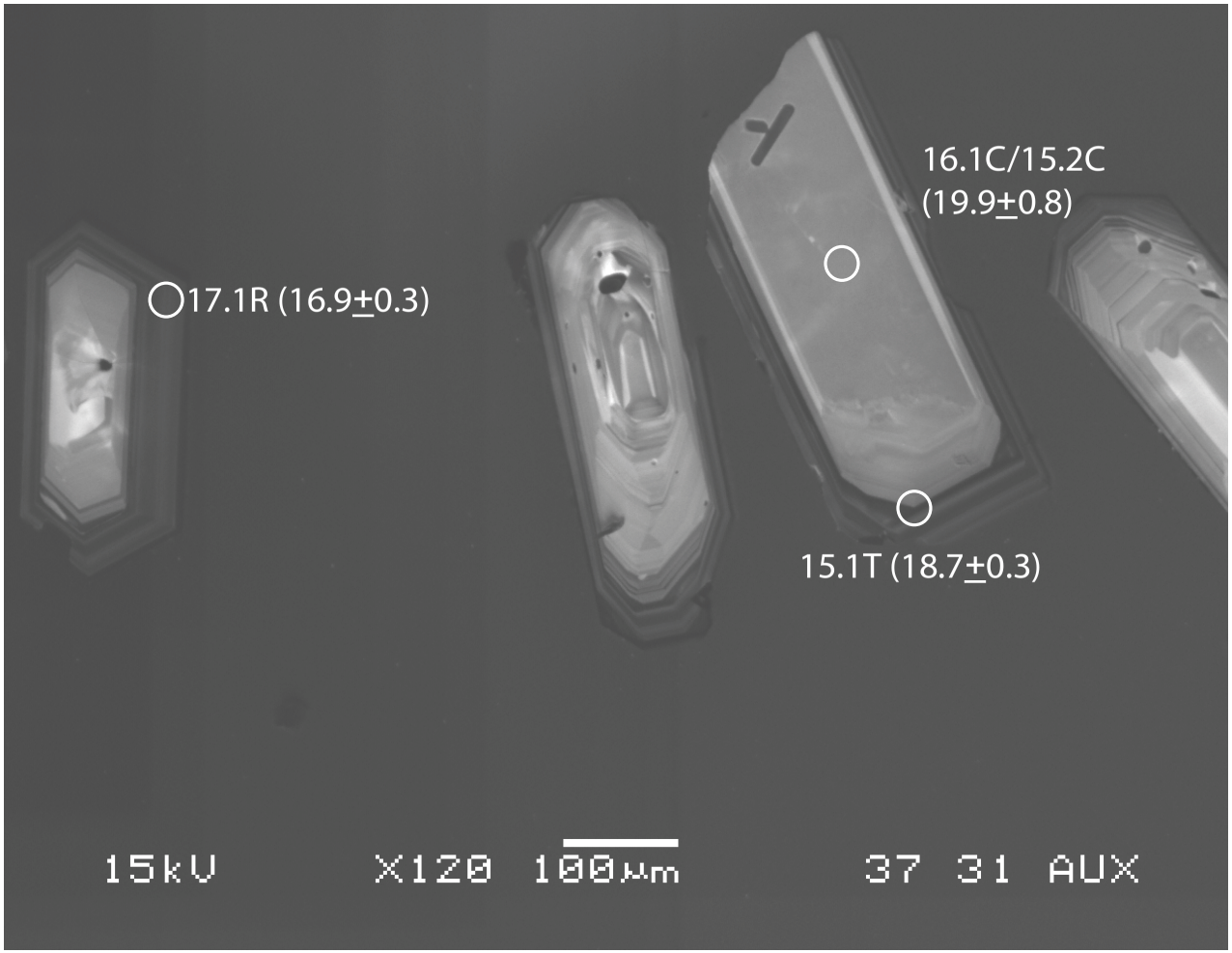
16.1C/15.2C
(19.9±0.8)
17.1R (16.9±0.3)
15.1T (18.7±0.3)
15kV
X120 100µm
37 31 AUX

15kV X120 100µm 37 31 AUX

Figure C2:
Cathodoluminsecence images of zircons from sample SML54z with spots from U-Pb SHRIMP-RG analyses marked

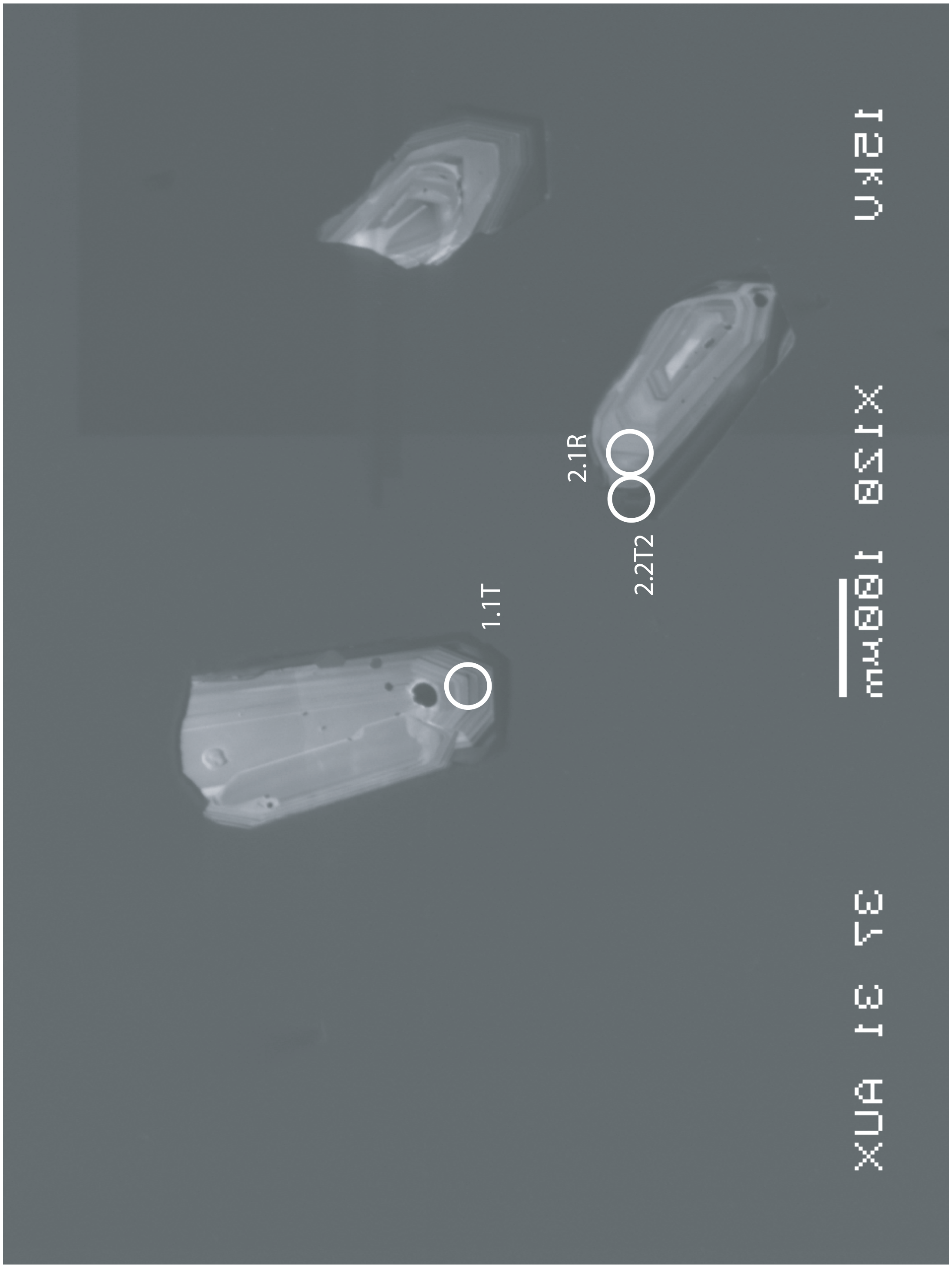
1.1T
2.1R
2.2T2
15kV
X150
100µm

5.1T
4.1T
3.1T
4.2R
100μm
X150 05IX
12kV

20.1R
6.1T
7.1C
8.1T
9.1C
9.2T
100µm
XL30 ESEM
12kV

XUA 13 32
10.1T
11.1C
12.1T
13.1T
100µm
X150 05:X
12kV U121

15.2C
15.1T
14.1R
100μm
X150 05IX
12kV

16.1C
18.1C
16.2T
17.1T
100μm
X150 05IX
12kV

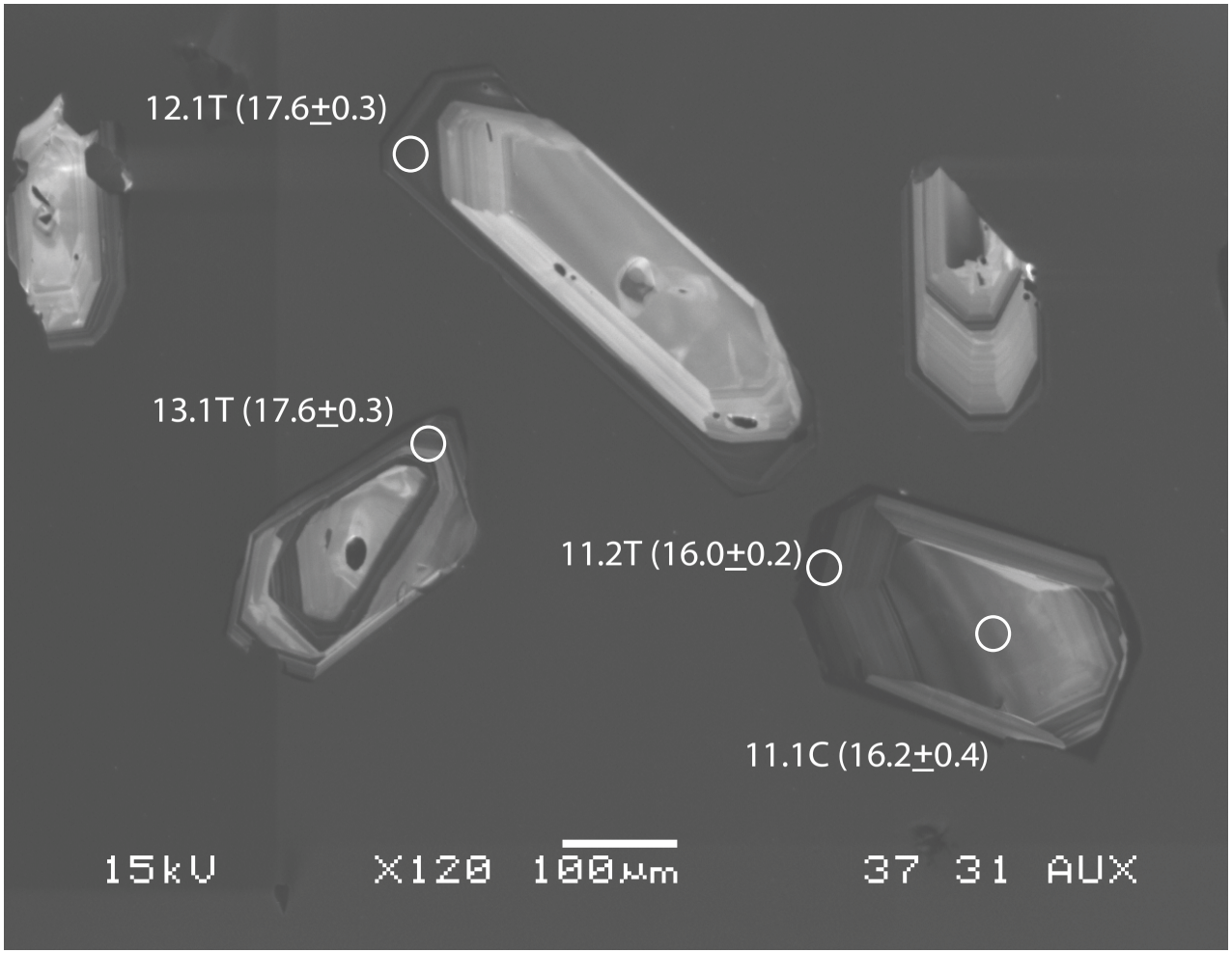
12.1T (17.6±0.3)
13.1T (17.6±0.3)
11.2T (16.0±0.2)
11.1C (16.2±0.4)
15kV X120 100µm 37 31 AUX

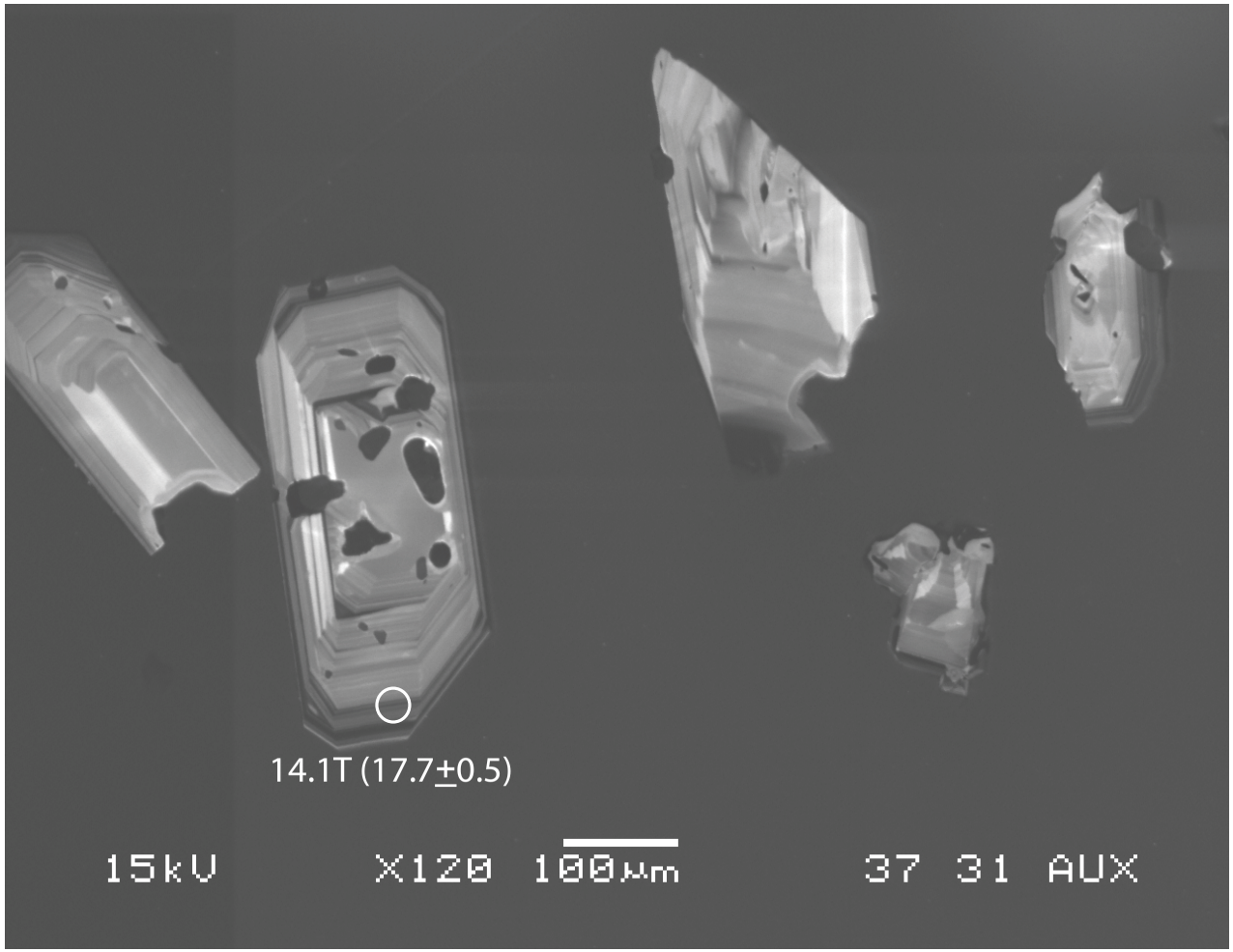
14.1T (17.7±0.5)
15kV
X120 100µm
37 31 AUX

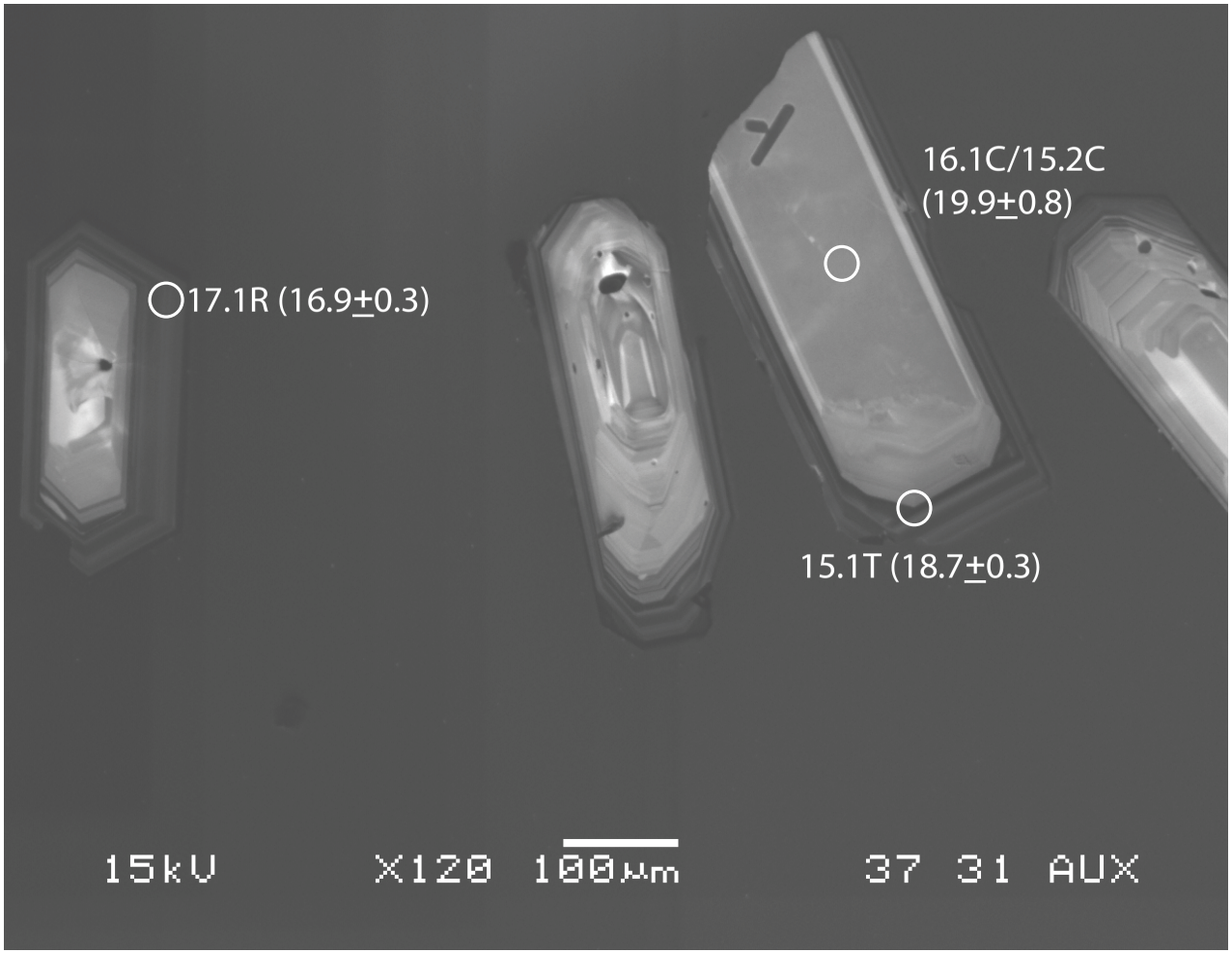
16.1C/15.2C
(19.9±0.8)
17.1R (16.9±0.3)
15.1T (18.7±0.3)
15kV X120 100µm 37 31 AUX

15kV X120 100µm 37 31 AUX

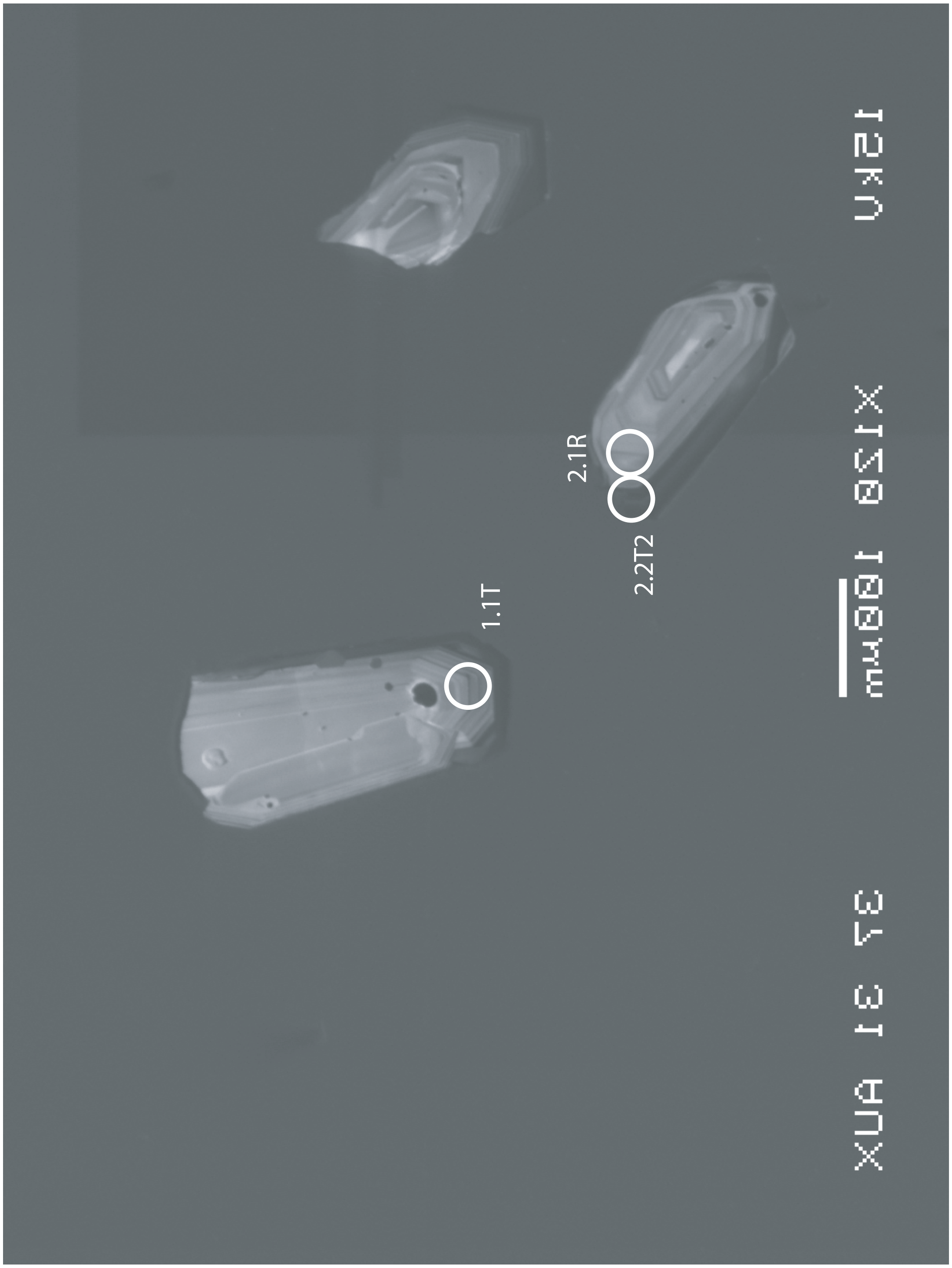
1.1T
2.1R
2.2T2
15kV
X150
100µm

5.1T
4.1T
3.1T
4.2R
100μm
X150 05IX
12KV

20.1R
6.1T
7.1C
8.1T
9.1C
9.2T
100μm

12kV UW21
X150 100μm
19.1T
XUA 12 31 37

12kV X150 100μm 35 31 AUX

1.1T
2.1T
3.1C
4.1R
100μm
X150 05:X
12kV

XUA 13 32
X150 OSIX 100μm
12kV UNLT
5.1T
6.1C
7.1C

12kV U421
X150 100μm
19.1T
XUA 12 31 37

XUA 31 35
X150 100μm
12kV

Figure C3:
Cathodoluminsecence images of zircons from sample SML59z with spots from U-Pb SHRIMP-RG analyses marked

XUA 15 32
100µm
X150 05IX
12kV
1.1T
2.1T
3.1C
4.1R

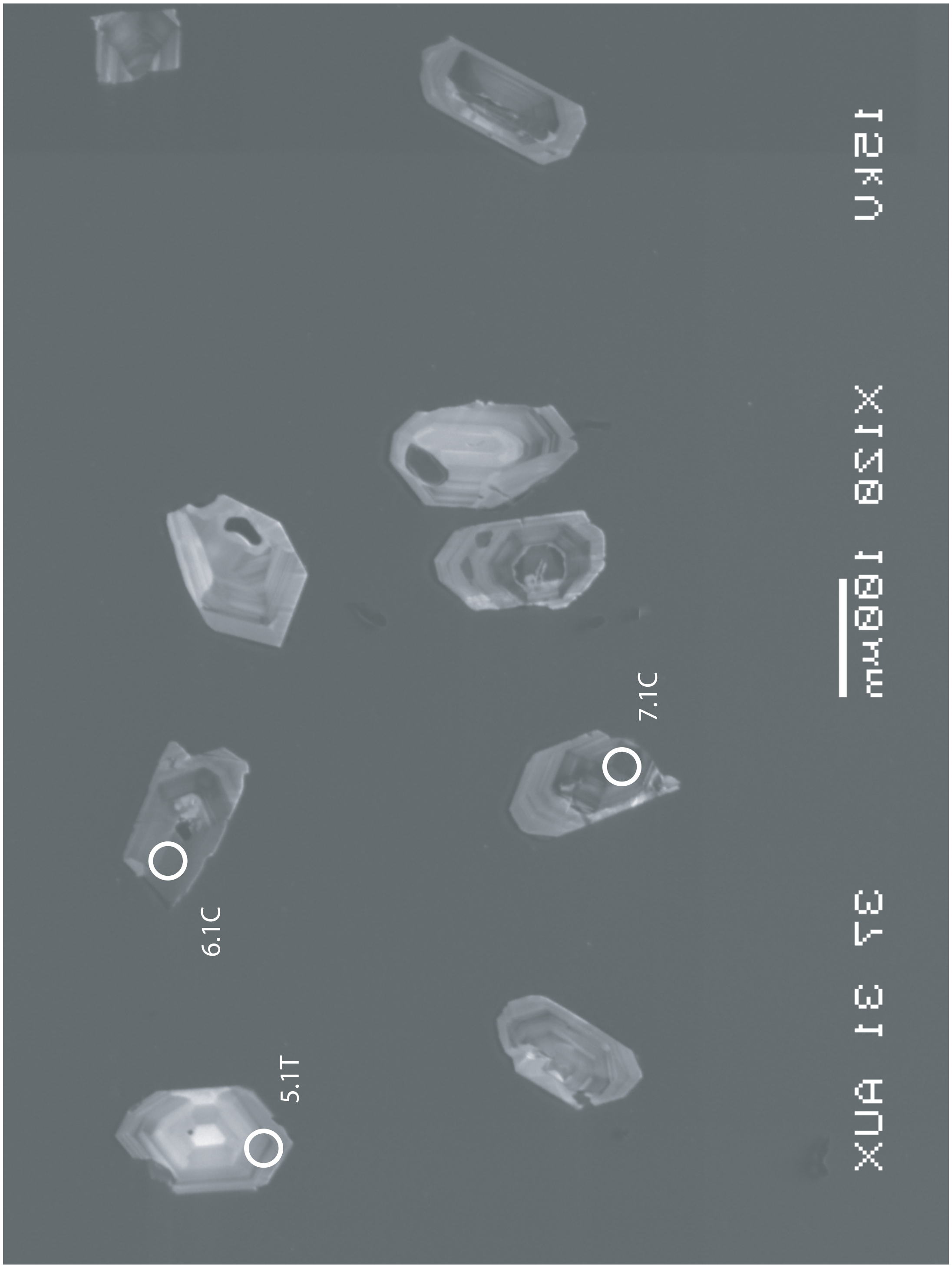
5.1T
6.1C
7.1C
15kV
X150
100µm

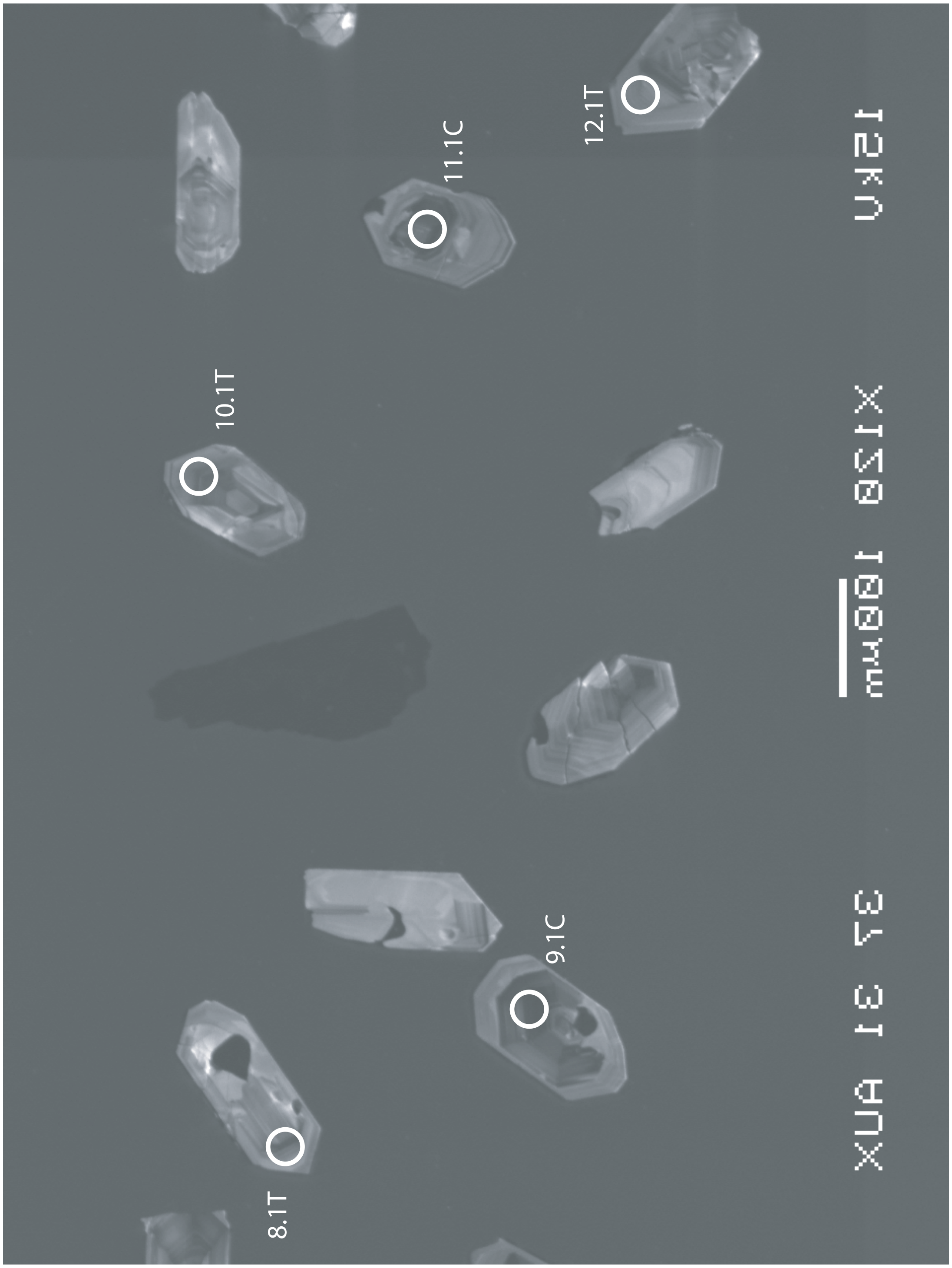
8.1T
9.1C
10.1T
11.1C
12.1T

13.1T
13.2C
14.1C
15.1C
16.1T
100μm
X150 05IX
12kV

XUA 15 31 35
X150 100µm
12kV UNM
17.1C
18.1T

12kV X150 100μm
35 31 AUX

12kV X150 100μm
XL30 ESEM

Figure C4:
Cathodoluminsecence images of zircons from sample SML120z with spots from U-Pb SHRIMP-RG analyses marked

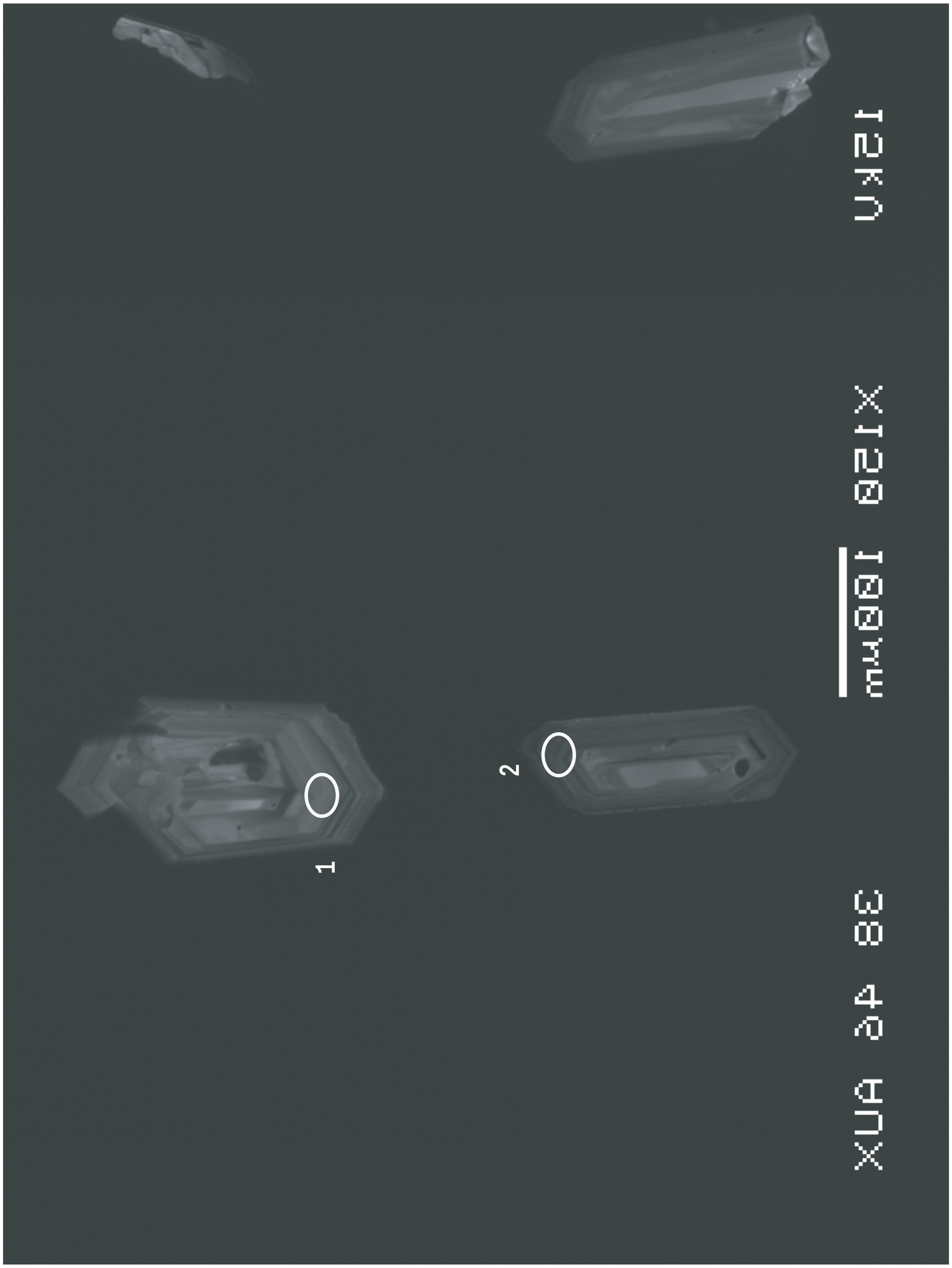
1
2

XUA 24 8C
3.2
3.1C
4.1C
5.1I

8.2R
8.1I
7.2I
7.1T
6.1I
6.2R

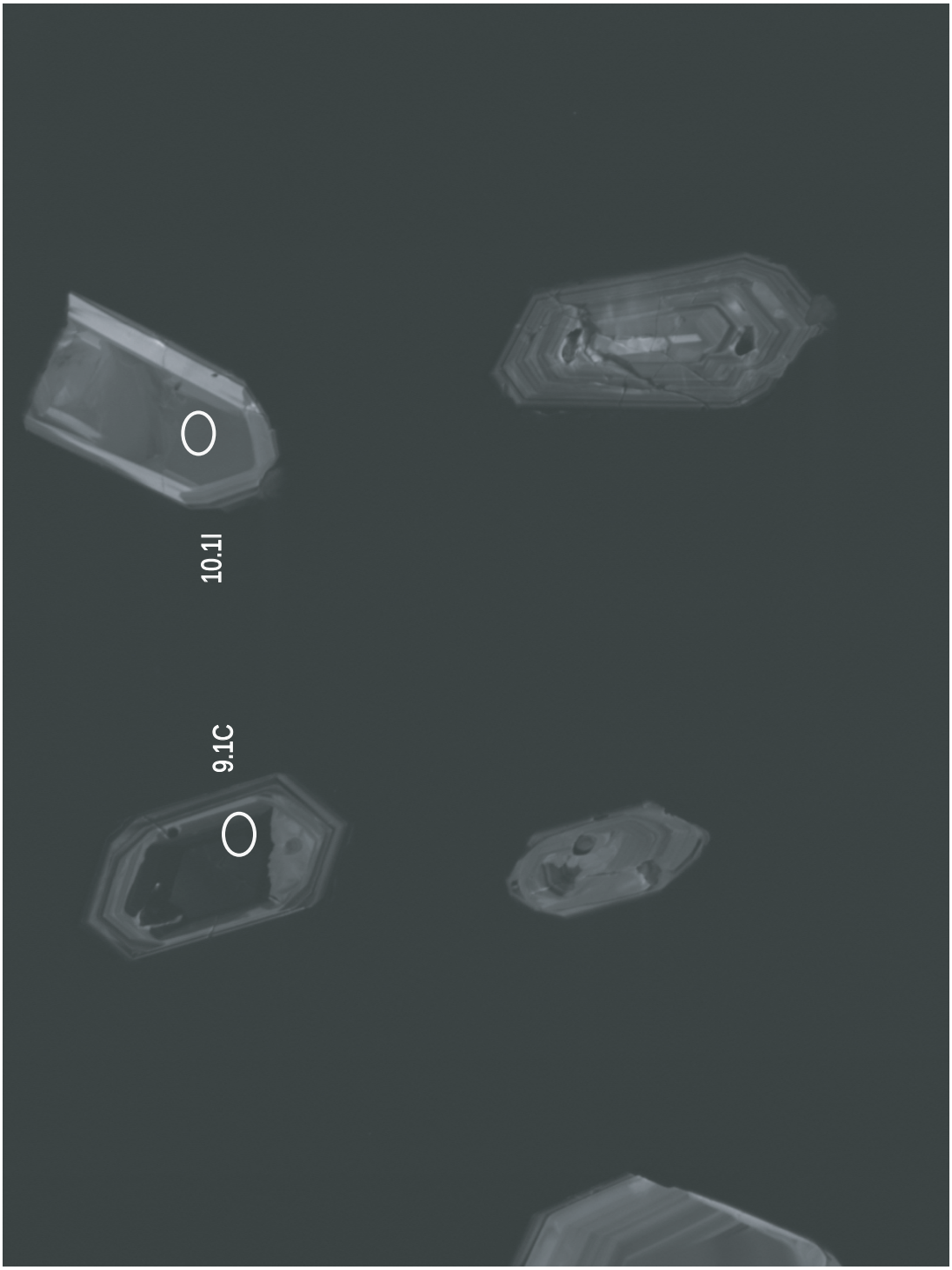
10.1I
9.1C

11.2I
11.1R

13.2R
13.1I
12.2R
12.1I
XUA 24 88
100µm 020X 12kV

14.1R
100µm
X180
12kV

17.1R
15.2C
15.1R
16.1C
100µm
X150 015
12kV UNR
XUA 24 88 38

18.1R
XUA 24 88
100µm
X120 021X
12kV UN21

Figure C5:
Cathodoluminsecence images of zircons from sample SML129z with spots from U-Pb SHRIMP-RG analyses marked

XUA 24 22
100mW
Uk2t
1
2R

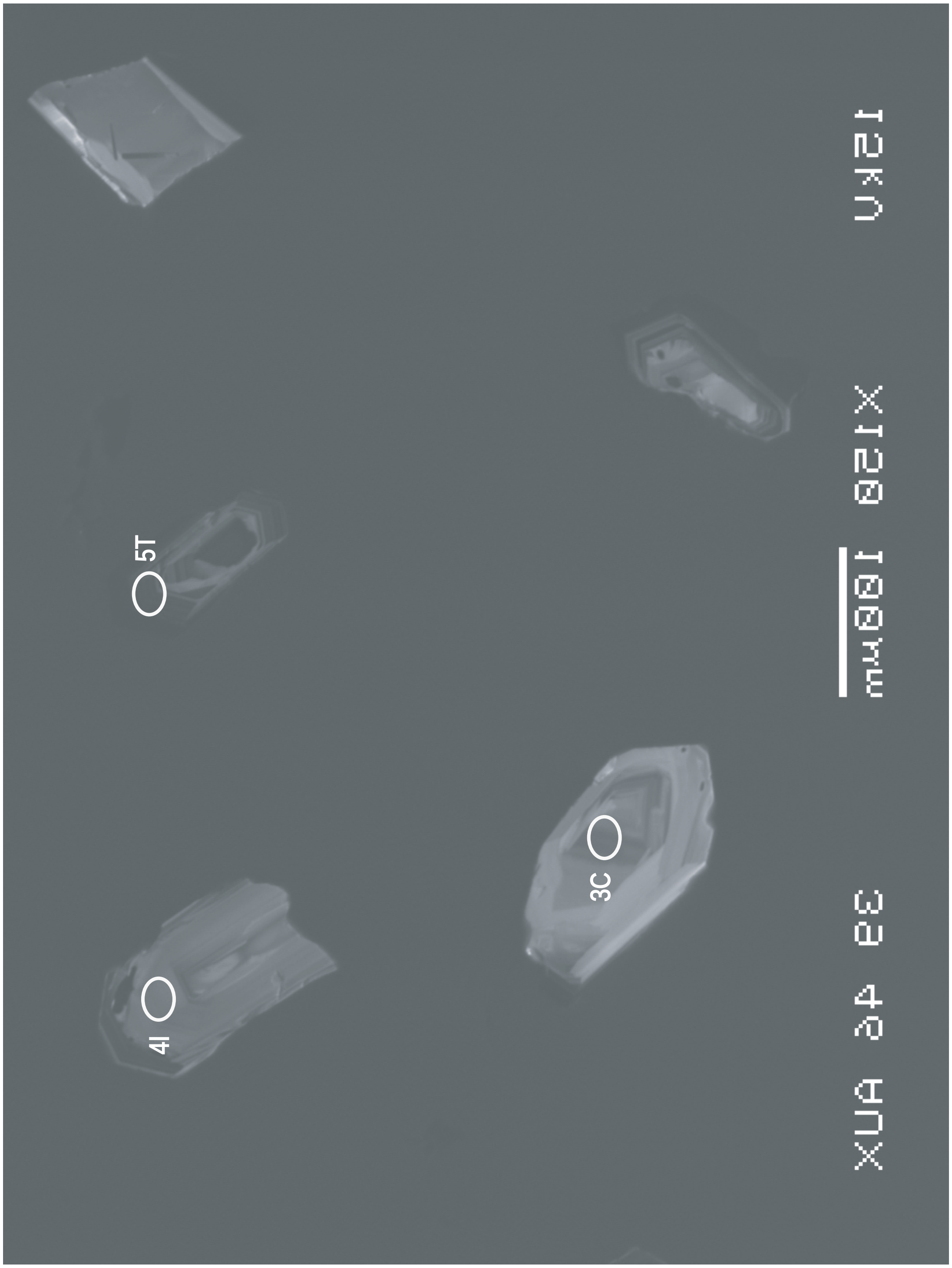
5T
3C
4I

XUA 24 8C
6C
7T
8.1C
8.2R
100µm
021X
UK21

XUA 24 8C
100µm
X120 021
12kV U121
9C
11.2R
11.1C
10R
12R

13R
12kV
X140 041X
100μm
24 Aug 38

12kV
X140 04
100mm
XUA 24 8C

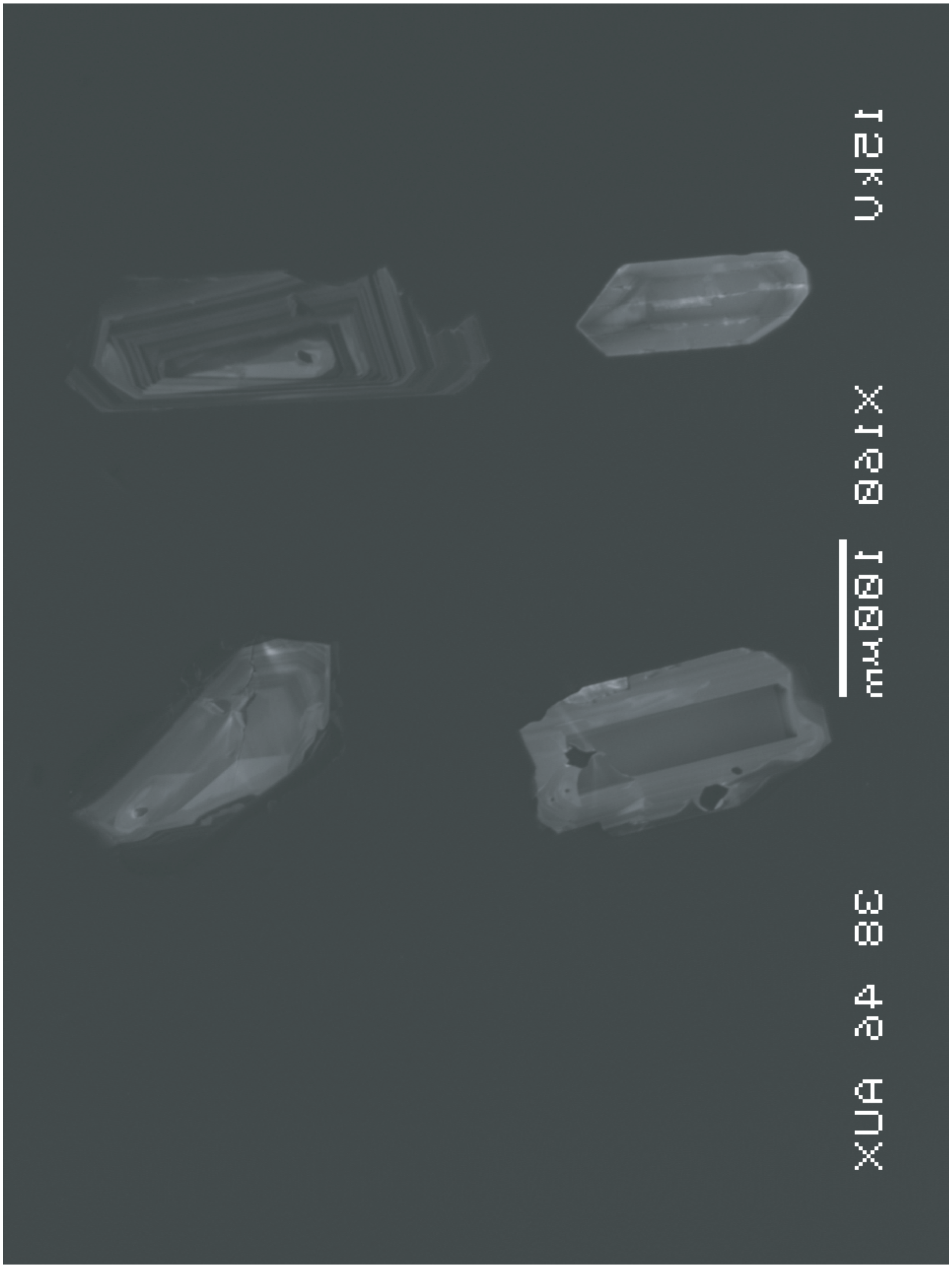

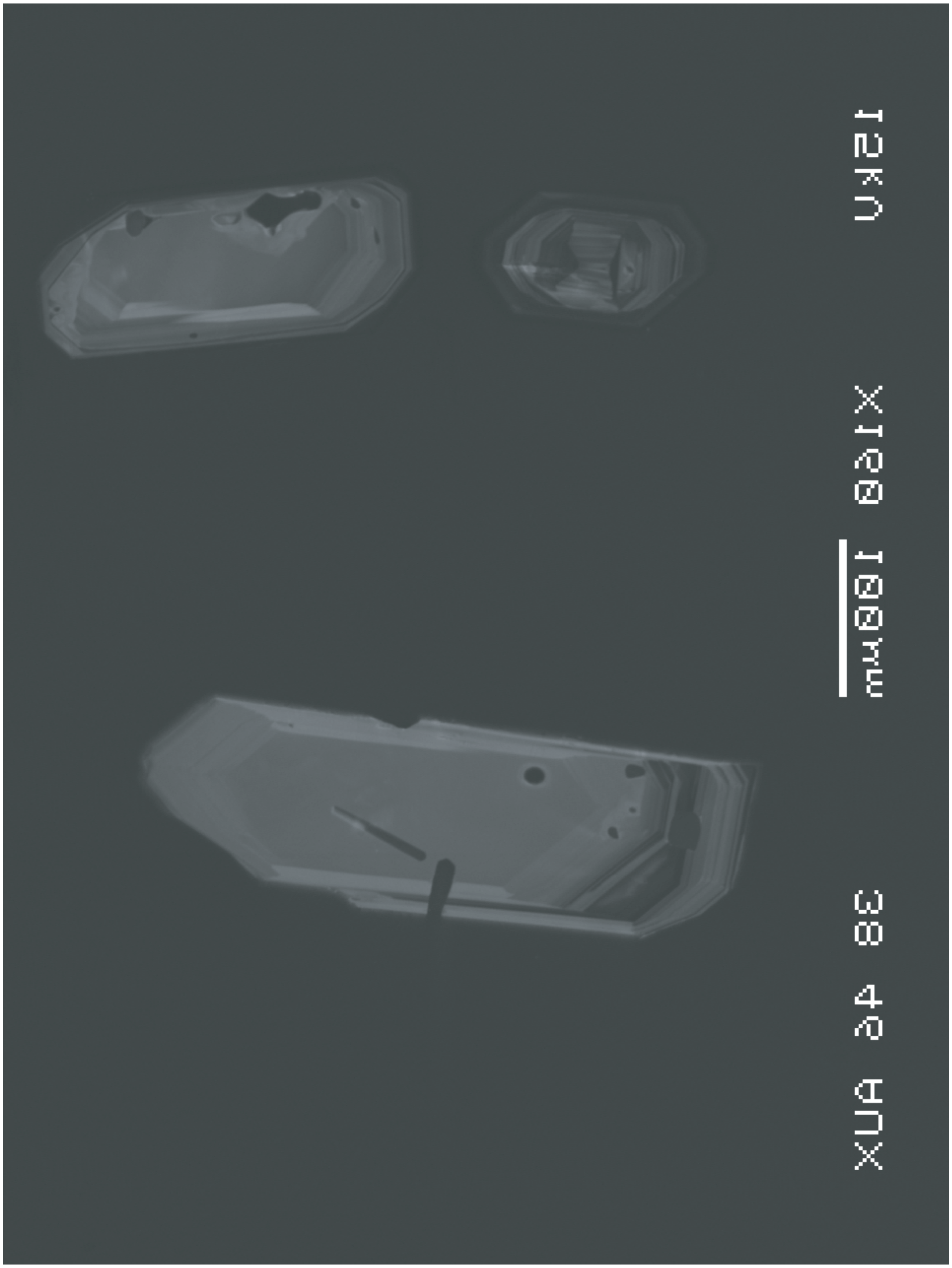

Figure C6:
Cathodoluminsecence images of zircons from sample MPL53z with spots from U-Pb SHRIMP-RG analyses marked

18.1T
1.1R
2.2C
2.3T
2.1
17.1
XUA 12 32
100µm
X130 001X
12kV U121

12kV UNK
X130 100μm
35 31 AUX
18.1T

6.1C
5.1C
4.1T
12kV X130 100µm
XUA 31 35

XUA 31 32
8.1T
7.1T
X130 100μm
12kV UNM

12kV X130 100μm 35 31 XUA
11.1T
10.1C
9.1C

12.1C
13.1C
14.1C
100µm
X130 031X
12kV UNK
XUA 31 32

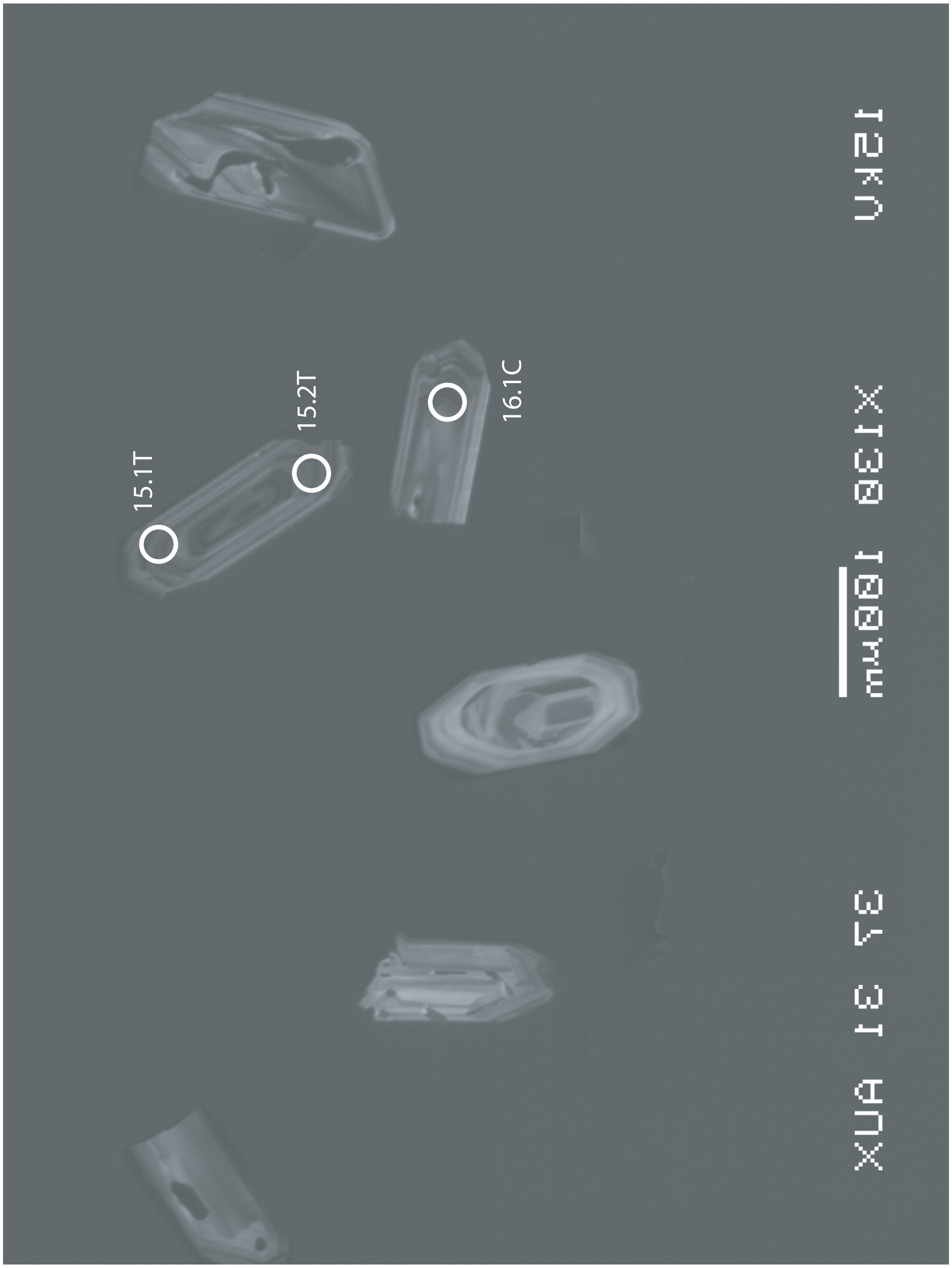
15.1T
15.2T
16.1C
15kV
X130
100µm

APPENDIX D:

Zircon Elemental Data and

Cathodoluminescence Images from the

Spirit Mountain Batholith,

SHRIMP-RG Analyses from September, 2005

Table D1: Complete TE data from 9/05 SHRIMP-RG analysis of zircons from SMB. * indicates data omitted due to high Fe.

	P ppm	Ca Rel to CZ3	Fe Rel to CZ3	Ti49 ppm	Y ppm	Yb ppm	Y/Yb	Hf ppm	Th ppm	U ppm	Th/U
LGZTE-1.1C	140	0.6	0.8	4.8	1822	945	1.9	13557	2702	1230	2.20
LGZTE-1.2T	170	0.9	1.5	4.7	2321	1431	1.6	15630	2600	2082	1.25
LGZTE-1.3T2	150	0.8	0.7	7.5	642	236	2.7	11213	76	69	1.10
LGZTE-2.1C	166	0.8	0.6	9.4	1352	415	3.3	10051	136	68	2.00
LGZTE-2.2T	173	0.9	2.3	4.6	2555	1464	1.7	14762	2752	1625	1.69
LGZTE-2.3T2*	1963	385	1582	36.1	1218	683	1.8	13853	445	397	1.12
LGZTE-2.4T2*	199	1.9	133	9.3	1513	715	2.1	13793	529	401	1.32
LGZTE-3.1T1	171	0.9	1.8	5.9	2882	1586	1.8	14332	3053	2268	1.35
LGZTE-3.2T2	108	1.2	1.2	3.2	1659	950	1.7	16716	951	1102	0.86
LGZTE-3.3C	175	1.2	1.5	24.6	1476	387	3.8	7536	103	29	3.57
LGZTE-3.4C2*	329	1.3	331	13.1	1551	451	3.4	10129	225	117	1.92
LGZTE-4.1C	392	1.0	0.8	17.9	4416	1156	3.8	7766	803	251	3.20
LGZTE-4.2	224	0.9	0.8	17.2	993	329	3.0	9156	132	69	1.91
LGZTE-4.3T	228	20.9	5.8	6.3	1221	645	1.9	12930	385	322	1.20
LGZTE-4.4X	309	0.9	0.8	19.7	2246	634	3.5	8408	505	180	2.80
LGZTE-5.1C	380	1.2	1.3	7.0	2902	978	3.0	12417	1218	641	1.90
LGZTE-5.2	287	1.2	0.9	8.7	1372	441	3.1	10653	382	203	1.88
LGZTE-5.3T	624	88	1.0	5.2	1154	515	2.2	13093	815	475	1.72
LGZTE-6.1C*	273	3.8	817	85.6	2411	1180	2.0	10032	3806	1938	1.96
LGZTE-6.2*	223	1.4	369	12.8	1504	613	2.5	11512	868	532	1.63
LGZTE-6.3T*	332	1.2	104	11.7	5587	2884	1.9	13608	13141	4823	2.72
LGZTE-7.1C	192	1.2	30.6	4.9	2637	1258	2.1	14884	3534	1862	1.90
LGZTE-7.2T	1393	302	2.7	7.6	1206	419	2.9	10182	208	151	1.38
LGZTE-7.3	170	2.0	7.0	5.9	843	339	2.5	11291	115	108	1.07
LGZTE-8.1C	431	2.0	1.3	3.3	1934	963	2.0	13812	921	756	1.22
LGZTE-8.2T	231	2.8	0.8	7.7	1084	408	2.7	10979	161	121	1.33
LGZTE-8.3T2	223	1.6	1.8	10.2	1215	448	2.7	10601	210	228	0.92

Table D1: Complete TE data from 9/05 SHRIMP-RG analysis of zircons from SMB. * indicates data omitted due to high Fe.

	P ppm	Ca Rel to CZ3	Fe Rel to CZ3	Ti49 ppm	Y ppm	Yb ppm	Y/Yb	Hf ppm	Th ppm	U ppm	Th/U
SWZTE-1.1T	154	0.8	0.9	10.6	728	242	3.0	9773	110	79	1.40
SWZTE-1.2C	156	0.9	1.0	6.4	764	278	2.7	10890	110	101	1.09
SWZTE-10.1C	190	0.8	0.9	7.2	1585	479	3.3	10669	188	108	1.75
SWZTE-10.2T	112	0.7	0.9	7.3	520	184	2.8	10462	63	61	1.03
SWZTE-10.3T2	171	0.6	0.7	5.1	1341	617	2.2	11402	273	277	0.98
SWZTE-2.1C	217	0.8	1.1	5.3	1906	624	3.1	10948	315	188	1.68
SWZTE-2.2T	162	0.8	0.8	9.9	745	252	3.0	9582	110	71	1.55
SWZTE-3.1T	123	0.7	0.9	11.8	505	171	2.9	9658	80	52	1.54
SWZTE-3.2C	315	0.9	1.2	10.8	2947	809	3.6	9021	646	205	3.15
SWZTE-3.3T2	309	0.7	1.1	12.4	1742	556	3.1	8837	265	141	1.89
SWZTE-4.1C	172	0.8	0.9	15.2	1615	460	3.5	8168	175	65	2.71
SWZTE-4.2T1	167	1.2	1.4	29.6	884	292	3.0	10813	164	144	1.15
SWZTE-4.3T2	184	0.7	0.8	14.4	953	331	2.9	8296	101	70	1.45
SWZTE-4.4T3	151	0.7	0.8	13.3	605	213	2.8	9165	80	49	1.62
SWZTE-4.5T4	234	0.5	0.6	5.7	1347	456	3.0	11448	233	203	1.15
SWZTE-4.6T5	209	0.5	0.6	12.7	978	324	3.0	9978	203	123	1.65
SWZTE-4.7T6	249	0.7	1.4	5.8	1459	523	2.8	11496	220	214	1.03
SWZTE-5.1C	364	0.7	1.0	14.8	4244	1082	3.9	8099	733	242	3.03
SWZTE-5.2T	221	0.6	0.9	13.6	1030	322	3.2	8914	221	106	2.08
SWZTE-6.1C	141	0.9	0.8	19.4	879	253	3.5	8468	89	41	2.16
SWZTE-6.2T	341	0.8	1.0	10.3	2057	620	3.3	10003	640	283	2.26
SWZTE-7.1C	344	1.0	1.3	5.3	2307	1109	2.1	12453	1258	925	1.36
SWZTE-7.2T	188	1.6	1.0	11.9	800	273	2.9	9390	137	77	1.77
SWZTE-7.3T2	167	1.0	0.8	16.9	676	218	3.1	8464	90	51	1.79
SWZTE-8.1C	242	0.8	0.8	32.3	1819	499	3.6	7472	162	48	3.36
SWZTE-8.1T	299	0.8	0.9	11.6	1578	471	3.4	9507	468	192	2.43
SWZTE-8.3T	495	0.9	0.9	25.5	2493	698	3.6	7847	757	196	3.86
SWZTE-8.4T	274	0.3	0.5	14.3	1264	369	3.4	8477	284	119	2.39
SWZTE-9.1C	287	0.9	1.5	5.9	1706	973	1.8	15037	1081	850	1.27
SWZTE-9.2T	166	0.8	0.7	11.1	765	245	3.1	9084	104	66	1.59

Table D1: Complete TE data from 9/05 SHRIMP-RG analysis of zircons from SMB. * indicates data omitted due to high Fe.

	P ppm	Ca Rel to CZ3	Fe Rel to CZ3	Ti49 ppm	Y ppm	Yb ppm	Y/Yb	Hf ppm	Th ppm	U ppm	Th/U
SWZTE-9.3T2	156	0.8	0.8	5.2	832	320	2.6	11609	269	196	1.37

Figure D1:
Cathodoluminsecence images of zircons from sample LGZTE with spots from Trace Element SHRIMP-RG analyses marked

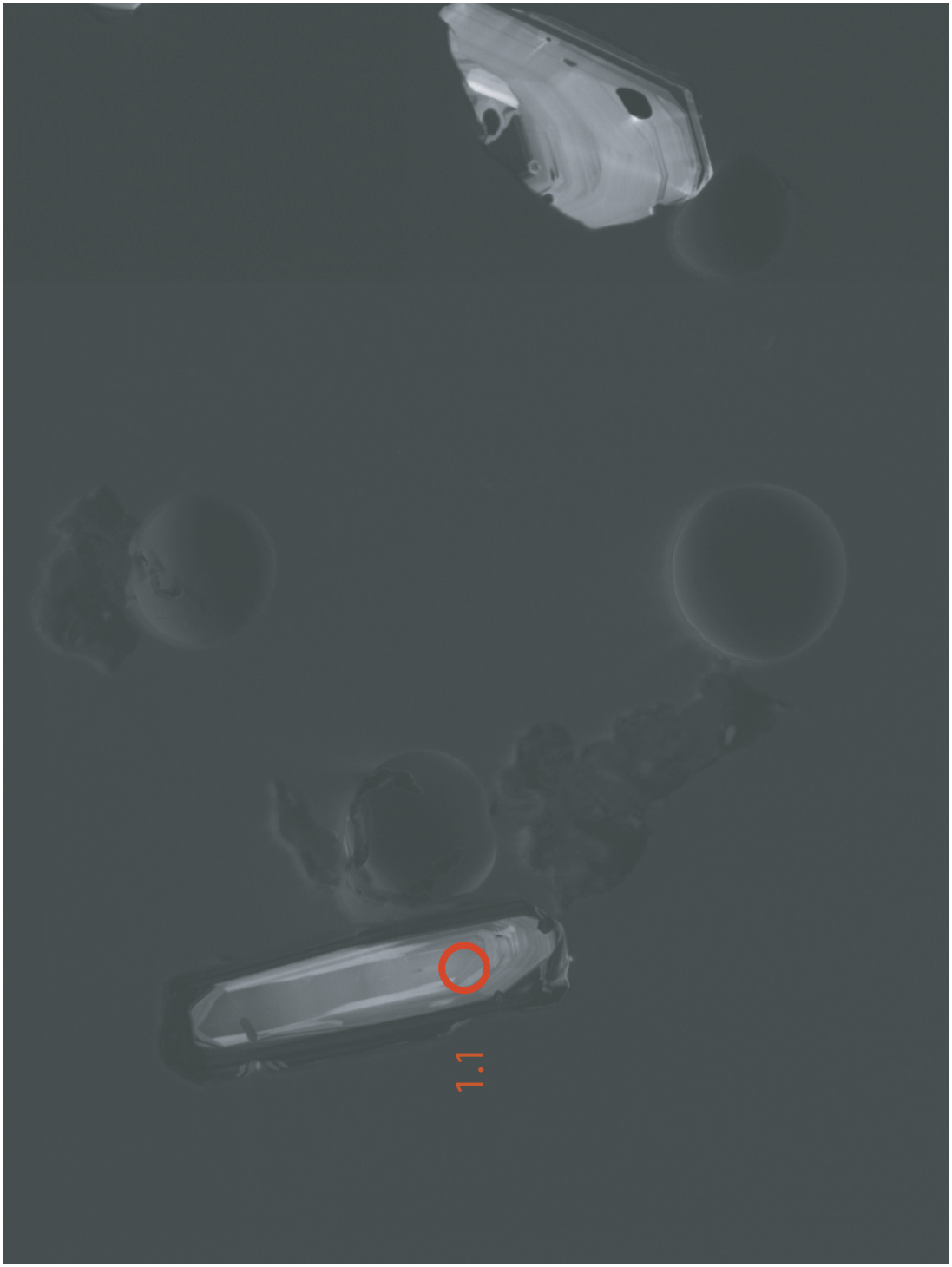
1:1

1.2T
1.3T2
1.1C

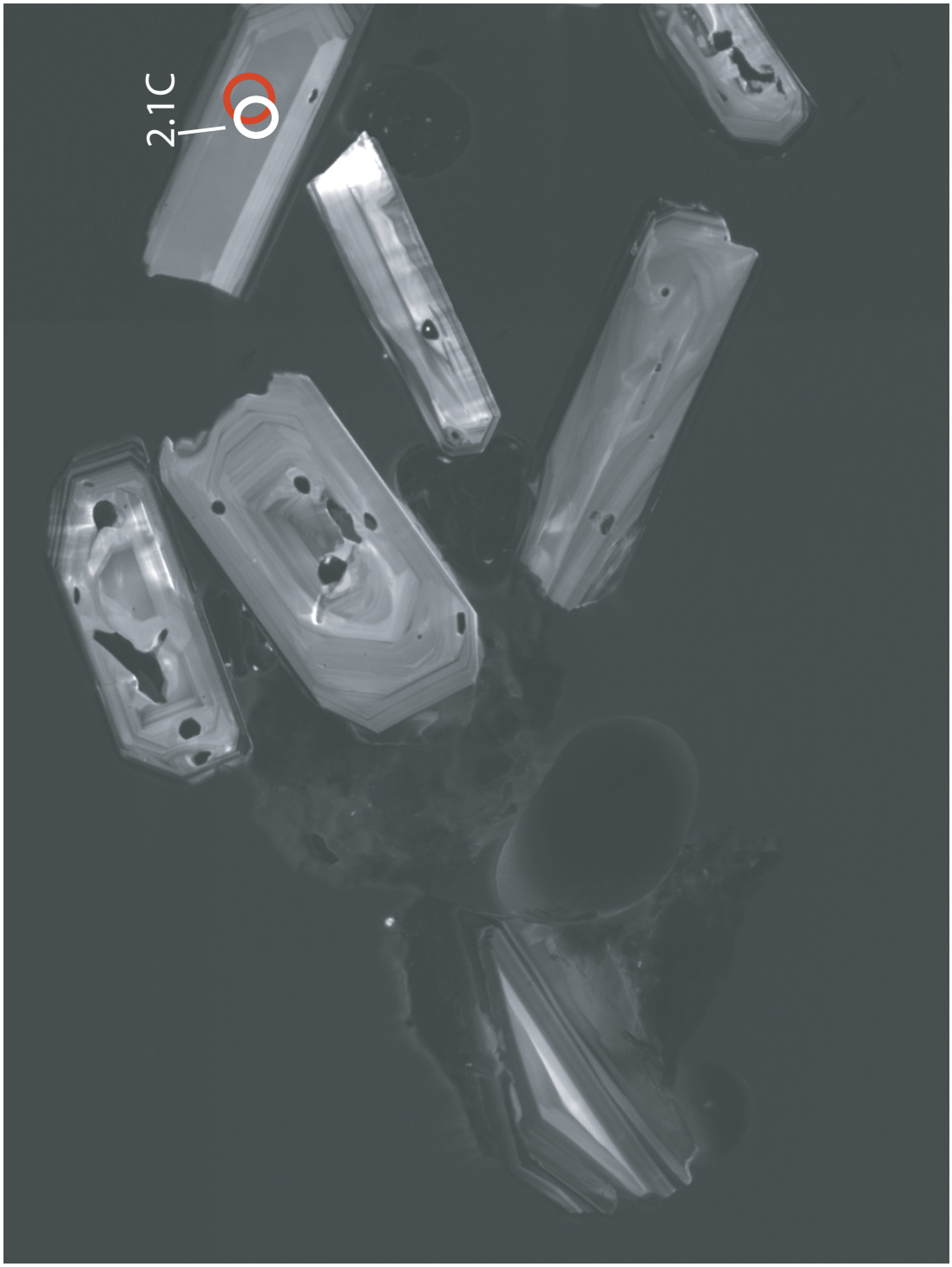
2.1C

8.1
5.1
4.1
6.1
2.2T
2.4T3
2.1C

10.1
10.2
7.1
9.1
8.1

14.1
4.3T
4.2
4.1C
3.4C2
3.3C
3.2T2
3.1T

14.1
8.1C
8.3T2
8.2T
4.3T
16.1
6.2
6.1C
7.3

18.1
7.3
7.1C
7.2T

Figure D2:
Cathodoluminsecence images of zircons from sample SWZTE with spots from Trace Element SHRIMP-RG analyses marked

SWZ-7

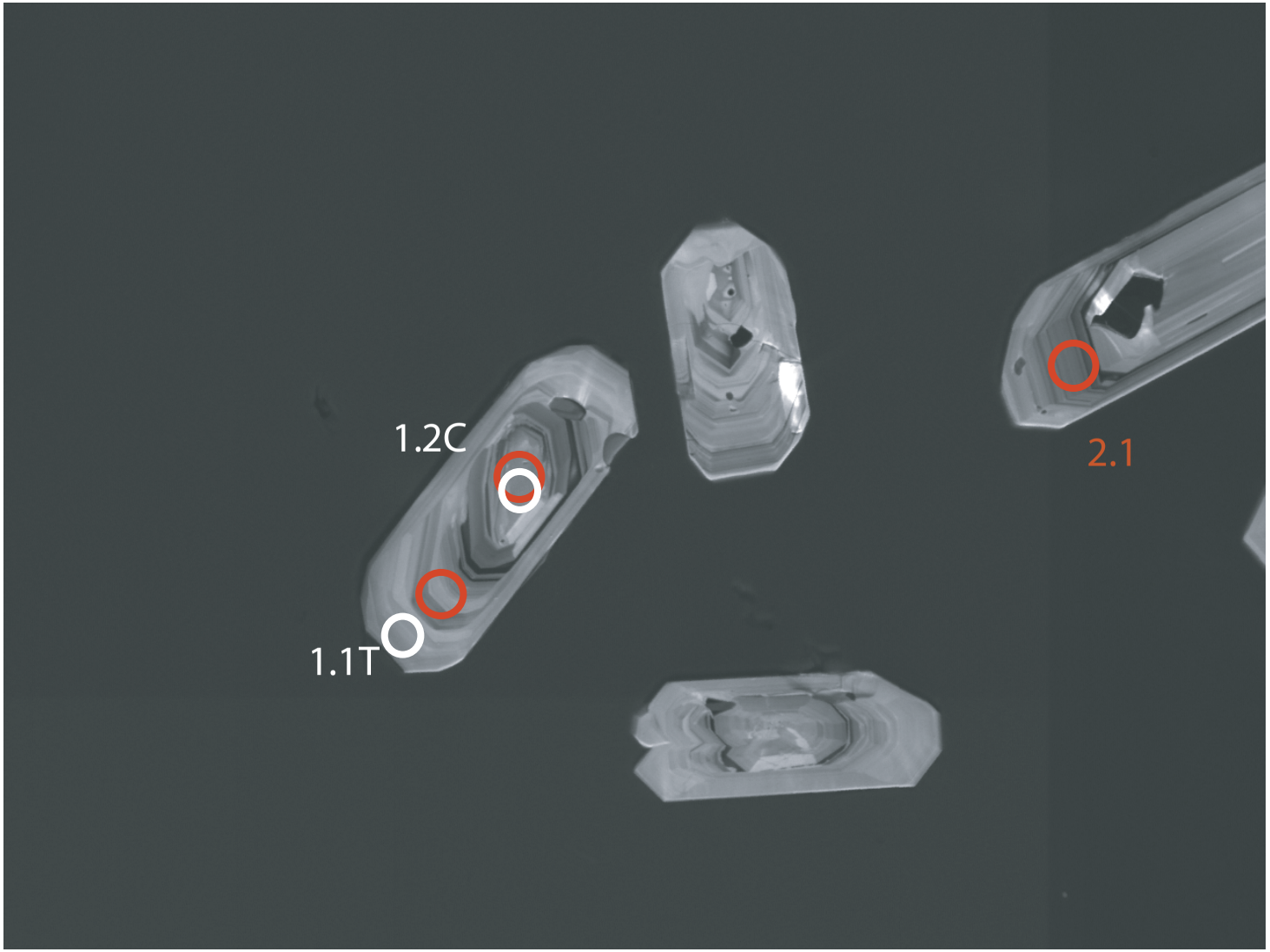

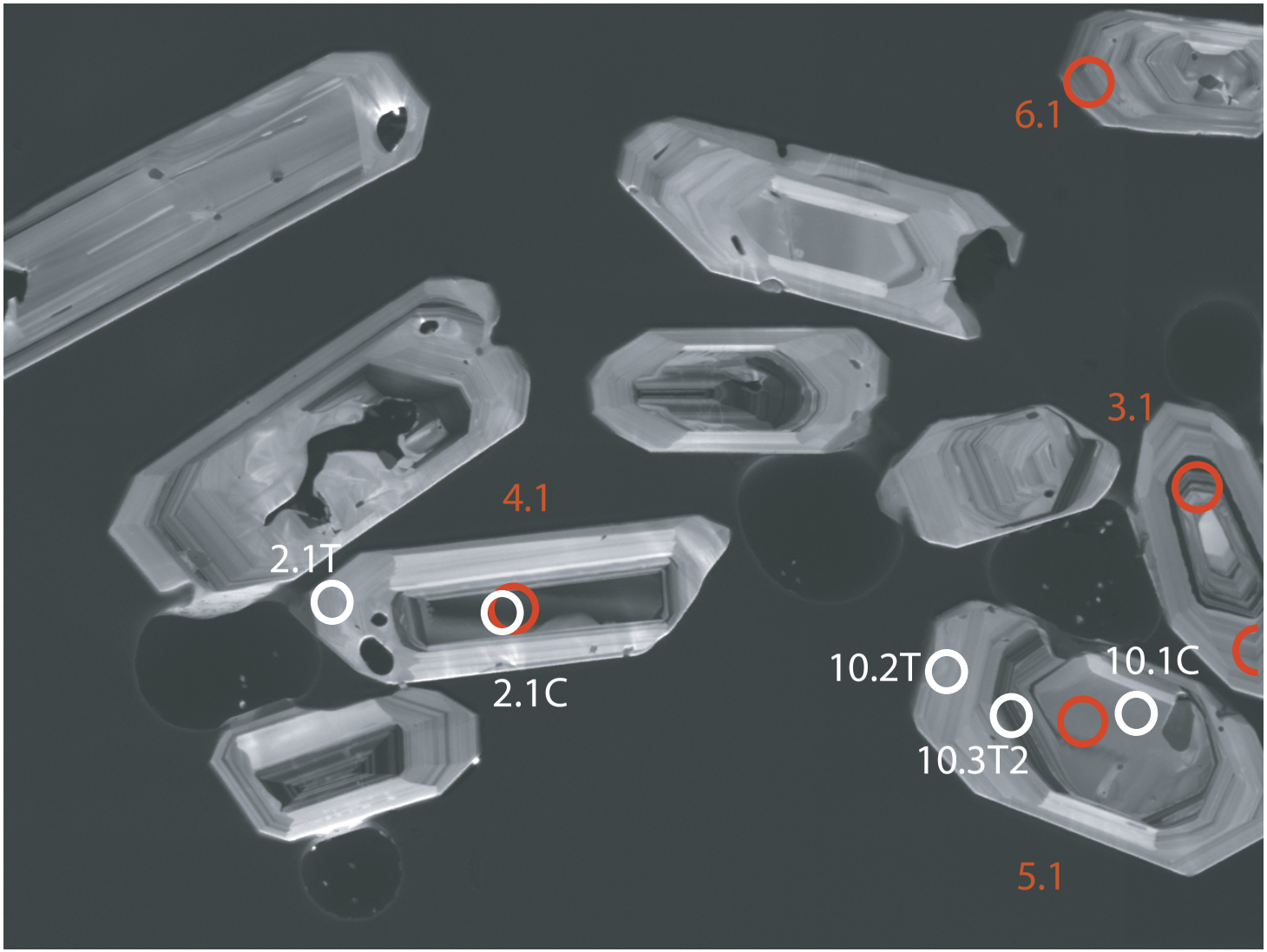
6.1
3.1
4.1
2.1T
2.1C
10.2T
10.1C
10.3T2
5.1

3.1T
3.3T2
7.2
7.1
3.2C
3.2
5.2

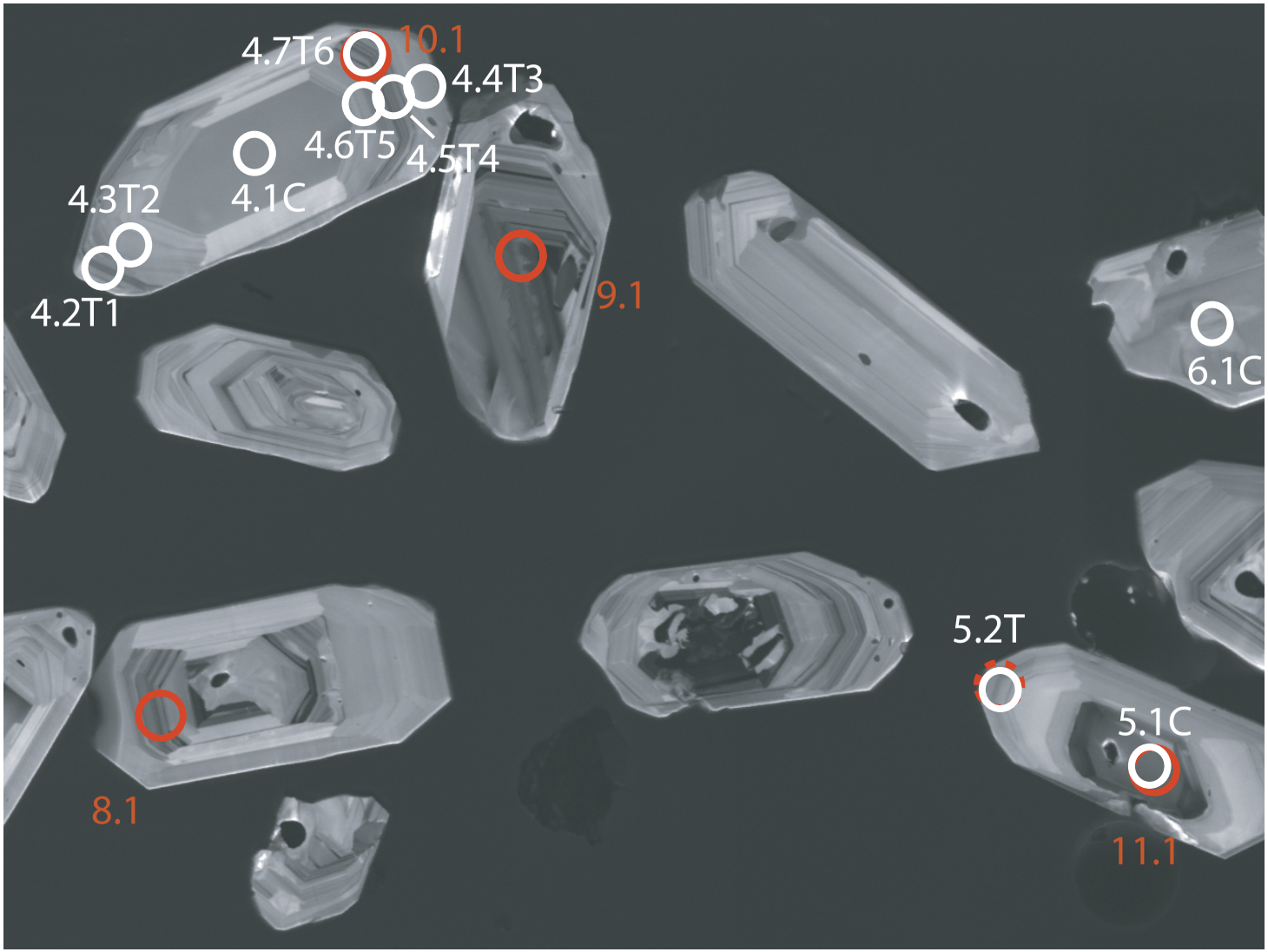
4.7T6
10.1
4.4T3
4.6T5
4.5T4
4.1C
4.3T2
4.2T1
9.1
6.1C
5.2T
5.1C
8.1
11.1

12.1
6.2T
13.1
14.1
6.1C

15.2
8.1C
8.3T
8.1T
15.1
8.4T
16.2
7.2T
16.1
7.3T2
7.1C

9.1C
9.3T2
17.1
9.2T
17.2

APPENDIX E:

Zircon Elemental Data and

Cathodoluminescence Images from the

Spirit Mountain Batholith,

SHRIMP-RG Analyses from March, 2006

Table D2: Complete trace element data from March, 2006 SHRIMP-RG analysis of zircons from the Spirit Mountain batholith.

	P ppm	Ca Rel to CZ3	Sc ppm	Ti48 ppm	Ti49 ppm	Fe Rel to CZ3	Y ppm	Zr96	Zr (Zr2O)	Hf ppm	Pb206	Th ppm	U ppm	Th/U
BC101-1.5	267.2	1.0	23.7	4.3	4.4	0.8	1275	472663	454883	11054	0.6	322	241	1.34
BC101-1.6R	341.8	0.7	44.1	15.7	15.2	0.5	926	463627	426369	7789	0.1	64	30	2.14
BC101-1E	256.6	18.4	62.9	137.3	105.3	27.6	1189	483142	565936	11032	2.9	341	436	0.78
BC101-1E2	223.7	1.7	17.0	5.6	5.6	1.2	796	468632	469072	10381	0.4	154	117	1.32
BC101-1LGC	424.4	1.4	22.5	8.7	8.6	1.0	2488	450201	424800	9149	0.3	253	103	2.46
BC101-1LGI	263.3	1.6	18.2	5.6	5.9	0.9	908	477299	451121	10128	0.3	144	108	1.33
BC101-2.1T	243.4	1.3	22.7	7.7	7.7	1.2	868	470475	463742	10178	0.3	150	112	1.35
BC101-2.2C	335.2	1.3	51.9	12.9	13.0	0.9	2402	456487	434697	6696	0.2	214	70	3.06
BC101-2.3I	211.3	1.2	20.6	9.2	9.7	0.9	601	457048	424938	7443	0.2	113	54	2.09
BC101-2.4I	200.8	1.9	21.6	4.3	4.2	1.1	885	451719	407586	10878	0.5	222	177	1.25
BC101-2.5T2	300.6	3.5	27.6	6.7	6.7	0.9	1174	443707	415154	9512	0.4	183	116	1.58
BC101-3.1T	159.4	14.8	40.5	4.5	4.2	1.6	671	437817	402216	10545	0.8	402	241	1.67
BC101-3.2I	263.4	1.5	24.3	4.4	4.8	1.0	1388	446017	387085	10472	1.0	964	419	2.30
BC101-3.3R	776.9	365.6	42.4	10.9	3.8	0.1	698	425912	413086	11101	0.7	299	226	1.33
BC101-3.4C	216.2	2.5	36.1	5.0	9.4	1.2	1170	441203	379580	7836	0.2	125	49	2.54
BC101-3.5T2	210.3	2.9	33.8	4.9	4.6	2.1	1069	447820	399159	10828	1.1	509	326	1.56
BC101-4.1R	216.9	1.8	29.9	4.7	4.7	1.4	1216	456314	429958	10489	0.6	336	234	1.44
BC101-4.2I	247.9	1.2	20.1	4.9	5.8	0.8	890	441747	424790	9912	0.3	137	105	1.31
BC101-4.3C	222.7	1.6	47.8	4.6	3.3	1.2	1502	450294	400662	11800	2.3	1580	887	1.78
BC101-5.1I	217.6	0.7	19.8	6.0	6.2	0.5	810	498075	463991	11120	0.3	140	95	1.46
BC101-5.2R	329.0	1.4	32.2	11.4	11.2	1.3	871	456532	395801	8805	0.3	156	70	2.23
BC101-6.1I	260.0	1.4	41.3	15.0	15.0	1.0	1712	446986	418727	7562	0.2	195	61	3.18
BC101-7.1I	263.2	1.2	22.5	5.7	5.6	1.3	1412	458518	414461	9442	0.3	160	84	1.91
BC101-7.2R	243.6	1.8	48.5	3.7	3.6	2.2	1686	467174	405547	13544	3.1	1719	1096	1.57
BC101-8.1R	283.7	2.7	19.0	6.2	6.4	1.0	1014	457892	409614	9658	0.4	164	111	1.47
BC101-8.2I	280.1	2.4	20.5	5.6	5.6	1.0	973	446219	413081	9107	0.4	198	125	1.58

Table D2: Complete trace element data from March, 2006 SHRIMP-RG analysis of zircons from the Spirit Mountain batholith.

	P ppm	Ca Rel to CZ3	Sc ppm	Ti48 ppm	Ti49 ppm	Fe Rel to CZ3	Y ppm	Zr96	Zr (Zr2O)	Hf ppm	Pb206	Th ppm	U ppm	Th/U
BC101-9.1R	189.4	1.5	29.0	5.4	5.4	2.5	593	486066	453597	11784	0.5	186	165	1.13
BC101-9.2IR	394.9	1.1	80.2	6.4	6.3	0.7	2667	449643	417028	9738	1.5	895	528	1.69
BC101-9.3I	157.9	2.1	19.1	6.8	6.9	1.0	1042	449394	408313	9315	0.3	182	104	1.76
BC101-9.4C	212.3	1.5	21.2	5.4	5.6	0.8	1080	461279	433895	9406	0.3	151	86	1.75
BC101-10.1R	191.4	1.2	24.7	4.3	4.4	1.1	998	465718	416466	10746	0.6	348	232	1.50
BC101-10.2C	624.1	1.2	71.6	8.6	8.6	1.6	2507	447196	405081	7704	0.8	839	260	3.22
BC101-10.3I	288.4	1.1	50.3	4.6	4.7	1.4	2143	455370	413795	12465	3.0	1688	1048	1.61
BC101-11.1R	307.0	1.4	34.8	15.6	16.3	1.0	788	486601	447264	8584	0.1	85	36	2.37
BC101-11.2I	313.4	1.2	22.6	5.4	5.7	0.7	1322	454664	433513	10207	0.5	234	160	1.46
BC101-11.3R	290.6	1.1	29.1	8.1	8.1	0.9	1024	466289	451986	9613	0.4	151	119	1.26
BC101-12.1T	256.1	2.4	47.3	5.0	5.0	1.6	1098	448393	396441	9959	1.0	483	281	1.72
BC101-12.2I	405.6	4.0	31.4	6.4	6.2	3.3	1794	467474	400512	10584	1.3	670	444	1.51
BC101-12.3C	264.6	2.4	20.4	16.4	16.5	55.7	853	465854	465553	11169	0.3	143	103	1.39
BC101-12.4C	320.1	0.5	27.0	5.9	6.0	1.5	1128	545950	536961	11303	0.2	135	100	1.36
BC101-13.1C	244.2	2.9	21.5	5.5	5.3	1.2	1974	473604	423751	9697	0.6	322	145	2.22
BC101-13.2IR	275.8	5.0	24.1	4.4	4.6	1.4	1327	445993	409298	11128	0.9	396	273	1.45
BC101-13.3R	315.5	8.4	38.0	7.9	7.6	1.2	1056	459913	431815	9387	0.3	162	104	1.57
BC101-14.1C	312.4	2.2	61.6	15.3	15.2	1.5	1996	452651	411001	7534	0.2	227	72	3.13
BC101-14.2IR	358.7	1.8	32.9	4.6	4.8	1.0	1889	454067	402464	10550	0.8	363	287	1.27
BC101-14.3I	294.3	2.1	32.2	8.2	8.2	1.9	1189	493319	472456	9952	0.4	258	132	1.96
BC101-14.4IR	286.8	2.0	17.6	5.1	4.9	1.4	1070	447800	397553	10015	0.6	236	186	1.27
BC101-14.5R	276.8	1.7	25.4	8.6	8.7	1.0	910	434879	379381	8830	0.3	150	90	1.66

Table D2: Complete trace element data from March, 2006 SHRIMP-RG analysis of zircons from the Spirit Mountain batholith.

	P ppm	Ca Rel to CZ3	Sc ppm	Ti48 ppm	Ti49 ppm	Fe Rel to CZ3	Y ppm	Zr96	Zr (Zr2O)	Hf ppm	Pb206	Th ppm	U ppm	Th/U
DSCG-1.1T	290.7	2.1	32.2	9.0	9.2	1.5	999	477343	442198	8701	0.3	151	81	1.87
DSCG-1.2IR	305.4	3.0	38.4	5.7	5.6	2.2	1329	458487	427277	9978	1.0	576	322	1.79
DSCG-1.3C	259.5	3.1	35.7	7.3	7.3	2.0	808	465879	418313	8950	0.3	87	67	1.29
DSCG-10.1C	440.5	2.1	55.9	4.3	4.3	2.6	1638	462337	396236	12088	2.5	1372	796	1.72
DSCG-10.2IR	443.7	2.6	38.8	12.5	12.5	2.3	1071	446132	397025	8379	0.3	178	86	2.08
DSCG-11.1C	509.1	2.1	47.6	5.2	5.3	4.2	4798	464647	393190	10907	2.6	2084	926	2.25
DSCG-11.2I	419.5	1.7	64.7	5.2	5.1	3.3	2985	446879	386059	11105	4.7	3528	1607	2.19
DSCG-11.3R	181.7	2.1	24.1	3.9	3.8	2.0	868	439505	374817	10107	0.7	326	233	1.40
DSCG-12.1R	346.3	2.6	32.1	8.4	8.4	3.1	1259	469646	409499	9573	0.4	237	130	1.83
DSCG-12.2I	383.6	2.8	26.1	7.7	7.9	1.9	1435	456772	397905	8920	0.3	171	100	1.71
DSCG-13.1C	364.5	2.9	44.6	25.7	25.6	1.9	1371	470990	393742	7606	0.1	108	28	3.78
DSCG-13.2I	395.4	1.5	40.6	15.1	15.5	1.0	983	441824	394908	7530	0.1	128	48	2.68
DSCG-13.3T	309.1	2.2	28.5	9.1	9.3	2.2	830	459882	372022	9265	0.3	151	95	1.60
DSCG-14.1I	189.2	1.9	15.1	5.1	4.9	2.8	707	454777	411190	11205	0.4	133	113	1.17
DSCG-14.2R	406.8	1.8	50.6	8.7	9.2	1.8	1493	460406	396985	8884	0.3	163	114	1.44
DSCG-15.1R	343.4	1.5	39.9	6.5	6.8	1.7	1240	462341	434358	9410	0.5	266	162	1.64
DSCG-15.2I	181.6	1.7	27.3	13.5	13.7	1.3	419	444089	389432	7749	0.1	46	23	1.99
DSCG-16.1C	551.7	2.2	125.7	8.4	8.6	6.3	6251	466111	405664	10502	14.7	23287	4717	4.94
DSCG-16.2R	360.9	2.2	34.6	7.9	7.8	2.6	1362	474324	442869	9939	0.5	222	152	1.46
DSCG-17.1C	467.5	9.2	159.0	8.7	8.6	11.2	5645	448080	382225	11913	15.1	12991	4746	2.74
DSCG-17.2R	307.3	4.3	29.2	7.3	7.8	2.2	1335	444081	420723	9368	0.4	215	116	1.85
DSCG-18.1R	133.5	2.5	39.8	4.1	3.9	1.9	626	459311	420501	10603	0.5	209	166	1.26
DSCG-19.1IR	212.1	2.6	56.7	4.4	4.3	2.2	964	452162	408378	10059	1.1	684	358	1.91
DSCG-2.1T	343.1	2.7	28.9	5.3	4.9	2.2	1405	511279	469187	11512	0.9	501	340	1.48
DSCG-2.2I	226.3	4.4	24.3	8.9	8.6	2.2	540	471848	410382	9593	0.3	83	65	1.28
DSCG-2.3C	266.2	10.2	45.0	6.3	5.3	6.1	1733	454124	399988	13848	1.6	815	527	1.55
DSCG-2.3C2	493.9	2.3	42.8	10.4	10.6	1.8	1489	505384	438078	9570	0.4	196	102	1.93
DSCG-20.1R	224.6	2.5	43.8	4.4	3.9	1.7	1000	461562	420051	10508	0.8	335	243	1.38
DSCG-20.2I	271.5	2.5	41.8	15.1	15.0	1.3	825	460692	414144	7669	0.2	125	49	2.53
DSCG-21.1C	373.2	2.4	44.3	18.7	18.9	1.5	1961	464978	432510	7555	0.2	170	49	3.46
DSCG-21.2I	294.6	2.7	36.8	16.2	16.3	1.5	723	470424	439567	8490	0.2	85	37	2.31
DSCG-3.2C	344.4	3.1	52.1	16.4	15.8	1.8	2231	466806	400308	7047	0.3	255	68	3.77
DSCG-3.3IR	292.1	24.6	63.5	5.2	5.3	1.9	1164	470477	437868	10340	0.5	238	206	1.16
DSCG-4.1T	294.5	6.1	44.6	5.0	5.9	2.8	1055	517779	455253	11664	1.0	541	328	1.65

Table D2: Complete trace element data from March, 2006 SHRIMP-RG analysis of zircons from the Spirit Mountain batholith.

	P ppm	Ca Rel to CZ3	Sc ppm	Ti48 ppm	Ti49 ppm	Fe Rel to CZ3	Y ppm	Zr96	Zr (Zr2O)	Hf ppm	Pb206	Th ppm	U ppm	Th/U
DSCG-4.2R	274.3	4.2	52.1	5.3	5.3	2.3	1348	441183	388490	9683	0.7	268	212	1.26
DSCG-4.3IR	256.4	2.5	43.1	14.1	14.2	1.6	1123	460035	409388	7483	0.1	100	33	3.01
DSCG-4.4C	447.4	5.9	87.2	19.4	19.6	2.2	2495	448243	389739	6915	0.2	313	65	4.83
DSCG-5.1T	355.6	1.8	31.4	7.0	7.5	1.7	1053	448047	400125	9330	0.4	196	118	1.65
DSCG-5.2IR	561.6	213.0	35.6	4.6	4.6	0.0	545	491569	412718	12264	0.6	238	188	1.27
DSCG-5.3IR	144.1	8.7	46.8	12.9	14.2	16.0	566	497713	526512	12535	0.8	333	240	1.39
DSCG-5.4IR	330.4	4.7	26.8	7.2	6.8	1.8	1079	449448	409158	9673	0.3	226	130	1.74
DSCG-5.5C	288.8	3.9	71.6	4.7	4.7	3.5	2065	447356	403916	11706	2.4	1149	863	1.33
DSCG-5.6I	102.6	11.0	30.9	4.2	3.5	1.4	493	451082	395502	11038	0.3	116	100	1.16
DSCG-6.1T	151.8	3.7	71.6	4.4	4.6	2.8	757	448051	387690	11444	1.2	580	415	1.40
DSCG-6.2C	476.1	3.5	77.1	5.4	5.5	3.4	2460	473272	421051	11872	3.5	1810	1079	1.68
DSCG-7.1C	358.9	3.2	60.7	5.1	5.0	3.2	2510	516892	460693	13665	4.4	3408	1551	2.20
DSCG-7.2IR	427.9	2.6	39.9	8.8	8.6	143.9	1676	457568	422478	8943	0.8	605	230	2.63
DSCG-7.3IR	399.2	2.8	39.4	10.6	10.4	3.1	1341	498615	468435	9401	0.4	254	117	2.16
DSCG-7.4T	320.8	3.2	25.5	6.5	6.4	2.8	1073	476184	417746	10385	0.4	194	140	1.39
DSCG-8.1C	329.6	2.7	31.6	5.5	4.9	4.2	951	463518	415920	11336	0.7	322	242	1.33
DSCG-8.2IR	413.5	2.5	43.8	5.4	5.0	3.0	1610	452344	392029	10162	0.8	342	266	1.28
DSCG-8.3IR	301.5	3.4	28.0	11.5	11.2	2.6	785	441299	378279	8149	0.3	149	72	2.07
DSCG-8.4T	181.8	2.8	29.4	4.7	4.6	2.4	699	453043	379257	10656	0.7	322	208	1.54
DSCG-9.1C	1264.1	2.5	121.6	10.4	11.0	4.0	8890	455977	386240	7214	2.7	2932	833	3.52
DSCG-9.2IR	420.6	3.0	39.3	17.1	17.1	1.7	1042	488118	409684	8452	0.2	143	51	2.79
DSCG-9.3R	348.2	3.3	34.6	11.1	11.1	3.5	973	466380	389352	9270	0.3	171	99	1.72
DSCG-9.4IR	233.9	14.5	23.1	5.7	6.0	2.3	720	465847	436485	10304	0.5	243	153	1.59

Table D2: Complete trace element data from March, 2006 SHRIMP-RG analysis of zircons from the Spirit Mountain batholith.

	P ppm	Ca Rel to CZ3	Sc ppm	Ti48 ppm	Ti49 ppm	Fe Rel to CZ3	Y ppm	Zr96	Zr (Zr2O)	Hf ppm	Pb206	Th ppm	U ppm	Th/U
LGZ-1.2IC	340.3	1.3	60.6	17.0	17.5	1.4	1820	497399	477282	7860	0.2	201	68	2.97
LGZ-1.2T	335.4	2.7	154.0	7.5	6.9	119.4	4227	469253	406806	12147	10.0	9763	3590	2.72
LGZ-10.1I	280.6	2.2	48.4	21.6	21.3	27.5	1791	500257	433697	8003	0.1	125	30	4.15
LGZ-11.1IR	314.8	2.0	51.9	14.8	14.8	1.1	1045	452887	417795	7392	0.2	86	44	1.97
LGZ-2.1C	184.4	1.5	79.5	4.4	4.2	1.4	1698	449723	409869	12885	3.0	2151	973	2.21
LGZ-2.2R	203.2	1.5	102.8	4.1	3.9	2.6	2177	436952	363867	13107	4.2	1688	1424	1.19
LGZ-2.3I	215.5	1.7	20.5	7.4	7.1	1.4	596	457286	408338	9287	0.2	64	50	1.30
LGZ-3.1I	375.6	1.3	20.1	4.5	4.6	1.2	1768	459501	431708	11180	0.9	382	257	1.48
LGZ-4.1C	279.9	1.6	41.1	4.3	4.4	1.8	1971	486781	432483	13310	1.4	651	502	1.30
LGZ-5.1I	221.0	1.5	28.2	7.4	7.6	1.2	865	481483	443177	9335	0.2	108	70	1.54
LGZ-6.1T	192.7	8.1	52.9	4.2	4.4	1.8	1259	526217	468579	14445	1.9	971	629	1.54
LGZ-6.2I	560.0	1.6	62.4	18.4	18.1	1.3	3796	455006	389774	6983	0.2	436	100	4.36
LGZ-7.1I	269.8	1.6	67.1	3.8	3.6	2.6	2923	453260	397330	13803	5.8	5088	2087	2.44
LGZ-8.1I	586.0	1.6	77.0	20.6	20.7	1.3	3927	450214	394418	6357	0.4	516	120	4.31
LGZ-8.2IR	248.8	11.3	28.8	5.4	5.3	1.4	1016	470852	401109	11131	0.8	348	248	1.40
LGZ-9.1I	264.5	1.9	48.7	13.2	13.1	1.4	910	450628	384619	7300	0.1	77	41	1.88
LGZ-11.2I	554.1	2.0	61.6	13.6	13.1	1.0	4658	478108	424809	7539	0.7	819	219	3.74
LGZ-12.1I	156.1	2.7	45.4	3.0	3.0	2.5	997	456556	404950	13519	2.2	1273	712	1.79
LGZ-13.1C	200.1	2.4	60.3	4.6	4.2	2.5	1819	440414	386808	13149	2.7	1569	936	1.68

Table D2: Complete trace element data from March, 2006 SHRIMP-RG analysis of zircons from the Spirit Mountain batholith.

	P ppm	Ca Rel to CZ3	Sc ppm	Ti48 ppm	Ti49 ppm	Fe Rel to CZ3	Y ppm	Zr96	Zr (Zr2O)	Hf ppm	Pb206	Th ppm	U ppm	Th/U
SWZ-1.1I	277.8	7.4	26.5	9.3	9.4	1.6	865	476078	437340	9536	0.3	127	76	1.67
SWZ-10.1C	199.7	2.4	42.1	10.2	10.4	1.1	944	435840	394281	7813	0.6	296	185	1.60
SWZ-11.1IR	223.3	1.8	16.5	4.7	4.7	1.4	708	418994	392739	8758	0.3	123	90	1.37
SWZ-11.2I	145.3	2.0	12.1	4.8	4.7	1.3	356	437997	409378	9641	0.2	51	44	1.16
SWZ-11.3C	873.9	196.3	28.8	3.1	2.9	0.0	851	437022	387327	12633	1.3	426	455	0.93
SWZ-11.4R	216.4	5.9	26.1	9.6	9.6	1.4	546	430174	374999	7903	0.1	71	39	1.82
SWZ-11.5IR	266.6	3.1	66.9	5.5	5.3	2.2	1800	410462	324930	9455	1.1	653	426	1.53
SWZ-2.1IR	187.8	3.0	22.4	4.2	4.3	1.8	881	460318	429720	10930	0.5	218	187	1.17
SWZ-2.2I	287.3	2.6	61.7	16.8	16.5	1.6	1705	490258	453320	7474	0.3	213	73	2.92
SWZ-3.1R	352.4	2.2	29.1	7.5	7.4	2.2	1375	458901	443325	9184	0.5	339	170	2.00
SWZ-4.1IC	234.9	2.0	28.9	4.5	3.8	1.8	1045	460926	434698	10311	0.5	193	176	1.10
SWZ-4.2R	440.8	2.7	40.2	9.9	9.5	2.3	1467	465925	408593	8511	0.5	420	158	2.66
SWZ-5.1R	304.5	3.0	31.3	9.4	9.0	2.0	983	467404	421408	8633	0.3	150	80	1.87
SWZ-5.2IC	327.9	2.3	30.7	6.6	6.4	2.4	1090	468150	433789	9271	0.4	255	137	1.86
SWZ-6.1IC	1018.3	4.0	144.7	16.2	16.6	4.0	7417	460471	413474	6995	1.0	1574	314	5.02
SWZ-6.2R	373.6	3.1	37.6	10.1	10.0	2.2	1117	449204	406004	8221	0.3	275	111	2.48
SWZ-7.1R	463.5	2.2	40.4	9.9	9.7	2.1	1590	466993	427999	8791	0.6	491	185	2.65
SWZ-8.1R	302.6	3.8	29.9	10.1	9.9	3.1	890	471372	445431	8887	0.3	145	78	1.85
SWZ-8.2IR	241.4	2.6	46.6	4.0	4.1	1.5	1268	451973	424835	10714	0.7	286	258	1.11
SWZ-8.3I	172.9	2.8	12.5	4.5	4.5	1.3	447	440945	422428	9516	0.2	50	47	1.06
SWZ-8.4C	767.0	2.6	136.1	13.4	13.5	3.2	3790	473026	445538	8078	2.1	3285	727	4.52
SWZ-9.1C	174.9	1.7	36.7	13.2	13.8	1.1	1238	462486	423598	8156	0.2	108	40	2.73
SWZ-9.2I	270.5	1.5	29.8	7.6	7.3	1.0	823	455708	397467	8368	0.2	124	79	1.58
SWZ-9.3IR	204.5	2.4	31.7	14.9	15.2	0.9	520	469974	409217	7680	0.1	83	39	2.12
SWZ-9.4R	262.5	1.7	23.2	6.6	6.4	1.6	928	441577	435487	9648	0.3	151	101	1.50

Table D2: Complete trace element data from March, 2006 SHRIMP-RG analysis of zircons from the Spirit Mountain batholith.

	P ppm	Ca Rel to CZ3	Sc ppm	Ti48 ppm	Ti49 ppm	Fe Rel to CZ3	Y ppm	Zr96	Zr (Zr2O)	Hf ppm	Pb206	Th ppm	U ppm	Th/U
SML49Z-1.1C	649.7	201.0	40.6	8.5	7.4	0.0	2624	478480	454767	7866	0.6	520	189	2.75
SML49Z-1.2R	315.3	1.4	51.1	5.3	5.5	1.2	2165	482195	487750	10573	1.4	715	503	1.42
SML49Z-1.3I	273.1	1.4	20.4	5.1	5.1	1.1	1204	490430	508100	10327	0.3	151	104	1.45
SML49Z-10.1R	332.6	1.5	38.2	4.5	4.2	1.3	1932	455309	409558	10610	1.4	738	504	1.46
SML49Z-10.2IR	285.8	49.5	26.1	4.2	4.1	0.0	3455	441421	485775	9496	0.7	652	326	2.00
SML49Z-10.3C	391.2	22.5	11.9	4.4	4.1	2.6	1465	455963	480550	10436	0.2	87	78	1.12
SML49Z-10.4C	222.5	1.4	15.5	4.4	4.3	0.9	795	490797	466177	11041	0.2	96	84	1.14
SML49Z-10.5IR	170.2	1.1	53.6	3.5	3.4	1.0	1335	439756	390335	11432	1.0	462	405	1.14
SML49Z-10.6IR	120.0	1.3	8.3	3.6	3.7	0.9	332	455817	418611	11019	0.2	72	68	1.07
SML49Z-11.1C	195.9	1.4	16.8	5.4	5.5	1.4	610	449464	382539	9189	0.2	79	69	1.15
SML49Z-11.2IR	237.0	3.3	37.6	7.3	8.0	1.2	809	431641	383165	7845	0.1	79	51	1.53
SML49Z-11.3R	245.1	1.6	58.0	3.7	3.6	1.3	1702	472849	412177	11919	1.8	873	687	1.27
SML49Z-12.1IC	235.1	1.1	23.9	4.8	4.7	0.9	1362	438498	383871	8923	0.3	172	87	1.97
SML49Z-12.2T	248.8	1.2	65.7	3.7	3.6	1.0	2001	443751	396030	11204	2.4	1146	855	1.34
SML49Z-13.1IC	327.7	1.4	12.9	5.1	5.4	1.2	1769	427702	403191	9951	0.3	161	78	2.06
SML49Z-13.2IR	193.2	1.3	16.4	5.0	5.3	1.0	754	428587	419808	9603	0.3	132	98	1.34
SML49Z-13.3T	234.0	1.4	36.4	3.9	3.6	1.6	1345	457150	439019	11639	1.5	957	508	1.88
SML49Z-2.1C	104.0	1.2	32.9	10.1	9.9	1.1	518	458365	410645	7753	0.1	55	33	1.67
SML49Z-2.2T	260.5	0.8	104.0	3.9	3.7	1.1	2661	458001	448805	12724	2.5	1175	907	1.29
SML49Z-2.3IR	293.3	1.9	57.1	9.9	10.0	1.9	1223	483556	453925	8916	0.3	138	94	1.48
SML49Z-3.1I	194.1	1.4	30.9	10.0	10.0	1.6	1498	476487	447714	8316	0.2	137	56	2.45
SML49Z-3.2R	213.6	1.1	37.4	5.2	5.3	1.2	1098	484547	510565	11406	0.5	218	186	1.17
SML49Z-4.1C	219.5	1.2	26.7	6.3	6.3	1.2	1425	483580	469169	9213	0.2	169	76	2.22
SML49Z-4.2T	223.3	1.2	53.6	3.5	3.7	1.4	1843	468828	472430	12307	1.9	992	714	1.39
SML49Z-5.1C	323.9	1.3	23.0	5.2	5.4	1.1	1904	456863	435876	9843	0.4	295	143	2.07
SML49Z-5.2R	200.6	1.8	83.6	3.7	3.8	1.3	1958	455071	432245	12250	1.9	737	652	1.13
SML49Z-5.3IR	207.8	1.5	16.0	5.0	5.1	1.0	732	467510	443765	9744	0.3	133	100	1.33
SML49Z-6.1R	177.9	1.5	42.0	2.5	2.4	1.4	2032	450545	396797	11816	1.5	910	511	1.78
SML49Z-6.2IR	514.7	1.4	79.6	12.2	12.3	1.3	2006	448680	388405	7475	0.8	1225	270	4.53
SML49Z-6.3IR	193.4	1.4	21.3	5.7	5.6	1.2	605	462555	448167	9082	0.2	115	73	1.57
SML49Z-7.1R	248.9	1.4	93.4	3.7	4.0	1.3	2001	457226	395706	12532	2.2	985	846	1.16
SML49Z-7.2IR	271.1	1.6	25.0	5.7	5.9	1.2	861	473173	427067	9168	0.3	139	103	1.35
SML49Z-7.3C	135.8	1.5	20.3	6.5	6.4	1.0	507	471363	431357	8764	0.1	38	30	1.27
SML49Z-7.4IR	233.7	0.7	24.3	5.4	5.6	0.8	831	449313	438609	8947	0.2	135	97	1.39
SML49Z-8.1C	197.7	1.4	18.8	4.5	4.2	1.1	880	437660	395585	9017	0.2	94	68	1.38
SML49Z-8.2IR	365.8	6.1	57.3	4.8	4.6	1.8	2550	414403	370881	10129	1.3	652	473	1.38
SML49Z-8.3R	253.3	1.4	60.4	3.0	3.4	1.1	1943	436773	386128	12551	3.0	1723	1251	1.38
SML49Z-8.4IR	319.1	1.6	38.5	3.9	4.1	1.2	1961	457232	396762	11169	1.7	936	631	1.48
SML49Z-8.5C	202.8	1.3	19.6	4.9	5.0	1.2	635	454997	419019	10511	0.2	81	66	1.23
SML49Z-9.1C	149.4	1.4	33.0	11.8	11.7	1.0	770	450062	411088	7495	0.1	68	29	2.38
SML49Z-9.2IR	227.4	1.2	48.8	9.3	9.1	1.1	853	444592	404309	7779	0.2	84	54	1.55

Table D2: Complete trace element data from March, 2006 SHRIMP-RG analysis of zircons from the Spirit Mountain batholith.

	P ppm	Ca Rel to CZ3	Sc ppm	Ti48 ppm	Ti49 ppm	Fe Rel to CZ3	Y ppm	Zr96	Zr (Zr2O)	Hf ppm	Pb206	Th ppm	U ppm	Th/U
SML49Z-9.3R	306.2	1.3	102.0	4.8	4.6	1.2	2762	460128	389700	11925	2.5	1299	877	1.48

Table D2: Complete trace element data from March, 2006 SHRIMP-RG analysis of zircons from the Spirit Mountain batholith.

	P ppm	Ca Rel to CZ3	Sc ppm	Ti48 ppm	Ti49 ppm	Fe Rel to CZ3	Y ppm	Zr96	Zr (Zr2O)	Hf ppm	Pb206	Th ppm	U ppm	Th/U
SML54Z-1.1I	228.8	1.3	37.8	10.1	10.2	1.9	1267	442805	443747	8403	0.2	136	59	2.29
SML54Z-1.2R	102.5	1.6	162.6	2.6	2.4	1.9	2101	512678	533125	15035	2.5	1421	902	1.58
SML54Z-10.1C	705.2	3.2	56.9	6.6	6.9	3.9	2016	461931	437308	12012	1.8	887	695	1.28
SML54Z-10.2R	292.8	2.3	18.6	5.5	5.9	3.0	984	467563	459136	10123	0.5	216	145	1.49
SML54Z-2.1I	196.2	1.2	38.7	16.2	15.9	2.1	1111	460376	457368	6986	0.1	81	33	2.42
SML54Z-3.1C	382.7	1.7	71.9	10.2	10.5	1.9	2979	489229	467944	8010	0.4	461	138	3.33
SML54Z-3.2I	307.8	1.4	37.3	10.6	10.6	1.5	1134	470901	455269	8542	0.3	298	105	2.85
SML54Z-3.3T	176.6	1.6	402.9	3.9	3.9	1.8	2377	456594	442160	15056	4.6	1821	1743	1.04
SML54Z-4.1C	169.7	1.0	25.8	7.0	6.9	1.3	593	459038	441123	9143	0.2	68	53	1.28
SML54Z-4.2IR	314.5	1.3	62.5	9.2	9.2	1.6	1341	456390	449669	8174	0.3	148	100	1.48
SML54Z-4.3T	282.0	1.7	27.7	4.2	4.2	3.8	1534	478650	464896	12560	1.4	762	529	1.44
SML54Z-5.1C	143.2	1.4	13.4	4.9	4.8	1.4	404	480000	459446	10188	0.2	44	43	1.02
SML54Z-5.2IIR	299.5	2.9	29.5	6.7	6.7	1.4	1056	465610	459139	9543	0.3	104	79	1.31
SML54Z-5.3IR	311.2	1.4	27.6	6.2	6.3	1.8	1087	465547	455403	9743	0.4	186	118	1.57
SML54Z-6.1C	327.6	1.3	56.6	14.1	13.8	1.3	2552	478778	454927	7622	0.3	367	100	3.66
SML54Z-6.2IR	405.7	56.8	35.3	11.5	11.2	0.0	1060	458338	438460	8555	0.3	301	118	2.54
SML54Z-7.1C	299.0	1.3	56.8	4.2	4.3	1.6	2214	483419	438863	12778	2.5	1441	944	1.53
SML54Z-7.2IR	230.6	1.2	19.9	4.7	4.7	1.4	886	465494	441926	10596	0.4	168	129	1.30
SML54Z-7.3T	194.1	1.3	97.1	3.8	4.0	1.5	1400	472921	462652	11864	1.9	921	663	1.39
SML54Z-8.1IC	155.9	1.2	36.0	14.6	15.0	1.2	617	472861	453515	7586	0.1	52	20	2.59
SML54Z-8.2T	347.8	1.3	15.8	5.3	5.3	1.5	1244	471343	442711	10492	0.5	221	166	1.33
SML54Z-9.1C	257.7	1.3	37.0	12.1	12.2	1.3	1796	455335	421766	7506	0.2	189	58	3.24
SML54Z-9.2IR	253.1	1.4	36.1	8.7	9.1	1.5	983	460855	433278	8592	0.2	125	69	1.81
SML54Z-9.3T	140.7	1.5	356.7	3.7	3.7	1.8	1910	462720	416554	14463	3.7	1410	1302	1.08

Table D2: Complete trace element data from March, 2006 SHRIMP-RG analysis of zircons from the Spirit Mountain batholith.

	P ppm	Ca Rel to CZ3	Sc ppm	Ti48 ppm	Ti49 ppm	Fe Rel to CZ3	Y ppm	Zr96	Zr (Zr2O)	Hf ppm	Pb206	Th ppm	U ppm	Th/U
CZ3-7.1JW145	14.3	1.4	4.3	5.0	5.0	1.1	43	451285	418969	10876	43.2	27	467	0.06
CZ3-8.1JW145	14.9	1.4	4.6	4.9	4.9	1.1	47	475217	443070	11172	44.8	31	505	0.06
CZ3-8.2JW145	14.3	1.4	4.3	4.6	4.3	1.1	44	449413	421201	10587	43.7	28	479	0.06
Average	14.5	1.4	4.4	4.8	4.7	1.1	44	458638	427747	10878	43.9	29	484	0.06
CZ3-10.1-189	14.2	1.3	4.3	5.3	5.2	1.0	49	502163	505593	12102	46.9	32	554	0.06
CZ3-9.1-189	15.3	1.1	4.4	5.2	5.2	0.9	48	487841	508018	11696	44.5	31	532	0.06
CZ3-6.1-251	12.5	0.9	4.3	5.0	5.0	0.9	42	470716	473297	11263	43.9	29	489	0.06
CZ3-7.1-251	11.8	0.9	4.2	5.0	5.1	1.0	41	466118	490208	11039	43.1	28	493	0.06
CZ3-7.2-251	12.9	0.9	4.6	5.1	5.2	1.2	44	501865	485261	11703	45.8	30	516	0.06
CZ3-8.1-251	12.5	1.1	4.5	5.7	5.6	1.1	46	513705	468737	12704	0.0	0	788	0.00
CZ3-8.2-251	11.7	0.7	4.5	5.1	5.2	0.9	44	472053	483346	10693	39.9	27	479	0.06
Average	13.0	1.0	4.4	5.2	5.2	1.0	45	487780	487780	11600	44.0	30	550	0.05
R33A206-19	171.9	1.2	15.1	6.0	6.2	29.6	1697	454583	465939	9341	14.8	176	229	0.77
R33-30A206	174.9	1.0	15.6	7.0	6.9	9.3	1448	423203		7491	0.0	67	92	0.73

	La ppm	Ce ppm	Pr Calc	Nd ppm	Sm ppm	Eu ppm	Ho ppm	Gd ppm	Tb ppm	Dy ppm	Er ppm	Tm pm	Yb ppm	Lu ppm
BC101-1.5	0.00	65.0	0.0	0.4	2.1	0.4	47.1	21.3	8.2	106.8	253.5	57.2	492.9	95.6
BC101-1.6R	0.00	39.1	0.0	0.8	2.8	0.6	36.9	25.1	8.5	92.3	173.2	37.7	300.9	59.5
BC101-1E	4.42	77.3	0.0	2.2	2.4	0.5	42.8	18.9	7.5	94.2	198.6	48.3	397.8	92.0
BC101-1E2	0.00	47.4	0.0	0.3	1.6	0.4	31.8	15.5	5.8	72.0	159.5	35.5	304.6	59.9
BC101-1LGC	0.01	77.2	0.0	2.1	9.4	1.1	109.1	80.0	26.4	284.0	474.8	89.0	673.0	120.9
BC101-1LGI	0.00	49.2	0.0	0.3	1.7	0.4	32.7	17.0	6.3	75.8	165.1	36.6	307.1	60.0
BC101-2.1T	0.00	47.7	0.0	0.4	1.8	0.4	33.1	17.5	6.8	77.9	165.0	35.9	303.1	58.4
BC101-2.2C	0.05	111.6	0.0	5.3	16.0	4.6	104.5	102.0	30.1	294.5	451.2	87.2	691.0	129.9
BC101-2.3I	0.00	50.2	0.0	0.4	1.7	0.5	23.9	14.4	4.8	54.7	117.1	26.0	231.2	48.1
BC101-2.4I	0.01	46.7	0.0	0.2	1.1	0.2	31.8	12.1	4.9	69.8	171.5	40.8	362.1	74.6
BC101-2.5T2	0.06	69.3	0.0	0.7	2.8	0.6	44.9	24.8	9.7	109.6	219.8	46.2	367.7	69.8
BC101-3.1T	0.01	48.6	0.0	0.3	1.0	0.2	22.9	10.5	4.3	50.8	129.7	32.3	318.7	72.6
BC101-3.2I	0.00	80.5	0.0	0.4	2.1	0.4	52.8	22.0	9.2	112.8	275.5	61.0	531.0	103.3
BC101-3.3R	6.32	75.0	0.0	5.0	2.9	0.4	23.2	12.5	3.7	48.9	135.7	34.3	339.1	80.0
BC101-3.4C	0.01	46.3	0.0	1.2	4.7	1.4	48.3	39.7	12.0	125.9	222.2	44.3	371.8	72.1
BC101-3.5T2	0.11	62.9	0.0	0.3	1.4	0.3	35.9	14.3	5.6	75.1	202.3	49.2	470.6	97.8
BC101-4.1R	0.00	66.2	0.0	0.4	1.9	0.4	44.3	19.5	7.8	100.2	235.7	53.1	466.8	91.0
BC101-4.2I	0.00	50.7	0.0	0.4	2.0	0.4	36.7	18.0	7.1	84.4	178.3	39.4	311.0	58.4
BC101-4.3C	0.00	95.5	0.0	0.3	1.3	0.2	47.2	14.7	6.3	86.9	288.8	72.5	719.3	152.2
BC101-5.1I	0.01	51.8	0.0	0.5	1.9	0.4	33.6	18.4	7.1	80.3	166.8	34.2	284.2	54.4
BC101-5.2R	0.00	58.9	0.0	0.6	2.4	0.6	37.1	23.6	8.5	92.4	180.4	38.0	313.6	56.4
BC101-6.1I	0.03	62.7	0.0	3.7	9.9	2.9	77.2	69.6	21.6	209.3	344.0	66.1	520.0	99.5
BC101-7.1I	0.00	55.8	0.0	0.8	3.9	0.8	59.9	35.6	13.0	148.9	282.3	58.5	466.5	87.0
BC101-7.2R	0.00	109.2	0.0	0.2	1.4	0.2	55.1	15.0	7.2	102.0	352.7	94.5	923.8	197.7
BC101-8.1R	0.00	52.4	0.0	0.5	2.1	0.4	41.3	20.3	8.2	91.5	195.0	41.7	336.7	60.0
BC101-8.2I	0.02	56.0	0.0	0.4	2.0	0.5	39.0	18.8	7.7	90.9	191.5	42.4	350.0	67.3

	La ppm	Ce ppm	Pr Calc	Nd ppm	Sm ppm	Eu ppm	Ho ppm	Gd ppm	Tb ppm	Dy ppm	Er ppm	Tm pm	Yb ppm	Lu ppm
BC101-9.1R	0.00	31.3	0.0	0.1	0.8	0.2	22.6	8.9	3.7	49.6	122.5	29.0	264.5	57.4
BC101-9.2IR	0.00	139.2	0.0	0.6	3.4	0.8	100.7	40.8	17.3	227.9	544.9	123.8	1049.0	196.6
BC101-9.3I	0.00	44.7	0.0	0.4	2.8	0.5	46.5	26.7	10.1	115.5	228.6	47.6	385.2	69.8
BC101-9.4C	0.00	51.3	0.0	0.4	2.0	0.5	45.4	22.0	8.8	108.9	217.2	46.4	375.0	72.4
BC101-10.1R	0.00	52.9	0.0	0.3	1.4	0.3	35.9	14.2	6.1	80.0	192.0	45.1	407.6	79.2
BC101-10.2C	0.02	123.7	0.0	2.3	9.0	2.1	101.9	74.7	25.0	262.1	464.8	91.6	734.9	135.4
BC101-10.3I	0.03	129.4	0.0	0.4	2.0	0.2	72.2	23.3	10.5	145.1	417.8	104.7	996.3	200.2
BC101-11.1R	0.01	43.6	0.0	0.6	2.5	0.5	30.3	19.8	7.1	79.6	144.1	28.3	246.3	47.7
BC101-11.2I	0.00	62.7	0.0	0.5	2.3	0.4	51.2	26.8	10.6	127.0	260.8	52.4	438.0	78.4
BC101-11.3R	0.00	54.1	0.0	0.4	2.1	0.4	42.6	19.9	7.6	92.4	202.6	44.2	351.8	66.7
BC101-12.1T	0.00	57.3	0.0	0.4	1.8	0.4	41.7	20.8	7.4	94.3	212.4	47.4	415.0	80.8
BC101-12.2I	0.01	100.2	0.0	0.6	2.7	0.6	78.1	35.8	13.5	181.5	396.3	88.2	692.3	129.3
BC101-12.3C	0.00	38.2	0.0	0.3	1.5	0.4	33.8	18.5	7.0	83.9	179.2	39.7	347.2	74.6
BC101-12.4C	0.00	49.1	0.0	0.4	2.0	0.5	42.9	21.9	8.7	101.0	215.8	44.7	378.8	75.4
BC101-13.1C	0.01	74.2	0.0	1.1	5.1	1.2	77.3	45.8	17.5	191.8	364.6	76.3	607.4	113.6
BC101-13.2IR	0.07	64.6	0.0	0.4	1.9	0.3	50.8	19.6	8.8	112.6	265.7	58.4	498.2	96.1
BC101-13.3R	0.12	59.8	0.0	0.6	2.4	0.4	40.6	21.4	8.2	94.9	196.1	42.3	350.4	69.1
BC101-14.1C	0.05	104.9	0.0	5.9	15.1	3.7	85.0	90.4	26.1	239.1	363.8	70.3	552.9	107.3
BC101-14.2IR	0.00	76.9	0.0	0.2	1.9	0.3	69.9	23.3	10.3	144.1	383.4	86.7	721.5	139.2
BC101-14.3I	0.03	79.2	0.0	0.9	3.4	0.8	48.3	28.9	10.8	117.7	224.2	46.6	378.5	72.4
BC101-14.4IR	0.00	56.5	0.0	0.3	1.8	0.3	45.2	19.6	7.8	100.3	222.6	49.0	410.8	75.6
BC101-14.5R	0.00	52.3	0.0	0.4	2.2	0.4	35.4	19.7	7.1	86.4	174.6	35.5	297.2	56.4

	La ppm	Ce ppm	Pr Calc	Nd ppm	Sm ppm	Eu ppm	Ho ppm	Gd ppm	Tb ppm	Dy ppm	Er ppm	Tm pm	Yb ppm	Lu ppm
DSCG-1.1T	0.00	62.5	0.0	0.8	2.9	0.7	40.6	25.9	8.7	100.2	185.2	37.6	324.8	61.0
DSCG-1.2IR	0.00	86.7	0.0	0.4	2.1	0.4	54.5	23.1	9.2	118.1	275.8	64.6	580.4	112.4
DSCG-1.3C	0.01	44.9	0.0	0.2	1.6	0.4	32.9	16.4	6.5	75.3	167.9	35.2	313.2	62.4
DSCG-10.1C	0.01	88.1	0.0	0.3	1.3	0.2	51.9	14.9	6.1	101.9	334.1	86.1	866.9	188.0
DSCG-10.2IR	0.01	68.6	0.0	0.8	3.1	0.7	49.8	29.6	10.4	122.2	241.0	49.0	397.9	75.3
DSCG-11.1C	0.05	179.9	0.0	2.0	6.8	1.0	165.1	69.5	29.1	357.9	884.3	199.1	1756.5	332.8
DSCG-11.2I	0.01	197.4	0.0	0.6	2.8	0.4	100.4	36.4	14.4	210.2	566.7	137.4	1259.8	255.9
DSCG-11.3R	0.00	48.1	0.0	0.2	1.0	0.2	31.4	11.3	4.7	65.7	174.1	39.8	358.4	74.3
DSCG-12.1R	0.03	69.3	0.0	0.9	3.3	0.7	50.0	30.5	11.0	126.9	245.1	49.6	425.5	77.4
DSCG-12.2I	0.02	53.1	0.0	1.4	4.2	1.2	58.0	38.2	12.8	140.3	271.6	55.2	439.9	82.0
DSCG-13.1C	0.03	43.1	0.0	3.2	6.8	1.6	62.6	55.0	16.8	170.3	280.2	52.8	416.6	79.5
DSCG-13.2I	0.00	54.6	0.0	1.1	3.7	0.8	40.1	29.3	9.6	104.5	191.4	38.2	310.2	57.2
DSCG-13.3T	0.00	49.5	0.0	0.4	1.3	0.4	35.1	18.2	6.7	86.1	172.2	37.2	305.4	58.1
DSCG-14.1I	0.07	30.0	0.0	0.1	0.8	0.2	24.7	8.6	3.8	53.2	143.5	33.0	298.2	58.6
DSCG-14.2R	0.04	62.2	0.0	0.6	3.3	0.7	58.1	28.8	11.0	133.6	291.8	60.6	521.2	100.6
DSCG-15.1R	0.01	61.5	0.0	0.6	2.7	0.6	48.5	24.5	9.8	107.8	228.0	49.1	404.5	76.5
DSCG-15.2I	0.00	38.9	0.0	0.4	1.6	0.5	17.7	13.8	4.6	46.3	86.8	17.4	148.6	30.3
DSCG-16.1C	0.04	612.6	0.0	2.4	8.7	1.2	215.9	88.2	34.6	446.6	1236.1	293.7	2729.0	545.4
DSCG-16.2R	0.01	66.4	0.0	0.6	2.6	0.5	52.3	27.0	10.9	124.8	264.6	55.4	458.6	84.8
DSCG-17.1C	0.23	547.2	0.0	1.5	5.0	0.5	156.7	44.7	20.1	276.6	1045.4	277.3	2957.2	634.4
DSCG-17.2R	0.06	66.7	0.0	0.8	3.6	0.8	54.4	31.4	11.0	130.1	268.3	55.2	443.3	79.3
DSCG-18.1R	0.00	41.0	0.0	0.3	1.1	0.3	23.3	11.4	3.8	53.0	123.7	29.1	289.1	62.8
DSCG-19.1IR	0.00	68.8	0.0	0.3	1.8	0.4	34.4	15.7	5.8	80.1	194.1	44.6	429.3	92.8
DSCG-2.1T	0.00	77.3	0.0	0.4	2.0	0.4	54.8	24.6	9.0	121.0	277.9	62.0	544.0	102.2
DSCG-2.2I	0.01	40.4	0.0	0.2	1.4	0.3	23.3	12.3	5.0	56.9	117.0	24.0	208.7	41.2
DSCG-2.3C	0.06	74.2	0.0	0.4	1.7	0.2	58.0	16.7	7.8	112.1	347.0	92.8	917.8	208.3
DSCG-2.3C2	0.00	79.2	0.0	1.0	4.0	0.9	63.4	38.3	13.7	160.2	306.0	63.9	508.6	94.0
DSCG-20.1R	0.00	55.0	0.0	0.4	1.8	0.4	37.1	18.1	6.9	85.2	197.2	45.3	418.0	83.5
DSCG-20.2I	0.01	67.4	0.0	1.1	3.8	1.0	34.1	27.7	8.0	86.0	152.1	31.5	267.4	53.0
DSCG-21.1C	0.02	53.4	0.0	3.8	10.1	2.8	81.5	75.7	22.6	228.6	353.7	67.0	534.7	95.6
DSCG-21.2I	0.01	48.9	0.0	0.7	2.9	0.7	31.9	21.5	7.5	79.6	143.6	28.8	246.8	48.6
DSCG-3.2C	0.06	104.0	0.0	5.2	14.2	4.1	98.2	100.6	28.0	273.0	419.1	78.7	632.5	116.4
DSCG-3.3IR	0.42	59.6	0.0	0.8	1.8	0.4	42.7	17.2	7.1	92.4	237.4	54.3	509.5	107.5
DSCG-4.1T	0.01	65.5	0.0	0.4	1.8	0.5	40.6	18.5	7.7	88.0	205.0	47.6	424.5	87.2

	La ppm	Ce ppm	Pr Calc	Nd ppm	Sm ppm	Eu ppm	Ho ppm	Gd ppm	Tb ppm	Dy ppm	Er ppm	Tm pm	Yb ppm	Lu ppm
DSCG-4.2R	0.00	60.9	0.0	0.4	1.7	0.4	51.9	20.2	9.0	113.2	271.1	60.4	542.6	105.9
DSCG-4.3IR	0.02	53.1	0.0	2.2	6.2	1.7	45.5	42.3	12.3	122.5	202.0	40.2	310.8	60.7
DSCG-4.4C	0.13	149.2	0.0	9.7	21.9	5.9	113.6	126.3	34.9	325.1	450.7	83.8	617.5	117.6
DSCG-5.1T	0.00	57.3	0.0	0.5	2.4	0.5	44.4	22.5	8.7	108.5	218.1	45.3	380.6	69.6
DSCG-5.2IR	3.05	49.7	0.0	1.6	1.0	0.2	17.8	7.5	2.8	35.9	110.5	29.1	300.4	69.6
DSCG-5.3IR	2.24	57.3	0.0	0.8	0.9	0.2	19.3	7.3	2.8	39.5	119.9	32.9	335.3	81.9
DSCG-5.4IR	0.00	67.3	0.0	0.5	2.8	0.7	45.8	26.9	9.6	109.0	223.3	47.4	382.1	69.1
DSCG-5.5C	0.03	114.0	0.0	0.4	1.4	0.3	62.7	18.7	7.5	121.2	381.7	102.6	994.9	212.9
DSCG-5.6I	0.00	28.0	0.0	0.1	0.6	0.2	16.2	7.3	2.7	35.6	94.4	24.0	248.8	60.1
DSCG-6.1T	0.01	39.0	0.0	0.2	1.0	0.3	26.2	10.9	3.9	56.4	137.8	36.4	335.2	81.1
DSCG-6.2C	0.01	136.7	0.0	0.3	1.9	0.3	71.0	20.8	9.5	135.7	444.8	117.1	1137.3	241.4
DSCG-7.1C	0.00	165.2	0.0	0.4	2.3	0.3	78.0	26.1	10.7	162.2	459.1	113.2	1080.1	224.8
DSCG-7.2IR	0.01	104.2	0.0	1.0	4.6	1.0	66.4	41.3	14.6	168.5	302.1	60.2	483.7	88.6
DSCG-7.3IR	0.00	89.6	0.0	1.0	4.0	1.0	56.4	34.5	11.9	135.8	256.4	51.6	426.3	76.9
DSCG-7.4T	0.00	53.4	0.0	0.3	1.6	0.3	41.6	19.9	7.5	94.9	208.0	46.0	388.5	74.2
DSCG-8.1C	0.05	41.5	0.0	0.2	0.9	0.2	30.9	10.9	4.6	66.3	191.2	47.9	442.7	92.9
DSCG-8.2IR	0.01	67.0	0.0	0.2	1.5	0.3	55.3	20.0	8.2	110.5	304.5	69.1	630.2	129.3
DSCG-8.3IR	0.01	54.7	0.0	0.6	2.4	0.7	34.2	20.8	7.4	82.7	156.9	31.8	259.2	51.5
DSCG-8.4T	0.00	44.6	0.0	0.2	0.9	0.2	25.6	11.5	4.2	55.7	142.5	34.0	321.2	67.1
DSCG-9.1C	0.09	421.3	0.0	8.7	29.2	8.5	372.6	288.3	94.9	1001.1	1661.2	311.4	2461.6	424.5
DSCG-9.2IR	0.01	75.7	0.0	1.1	4.0	0.6	42.7	32.3	10.2	111.5	192.5	38.4	321.6	61.0
DSCG-9.3R	0.01	56.7	0.0	0.6	2.7	0.6	38.5	23.4	8.5	96.1	195.8	41.0	343.9	66.4
DSCG-9.4IR	0.57	41.7	0.0	0.7	1.2	0.3	26.8	12.9	4.6	60.5	141.0	33.0	289.3	54.3

	La ppm	Ce ppm	Pr Calc	Nd ppm	Sm ppm	Eu ppm	Ho ppm	Gd ppm	Tb ppm	Dy ppm	Er ppm	Tm pm	Yb ppm	Lu ppm
LGZ-1.2IC	0.03	78.2	0.0	3.9	11.4	3.9	86.1	74.6	22.7	225.9	360.7	70.4	575.2	109.9
LGZ-1.2T	0.06	377.8	0.0	0.9	3.4	0.4	125.7	35.0	15.1	203.8	730.7	202.0	2068.3	449.5
LGZ-10.1I	0.12	85.0	0.0	5.1	13.8	3.1	74.1	84.8	22.9	207.6	300.3	55.1	434.7	81.3
LGZ-11.1IR	0.01	58.0	0.0	1.0	3.7	1.1	41.1	28.0	9.1	101.0	192.2	41.0	336.5	66.7
LGZ-2.1C	0.00	159.3	0.0	0.4	1.4	0.2	52.7	16.2	6.8	96.9	337.9	94.3	988.6	231.3
LGZ-2.2R	0.00	152.2	0.0	0.3	1.3	0.2	61.9	15.2	7.1	109.5	428.0	119.9	1318.6	298.3
LGZ-2.3I	0.00	38.5	0.0	0.3	1.6	0.3	23.9	14.3	5.0	58.5	117.0	26.0	217.1	42.0
LGZ-3.1I	0.00	81.9	0.0	0.5	2.5	0.2	73.4	31.1	13.6	166.1	361.9	74.9	612.6	112.8
LGZ-4.1C	0.01	105.2	0.0	0.3	1.6	0.1	69.3	20.2	9.8	136.0	384.2	95.8	866.3	172.4
LGZ-5.1I	0.00	52.7	0.0	0.5	2.0	0.5	34.8	19.4	7.2	80.0	167.7	34.4	290.1	56.4
LGZ-6.1T	0.17	91.3	0.0	0.3	1.3	0.2	39.9	12.4	5.2	72.6	241.4	64.2	653.1	149.6
LGZ-6.2I	0.08	180.3	0.0	7.5	23.1	6.2	156.8	161.4	45.6	422.0	645.0	120.5	928.7	169.8
LGZ-7.1I	0.00	218.3	0.0	0.4	1.8	0.1	86.5	26.2	11.7	165.1	522.7	129.9	1286.3	275.3
LGZ-8.1I	0.11	136.0	0.0	7.3	26.7	10.3	170.2	177.1	51.9	477.8	695.1	129.5	979.0	182.0
LGZ-8.2IR	0.22	63.2	0.0	0.4	1.7	0.3	36.4	16.2	6.4	78.8	199.1	47.4	432.7	91.6
LGZ-9.1I	0.00	64.8	0.0	1.0	3.4	0.9	37.5	27.3	8.5	93.6	178.8	39.3	316.9	67.8
LGZ-11.2I	0.11	253.4	0.0	8.8	28.4	7.1	205.4	198.8	58.8	565.1	830.4	157.6	1227.0	223.5
LGZ-12.1I	0.00	93.7	0.0	0.3	0.7	0.1	34.0	9.1	4.4	58.9	218.7	58.9	598.8	138.8
LGZ-13.1C	0.08	129.0	0.0	0.3	1.3	0.1	54.0	15.8	6.8	100.1	333.4	87.7	873.8	195.6

	La ppm	Ce ppm	Pr Calc	Nd ppm	Sm ppm	Eu ppm	Ho ppm	Gd ppm	Tb ppm	Dy ppm	Er ppm	Tm pm	Yb ppm	Lu ppm
SWZ-1.1I	0.00	53.8	0.0	0.5	2.2	0.5	34.5	21.7	7.3	83.3	166.1	33.3	279.6	53.3
SWZ-10.1C	0.00	49.8	0.0	0.5	2.3	0.7	31.7	19.1	6.6	73.1	159.1	35.5	320.1	63.2
SWZ-11.1IR	0.00	39.8	0.0	0.2	1.2	0.3	25.6	12.7	5.0	59.8	133.1	28.7	249.8	48.0
SWZ-11.2I	0.00	24.6	0.0	0.1	0.5	0.1	14.0	5.3	2.3	31.5	71.9	16.2	143.0	29.4
SWZ-11.3C	2.09	46.2	0.0	1.9	1.4	0.1	29.2	8.1	3.7	55.1	186.4	49.5	467.5	104.4
SWZ-11.4R	0.04	46.6	0.0	0.4	1.8	0.5	22.6	14.8	5.3	55.8	108.7	21.7	182.6	36.1
SWZ-11.5IR	0.03	100.8	0.0	0.3	1.3	0.2	59.8	16.8	7.5	109.8	339.4	85.5	805.2	171.0
SWZ-2.1IR	0.00	45.6	0.0	0.2	1.1	0.2	32.2	13.1	5.5	69.3	181.3	41.5	370.9	73.2
SWZ-2.2I	0.04	63.3	0.0	4.7	12.4	4.3	74.3	79.4	21.1	204.5	313.1	63.0	505.3	96.1
SWZ-3.1R	0.00	82.6	0.0	0.8	3.7	0.7	54.3	31.7	12.0	135.7	256.3	52.7	423.7	79.4
SWZ-4.1IC	0.00	45.0	0.0	0.2	1.2	0.3	39.0	14.4	6.4	80.3	207.3	47.8	437.0	89.8
SWZ-4.2R	0.00	94.1	0.0	1.1	4.7	1.0	59.5	38.5	13.3	144.6	272.8	54.8	443.2	82.7
SWZ-5.1R	0.01	61.8	0.0	0.7	2.8	0.7	39.6	23.6	8.3	93.9	180.3	36.8	300.5	58.1
SWZ-5.2IC	0.07	68.5	0.0	0.5	2.6	0.6	44.9	23.1	8.8	102.5	224.2	47.1	416.6	79.9
SWZ-6.1IC	0.18	395.2	0.0	16.8	54.2	18.4	328.6	367.4	97.7	956.9	1386.3	262.0	2037.0	360.2
SWZ-6.2R	0.00	79.5	0.0	1.0	3.5	0.9	48.3	31.9	10.6	118.1	219.4	43.2	367.1	68.8
SWZ-7.1R	0.01	103.6	0.0	1.2	4.8	1.1	69.4	43.4	15.5	167.4	312.8	61.0	487.3	89.6
SWZ-8.1R	0.01	61.3	0.0	0.6	2.9	0.6	38.7	22.4	8.2	93.2	177.8	36.6	298.0	59.0
SWZ-8.2IR	0.00	59.4	0.0	0.2	1.3	0.2	44.6	13.4	6.0	86.5	254.1	65.4	599.0	129.8
SWZ-8.3I	0.00	25.6	0.0	0.1	0.6	0.2	17.5	7.6	3.0	37.9	92.4	20.1	181.3	35.5
SWZ-8.4C	0.03	445.8	0.0	3.9	17.7	4.2	160.7	138.7	43.6	443.7	720.5	144.2	1165.9	211.4
SWZ-9.1C	0.02	50.6	0.0	2.8	7.9	2.8	49.5	49.8	14.4	139.6	218.4	41.6	347.8	65.4
SWZ-9.2I	0.00	54.4	0.0	0.5	2.1	0.5	31.8	18.5	6.7	77.2	150.3	30.8	263.1	50.8
SWZ-9.3IR	0.00	45.0	0.0	0.4	1.8	0.6	20.2	14.6	4.6	49.6	94.1	19.6	163.8	33.4
SWZ-9.4R	0.00	52.2	0.0	0.4	2.1	0.5	37.7	19.7	7.5	89.7	183.2	38.4	305.2	57.3

	La ppm	Ce ppm	Pr Calc	Nd ppm	Sm ppm	Eu ppm	Ho ppm	Gd ppm	Tb ppm	Dy ppm	Er ppm	Tm pm	Yb ppm	Lu ppm
SML49Z-1.1C	3.25	143.1	0.0	6.4	14.8	3.0	125.7	100.1	32.6	330.9	577.7	112.8	898.7	163.6
SML49Z-1.2R	0.00	107.4	0.0	0.4	2.3	0.3	76.2	25.7	11.1	150.5	411.3	97.4	878.6	178.2
SML49Z-1.3I	0.01	50.4	0.0	0.4	2.5	0.5	48.7	24.1	9.7	113.3	238.1	50.1	413.8	78.5
SML49Z-10.1R	0.00	106.4	0.0	0.4	2.3	0.4	70.4	26.2	11.1	144.8	381.7	87.3	772.9	150.6
SML49Z-10.2IR	2.28	106.5	0.0	10.1	21.4	2.1	130.7	89.7	29.6	297.5	560.4	119.1	951.0	178.9
SML49Z-10.3C	1.72	49.0	0.0	7.9	14.1	1.3	59.2	50.1	15.9	151.5	237.6	47.9	379.4	65.8
SML49Z-10.4C	0.00	37.1	0.0	0.1	1.0	0.2	31.3	11.7	5.2	67.0	161.7	35.6	306.8	59.3
SML49Z-10.5IR	0.00	71.3	0.0	0.2	0.9	0.1	41.4	10.5	5.2	71.5	246.4	64.5	644.0	143.8
SML49Z-10.6IR	0.00	22.8	0.0	0.1	0.4	0.1	13.5	5.0	2.1	27.8	72.8	17.4	153.2	30.7
SML49Z-11.1C	0.00	34.0	0.0	0.2	1.0	0.2	24.6	10.5	4.0	52.4	127.2	27.8	242.5	48.8
SML49Z-11.2IR	0.05	44.5	0.0	0.5	1.8	0.5	30.1	17.0	6.2	71.9	148.5	31.0	268.7	52.8
SML49Z-11.3R	0.00	102.9	0.0	0.3	1.2	0.2	54.8	15.6	6.9	98.8	334.6	85.3	838.1	180.8
SML49Z-12.1IC	0.00	60.1	0.0	0.6	3.1	0.7	51.3	29.9	10.8	122.1	247.6	50.9	408.2	76.2
SML49Z-12.2T	0.01	124.0	0.0	0.3	1.6	0.2	62.3	17.4	7.9	112.7	371.1	95.0	932.6	199.1
SML49Z-13.1IC	0.00	68.6	0.0	0.5	3.3	0.5	73.6	40.6	15.9	185.4	333.0	64.3	489.0	85.0
SML49Z-13.2IR	0.00	44.7	0.0	0.2	1.4	0.3	29.7	14.4	5.5	69.3	153.0	33.0	281.0	52.1
SML49Z-13.3T	0.00	80.4	0.0	0.3	1.6	0.3	48.9	17.5	7.3	100.9	278.3	67.8	627.9	127.5
SML49Z-2.1C	0.00	36.9	0.0	0.5	1.8	0.6	22.3	15.7	5.0	53.6	106.4	22.1	186.2	37.4
SML49Z-2.2T	0.00	140.0	0.0	0.2	1.2	0.1	75.1	14.8	7.6	120.3	486.5	128.8	1400.1	305.6
SML49Z-2.3IR	0.00	71.6	0.0	0.8	3.2	0.9	51.9	29.2	10.5	122.8	256.2	55.1	469.6	93.9
SML49Z-3.1I	0.01	63.4	0.0	2.2	7.8	1.9	67.2	57.0	17.2	175.1	293.8	57.5	459.2	86.7
SML49Z-3.2R	0.00	54.6	0.0	0.3	1.3	0.3	40.9	15.1	6.8	81.5	218.0	50.2	465.8	97.4
SML49Z-4.1C	0.01	64.1	0.0	1.2	5.6	1.4	66.4	47.4	15.6	171.3	306.4	59.9	482.1	88.1
SML49Z-4.2T	0.00	100.3	0.0	0.4	1.7	0.3	60.3	18.8	8.1	115.6	357.8	90.7	876.7	185.0
SML49Z-5.1C	0.00	70.7	0.0	1.1	5.1	1.1	83.6	47.6	17.5	198.0	387.0	78.1	631.9	113.8
SML49Z-5.2R	0.00	104.8	0.0	0.2	1.1	0.2	61.3	13.9	6.8	107.0	392.6	106.8	1075.9	233.0
SML49Z-5.3IR	0.00	41.8	0.0	0.2	1.3	0.3	28.9	14.1	5.2	63.8	142.2	31.7	276.9	51.6
SML49Z-6.1R	0.00	73.8	0.0	0.5	2.0	0.3	64.6	21.7	9.2	129.2	395.2	98.9	966.8	202.1
SML49Z-6.2IR	0.01	210.7	0.0	2.4	9.3	3.0	94.1	76.2	24.3	246.8	401.5	75.7	577.2	107.0
SML49Z-6.3IR	0.00	42.8	0.0	0.3	1.4	0.4	24.0	13.1	4.6	56.4	116.5	24.3	211.7	40.0
SML49Z-7.1R	0.00	118.0	0.0	0.2	1.0	0.1	63.0	13.3	6.7	104.9	438.2	121.2	1268.7	278.2
SML49Z-7.2IR	0.00	50.6	0.0	0.3	1.8	0.4	34.2	17.4	6.5	78.7	164.8	35.5	297.2	55.8
SML49Z-7.3C	0.00	32.2	0.0	0.2	1.0	0.3	19.2	9.9	3.6	44.1	96.0	20.4	171.6	34.0
SML49Z-7.4IR	0.00	48.5	0.0	0.4	1.9	0.4	32.8	16.2	6.2	74.8	157.2	33.2	269.2	53.2
SML49Z-8.1C	0.01	39.0	0.0	0.2	1.4	0.3	31.3	14.9	6.2	69.0	155.1	32.4	268.5	52.3
SML49Z-8.2IR	0.16	121.8	0.0	0.6	2.4	0.4	81.5	23.9	10.5	153.0	460.8	107.8	1028.3	204.9
SML49Z-8.3R	0.01	121.0	0.0	0.3	1.2	0.1	56.2	14.0	6.5	96.7	363.2	97.7	1006.7	221.3
SML49Z-8.4IR	0.01	104.4	0.0	0.4	2.1	0.3	63.9	21.8	9.6	131.4	360.4	84.9	786.5	156.5
SML49Z-8.5C	0.00	34.7	0.0	0.2	1.1	0.2	24.2	11.4	4.4	56.6	130.4	28.5	253.9	48.9
SML49Z-9.1C	0.01	37.0	0.0	0.9	3.6	1.2	33.6	27.1	8.6	85.2	149.4	29.3	240.8	46.6
SML49Z-9.2IR	0.00	53.6	0.0	0.6	2.6	0.7	35.5	21.8	7.4	84.0	173.1	37.0	315.6	65.4

	La ppm	Ce ppm	Pr Calc	Nd ppm	Sm ppm	Eu ppm	Ho ppm	Gd ppm	Tb ppm	Dy ppm	Er ppm	Tm pm	Yb ppm	Lu ppm
SML49Z-9.3R	0.00	161.1	0.0	0.3	1.6	0.2	86.8	21.4	10.4	156.4	558.7	145.1	1430.3	304.6

	La ppm	Ce ppm	Pr Calc	Nd ppm	Sm ppm	Eu ppm	Ho ppm	Gd ppm	Tb ppm	Dy ppm	Er ppm	Tm pm	Yb ppm	Lu ppm
SML54Z-1.1I	0.01	57.6	0.0	1.3	5.2	1.3	51.8	38.9	13.0	136.3	239.4	45.7	372.2	71.5
SML54Z-1.2R	0.00	73.7	0.0	0.8	2.8	0.5	59.3	23.8	8.5	111.0	382.8	109.8	1247.2	308.0
SML54Z-10.1C	0.08	69.3	0.0	0.3	1.4	0.2	64.6	17.3	8.1	123.0	395.1	98.7	978.8	199.4
SML54Z-10.2R	0.07	52.8	0.0	0.4	1.9	0.4	40.6	18.9	7.4	92.7	197.8	42.4	351.6	63.5
SML54Z-2.1I	0.02	41.3	0.0	2.6	7.5	2.5	46.3	46.4	12.8	122.1	194.3	38.7	309.6	60.5
SML54Z-3.1C	0.06	137.7	0.0	5.3	17.5	5.6	127.9	122.4	36.4	355.5	551.1	104.1	827.9	145.1
SML54Z-3.2I	0.01	93.8	0.0	1.2	4.2	1.1	51.2	34.7	11.5	126.5	235.1	46.5	376.3	72.4
SML54Z-3.3T	0.00	123.4	0.0	0.2	1.0	0.2	63.1	12.5	5.8	95.9	465.2	147.3	1812.8	477.1
SML54Z-4.1C	0.00	34.9	0.0	0.2	1.2	0.3	24.7	13.2	4.9	57.5	121.4	26.8	226.1	45.5
SML54Z-4.2IR	0.00	70.1	0.0	0.7	3.1	0.8	53.0	29.4	10.2	121.9	258.4	53.9	466.7	91.7
SML54Z-4.3T	0.01	79.5	0.0	0.3	2.0	0.3	60.0	21.8	9.8	121.3	317.8	72.7	644.4	125.1
SML54Z-5.1C	0.00	24.6	0.0	0.1	0.5	0.2	15.0	6.3	2.6	33.2	81.0	18.4	158.9	31.0
SML54Z-5.2IIR	0.03	45.6	0.0	0.4	2.0	0.5	44.3	22.2	8.3	106.1	216.8	45.8	383.9	71.8
SML54Z-5.3IR	0.05	65.8	0.0	0.6	2.7	0.6	48.0	24.7	9.2	108.4	229.8	46.4	394.0	71.5
SML54Z-6.1C	0.06	125.8	0.0	5.6	16.7	4.8	110.7	111.2	31.9	305.0	466.9	86.8	677.8	124.0
SML54Z-6.2IR	0.93	85.4	0.0	1.9	3.8	1.0	47.1	31.9	10.9	118.7	216.5	42.3	362.2	66.9
SML54Z-7.1C	0.00	133.6	0.0	0.5	1.6	0.3	74.7	24.6	10.6	146.1	438.5	105.5	1012.4	210.1
SML54Z-7.2IR	0.01	47.0	0.0	0.3	1.7	0.3	35.7	16.6	6.4	82.7	185.9	39.8	346.6	64.0
SML54Z-7.3T	0.01	96.4	0.0	0.4	1.8	0.4	49.0	18.4	7.3	103.0	288.8	73.2	737.3	164.7
SML54Z-8.1IC	0.01	43.3	0.0	1.0	3.3	1.0	27.1	24.7	7.7	76.2	130.6	25.7	213.4	42.5
SML54Z-8.2T	0.00	55.7	0.0	0.3	2.1	0.3	51.6	23.9	9.4	120.0	253.1	52.4	412.7	72.8
SML54Z-9.1C	0.02	74.6	0.0	3.6	10.6	2.6	77.0	70.8	20.6	205.9	331.8	63.3	506.0	93.1
SML54Z-9.2IR	0.00	63.3	0.0	0.7	3.0	0.7	42.0	25.8	9.1	104.3	200.5	41.3	351.1	67.3
SML54Z-9.3T	0.00	108.7	0.0	0.2	1.0	0.2	53.3	11.5	5.0	82.7	399.3	119.7	1485.1	393.5

	La ppm	Ce ppm	Pr Calc	Nd ppm	Sm ppm	Eu ppm	Ho ppm	Gd ppm	Tb ppm	Dy ppm	Er ppm	Tm pm	Yb ppm	Lu ppm
CZ3-7.1JW145	0.04	0.5	0.0	0.0	0.1	0.0	1.6	1.1	0.4	4.9	8.3	1.7	14.5	2.6
CZ3-8.1JW145	0.03	0.6	0.0	0.1	0.1	0.0	1.9	1.0	0.4	4.4	8.6	1.8	16.0	2.7
CZ3-8.2JW145	0.04	0.6	0.0	0.1	0.1	0.0	1.7	1.0	0.3	4.1	8.2	1.7	14.4	2.4
Average	0.04	0.6	0.0	0.1	0.1	0.0	1.7	1.1	0.4	4.5	8.3	1.7	14.9	2.6
CZ3-10.1-189	0.02	0.4	0.0	0.1	0.1	0.1	1.9	1.0	0.5	5.4	9.0	2.0	16.6	3.0
CZ3-9.1-189	0.04	0.6	0.0	0.1	0.1	0.0	1.9	1.0	0.4	4.6	9.1	1.9	16.1	2.8
CZ3-6.1-251	0.03	0.5	0.0	0.1	0.1	0.0	1.7	1.1	0.4	4.4	8.4	1.7	14.4	2.9
CZ3-7.1-251	0.03	0.5	0.0	0.1	0.1	0.0	1.9	1.1	0.4	4.7	8.5	1.7	14.7	2.7
CZ3-7.2-251	0.04	0.5	0.0	0.1	0.1	0.0	1.9	1.1	0.4	4.6	8.9	1.9	14.8	2.7
CZ3-8.1-251	0.03	0.5	0.0	0.1	0.1	0.1	2.0	1.2	0.4	5.6	9.9	2.1	19.1	2.8
CZ3-8.2-251	0.03	0.5	0.0	0.1	0.1	0.1	1.8	0.9	0.3	4.3	8.4	1.7	14.8	2.5
Average	0.03	0.5	0.0	0.1	0.1	0.1	1.9	1.1	0.4	4.8	8.9	1.9	15.8	2.8
R33A206-19	0.03	5.1	0.0	1.0	3.8	0.9	66.6	34.0	11.8	144.7	324.2	69.9	611.6	122.3
R33-30A206	0.01	3.8	0.0	0.6	3.0	0.8	50.7	30.1	10.6	121.0	234.0	48.4	414.1	76.9

	Y/Yb	Er/Yb	Yb/Lu	Dy/Lu	Sm/Eu	Th/Yb	Ce/Nd	Sc+Y/3	(ScY/3)/P	Ce/Ce*	Eu/Eu*
BC101-1.5	2.59	0.51	5.15	1.12	5.47	0.65	166.57	448.73	1.68	2371.40	0.17
BC101-1.6R	3.08	0.58	5.06	1.55	5.12	0.21	50.95	352.88	1.03	752.57	0.20
BC101-1E	2.99	0.50	4.32	1.02	5.15	0.86	34.97	459.14	1.79	10.67	0.21
BC101-1E2	2.61	0.52	5.09	1.20	4.39	0.51	162.93	282.47	1.26	2107.57	0.22
BC101-1LGC	3.70	0.71	5.57	2.35	8.23	0.38	37.56	851.71	2.01	873.69	0.13
BC101-1LGI	2.96	0.54	5.12	1.26	4.38	0.47	153.35	320.74	1.22	2517.29	0.22
BC101-2.1T	2.87	0.54	5.19	1.33	4.70	0.50	130.31	312.19	1.28	1181.74	0.21
BC101-2.2C	3.48	0.65	5.32	2.27	3.49	0.31	20.90	852.62	2.54	237.49	0.35
BC101-2.3I	2.60	0.51	4.81	1.14	3.35	0.49	114.49	220.81	1.05	1233.73	0.31
BC101-2.4I	2.44	0.47	4.85	0.93	5.61	0.61	247.15	316.49	1.58	677.43	0.16
BC101-2.5T2	3.19	0.60	5.27	1.57	4.66	0.50	103.75	418.89	1.39	263.91	0.22
BC101-3.1T	2.11	0.41	4.39	0.70	4.39	1.26	189.26	264.20	1.66	906.80	0.21
BC101-3.2I	2.61	0.52	5.14	1.09	5.87	1.81	212.31	487.00	1.85	2901.42	0.16
BC101-3.3R	2.06	0.40	4.24	0.61	7.41	0.88	14.88	275.02	0.35	6.19	0.20
BC101-3.4C	3.15	0.60	5.16	1.75	3.47	0.34	37.51	426.18	1.97	559.14	0.30
BC101-3.5T2	2.27	0.43	4.81	0.77	4.08	1.08	202.28	390.29	1.86	194.81	0.23
BC101-4.1R	2.61	0.50	5.13	1.10	4.67	0.72	162.36	435.24	2.01	2216.92	0.20
BC101-4.2I	2.86	0.57	5.33	1.45	4.75	0.44	118.76	316.80	1.28	1867.40	0.22
BC101-4.3C	2.09	0.40	4.73	0.57	6.65	2.20	280.19	548.38	2.46	4861.06	0.14
BC101-5.1I	2.85	0.59	5.22	1.48	4.48	0.49	114.32	289.79	1.33	735.15	0.22
BC101-5.2R	2.78	0.58	5.56	1.64	4.26	0.50	93.60	322.53	0.98	1466.76	0.23
BC101-6.1I	3.29	0.66	5.23	2.10	3.46	0.37	16.95	611.84	2.35	201.07	0.33
BC101-7.1I	3.03	0.61	5.36	1.71	4.70	0.34	73.36	493.20	1.87	1361.27	0.21
BC101-7.2R	1.83	0.38	4.67	0.52	7.51	1.86	495.05	610.53	2.51	3323.40	0.12
BC101-8.1R	3.01	0.58	5.61	1.53	5.20	0.49	116.14	356.95	1.26	1861.40	0.19
BC101-8.2I	2.78	0.55	5.20	1.35	4.46	0.57	140.11	344.79	1.23	520.85	0.22

	Y/Yb	Er/Yb	Yb/Lu	Dy/Lu	Sm/Eu	Th/Yb	Ce/Nd	Sc+Y/3	(ScY/3)/P	Ce/Ce*	Eu/Eu*
BC101-9.1R	2.24	0.46	4.61	0.86	4.86	0.70	272.62	226.82	1.20	1402.64	0.19
BC101-9.2IR	2.54	0.52	5.33	1.16	4.15	0.85	237.80	969.35	2.45	5823.35	0.21
BC101-9.3I	2.71	0.59	5.52	1.66	5.06	0.47	104.41	366.56	2.32	1284.80	0.19
BC101-9.4C	2.88	0.58	5.18	1.50	3.71	0.40	134.33	381.38	1.80	2822.37	0.25
BC101-10.1R	2.45	0.47	5.15	1.01	4.84	0.85	183.48	357.43	1.87	2125.78	0.20
BC101-10.2C	3.41	0.63	5.43	1.94	4.28	1.14	53.07	907.25	1.45	639.98	0.25
BC101-10.3I	2.15	0.42	4.98	0.72	9.16	1.69	318.63	764.59	2.65	803.49	0.10
BC101-11.1R	3.20	0.59	5.16	1.67	5.10	0.35	71.72	297.45	0.97	759.22	0.21
BC101-11.2I	3.02	0.60	5.59	1.62	5.53	0.53	136.49	463.10	1.48	3265.47	0.16
BC101-11.3R	2.91	0.58	5.28	1.39	4.94	0.43	130.03	370.28	1.27	2832.57	0.20
BC101-12.1T	2.65	0.51	5.14	1.17	4.12	1.16	142.83	413.39	1.61	1443.66	0.22
BC101-12.2I	2.59	0.57	5.35	1.40	4.79	0.97	181.15	629.40	1.55	1849.14	0.17
BC101-12.3C	2.46	0.52	4.66	1.12	4.11	0.41	127.80	304.80	1.15	1261.60	0.21
BC101-12.4C	2.98	0.57	5.03	1.34	3.98	0.36	120.47	402.96	1.26	1855.16	0.23
BC101-13.1C	3.25	0.60	5.35	1.69	4.21	0.53	65.05	679.46	2.78	644.64	0.24
BC101-13.2IR	2.66	0.53	5.19	1.17	7.62	0.79	182.24	466.42	1.69	268.77	0.13
BC101-13.3R	3.01	0.56	5.07	1.37	5.51	0.46	96.84	389.95	1.24	137.98	0.18
BC101-14.1C	3.61	0.66	5.15	2.23	4.08	0.41	17.89	726.74	2.33	199.50	0.30
BC101-14.2IR	2.62	0.53	5.18	1.04	7.01	0.50	318.83	662.50	1.85	3007.33	0.12
BC101-14.3I	3.14	0.59	5.23	1.63	4.33	0.68	92.15	428.58	1.46	455.71	0.24
BC101-14.4IR	2.60	0.54	5.43	1.33	5.78	0.57	193.65	374.20	1.30	2170.23	0.16
BC101-14.5R	3.06	0.59	5.27	1.53	4.90	0.51	117.55	328.78	1.19	1463.97	0.21

	Y/Yb	Er/Yb	Yb/Lu	Dy/Lu	Sm/Eu	Th/Yb	Ce/Nd	Sc+Y/3	(ScY/3)/P	Ce/Ce*	Eu/Eu*
DSCG-1.1T	3.08	0.57	5.33	1.64	4.00	0.46	78.54	365.33	1.26	1185.24	0.25
DSCG-1.2IR	2.29	0.48	5.17	1.05	4.80	0.99	211.52	481.44	1.58	1932.95	0.19
DSCG-1.3C	2.58	0.54	5.02	1.21	4.16	0.28	187.39	305.13	1.18	817.56	0.23
DSCG-10.1C	1.89	0.39	4.61	0.54	8.54	1.58	300.95	602.07	1.37	1606.46	0.10
DSCG-10.2IR	2.69	0.61	5.28	1.62	4.19	0.45	85.78	395.96	0.89	1114.22	0.24
DSCG-11.1C	2.73	0.50	5.28	1.08	6.81	1.19	91.05	1647.00	3.24	526.77	0.14
DSCG-11.2I	2.37	0.45	4.92	0.82	6.38	2.80	321.26	1059.82	2.53	2831.97	0.13
DSCG-11.3R	2.42	0.49	4.82	0.88	4.42	0.91	214.68	313.52	1.73	1888.55	0.21
DSCG-12.1R	2.96	0.58	5.49	1.64	4.48	0.56	80.12	451.67	1.30	374.95	0.22
DSCG-12.2I	3.26	0.62	5.37	1.71	3.53	0.39	38.70	504.25	1.31	367.03	0.29
DSCG-13.1C	3.29	0.67	5.24	2.14	4.14	0.26	13.60	501.51	1.38	158.21	0.26
DSCG-13.2I	3.17	0.62	5.43	1.83	4.84	0.41	48.72	368.15	0.93	1019.45	0.22
DSCG-13.3T	2.72	0.56	5.25	1.48	3.39	0.49	129.85	305.34	0.99	1795.46	0.24
DSCG-14.1I	2.37	0.48	5.09	0.91	4.92	0.45	297.44	250.79	1.33	188.42	0.18
DSCG-14.2R	2.86	0.56	5.18	1.33	4.41	0.31	97.95	548.24	1.35	310.18	0.23
DSCG-15.1R	3.06	0.56	5.29	1.41	4.55	0.66	100.00	453.10	1.32	1007.40	0.22
DSCG-15.2I	2.82	0.58	4.91	1.53	3.27	0.31	87.62	166.77	0.92	1247.47	0.31
DSCG-16.1C	2.29	0.45	5.00	0.82	7.23	8.53	254.93	2209.33	4.00	1989.06	0.13
DSCG-16.2R	2.97	0.58	5.41	1.47	4.84	0.48	105.77	488.75	1.35	683.11	0.20
DSCG-17.1C	1.91	0.35	4.66	0.44	10.18	4.39	357.92	2040.55	4.36	615.94	0.10
DSCG-17.2R	3.01	0.61	5.59	1.64	4.67	0.49	80.98	474.23	1.54	230.54	0.22
DSCG-18.1R	2.16	0.43	4.60	0.84	3.64	0.72	159.54	248.37	1.86	1227.56	0.25
DSCG-19.1IR	2.25	0.45	4.63	0.86	3.98	1.59	199.43	378.04	1.78	2576.16	0.26
DSCG-2.1T	2.58	0.51	5.32	1.18	4.71	0.92	191.77	497.23	1.45	2012.00	0.18
DSCG-2.2I	2.59	0.56	5.07	1.38	4.28	0.40	174.95	204.28	0.90	1060.38	0.24
DSCG-2.3C	1.89	0.38	4.41	0.54	9.61	0.89	209.70	622.74	2.34	332.44	0.10
DSCG-2.3C2	2.93	0.60	5.41	1.70	4.43	0.39	81.21	539.27	1.09	2099.12	0.22
DSCG-20.1R	2.39	0.47	5.01	1.02	4.16	0.80	151.06	377.19	1.68	1601.85	0.23
DSCG-20.2I	3.08	0.57	5.05	1.62	3.68	0.47	63.52	316.68	1.17	843.23	0.30
DSCG-21.1C	3.67	0.66	5.60	2.39	3.57	0.32	14.02	697.94	1.87	194.78	0.31
DSCG-21.2I	2.93	0.58	5.08	1.64	4.12	0.35	66.05	277.83	0.94	481.81	0.27
DSCG-3.2C	3.53	0.66	5.44	2.35	3.45	0.40	19.84	795.65	2.31	191.13	0.33
DSCG-3.3IR	2.28	0.47	4.74	0.86	4.80	0.47	75.16	451.46	1.55	55.21	0.21
DSCG-4.1T	2.49	0.48	4.87	1.01	3.24	1.28	183.17	396.25	1.35	850.00	0.29

	Y/Yb	Er/Yb	Yb/Lu	Dy/Lu	Sm/Eu	Th/Yb	Ce/Nd	Sc+Y/3	(ScY/3)/P	Ce/Ce*	Eu/Eu*
DSCG-4.2R	2.48	0.50	5.12	1.07	3.95	0.49	167.58	501.35	1.83	2992.41	0.22
DSCG-4.3IR	3.61	0.65	5.12	2.02	3.55	0.32	23.79	417.33	1.63	278.85	0.33
DSCG-4.4C	4.04	0.73	5.25	2.77	3.69	0.51	15.37	918.90	2.05	131.02	0.34
DSCG-5.1T	2.77	0.57	5.47	1.56	4.58	0.51	114.05	382.48	1.08	2421.68	0.22
DSCG-5.2IR	1.81	0.37	4.32	0.52	4.57	0.79	30.40	217.25	0.39	9.71	0.24
DSCG-5.3IR	1.69	0.36	4.10	0.48	4.25	0.99	72.73	235.36	1.63	17.55	0.24
DSCG-5.4IR	2.82	0.58	5.53	1.58	4.17	0.59	122.53	386.49	1.17	1561.58	0.23
DSCG-5.5C	2.08	0.38	4.67	0.57	5.44	1.15	290.91	759.84	2.63	737.36	0.15
DSCG-5.6I	1.98	0.38	4.14	0.59	3.15	0.47	244.67	195.11	1.90	1104.57	0.29
DSCG-6.1T	2.26	0.41	4.13	0.69	3.90	1.73	201.37	323.94	2.13	1015.17	0.23
DSCG-6.2C	2.16	0.39	4.71	0.56	7.55	1.59	426.92	897.17	1.88	2395.60	0.12
DSCG-7.1C	2.32	0.43	4.80	0.72	7.48	3.16	376.80	897.40	2.50	5459.69	0.12
DSCG-7.2IR	3.46	0.62	5.46	1.90	4.69	1.25	105.16	598.50	1.40	1037.74	0.22
DSCG-7.3IR	3.14	0.60	5.54	1.77	4.15	0.60	89.98	486.28	1.22	2052.78	0.25
DSCG-7.4T	2.76	0.54	5.24	1.28	5.09	0.50	166.23	383.25	1.19	2532.71	0.17
DSCG-8.1C	2.15	0.43	4.77	0.71	5.98	0.73	201.64	348.48	1.06	243.44	0.15
DSCG-8.2IR	2.56	0.48	4.87	0.85	4.38	0.54	270.07	580.44	1.40	1597.66	0.19
DSCG-8.3IR	3.03	0.61	5.03	1.61	3.48	0.58	98.71	289.72	0.96	822.53	0.30
DSCG-8.4T	2.18	0.44	4.79	0.83	4.08	1.00	209.02	262.43	1.44	2404.09	0.21
DSCG-9.1C	3.61	0.67	5.80	2.36	3.42	1.19	48.51	3084.85	2.44	500.90	0.28
DSCG-9.2IR	3.24	0.60	5.27	1.83	6.14	0.44	70.76	386.48	0.92	873.64	0.17
DSCG-9.3R	2.83	0.57	5.18	1.45	4.77	0.50	102.11	358.97	1.03	927.66	0.22
DSCG-9.4IR	2.49	0.49	5.33	1.11	4.67	0.84	58.51	263.07	1.12	32.99	0.20

	Y/Yb	Er/Yb	Yb/Lu	Dy/Lu	Sm/Eu	Th/Yb	Ce/Nd	Sc+Y/3	(ScY/3)/P	Ce/Ce*	Eu/Eu*
LGZ-1.2IC	3.16	0.63	5.23	2.06	2.97	0.35	20.11	667.08	1.96	237.50	0.40
LGZ-1.2T	2.04	0.35	4.60	0.45	8.00	4.72	406.19	1563.07	4.66	1197.47	0.12
LGZ-10.1I	4.12	0.69	5.35	2.55	4.39	0.29	16.52	645.27	2.30	95.81	0.28
LGZ-11.1IR	3.11	0.57	5.04	1.51	3.36	0.26	58.29	400.36	1.27	719.43	0.33
LGZ-2.1C	1.72	0.34	4.27	0.42	6.42	2.18	377.31	645.47	3.50	4936.34	0.14
LGZ-2.2R	1.65	0.32	4.42	0.37	8.25	1.28	547.13	828.48	4.08	4007.61	0.11
LGZ-2.3I	2.75	0.54	5.17	1.39	5.06	0.30	133.56	219.31	1.02	1214.05	0.20
LGZ-3.1I	2.89	0.59	5.43	1.47	11.18	0.62	175.98	609.31	1.62	1934.60	0.08
LGZ-4.1C	2.27	0.44	5.02	0.79	17.06	0.75	385.37	697.93	2.49	1558.19	0.05
LGZ-5.1I	2.98	0.58	5.14	1.42	3.95	0.37	114.18	316.33	1.43	1205.15	0.25
LGZ-6.1T	1.93	0.37	4.37	0.49	5.31	1.49	265.24	472.58	2.45	208.27	0.18
LGZ-6.2I	4.09	0.69	5.47	2.48	3.75	0.47	24.14	1327.70	2.37	238.73	0.31
LGZ-7.1I	2.27	0.41	4.67	0.60	14.64	3.96	549.35	1041.53	3.86	6318.66	0.05
LGZ-8.1I	4.01	0.71	5.38	2.62	2.59	0.53	18.68	1386.11	2.37	147.46	0.46
LGZ-8.2IR	2.35	0.46	4.72	0.86	5.15	0.81	152.77	367.58	1.48	111.81	0.19
LGZ-9.1I	2.87	0.56	4.67	1.38	3.67	0.24	65.59	352.06	1.33	1115.47	0.29
LGZ-11.2I	3.80	0.68	5.49	2.53	4.02	0.67	28.76	1614.19	2.91	261.62	0.29
LGZ-12.1I	1.66	0.37	4.31	0.42	5.94	2.13	371.78	377.73	2.42	3254.47	0.15
LGZ-13.1C	2.08	0.38	4.47	0.51	9.79	1.80	411.35	666.44	3.33	515.79	0.09

	Y/Yb	Er/Yb	Yb/Lu	Dy/Lu	Sm/Eu	Th/Yb	Ce/Nd	Sc+Y/3	(ScY/3)/P	Ce/Ce*	Eu/Eu*
SWZ-1.1I	3.09	0.59	5.25	1.56	4.45	0.45	112.84	314.85	1.13	1925.68	0.22
SWZ-10.1C	2.95	0.50	5.07	1.16	3.34	0.93	92.60	356.92	1.79	1049.54	0.32
SWZ-11.1IR	2.83	0.53	5.20	1.25	4.14	0.49	165.02	252.55	1.13	1947.02	0.23
SWZ-11.2I	2.49	0.50	4.86	1.07	3.87	0.36	275.67	130.71	0.90	928.54	0.25
SWZ-11.3C	1.82	0.40	4.48	0.53	11.43	0.91	24.25	312.28	0.36	11.02	0.11
SWZ-11.4R	2.99	0.60	5.06	1.55	3.73	0.39	115.69	208.17	0.96	282.03	0.29
SWZ-11.5IR	2.24	0.42	4.71	0.64	5.51	0.81	347.30	667.05	2.50	729.42	0.15
SWZ-2.1IR	2.38	0.49	5.07	0.95	4.34	0.59	204.36	316.01	1.68	1669.07	0.20
SWZ-2.2I	3.37	0.62	5.26	2.13	2.89	0.42	13.33	629.99	2.19	150.72	0.42
SWZ-3.1R	3.24	0.60	5.34	1.71	5.25	0.80	109.84	487.28	1.38	1617.05	0.20
SWZ-4.1IC	2.39	0.47	4.87	0.89	4.88	0.44	241.73	377.23	1.61	1999.48	0.18
SWZ-4.2R	3.31	0.62	5.36	1.75	4.49	0.95	87.37	529.13	1.20	1560.23	0.24
SWZ-5.1R	3.27	0.60	5.17	1.61	4.25	0.50	87.72	358.97	1.18	930.22	0.25
SWZ-5.2IC	2.62	0.54	5.22	1.28	4.40	0.61	133.56	393.87	1.20	249.49	0.23
SWZ-6.1IC	3.64	0.68	5.65	2.66	2.94	0.77	23.54	2617.04	2.57	231.87	0.40
SWZ-6.2R	3.04	0.60	5.33	1.72	4.08	0.75	83.21	410.10	1.10	2081.21	0.25
SWZ-7.1R	3.26	0.64	5.44	1.87	4.51	1.01	89.60	570.38	1.23	1266.91	0.22
SWZ-8.1R	2.99	0.60	5.05	1.58	4.58	0.49	110.24	326.67	1.08	1182.00	0.24
SWZ-8.2IR	2.12	0.42	4.62	0.67	7.16	0.48	310.29	469.21	1.94	2138.11	0.13
SWZ-8.3I	2.47	0.51	5.11	1.07	3.76	0.28	197.63	161.55	0.93	1532.01	0.23
SWZ-8.4C	3.25	0.62	5.52	2.10	4.23	2.82	114.25	1399.42	1.82	1363.16	0.26
SWZ-9.1C	3.56	0.63	5.32	2.13	2.78	0.31	18.23	449.43	2.57	269.88	0.44
SWZ-9.2I	3.13	0.57	5.18	1.52	4.11	0.47	115.33	304.12	1.12	1457.43	0.25
SWZ-9.3IR	3.17	0.57	4.90	1.48	3.07	0.51	105.17	204.97	1.00	1171.78	0.34
SWZ-9.4R	3.04	0.60	5.33	1.56	4.51	0.49	129.81	332.52	1.27	2067.15	0.22

	Y/Yb	Er/Yb	Yb/Lu	Dy/Lu	Sm/Eu	Th/Yb	Ce/Nd	Sc+Y/3	(ScY/3)/P	Ce/Ce*	Eu/Eu*
SML49Z-1.1C	2.92	0.64	5.49	2.02	4.91	0.58	22.40	915.19	1.41	17.02	0.24
SML49Z-1.2R	2.46	0.47	4.93	0.84	6.97	0.81	266.75	772.65	2.45	3426.68	0.13
SML49Z-1.3I	2.91	0.58	5.27	1.44	4.95	0.37	140.85	421.53	1.54	867.85	0.20
SML49Z-10.1R	2.50	0.49	5.13	0.96	6.20	0.95	248.71	682.04	2.05	6889.83	0.15
SML49Z-10.2IR	3.63	0.59	5.32	1.66	10.45	0.69	10.51	1177.65	4.12	13.76	0.14
SML49Z-10.3C	3.86	0.63	5.77	2.30	11.13	0.23	6.23	500.14	1.28	8.31	0.15
SML49Z-10.4C	2.59	0.53	5.17	1.13	4.69	0.31	248.99	280.62	1.26	1805.96	0.19
SML49Z-10.5IR	2.07	0.38	4.48	0.50	7.59	0.72	462.89	498.66	2.93	3725.12	0.11
SML49Z-10.6IR	2.17	0.47	5.00	0.91	5.21	0.47	387.08	118.97	0.99	1890.26	0.17
SML49Z-11.1C	2.52	0.52	4.97	1.07	3.90	0.32	151.17	220.21	1.12	1175.88	0.24
SML49Z-11.2IR	3.01	0.55	5.09	1.36	3.65	0.29	89.00	307.24	1.30	205.56	0.27
SML49Z-11.3R	2.03	0.40	4.64	0.55	6.46	1.04	331.91	625.37	2.55	4104.39	0.13
SML49Z-12.1IC	3.34	0.61	5.36	1.60	4.29	0.42	106.76	477.92	2.03	1473.65	0.23
SML49Z-12.2T	2.15	0.40	4.68	0.57	7.38	1.23	358.73	732.82	2.95	2919.20	0.12
SML49Z-13.1IC	3.62	0.68	5.75	2.18	7.04	0.33	149.84	602.63	1.84	2604.73	0.12
SML49Z-13.2IR	2.68	0.54	5.39	1.33	4.91	0.47	186.07	267.71	1.39	1837.93	0.19
SML49Z-13.3T	2.14	0.44	4.93	0.79	5.96	1.52	294.47	484.64	2.07	3724.28	0.15
SML49Z-2.1C	2.78	0.57	4.98	1.43	3.10	0.30	80.12	205.69	1.98	1142.93	0.33
SML49Z-2.2T	1.90	0.35	4.58	0.39	8.37	0.84	602.80	991.04	3.80	7608.63	0.10
SML49Z-2.3IR	2.60	0.55	5.00	1.31	3.57	0.29	95.05	464.76	1.58	1402.83	0.28
SML49Z-3.1I	3.26	0.64	5.30	2.02	4.08	0.30	28.80	530.19	2.73	534.19	0.28
SML49Z-3.2R	2.36	0.47	4.78	0.84	4.75	0.47	209.50	403.40	1.89	2278.83	0.19
SML49Z-4.1C	2.96	0.64	5.47	1.94	4.12	0.35	52.74	501.60	2.29	832.06	0.25
SML49Z-4.2T	2.10	0.41	4.74	0.62	6.72	1.13	269.38	668.03	2.99	3273.14	0.14
SML49Z-5.1C	3.01	0.61	5.55	1.74	4.58	0.47	64.01	657.54	2.03	1167.81	0.22
SML49Z-5.2R	1.82	0.36	4.62	0.46	6.75	0.69	472.68	736.17	3.67	3810.04	0.13
SML49Z-5.3IR	2.64	0.51	5.36	1.24	4.52	0.48	177.45	259.97	1.25	2070.72	0.21
SML49Z-6.1R	2.10	0.41	4.78	0.64	6.48	0.94	151.96	719.32	4.04	2754.23	0.14
SML49Z-6.2IR	3.48	0.70	5.39	2.31	3.09	2.12	87.85	748.31	1.45	1361.08	0.34
SML49Z-6.3IR	2.86	0.55	5.29	1.41	3.43	0.54	135.26	222.95	1.15	1246.85	0.29
SML49Z-7.1R	1.58	0.35	4.56	0.38	7.53	0.78	563.44	760.36	3.05	5101.24	0.11
SML49Z-7.2IR	2.90	0.55	5.33	1.41	4.29	0.47	158.36	311.86	1.15	1790.56	0.23
SML49Z-7.3C	2.95	0.56	5.05	1.30	3.67	0.22	162.70	189.35	1.39	1343.12	0.26
SML49Z-7.4IR	3.09	0.58	5.06	1.41	4.51	0.50	135.64	301.32	1.29	1771.38	0.23
SML49Z-8.1C	3.28	0.58	5.14	1.32	3.94	0.35	162.04	312.08	1.58	929.37	0.23
SML49Z-8.2IR	2.48	0.45	5.02	0.75	6.48	0.63	196.43	907.42	2.48	237.12	0.15
SML49Z-8.3R	1.93	0.36	4.55	0.44	8.61	1.71	402.69	708.19	2.80	2202.29	0.11
SML49Z-8.4IR	2.49	0.46	5.03	0.84	7.03	1.19	268.83	692.19	2.17	1726.53	0.13
SML49Z-8.5C	2.50	0.51	5.20	1.16	4.68	0.32	169.30	231.29	1.14	1236.28	0.20
SML49Z-9.1C	3.20	0.62	5.17	1.83	3.12	0.28	39.13	289.79	1.94	511.25	0.36
SML49Z-9.2IR	2.70	0.55	4.83	1.28	3.64	0.27	86.45	333.22	1.47	1133.24	0.29

	Y/Yb	Er/Yb	Yb/Lu	Dy/Lu	Sm/Eu	Th/Yb	Ce/Nd	Sc+Y/3	(ScY/3)/P	Ce/Ce*	Eu/Eu*
SML49Z-9.3R	1.93	0.39	4.70	0.51	6.88	0.91	593.72	1022.71	3.34	6253.55	0.12

	Y/Yb	Er/Yb	Yb/Lu	Dy/Lu	Sm/Eu	Th/Yb	Ce/Nd	Sc+Y/3	(ScY/3)/P	Ce/Ce*	Eu/Eu*
SML54Z-1.1I	3.40	0.64	5.21	1.91	4.00	0.36	45.47	459.96	2.01	605.78	0.28
SML54Z-1.2R	1.68	0.31	4.05	0.36	5.36	1.14	94.25	862.86	8.42	1619.88	0.19
SML54Z-10.1C	2.06	0.40	4.91	0.62	6.72	0.91	213.70	728.88	1.03	259.23	0.13
SML54Z-10.2R	2.80	0.56	5.53	1.46	5.04	0.61	136.53	346.75	1.18	199.51	0.19
SML54Z-2.1I	3.59	0.63	5.12	2.02	2.93	0.26	16.10	408.91	2.08	177.29	0.42
SML54Z-3.1C	3.60	0.67	5.70	2.45	3.10	0.56	26.11	1064.87	2.78	263.60	0.37
SML54Z-3.2I	3.01	0.62	5.20	1.75	3.72	0.79	79.32	415.26	1.35	1059.04	0.28
SML54Z-3.3T	1.31	0.26	3.80	0.20	5.14	1.00	619.25	1195.29	6.77	5601.76	0.16
SML54Z-4.1C	2.62	0.54	4.97	1.26	3.41	0.30	143.43	223.51	1.32	1691.53	0.27
SML54Z-4.2IR	2.87	0.55	5.09	1.33	3.93	0.32	99.33	509.70	1.62	1717.16	0.25
SML54Z-4.3T	2.38	0.49	5.15	0.97	7.88	1.18	234.16	538.97	1.91	1626.03	0.12
SML54Z-5.1C	2.54	0.51	5.13	1.07	3.48	0.28	254.04	147.96	1.03	1728.34	0.25
SML54Z-5.2IIR	2.75	0.56	5.35	1.48	4.24	0.27	109.39	381.38	1.27	285.07	0.22
SML54Z-5.3IR	2.76	0.58	5.51	1.52	4.61	0.47	117.69	389.99	1.25	268.52	0.22
SML54Z-6.1C	3.77	0.69	5.47	2.46	3.51	0.54	22.66	907.38	2.77	225.14	0.34
SML54Z-6.2IR	2.93	0.60	5.42	1.78	4.02	0.83	46.15	388.65	0.96	35.42	0.26
SML54Z-7.1C	2.19	0.43	4.82	0.70	6.14	1.42	292.88	794.81	2.66	3169.38	0.13
SML54Z-7.2IR	2.56	0.54	5.41	1.29	5.58	0.48	156.70	315.20	1.37	831.52	0.17
SML54Z-7.3T	1.90	0.39	4.48	0.63	4.61	1.25	237.87	563.94	2.91	1492.10	0.21
SML54Z-8.1IC	2.89	0.61	5.02	1.79	3.26	0.24	43.24	241.72	1.55	681.47	0.34
SML54Z-8.2T	3.01	0.61	5.67	1.65	6.03	0.54	162.97	430.43	1.24	2344.59	0.15
SML54Z-9.1C	3.55	0.66	5.44	2.21	4.07	0.37	20.83	635.60	2.47	328.97	0.29
SML54Z-9.2IR	2.80	0.57	5.22	1.55	3.95	0.36	88.96	363.89	1.44	1326.14	0.26
SML54Z-9.3T	1.29	0.27	3.77	0.21	5.66	0.95	456.61	993.50	7.06	5772.23	0.16

	Y/Yb	Er/Yb	Yb/Lu	Dy/Lu	Sm/Eu	Th/Yb	Ce/Nd	Sc+Y/3	(ScY/3)/P	Ce/Ce*	Eu/Eu*
CZ3-7.1JW145	2.98	0.57	5.67	1.92	3.47	1.88	12.50	18.71	1.31	5.93	0.31
CZ3-8.1JW145	2.93	0.54	5.89	1.62	2.70	1.92	10.32	20.17	1.36	7.22	0.40
CZ3-8.2JW145	3.03	0.57	5.96	1.71	3.26	1.95	10.20	18.85	1.31	6.02	0.32
Average	2.98	0.56	5.84	1.75	3.11	1.91	10.82	19.25	1.33		
CZ3-10.1-189	2.96	0.54	5.57	1.80	1.94	1.93	8.70	20.67	1.45	8.16	0.52
CZ3-9.1-189	2.95	0.57	5.75	1.64	2.79	1.94	6.38	20.30	1.32	5.58	0.37
CZ3-6.1-251	2.93	0.58	5.03	1.52	3.46	1.98	7.90	18.42	1.48	6.07	0.31
CZ3-7.1-251	2.80	0.58	5.51	1.75	3.34	1.89	9.75	17.97	1.52	7.41	0.32
CZ3-7.2-251	2.99	0.60	5.51	1.73	2.87	2.02	7.24	19.30	1.50	5.23	0.36
CZ3-8.1-251	2.41	0.52	6.72	1.98	1.92	0.00	8.78	19.89	1.59	6.68	0.54
CZ3-8.2-251	3.00	0.57	5.86	1.71	2.62	1.85	7.74	19.24	1.64	6.43	0.46
Average	2.85	0.56	5.70	1.73	2.60	1.87	7.88	19.40	1.49	6.31	0.41
R33A206-19	2.78	0.53	5.00	1.18	4.05	0.29	5.03	580.94	3.38	26.16	0.25
R33-30A206	3.50	0.56	5.39	1.57	3.74	0.16	5.98	498.14	2.85	45.07	0.25

Figure E1:
Cathodoluminsecence images of zircons from sample BC101z with spots from Trace Element SHRIMP-RG analyses marked

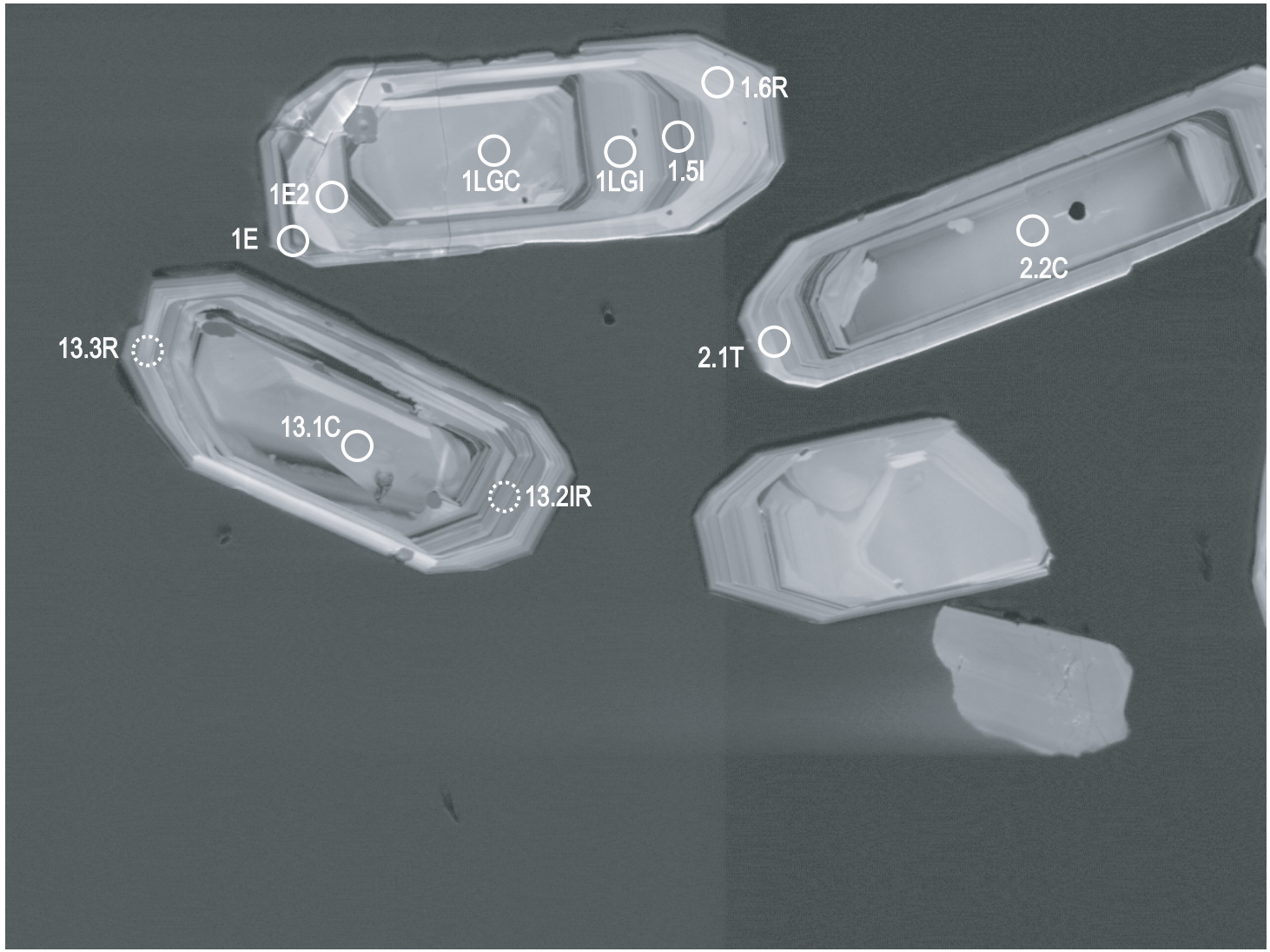
1.6R
1LGC
1LGI
1.5I
1E2
1E
2.2C
13.3R
2.1T
13.1C
13.2IR

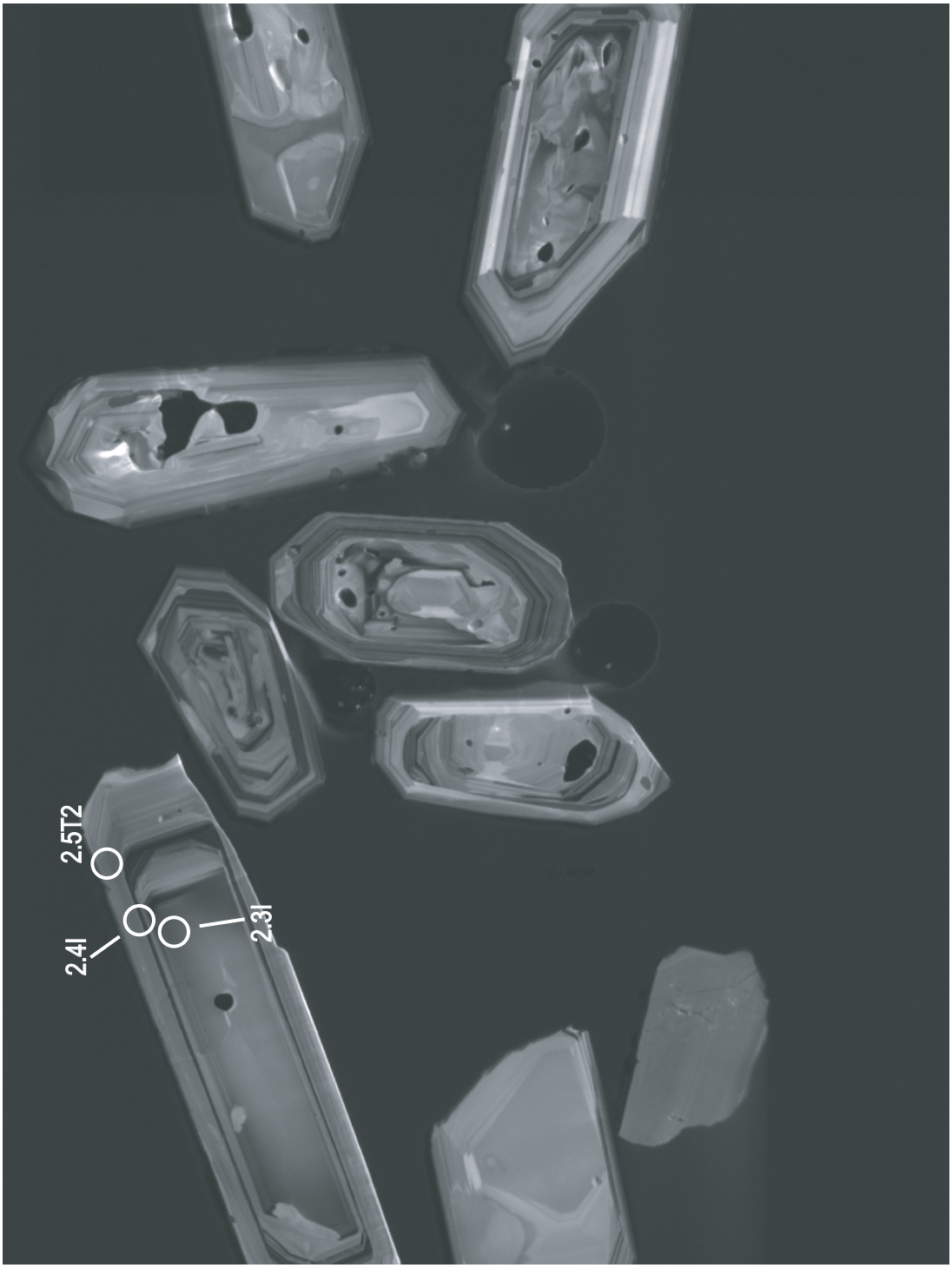
2.5T2
2.4I
2.3I

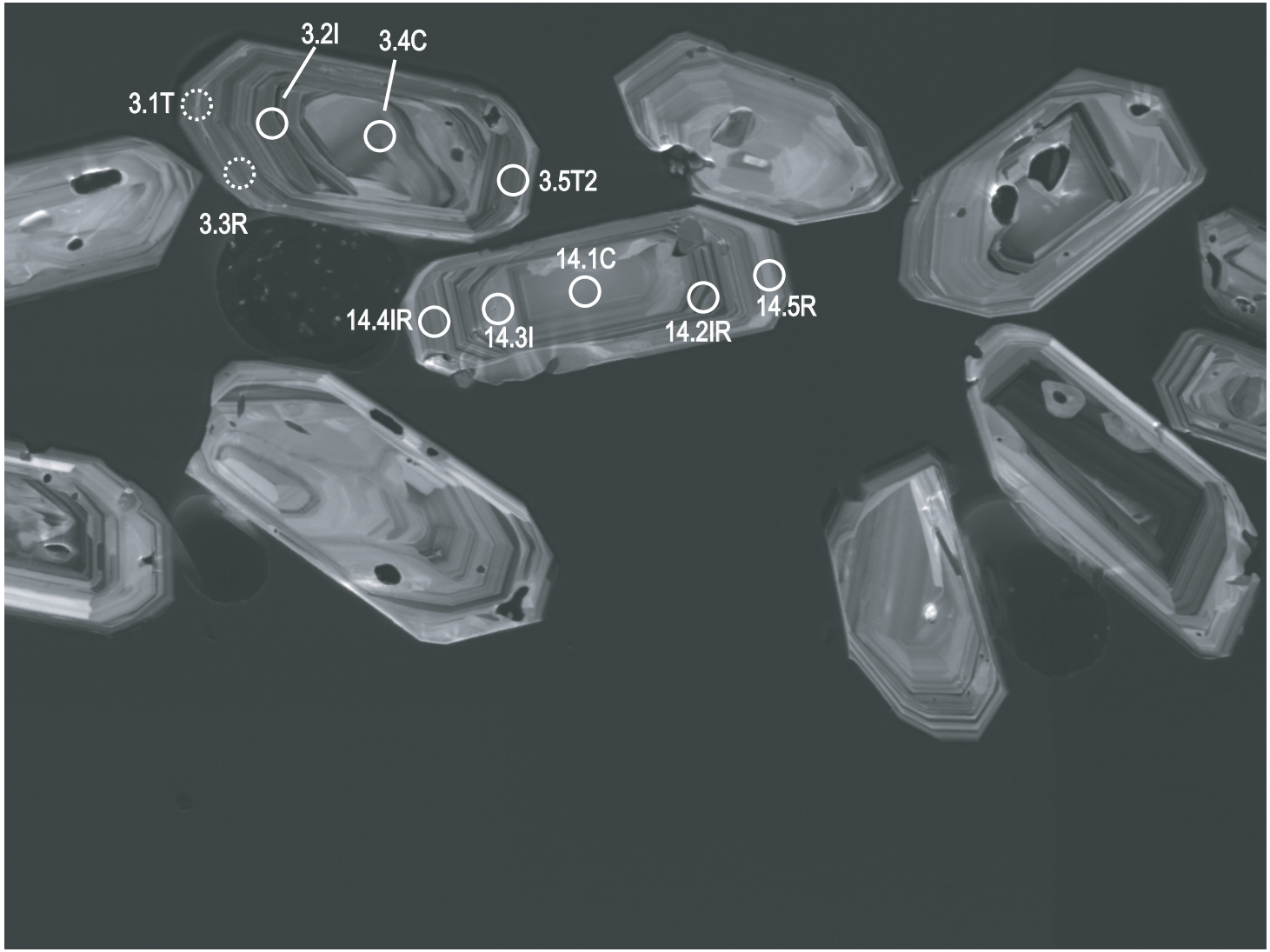
3.2I
3.4C
3.1T
3.5T2
3.3R
14.1C
14.4IR
14.3I
14.2IR
14.5R

4.2I
4.3C
4.1R
5.1I
5.2R

8.1R
8.2I
7.2R
7.1I
7.3R
6.1R

11.3R
11.2I
11.1R
10.3I
10.2C
10.1R
9.2IR
9.3I
9.4C
9.1R

12.1TO
12.2I
12.3C/12.4C

Figure E2:
Cathodoluminsecence images of zircons from sample DSCG with spots from Trace Element SHRIMP-RG analyses marked

3.3IR
3.2C
3.1T(2.3C2)
1.3C
1.1T
1.2IR

20.1R
20.2I
2.3C
2.2I
2.1T

4.2R
4.1T
4.3IR
4.4C
19.1i
18.1R

5.6I
5.5C
5.4IR
5.3IR
5.2IR
5.1T
6.1T
6.2C

7.1C
7.2IR
7.3IR
7.4T

8.4T
8.3IR
8.2IR
8.1C
16.2R
16.1C
10.1C
10.2I
9.2IR
9.1C
9.3R
17.1C
17.2R

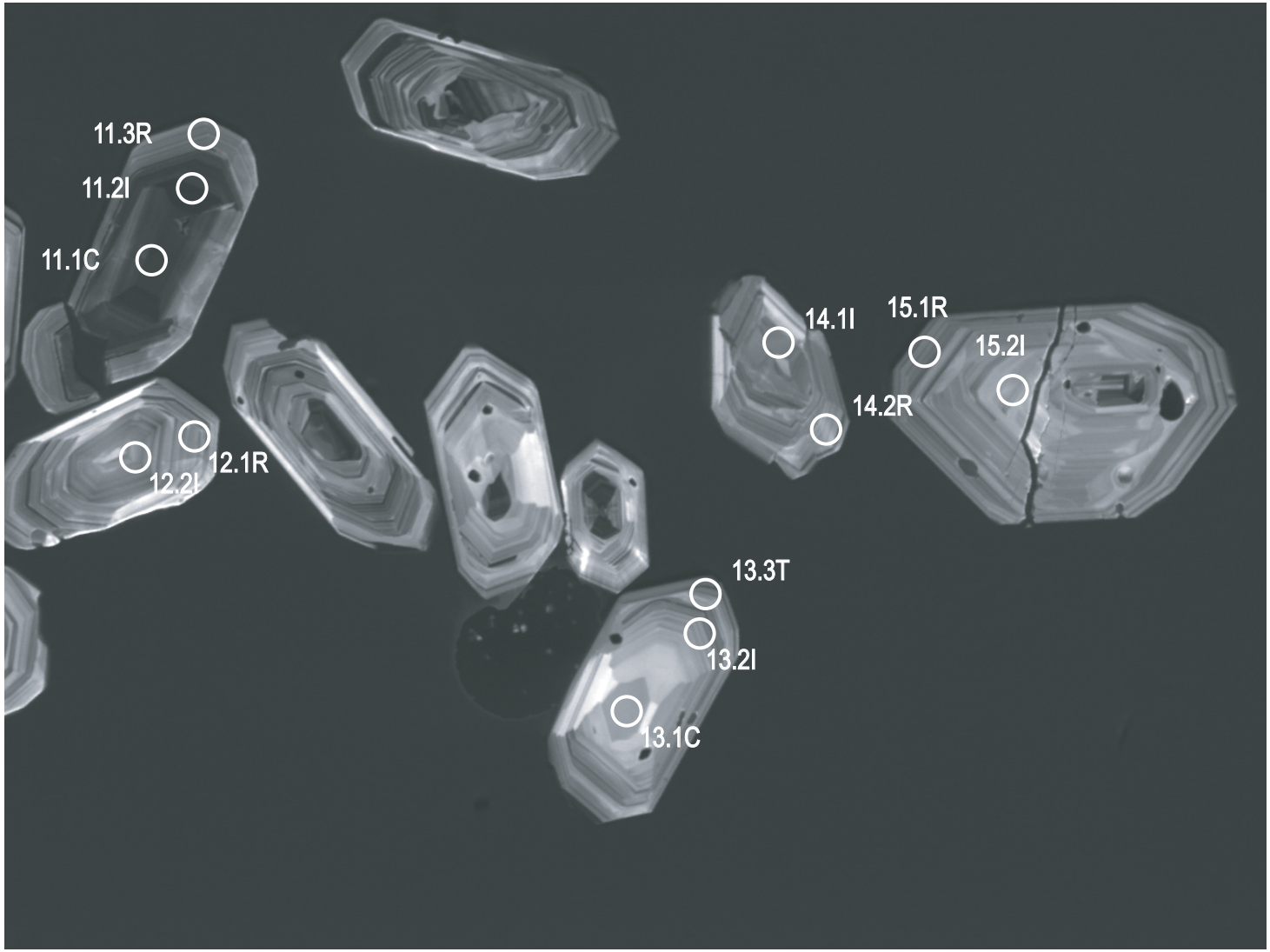
11.3R
11.2I
11.1C
14.1I
15.1R
15.2I
14.2R
12.2I
12.1R
13.3T
13.2I
13.1C

Figure E3:
Cathodoluminsecence images of zircons from sample LGZ with spots from Trace Element SHRIMP-RG analyses marked

1.2T
1.2IC

2.2R
2.3I
2.1C

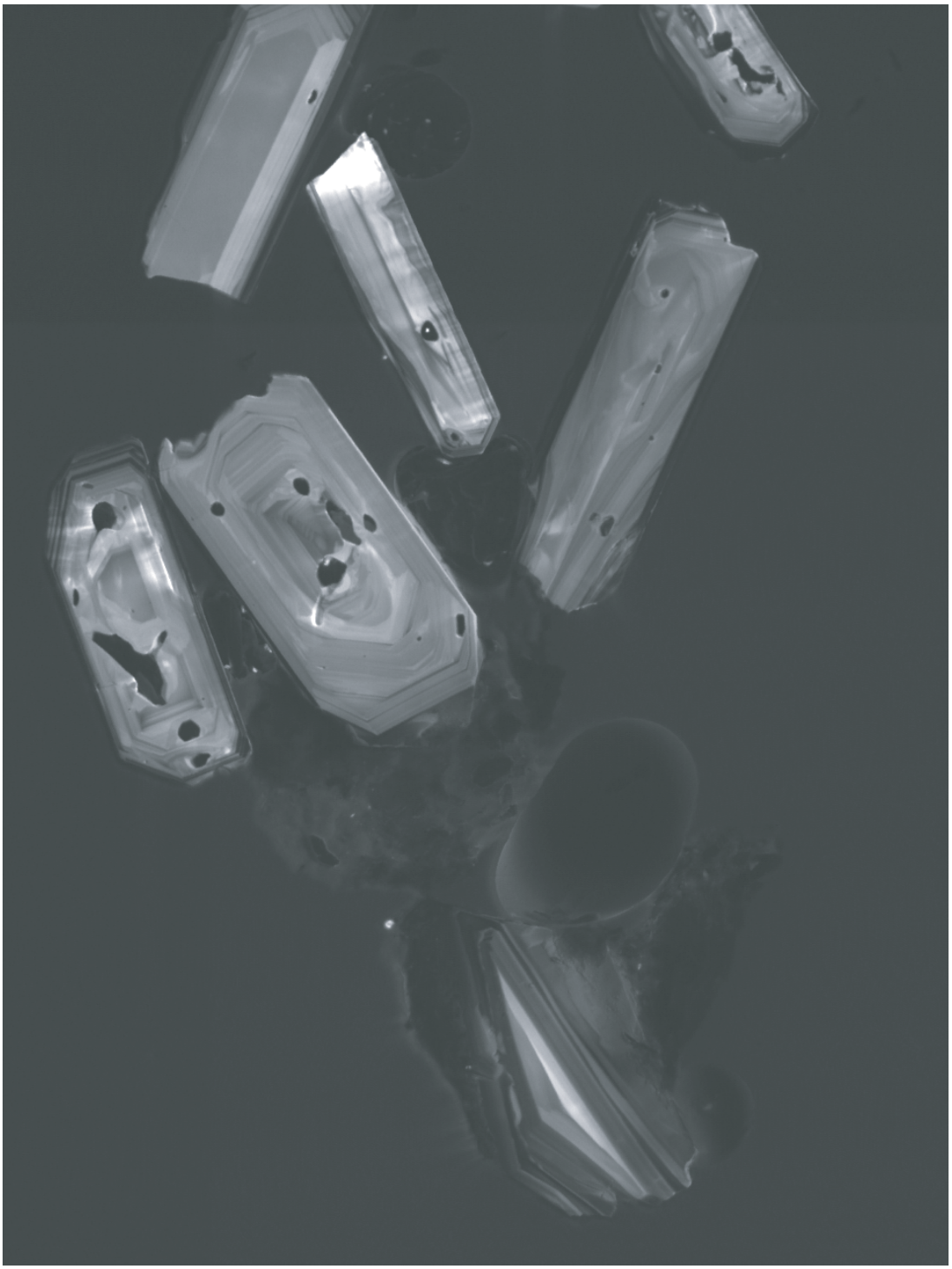

3.1I
4.1C

8.2IR
8.1I
7.1I
6.2I
6.1T
5.1I

11.1IR
11.1I
10.1I
9.1I

12.11
13.1C

Figure E4:
Cathodoluminsecence images of zircons from sample SWZ with spots from Trace Element SHRIMP-RG analyses marked

2.1IR
1.1I

3.1R
4.1IC
8.4C
8.3I
2.2I
8.2IR
8.1R

9.1C
9.2I
9.3IR
9.4R
5.2IC
5.1R
4.2R

10.1C
11.4R
11.2I
11.5IR
11.3C
11.1IR

6.1IC
7.1R

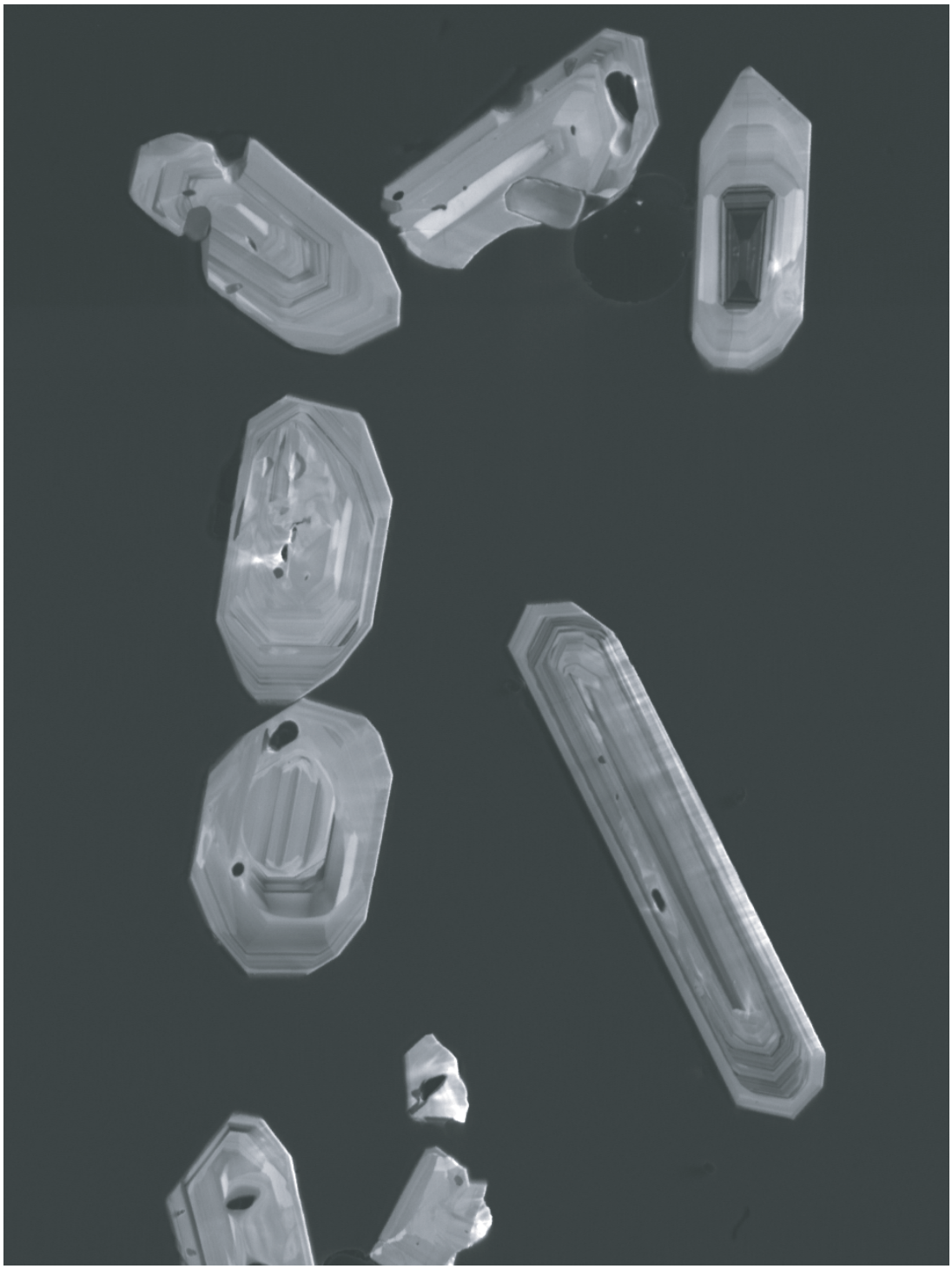

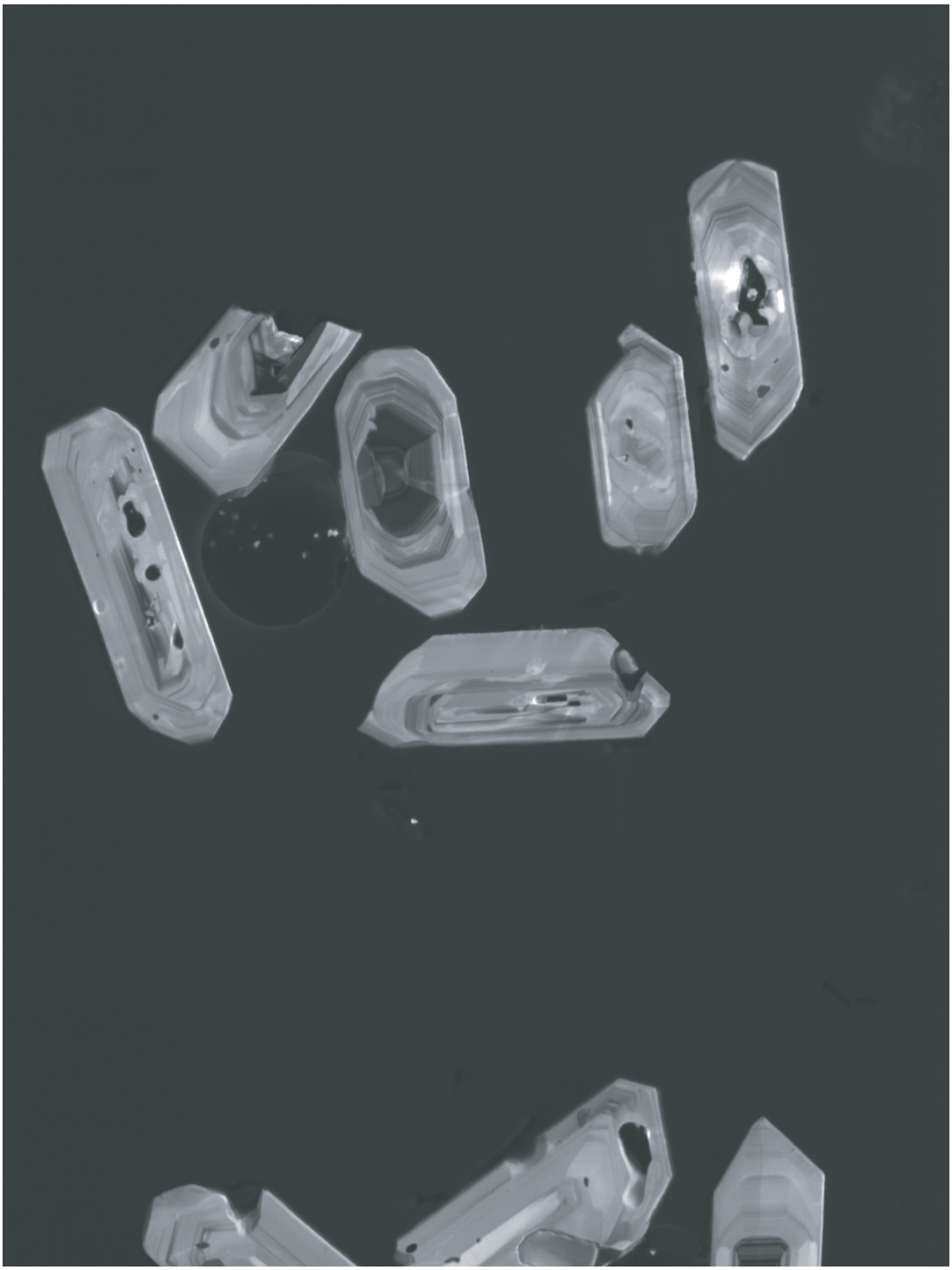

Figure E5:
Cathodoluminsecence images of zircons from sample SML49z with spots from Trace Element SHRIMP-RG analyses marked

1.1C
1.3I
1.2R
4.2T
4.1C
3.1I
3.2R
100mm
X120 05IX
12KV WD21
XUA 13 52 31

2.2T
2.3IR
2.1C
1.1C
1.2R
1.3I
4.2T
4.1C
100µm
X150 05:X
12kV

12kV X150 100mm 35 31 49X

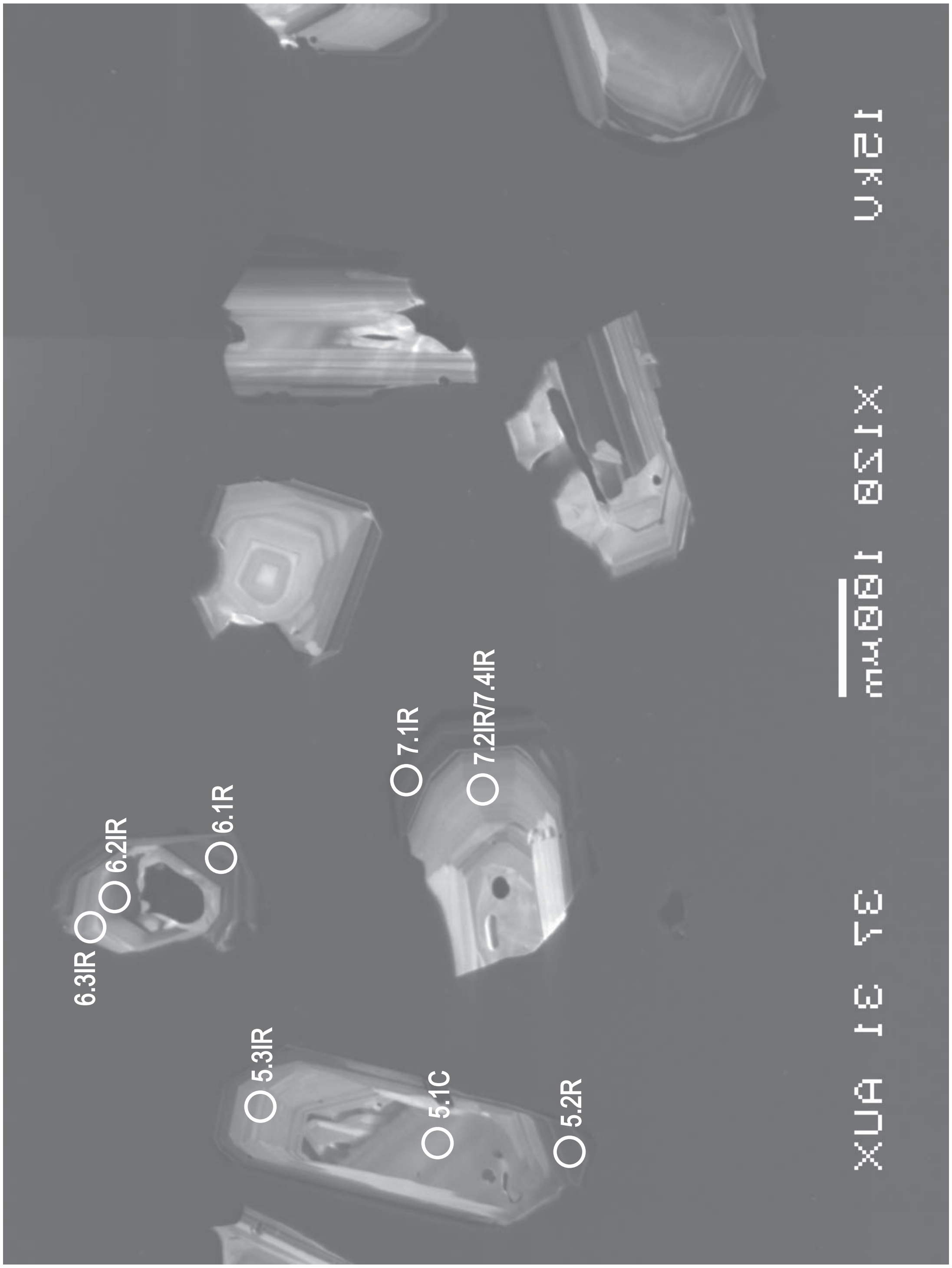
6.3IR
6.2IR
6.1R
7.1R
7.2IR/7.4IR
5.3IR
5.1C
5.2R

9.3R
9.2IR
9.1C
10.1R
10.3C
10.5IR
10.4C
10.2IR
10.6IR
8.3R
8.4IR
8.2IR
8.1C/8.5C

13.1IC
13.2IR
13.3T
100mm
X120 05IX
12KV WD21
XUA 13 52 31

12.1IC
12.2T
11.1C
11.2IR
11.3R
100mm
X120 0S1X
12KV

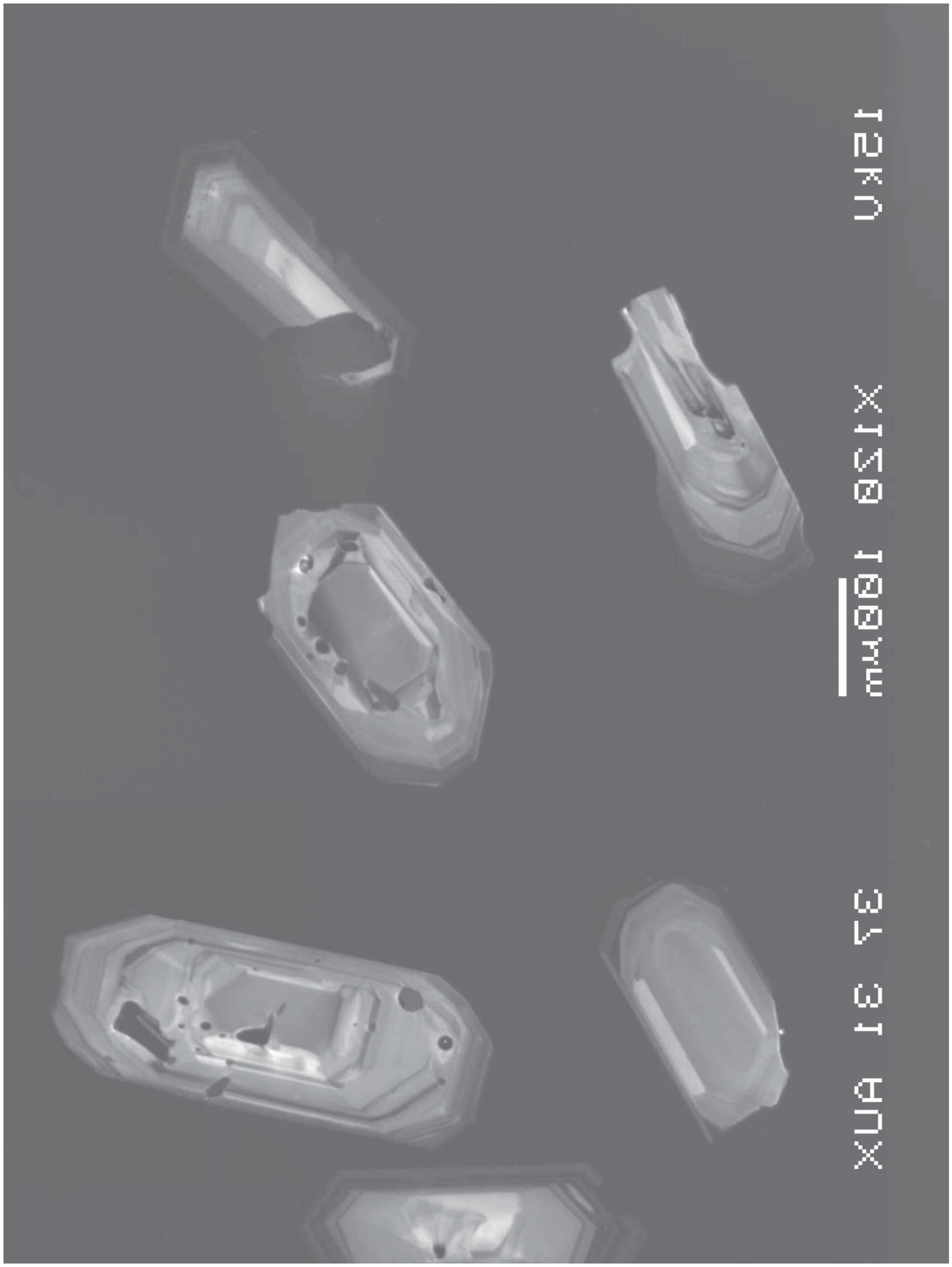

Figure E6:
Cathodoluminsecence images of zircons from sample SML54z with spots from Trace Element SHRIMP-RG analyses marked

2.1I
3.1C
3.2I
3.3T
1.1I
1.2R
100mm
XUA 1C 37

5.3IR
5.2IIR
5.1C
4.3T
4.1C
4.2IR
100mm
X120 05IX
12KV
XUA 13 32

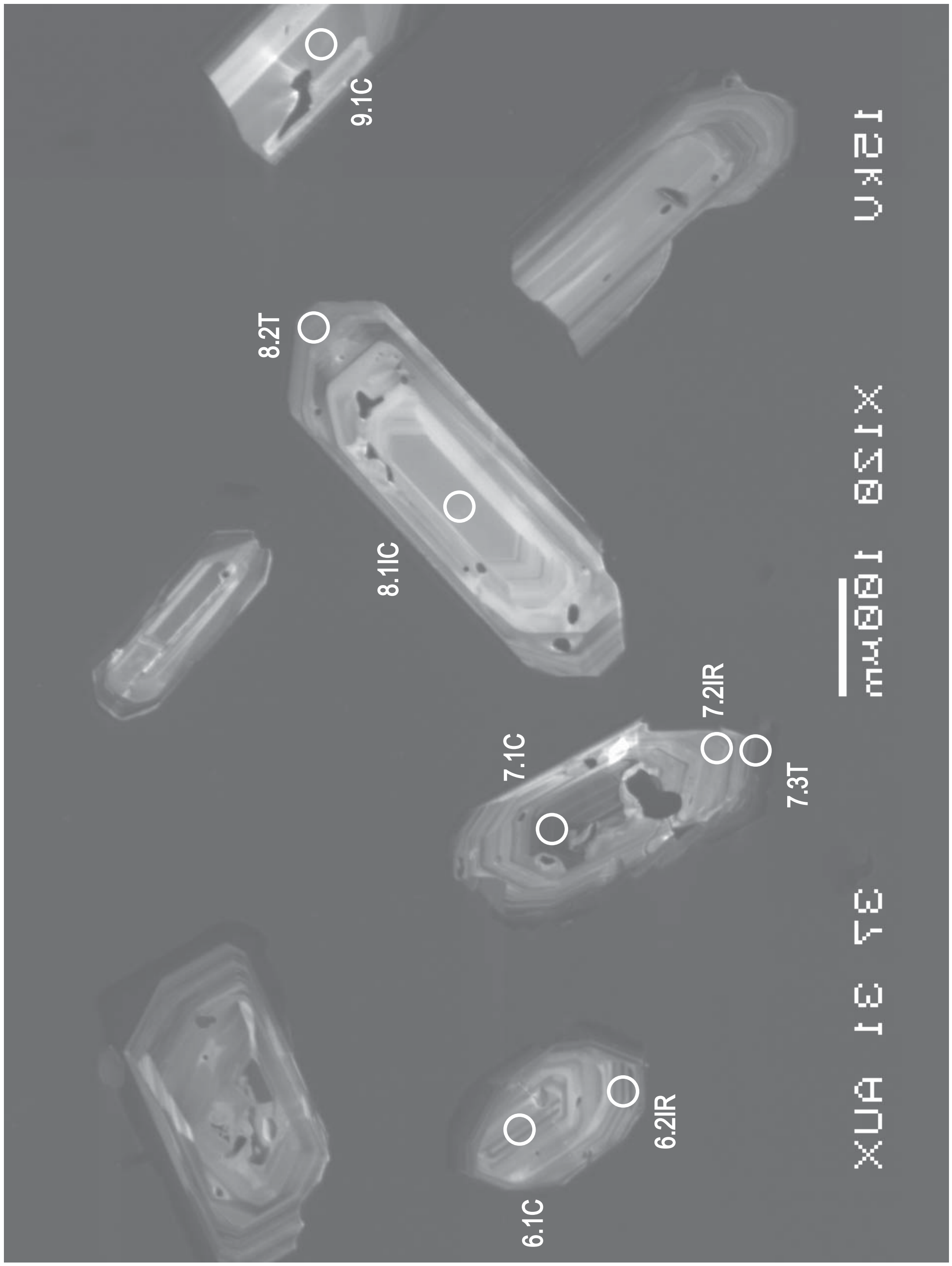
9.1C
8.2T
8.1IC
7.1C
7.2IR
7.3T
6.1C
6.2IR

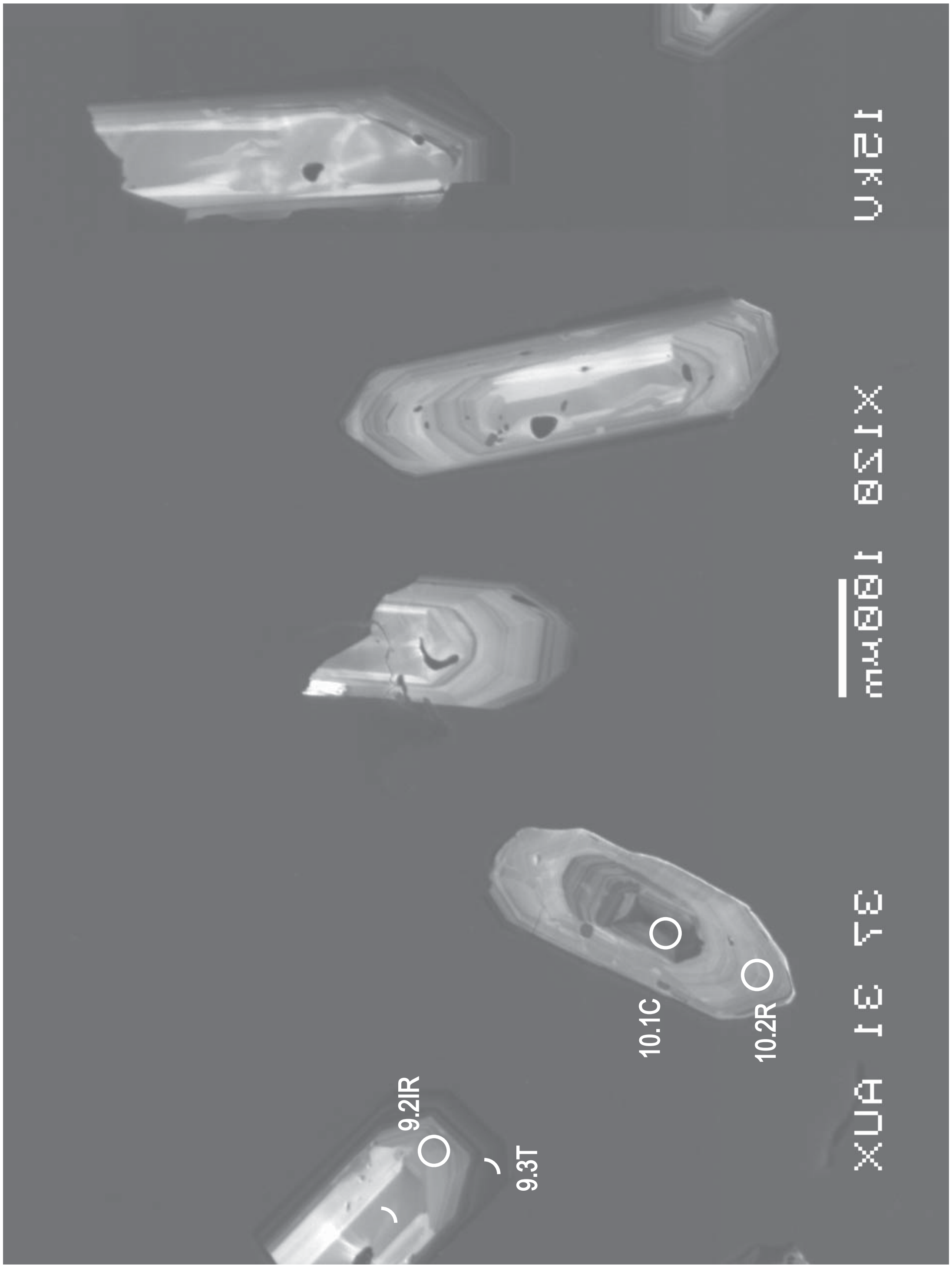
9.2IR
9.3T
10.1C
10.2R

12kV
X150 100nm
35 31 AUX

12kV
X150 100nm
35 31 XUA

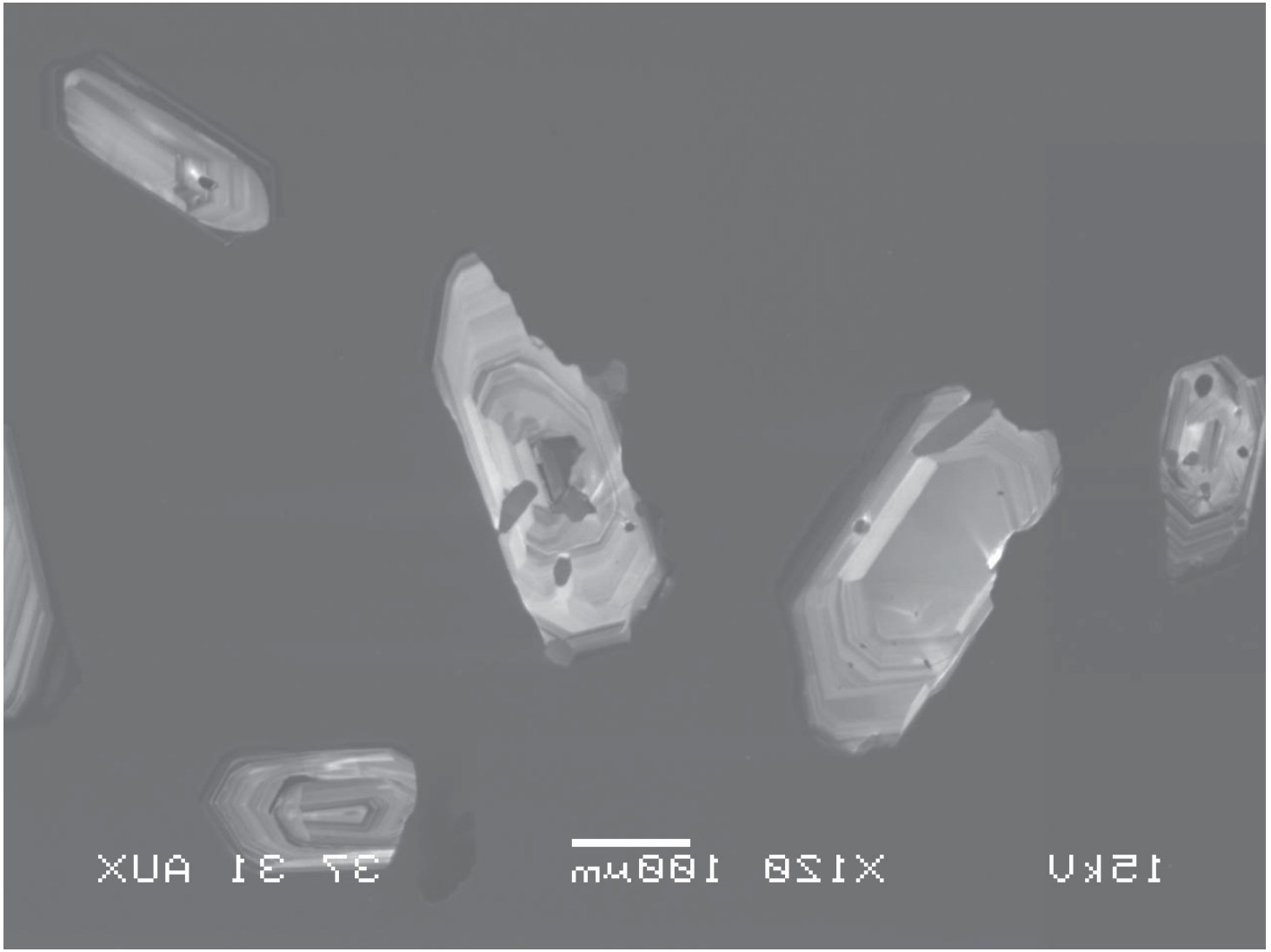
15kV X120 100µm 37 31 AUX

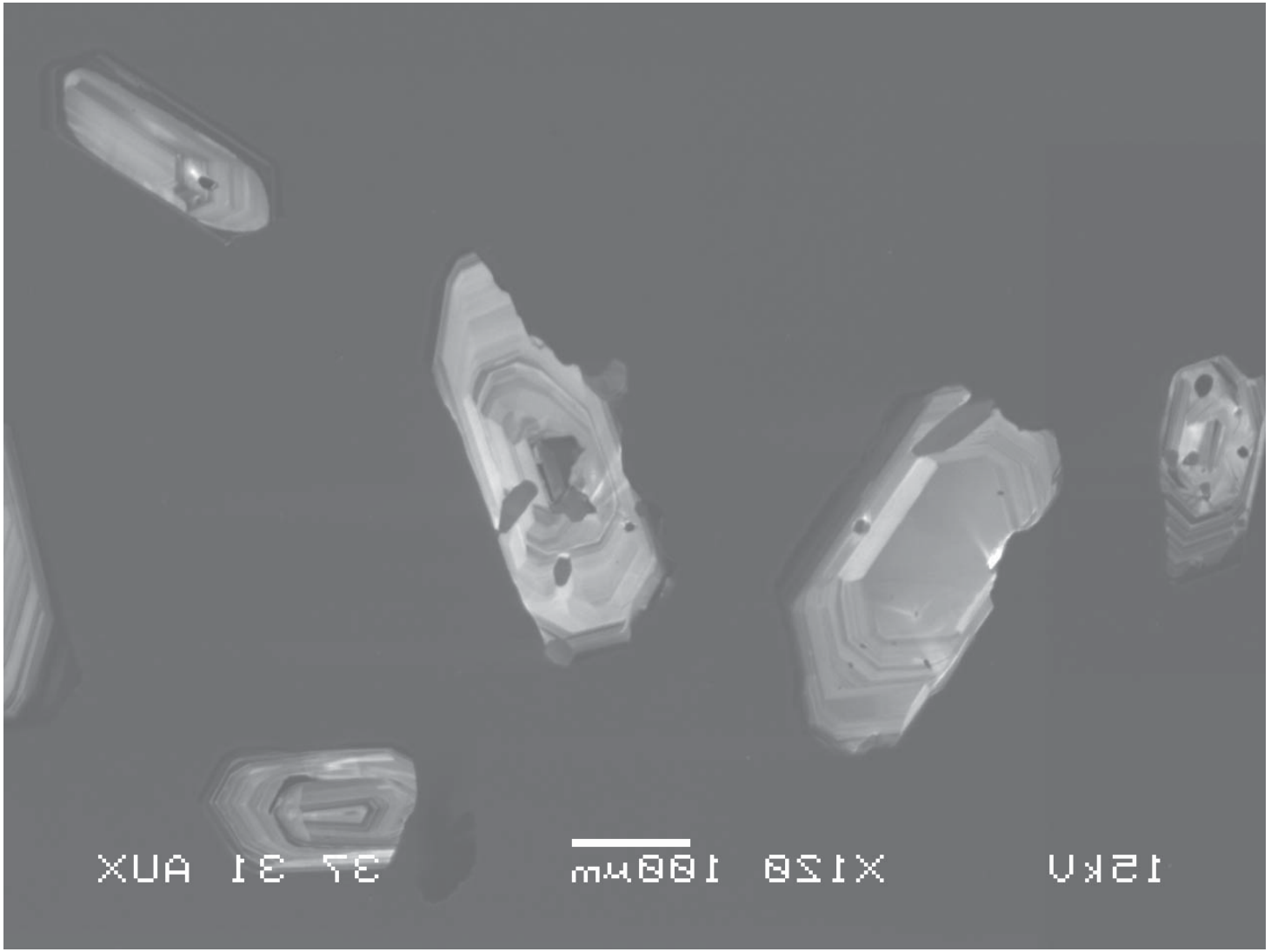
15kV X120 100µm 37 31 AUX

APPENDIX F:

Field Observations and of the Leucogranite Zone, Spirit Mountain Batholith

Table F-1: Field observations of aplite sheets within the leucogranite zone, Spirit Mountain batholith

location desc	lat	long	orientation	thickness	contact	rock desc	host rock	notes
above XTP camp	15.538	44.798	S80E, 80ºN	100 m	grad over 2 m	aplite	crunchy lg	more like a giant pod than a sheet
above XTP camp	15.549	44.767	N3E, 73ºW	100 m	grad over 1 m	aplite	crunchy lg	more like a giant pod than a sheet
above XTP camp	15.498	44.773	E/W	2 ft	sharp	aplite	crunchy lg	dike feeding into pod above (63)
above XTP camp	15.451	44.79	N/S	100 m		aplite	crunchy lg	southern contact of pod - long axis N/S
top of GVC, just off XTP headed W			N/S, 70ºW		sharp	aplite	CG	
top of GVC, just off XTP headed W			N25E, 40ºE		sharp	aplite	CG	
top of GVC, just off XTP headed W			E/W		sharp	aplite	CG	
top of GVC, just off XTP headed W			N30E, 40ºE		sharp	aplite	CG	
s. powerline rd, atop ridge	10.848	45.034	N87E	<5 m	?	fg porphyry	clg	
s. powerline rd, atop ridge	10.795	45.292	E/W, 79ºS	<5 m	?	fg porphyry	mglg	
atop RTR above XTP camp	15.242	45.063	?	1.5m x 0.5m	sharp	aplite	mglg	no apparent feeders, several pods here
atop RTR above XTP camp	15.242	45.063	255º, 68ºNE	6 cm	sharp	fglg	mglg	
atop RTR above XTP camp	15.242	45.063	N30E, 80ºW					small dikes pinch out into pegmatites
Juniper Mine	13.096	45.68	340º, 65ºE	3 m	grad over few cm	aplite	mglg	
Juniper Mine	13.118	45.769	355º		grad over few cm	crystalline aplite	mglg	
Juniper Mine	13.034	45.516	340º	0.75	grad over 0.5 m	aplite	mglg	
Juniper Mine	13.083	45.379	310º	3"	grad over 1 cm	aplite	mglg	contact is myrmekitic
Juniper Mine	13.246	45.61	110º, 20º@20º	3 m	grad over 0.5 m	aplite		
SM Proper	15.567	42.999	310º, 34º@220º	1 m	sharp	very fglg	mg crunchy	pegmatite at center
SM Proper	15.394	43.759	30º	6 m, 50 m long		aplite to porphyry	mglg	smaller dikes coming off this one
SM Proper	15.468	43.3612	E/W	1.5 m		aplite	mglg	
Juniper mine transect	12.006	44.515	20º, 60ºW	0.75 m		aplite	crunchy gran	
Juniper mine transect	12.344	44.031	145º, 35ºE	1 m		aplite	crunchy gran	
Juniper mine transect	12.508	44.545	140º, 40ºNE	MED-THICK				
Juniper mine transect	12.553	44.864	N/S, 45ºE	several m	sharp on E, grad on W (1cm)	aplite	mglg	subvertical, but with diff contacts
West front of Spirit Mountain	15.691	43.935	N/S, mod to E	1 m	grad over 0.5 m	aplite porphyry	mglg	looks like a pod or lens
RTR from JM	13.276	45.21	70º, steep W	5 - 7 m	grad over 5 cm	aplite	mglg	one small dike perpendicualr (15 cm) coming off
RTR from JM	13.276	45.21	340º, vert	5 m		aplite	mglg	may be pod or lens like
RTR from JM			N/Ne, W/NW	3 m	grad over 10 cm	aplite	mglg	
RTR from JM			E/W, vert	10 cm		aplite	mglg	may be pod or lens like
RTR from JM			N/S, steep W	2-4 m		aplite	mglg	
RTR from JM			N/S, mod to E	1.5 m	sharp	aplite	mglg	
RTR from JM			N/S, mod W dip	<1m	grad over 5 cm	aplite	mglg	
RTR from JM			N/S	1 m		aplite	mglg	can trace for 10 m, then lose; qtz veins and pockets
s. powerline rd transect	10.775	45.134	N/S, mod to W		grad	aplite	mglg	top of knob
s. powerline rd transect			5º, 40ºW	0.75 m	grad	aplite	mglg	>10m long
top of GVC	15.075	43.933	40º, 25ºSE	1 m	sharp	aplite	TLG	
top of GVC	15.06	44.014	54º, mod dip NW					
top of GVC	14.915	44.036	E/W, steep S; N/S w mod dip E	6" - 1'	sharp	aplite	TLG	network of aplites
top of GVC	14.969	43.909	100º, 24ºS	1.5 ft	sharp	aplite	CG	
top of GVC	14.626	43.668	5º, 64º W	1 ft	sharp	aplite	CG	fed by smaller at 100º, 59ºNE
top of GVC	15.543	43.755	25º, 61ºNW	1 m	sharp	aplite	CG	fed into by below
top of GVC	15.543	43.755	322º, steep NE	2 m	sharp	aplite	CG	feeds into previous
south of hwy	7.87	44.154	100º, steep N			aplite	cg	
s of SM Proper	15.593	43.184	25º, 65ºW	3 m		aplite	cg	several smaller aplites come together here
s of SM Proper	15.628	43.288	60º, mod NW	1 ft		aplite	cg	
south of hwy	9.186	45.737	40º, steep E	1 ft	sharp	aplite	mglg	top of knob
south of hwy	9.17	44.738	N/S, W		diffuse	aplite	cg	
south of hwy	9.17	44.738	20º, 65ºW	1.5 m		aplite	TLG	
south of hwy	8.204	46.782	N/S	1 m		aplite	cg	loads of these in upper cg here (and elsewhere)
south of hwy	8.043	47.06	355º, steep E	1 - 2 m	sharp	aplite porphyry	TLG	loads of these in upper cg here (and elsewhere)
E of SM proper	15.748	42.665	25º, 74ºW	1 m		aplite	cg	

APPENDIX G

Secret Pass Canyon, The Black Mountains:

Petrography, Whole-rock Geochemistry, Geochronology, and

Cathodoluminescence Images of Zircons

Table G1: Petrography of Secret Pass Canyon, Black Mountains

sample	date collected	latitude (35°N)	longitude (114°W)	field location	handsample description	unit	other analyses
BML19	5/05				gray gm with 15% plag phenos	trachydacite	
BML22z	5/05	9.822	24.826		some diorite xenocrysts, flow banding visible	trachydacite	GC, Z
BML25z	5/05	10.292	26.591			trachydacite	
BML26z	5/05	9.89	24.056	low silica rhyolite flow		rhyolite	GC, Z
BML27	5/05	10.242	23.723	high silica rhyolite flow		HSR	
BML28	5/05	10.283	23.785		flow banded HSR	HSR	
BML31Z	5/05	9.791	25.199	flat top mtn	HSR	HSR	GC, Z
BML33	5/05	9.674	25.166	flat top mtn	gray, mostly mafic phenos, fspar weathered out	LSR	
BML38	5/05	8.91	25.091	at top of intrusion?		trachydacite	
BML39	5/05	9.285	24.334		weathered out fiamme and plag phenos	possible PST	
BML42a	5/05	10.609	25.865	top of Thumb Butte		block and ash flows	
BML42b	5/05	10.609	25.865	top of Thumb Butte		block and ash flows	

Table G1: Petrography of Secret Pass Canyon, Black Mountains

Phenocrysts	other	ground-mass	alteration	texture	notes
15% plag		85		med-gr porphyry	lenses of anhedral qtz and a few kspar phenos, qtz phenos highly rounded
20% fspar		75	calcite	coarse-gr porphyry	
3% biotite, 5% plag	5% qtz lenses	87	calcite	med-gr porphyry	some yellowish mineral highly replaced (cpx?)
7% plag, 2% bio		91	no	med-gr porphyry	
3% qtz		97	no	fine grained porphyry	linear feature - flow band?
3% qtz	7% qtz lenses	90	no	med-gr porphyry	
5% qtz, 2% plag	<1% bio	93	no	very fine grained gm, med gr por	some qtz phenos rounded
2% opaque needles, 3% plag	<1% opaque rims on replaced xls, <1% bio	94	yes	coarse-gr porphyry	
8% plag, 2% qtz, 3% bio, 25 cpx	<1% opaques	85	no	coarse-gr porphyry	
	5% quartz filling veins	95		spherulitic in gm, porphyry	lots of qtz veins, no other phenos
7% plag	<1% opaques, <1% bio	93	calcite	coarsely crystalline gm	
3% plag	<1% opaques, <1% bio	97	calcite	coarsely crystalline gm	

Table G-2: Whole-rock Geochemistry of Secret Pass Canyon, Black Mountains
Oxides listed in wt%, all other elements listed in ppm.

	BML22Z	BML26Z
SiO2	63.30	67.64
Al2O3	16.19	17.07
Fe2O3	5.33	2.46
MnO	0.09	0.05
MgO	1.85	0.60
CaO	3.78	2.08
Na2O	3.84	4.55
K2O	4.23	5.10
TiO2	0.99	0.35
P2O5	0.40	0.11
Ba	1944	2229
Sr	704	1112
Y	29	18
Zr	345	376
Be	3	2
V	80	14
Ga	20	23
Ge	1.3	1
Rb	105	93
Nb		
Sn	21.3	18.1
Cs	< 1	< 1
Hf	2.2	1.5
Ta	91.5	133
Tl	179	245
Bi	20.2	26.7
Th	66.9	81.1
U		
Cu	10.8	11.3
Zn	2.49	2.3
Sc	7.1	5.65
Pb	1.05	0.76
Zr/Hf	5.18	3.44
Rb/Sr	1	0.6
Nb/Ta	2.87	1.64
La	0.398	0.241
Ce	2.44	1.57
Pr	0.362	0.216
Nd	8.7	9.8
Sm	1.2	1.1
Eu	0.61	0.8
Gd		
Tb	14.3	22.4
Dy	2.28	2.37
Ho	16	36
Er	73	65
Tm	10.4	3.06
Yb	17	30
Lu	39.66	38.37

Table G-3: Geochronology data from SHRIMP-RG analysis of zircons from Secret Pass Canyon, Black Mountains

Spot Name	% comm 206	ppm U	ppm Th	232Th /238U	207corr 206Pb /238U Age	1s err	7corr 206Pbr /238U	1s err	Total 238 /206	% err	Total 207 /206	% err
BML37-1	0.45	119	157	1.36	16.5	0.6	.0026	.0001	389.44	3.2	.0500	14.8
BML37-2	0.56	153	280	1.89	17.2	0.5	.0027	.0001	373.17	2.6	.0508	11.5
BML37-3	5.14	263	618	2.43	17.3	0.4	.0027	.0001	353.24	1.9	.0870	7.1
BML37-4	-0.41	114	248	2.25	18.5	0.5	.0029	.0001	348.80	2.8	.0432	13.9
BML37-5R	0.28	179	211	1.22	17.7	0.4	.0028	.0001	362.57	2.3	.0486	10.6
BML37-6R	0.68	167	357	2.20	16.3	0.4	.0025	.0001	391.69	2.5	.0518	10.9
BML37-7I	1.04	161	282	1.82	16.7	0.5	.0026	.0001	381.32	2.6	.0546	11.2
BML37-8I	31.06	111	173	1.61	18.0	1.1	.0028	.0002	247.08	2.4	.2919	9.3
BML37-9C	0.64	270	495	1.90	16.2	0.3	.0025	.0001	393.81	2.0	.0514	8.9
BML37-10R	0.54	135	208	1.59	17.7	0.5	.0027	.0001	362.07	2.7	.0507	13.3
BML37-11I	0.29	162	189	1.20	17.8	0.4	.0028	.0001	360.90	2.3	.0487	10.8
BML37-12I	1.86	110	164	1.55	17.2	0.5	.0027	.0001	367.44	2.9	.0611	12.1
BML37-13C	0.22	234	449	1.99	18.1	0.4	.0028	.0001	355.43	2.0	.0482	9.1
BML37-14IR	5.08	193	251	1.34	17.6	0.4	.0027	.0001	346.71	2.1	.0865	7.7
BML37-15I	0.22	91	163	1.86	17.2	0.6	.0027	.0001	373.36	3.3	.0481	15.1
BML37-16T	1.85	126	188	1.54	17.2	0.5	.0027	.0001	367.99	2.6	.0610	10.9
BML37-18C	1.20	196	369	1.94	16.5	0.4	.0026	.0001	384.79	2.2	.0559	9.3
BML37-19T	0.26	203	363	1.85	18.3	0.5	.0028	.0001	351.49	2.4	.0484	16.0
BML37-20R	3.17	81	97	1.23	17.2	0.7	.0027	.0001	363.46	3.9	.0714	15.0
BML37-21R	0.23	283	632	2.31	18.0	0.4	.0028	.0001	356.75	2.0	.0482	9.4
BML37-22T	-1.23	78	98	1.30	16.8	1.1	.0026	.0002	387.91	6.2	.0367	20.1

Table G-3: Geochronology data from SHRIMP-RG analysis of zircons from Secret Pass Canyon, Black Mountains

Spot Name	% comm 206	ppm U	ppm Th	232Th /238U	207corr 206Pb /238U Age	1s err	7corr 206Pbr /238U	1s err	Total 238 /206	% err	Total 207 /206	% err
BML65Z-1I	0.95	161	293	1.88	17.2	0.4	.0027	.0001	370.71	2.4	.0539	10.5
BML65Z-1.2T	2.02	43	61	1.48	16.4	0.8	.0026	.0001	384.03	4.5	.0623	17.7
BML65Z-3	2.98	75	101	1.39	17.2	0.6	.0027	.0001	362.09	3.2	.0700	12.4
BML65Z-2	3.89	52	85	1.68	19.0	0.8	.0030	.0001	324.84	3.9	.0772	14.4
BML65Z-4	0.61	47	90	1.96	18.3	0.8	.0028	.0001	349.43	4.1	.0512	17.9
BML65Z-5.1C	0.29	127	140	1.14	19.0	0.5	.0030	.0001	337.79	2.5	.0487	11.4
BML65Z-5.2T	1.96	71	104	1.51	18.1	0.6	.0028	.0001	348.18	3.4	.0619	13.7
BML65Z-6.1C	1.39	102	129	1.30	18.5	0.5	.0029	.0001	342.85	2.7	.0574	11.4
BML65Z-6.2T3	9.00	10	20	2.00	18.1	2.2	.0028	.0003	323.07	11.0	.1175	29.9
BML65Z-7.1C2	7.23	101	176	1.80	~~28.7~~	~~1.4~~	.0045	.0002	207.66	4.6	.1038	12.4
BML65Z-7.2T	0.40	32	39	1.28	19.6	1.1	.0030	.0002	326.93	5.2	.0496	22.9
BML65Z-8C	1.19	234	128	0.56	~~1481.6~~	~~5.9~~	.2584	.0012	3.82	0.4	.1029	0.9

Table G-3: Geochronology data from SHRIMP-RG analysis of zircons from Secret Pass Canyon, Black Mountains

Spot Name	% comm 206	ppm U	ppm Th	232Th /238U	207corr 206Pb /238U Age	1s err	7corr 206Pbr /238U	1s err	Total 238 /206	% err	Total 207 /206	% err
BML26Z-1.1T	54.03	234	459	2.02	~~15.1~~	~~0.7~~	.0023	.0001	196.14	1.9	.4733	3.0
BML26Z-2.1C	0.80	655	1306	2.06	17.9	0.3	.0028	.0000	357.72	1.3	.0527	6.5
BML26Z-3.1C	4.86	62	123	2.06	18.4	0.9	.0029	.0001	332.74	4.3	.0848	20.5
BML26Z-4.1T	0.65	264	497	1.94	17.0	0.4	.0026	.0001	376.17	2.1	.0515	11.2
BML26Z-5.1T	3.18	209	308	1.52	16.9	0.4	.0026	.0001	367.90	2.4	.0715	10.1
BML26Z-6.1C	3.01	93	176	1.96	16.4	0.6	.0025	.0001	381.85	3.5	.0701	14.7
BML26Z-7.1T	3.69	129	239	1.90	~~16.4~~	~~0.5~~	.0025	.0001	377.98	3.0	.0755	12.3
BML26Z-8.1T	4.65	89	109	1.26	16.4	0.7	.0025	.0001	374.46	3.7	.0831	15.8
BML26Z-9.1T	1.34	126	212	1.75	17.4	0.6	.0027	.0001	364.54	3.1	.0570	14.2
BML26Z-10.1C	5.90	94	213	2.34	17.6	0.7	.0027	.0001	343.47	3.4	.0930	12.7
BML26Z-11.1T	4.46	167	343	2.12	17.5	0.5	.0027	.0001	351.52	2.7	.0816	10.9
BML26Z-12.1T	1.48	145	257	1.83	17.9	0.5	.0028	.0001	353.54	2.9	.0581	12.8
BML26Z-13.1T	1.68	185	355	1.98	18.1	0.5	.0028	.0001	349.50	2.5	.0597	12.6
BML26Z-14.1T	0.36	290	61	0.22	~~950.3~~	~~6.1~~	.1588	.0011	6.27	0.7	.0737	1.1
BML26Z-15.1C	7.99	93	103	1.15	16.3	0.7	.0025	.0001	362.56	3.6	.1095	12.0
BML26Z-16.1C	-0.25	261	81	0.32	~~1734.4~~	~~9.6~~	.3087	.0020	3.25	0.6	.1040	0.7
BML26Z-16.2T	0.69	277	342	1.27	~~19.0~~	~~0.4~~	.0029	.0001	337.34	2.0	.0519	10.0
BML26Z-17.1T	2.99	184	246	1.38	18.4	0.5	.0029	.0001	339.28	2.5	.0701	10.4
BML26Z-18.1C	3.81	117	228	2.02	17.2	0.6	.0027	.0001	361.00	3.3	.0765	13.6
BML26Z-19.1T	2.45	107	154	1.49	17.9	0.6	.0028	.0001	351.62	3.3	.0658	15.5
BML26Z-20.1T	3.88	81	87	1.10	18.3	0.7	.0028	.0001	337.98	3.7	.0770	14.6
BML26Z-21.1	0.77	100	210	2.17	~~19.2~~	~~0.7~~	.0030	.0001	333.09	3.5	.0525	20.0
BML26Z-22.1	6.71	73	61	0.86	~~15.7~~	~~0.7~~	.0024	.0001	383.73	4.1	.0993	14.3
BML26Z-22.2T	0.68	272	344	1.31	18.2	0.4	.0028	.0001	351.18	2.1	.0517	10.9
BML26Z-23.1T	4.50	89	116	1.35	17.1	0.7	.0027	.0001	358.80	3.7	.0820	16.1

Figure G1:

Catholoduminescence Images of Zircons from BML 37z

with U-Pb SHRIMP analysis spots

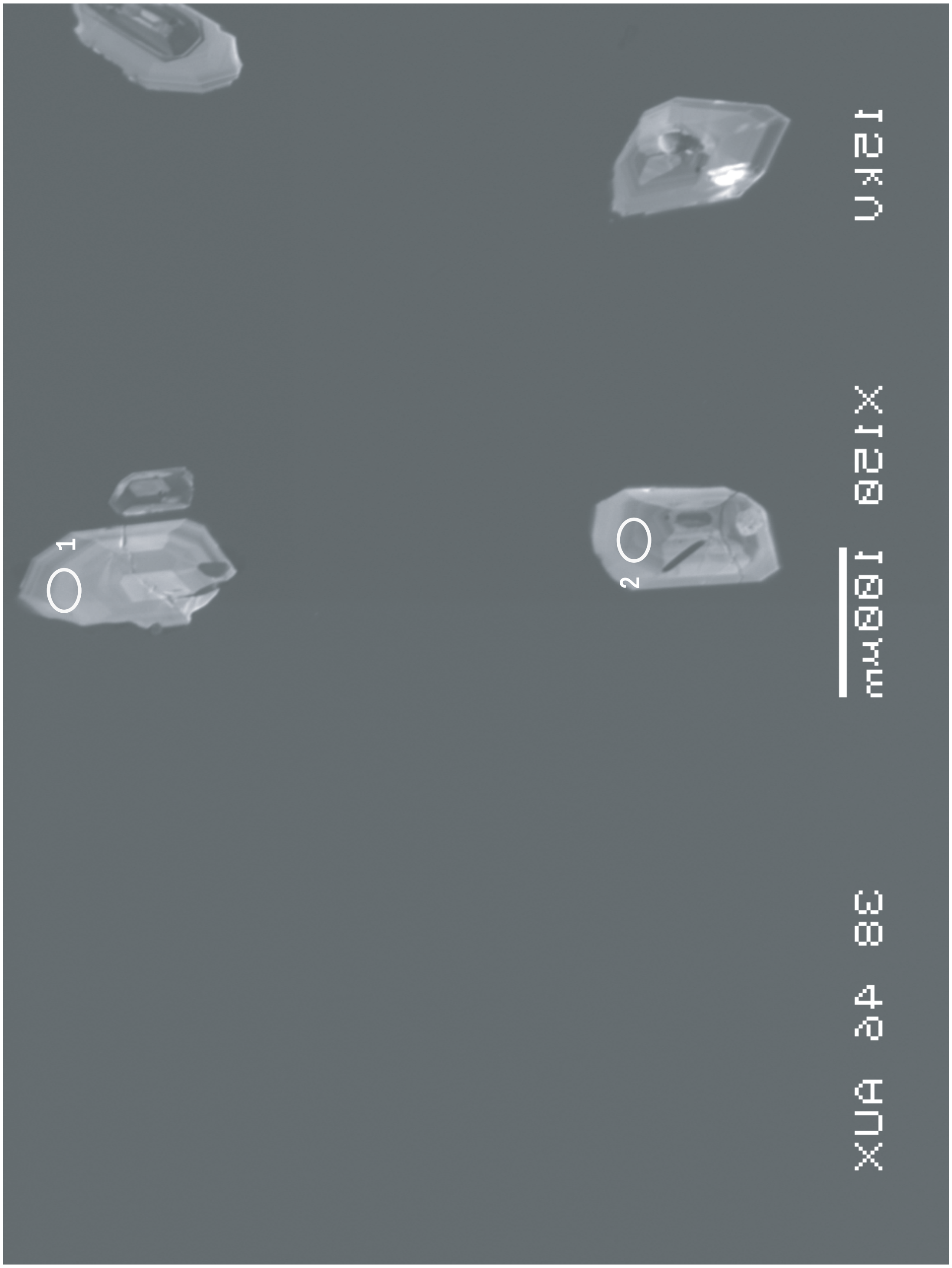
1
2
15kV
X120
100µm

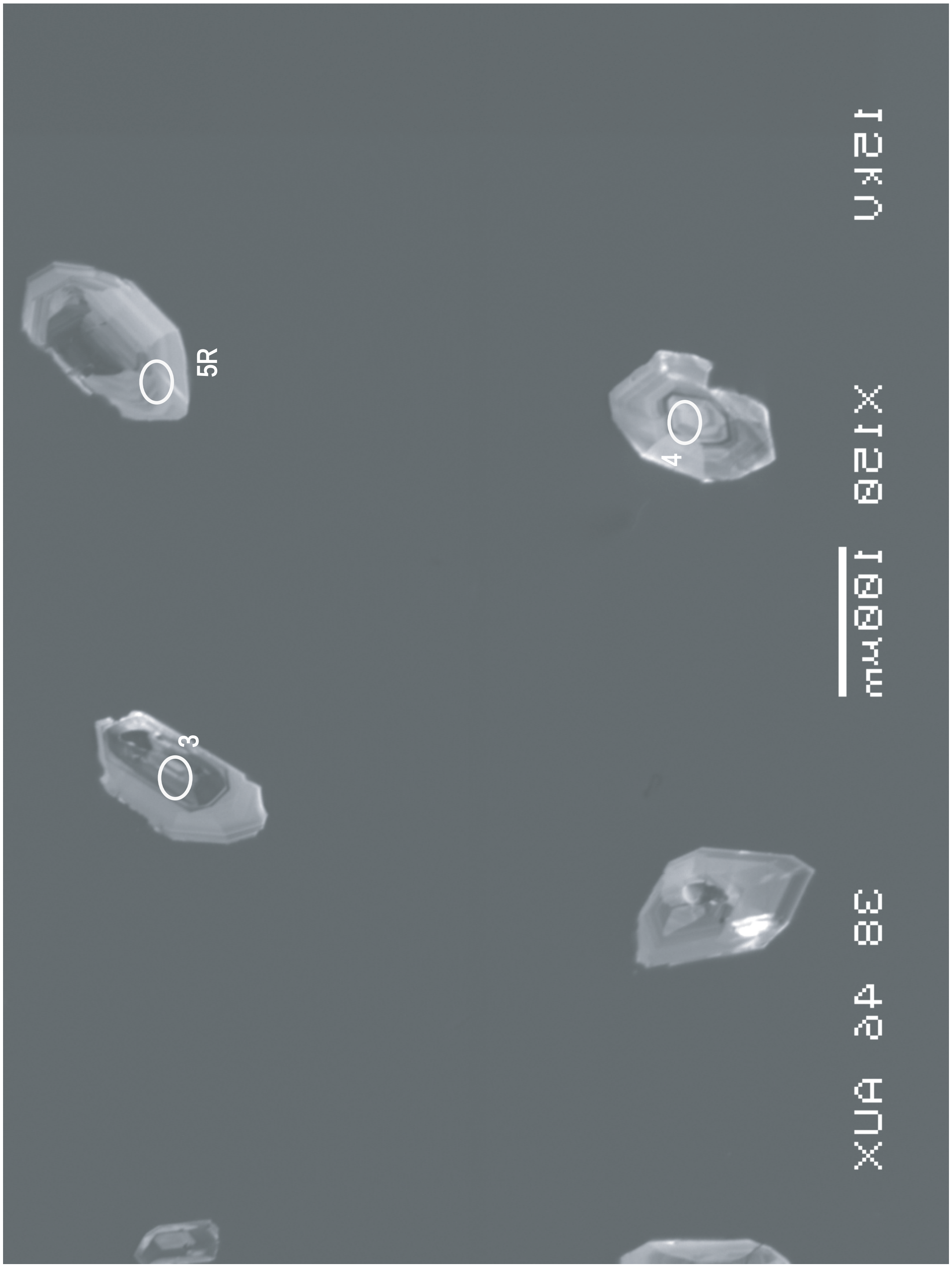
5R
3
4

XUA 24 88
6R
71
18
100µm
X120 021X
UK21
9C6

XWA 24 38 23
MW001 100%
X120 021X
12KN UNK

XUA 24 88
11I
10R
19T
12I
13C
100µm
X140 04:X
UKN 12

XUA 24 88
100µm
x120 001X
UK21
171
16T
15I
14IR

XUA 24 8C
mm001 04IX
UK2I
18C
21T
21R
20R

Figure G2:

Catholoduminescence Images of Zircons from BML 65z

with U-Pb SHRIMP analysis spots

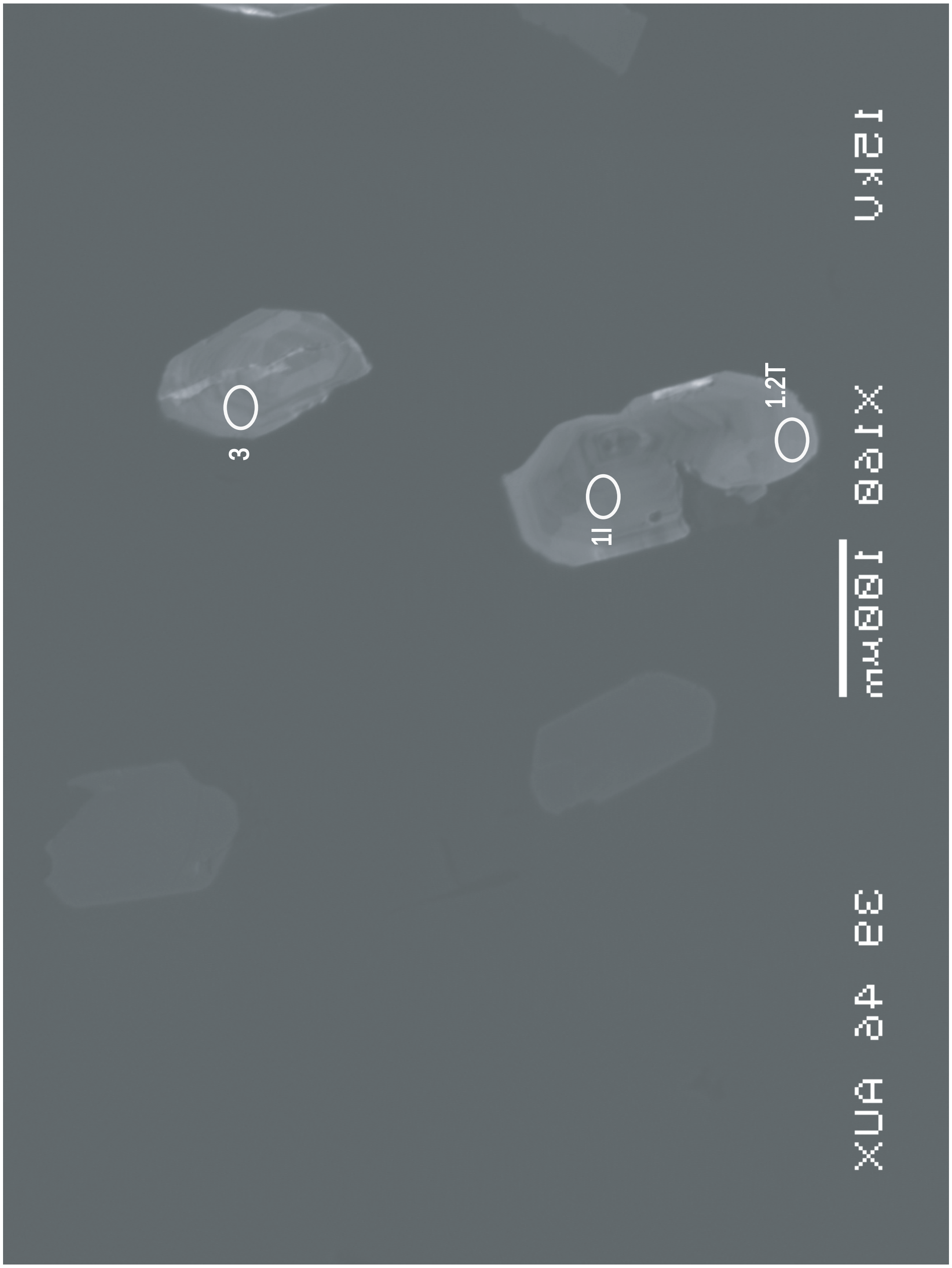
3
1I
1.2T

XUA 24 23
100mm
X120 021X
12kN U121
21

XUA 24 8G
100μm
X120 021X
12kV UNT

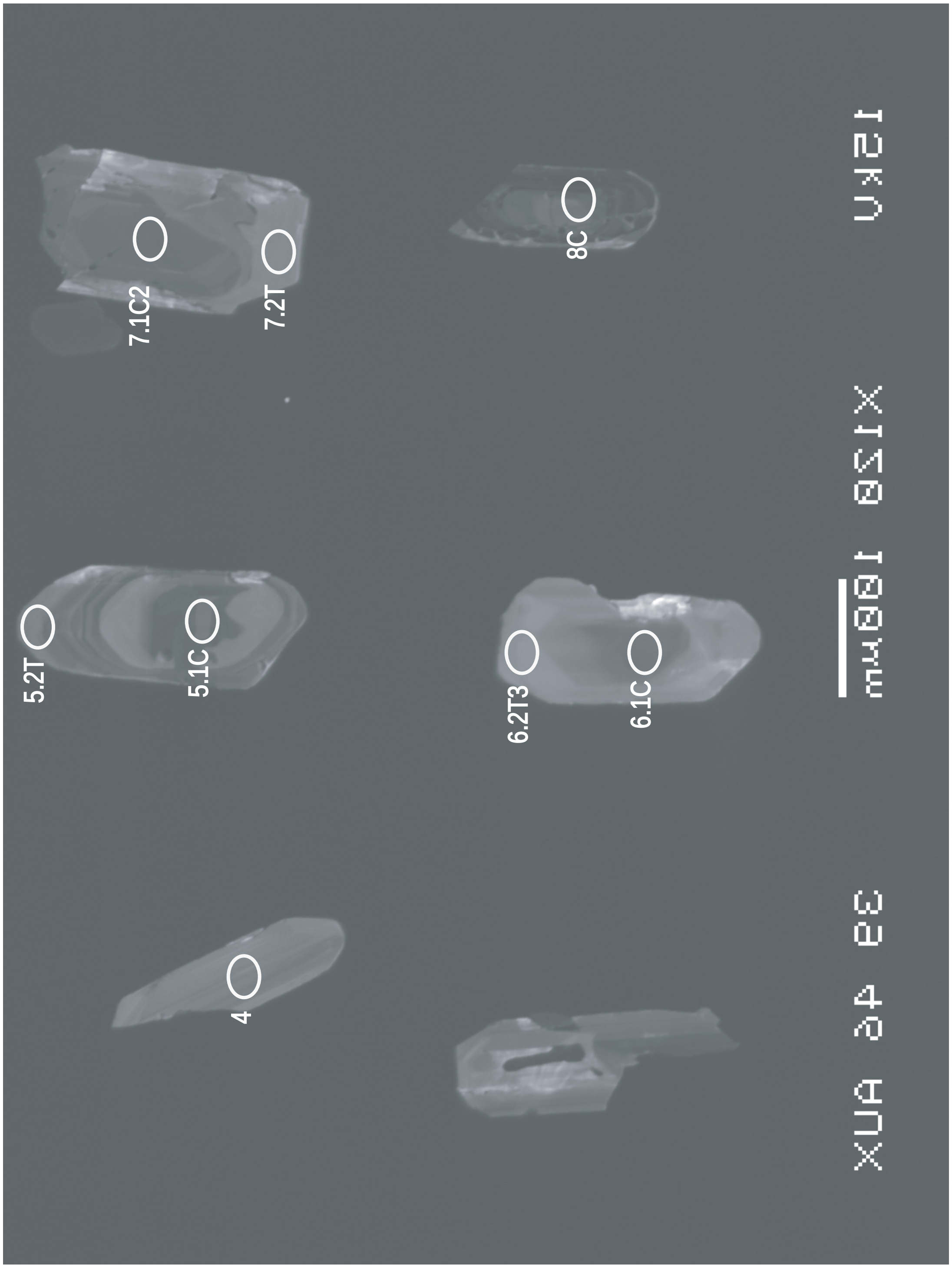
7.1C2
7.2T
8C
5.2T
5.1C
6.2T3
6.1C
4

Figure G3:

Catholoduminescence Images of Zircons from BML 26z

with U-Pb SHRIMP analysis spots

1.1T
2.1C
XU4 31 35
X130 100µm
12kV

XUA 12 32
2.1C
3.1C
4.1T
5.1T
7.1T
100µm
X130 03:X
12kV U121

XUA 15 52 35 31 AUX
8.1T
9.1T
10.1C
11.1T
100μm
X130 031X
12kV UN2L

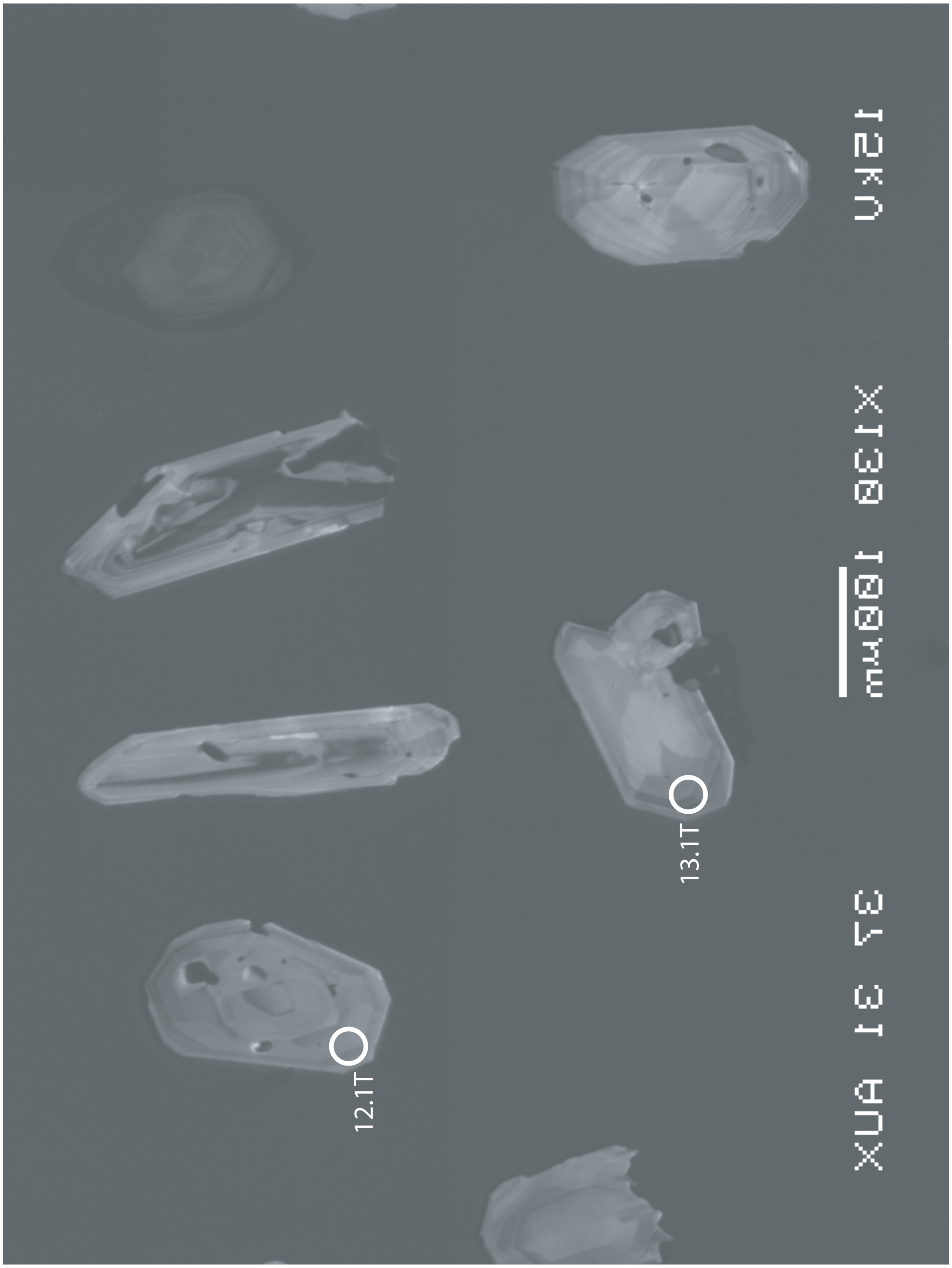
13.1T
12.1T

XUA 15 32
X130 031X
100µm
12kV UNLT
16.1C
16.2T

XUA 13 32
17.1T
18.1C
19.1T
20.1T
100μm
X130 031X
12kV UW21

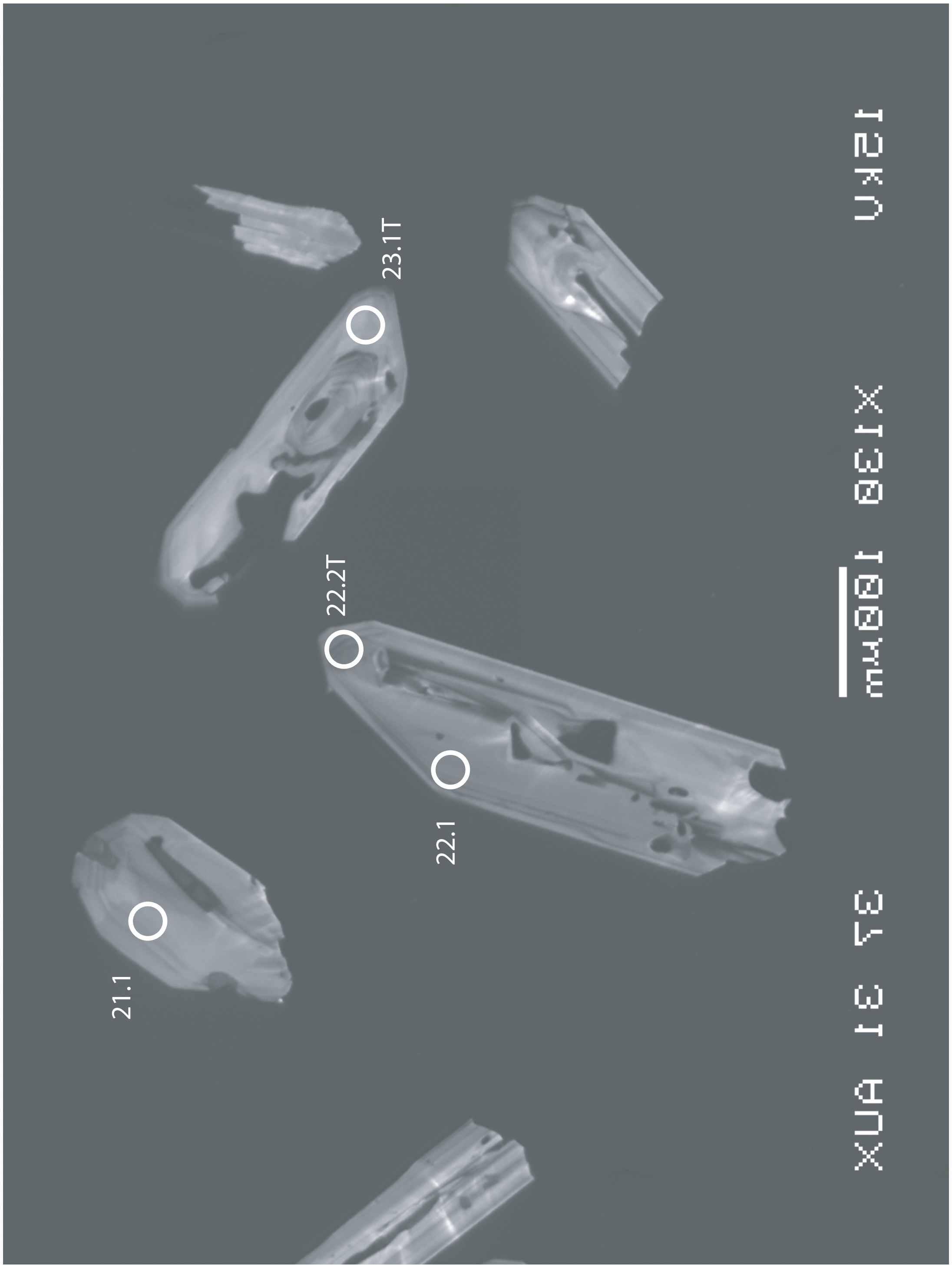
15kU X130 100µm
23.1T
22.2T
22.1
21.1

REFERENCES

Ahrens, L.H. and Erlank, A.J. (1969) Hafnium. *Handbook of Geochemistry*, **2-5**, sections B-O. Wedepohl, K.H. (ed).

*Anderson, A.T., Davis, A.M. and Lu, F. (2000) Evolution of the Bishop Tuff rhyolitic magma based onmelt and magnetite inclusions and zoned phenocrysts. *Journal of Petrology*, **41**, 449-473.

* Bachl, C.A. (1997) *The Searchlight pluton: An example of wholesale magmatic reconstruction of the upper crust during continental extension* [M.S. Thesis]: Nashville, Tennessee. Vanderbilt University, 114 p.

Bachmann, O. and Bergantz, G.W. (2004) On the Origin of Crystal-poor Rhyolites: Extracted from Batholithic Crystal Mushes. *Journal of Petrology,* **45**, 1565-1582.

Baker, D.R., Conte, A.M., Freda, C. and Ottolini, L. (2002) The effect of halogens on Zr diffusion and zircon dissolution in hydrous metaluminous granitic melts. Contributions to Mineralogy and Petrology, **142**, 666-678.

Bea, F. and Montero, P. (1999) Behavior of accessory phases and redistribution of Zr, REE, Y, Th, and U during metamorphism and partial melting of metapelites in the lower crust: An example from the Kinzigite Formation of Ivrea-Verbano, NW Italy. *Geochimica et Cosmochimica Acta*, **63**, 1113-1153.

Bea, F., Montero, P. and Ortega, M. (2006) A LA-ICPMS evaluation of Zr reservoirs in common crustal rocks: Implications for zircon-forming processes. *Canadian Mineralogist*, 44, 745 - 766.

Belousova, E.A., Griffin, W.L., O'Reilly, S.Y. and Fisher, N.I. (2002) Igneous zircon: trace element composition as an indicator of source rock type. *Contributions to Mineralogy and Petrology*, **143**, 602-622.

*Briggs, R.M., Gifford, M.G., Moyle, A.R., Taylor, S.R., Norman, M.D., Houghton, B.F. and Wilson, C.J.N. (1993) Geochemical zoning and eruptive mixing in ignimbrites from Mangakino volcano, Taupo Volcanic Zone, New Zealand. *Journal of Volcanology and Geothermal Research*, **56**, 175-203.

Brown, S.J.A. and Fletcher, I.R. (1999) SHRIMP U-Pb dating of the preerption growth history of zircons from the 340 ka Whakamaru Ignimbrite, New Zealand: Evidence for >250 k.y. magma residence times. *Geology*, **27**, 1035-1038.

Cates, N.L., Miller, J.S., Miller, C.F., Wooden, J.L., Erickson, S. and Means, M. (2003) Longevity of plutonic systems: SHRIMP evidence from Aztec Wash and Searchlight plutons, Nevada. *Abstracts with Programs – Geological Society of America*, **35**, 63.

Charlier, B.L.A., Wilson, C.J.N., Lowenstern, J.B., Blake, S., Van Calsteren, P.W. and Davidson, J.P. (2005) Magma generation at al large, hyperactive silicic volcano (Taupo, New Zealand) revealed by U-Th and U-Pb systematics in zircons. *Journal of Petrology*, **46**, 3-32.

Coleman, D.S., Gray, W. and Glazner, A.F. (2004) Rethinking the emplcament and evolution of zoned plutons: Geochronologic evidence for incremental assembly of the Tuolumne Intrusive Suite, California. *Geology*, **32**, 433-436.

Cooper, K.M. and Reid, M.R. (2003) Re-examination of crystal ages in recent Mount St. Helens lavas: implications for magma reservoir processes. *Earth and Planetary Science Letters*, **213**, 149-167.

Corfu, F, Hanchar, J.M., Hoskin, P.W.O. and Kinny, P.D. (2003) Atlas of zircon textures. *Reviews in Mineralogy and Geochemistry*, **53**, 469-500.

David, K., Schiano, P. and Allègre, C.J. (2000) Assessment of the Zr/Hf fractionation in oceanic basalts and continental materials during petrogenetic processes. *Earth and Planetary Science Letters*, **178**, 285-301.

Davidson, J.P. and Tepley, F.J.T. (1997) Recharge in volcanic systems: Evidence from isotope profiles of phenocrysts. *Science*, **275**, 826-829.

Davies, G.R., Halliday, A.N., Mahood, G.A. and Hall, C.M. (1994) Isotopic constrains on the production-rates, crystallization histories and residence times of pre-caldera silicic magmas, Long Valley, California. *Earth and Planetary Science Letters*, **125**, 17-37.

Faulds, J.E., Geissman, J.W., Mawer, C.K. (1990) Structural development of a major extensional accommodation zone in the Basin and Range Province, northwestern Arizona and southern Nevada: implications for kinematic models of continental extension. *Geologic Society of America, Memoir* **176**, 37-76.

Faulds, J.E., Feuerbach, D.L., Reagan, M.K., Metcalf, R.V., Gans, P. and Walker, J.D. (1995) The Mount Perkins Block, northwestern Airzona: an exposed cross section of an evolving, preextensional to synextensional magmatic system. *Journal of Geophysical Research, B, Solid Earth and Planets*, **100**, 15249-15266.

Faulds, J.E., Feuerbach, D.L., Miller, C.F. and Smith, E.I. (2001) Cenozoic evolution of the northern Colorado River Extensional Corridor, southern Nevada and Northwest Arizona. *Guidebook – Pacific Section, American Association of Petroleum Geologists*, **78**, 239-271.

Faulds, J.E., Geissman, J.W. and Shafiqullah, M. (1992) Implications of paleomagnetic

data on Miocene extension near a major accommodation zone in the Basin and Range province, northwestern Arizona and southern Nevada. *Tectonics*, **11**, 204-227.

Gans, P.B. and Bohrson, W.A. (1998) Suppression of volcanism during rapid extension in the Basin and Range province, United States. *Science*, **279**, 66-68.

Glazner, A.F., Bartley, J.M., Coleman, D.S., Gray, W. and Taylor, R.Z. (2004) Are plutons assembled over millions of years by amalgamation from small magma chambers? *GSA Today*, **14**, 4-11.

Haapala, I., Ramo, O.T. and Volborth, A. (1996) Petrogenesis of the Miocene granite of the Newberry Mountains, Colorado River extensional corridor, southern Nevada. *Abstracts with Programs – Geological Society of America*, **28**, 420.

Haapala, I., Ramo, O.T. and Frindt, S. (2005) Comparison of Proterozoic and Phanerozoic rift-related basaltic-granitic magmatism. *Lithos,* **80**, 1-32.

Hanchar, J.M. and Miller, C.F. (1993) Zircon zonation patterns as revealed by cathodoluminescence and backscattered electron images; implications for interpretation of complex crustal histories. *Chemical Geology*, **110**, 1–13.

Hanchar, J.M. and Watson, E.B. (2003) Zircon saturation thermometry. *Reviews in Mineralogy and Geochemistry*, **53**, 89-110.

Harper, B.E., Miller, C.F., Koteas, G.C., Cates, N.L., Wiebe, R.A., Lazzareschi, D.S. and Cribb, J.W. (2004) Granites, dynamic magma chamber processes and pluton construction: the Aztec Wash pluton, Eldorado Mountains, Nevada, USA. *Transactions of the Royal Society of Edinburgh – Earth Sciences*, **95**, 277-295.

Harrison, T.M. and Watson, E.B. (1983) Kinetics of zircon dissolution and zirconium diffusion and granitic melts of variable water content. *Contributions to Mineralogy and Petrology*, **84**, 66-72.

Heaman, L.M., Bowins, R. and Crocket, J.H. (1990) The chemical composition of igneous zircon suites: implications for geochemical tracer studies. *Geochimica et Cosmochimica Acta*, **54**, 1597-1607.

*Heumann, A. and Davies, G.R. (1997) Isotopic and chemical evolution of the post-caldera rhyolitic system at Long Valley, California. *Journal of Petrology*, **38**, 1661-1678.

Hopson, C.A., Gans, P.B., Baer, E., Blythe, A.E., Calvert, A. and Pinnow, J. (1994) Spirit Mountain Pluton, southern Nevada; a progress report. *Abstracts with Programs – Geological Society of America*, **26**, 60.

Hoskin, P.W.O. and Ireland, T.R. (2000) Rare earth element chemistry of zircon and its use as a provenance indicator. *Geology*, **28**, 627-630.

Hoskin, P.W.O. and Schaltegger, U. (2003) The composition of zircon and igneous and metamorphic petrogenesis. *Reviews in Mineralogy & Geochemistry: Zircon*, **53**, 27-62.

Howard, K.A., John, B.E. (1987) Crustal extension along a rooted system of imbricate low angle faults: Colorado River Extensional Corridor, California, and Arizona. In: Coward, M.P., Dewey, J.F., Hancock, P.L. (Eds.), *Continental Tectonics*: *Geological Society of London Special Publication*, **28**, 299–311.

Howard, K.A., Wooden, J.L., Simpson, R.W. and Pease, V.L. (1996) Extension-related plutonism along the Colorado River extensional corridor. *Abstracts with Programs – Geological Society of America*, **28**, 450.

Howard, K.A., John, B.E., Davis, G.A., Anderson, J.L. and Gans, P.B. (1994) A guide to Miocene extension and magmatism in the lower Colorado River region, Nevada, Arizona, and California. *U.S. Geological Survey Report,* **OF 94-0246**, 54 pp.

Jia, Y.Q. (1991) Crystal radii and effective ionic radii of the rare earth ions. *Journal of Solid State Chemistry*, **95**, 184-187.

*Johnson, J.A. and Grunder, A.L. (2000) The making of intermediate composition magma in a bimodal suite: Duck Butte Eruptive Center, Oregon, USA. *Journal of Volcanology and Geothermal Research*, **95**. 175-195.

Keppler, H. (1993) Influence of fluorine on the enrichment of high field strength trace elements in granitic rocks. *Contributions to Mineralogy and Petrology*, **114**, 479-488.

Linnen, R.L. (2005) The effect of water on accessory phase solubility in subaluminous and peralkaline granitic melts. *Lithos*, **80**, 267-280.

Linnen, R.L. and Keppler, H. (2002) Melt composition control of Zr/Hf fractionation in magmatic processes. *Geochimica et Cosmochimica Acta*, **66**, 3293-3301.

*Mahood, G.A. (1981) A summary of the geology and petrology of the Sierra La Primavera, Jalisco, Mexico. *Journal of Geophysical Research*, **86**, 10137-10152.

*Metz, J.M. and Mahood, G.A. (1991) Development of the Long Valley, California, magma chamber recorded in precaldera rhyolite lavas of Glass Mountain. *Contributions to Mineralogy and Petrology*, **106**, 379-397.

Miller, C.F., McDowell, S.M. and Mapes, R.W. (2003) Hot and cold granites?

Implications of zircon saturation temperatures and preservation of inheritance. *Geology*, **31**, 529-532.

Miller, C.F., Lowery, L.E. and Bea, F. (2005) Zircons and Zr/Hf: Assessing magmatic fractionation in the crust. *Goldschmidt Abstract with Programs,* **15**, A10.

Miller, J.S. and Wooden, J.L. (2004) Residence, resorption and recycling of zircons in Devils Kitchen rhyolite, Coso Volcanic field, California. *Journal of Petrology*, **45**, 2155-2170.

Miller, J.S., Miller, C.F., Cates, N.L., Wooden, J.L., Means, M.A. and Ericksen, S. (2004) Time scales of pulsatory magmatic construction and solidification in Miocene subvolcanic systems, Eldorado Mountains, Nevada (USA) *Transactions of the American Geophysical Union, Fall Meeting, EOS*, **85**, JA 496.

Pupin, J.P. (2000) Granite genesis related to geodynamics from Hf-Y in zircon. *Transactions of the Royal Society of Edinburgh: Earth Sciences*, **91**, 245 – 256.

Putnis, A., Fernandez-Diaz, L. and Prieto, M. (1992) Experimentally produced oscillatory zoning in the (Ba,Sr)SO_4 solid solution. *Nature*, **358**, 743-745.

*Reagan, M.K., Sims, K.W.W., Erich, J., Thomas, R.B., Cheng, H., Edwards, R.L., Layne, G. and Ball, L. (2003) Time-scales of differentiation from mafic parents to rhyolite in North American continental arcs. *Journal of Petrology*, **44**, 1703-1726.

Reid, M.R., Coath, C.D., Harrison, T.M. and McKeegan, K.D (1997) Prolonged residence times for the youngest rhyolites associated with Long Valley Caldera: (super 230) Th- (super 238) U ion microprobe dating of young zircons. *Earth and Planetary Science Letters*, **150**, 27-39.

Schmitt, A.K., Lindsay, J.M., de Silva, S. and Trumbull, R.B. (2003) U-Pb zircon chronostratigraphy of early-Pliocene ignimbrites from La Pacana, North Chile: implication for the formation of stratified magma chambers. *Journal of Volcanology and Geothermal Research*, **120**, 43-53.

Shannon, R.D. (1976) Revised effective ionic radii and systematic studies of interatomic distances in halies and chalcogenides. *Acta Crystallographica*, **A32**, 751-767.

Shore, M. and Fowler, A.D. (1996) Oscillatory zoning in minerals: a common phenomenon. *The Canadian Mineralogist*, **34**, 1111-1126.

*Stix, J., Goff, F., Gorton, M.P., Heiken, G. and Garcia, S.R. (1988) Restoration of compositional zonation in the Bandalier silicic magma chamber between two caldera-forming eruptions – Geochemistry and origin of the Cerro Toledo rhyolite, Jemez Mountains, New Mexico. *Journal of Geophysical Research*, **93**, 6129-6147.

*Stix, J. and Gorton, M.P. (1990) Changes in silicic melt structure between the two Bandalier Caldera-forming eruptions, New Mexico, USA: Evidence from zirconium and light rare earth elements. *Journal of Petrology*, **31**, 1261-1283.

Vazquez, J.A. and Reid, M.R. (2002) Timescales of magma storage and differentiation of voluminous high-silica rhyolites at Yellowstone caldera, Wyoming. *Contributions to Mineralogy and Petrology*, **144**, 274-285.

Vazquez, J.A. and Reid, M.R. (2004) Probing the Accumulation History of the Voluminous Toba Magma. *Science*, **305**, 991-993.

Volborth, A. (1973) Geology of the granite complex of the Eldorado, Newberry, and northern Dead Mountains, Clark County, Nevada. *Bulletin – Nevada Bureau of Mines and Geology*, **80**, 40 pp.

Walker, B.A., Miller, C.F., Lowery Claiborne, L., Wooden, J. & Miller, J.S. (in press) Batholith construction: New insights concerning timescales and physical processes from the Spirit Mountain Batholith, southern Nevada. *Journal of Volcanological and Geothermal Research.*

Walker, B.A., Miller, C.F., George, B.E., Ludington, S., Wooden, J.L., Bleick, H.A. and Miller, J.S. (2005) The Spirit Mountain batholith: Documenting magma storage in the upper crust one pulse at a time. *Transactions of the American Geophysical Union, Spring Meeting, EOS,* **86**, JA516.

Wallace, G.S. and Bergantz, G.W. (2002) Wavelet-based correlation (WBC) of zoned crystal populations and magma mixing. *Earth and Planetary Science Letters*, **202**, 133-145.

*Wark, D.A. and Miller, C.F. (1993) Accessory mineral behavior during differentiation of a granite suite: monazite, xenotime and zircon in the Sweetwater Wash pluton, southeastern California, U.S.A. *Chemical Geology*, **110**, 49-67.

Watson, E.B. and Harrison, T.M. (2005) Zircon thermometer reveals minimum melting conditions on earliest Earth. *Science*, **308**, 841-844.

Watson, E.B and Harrison, T.M. (1983) Zircon saturation revisited: temperature and composition effects in a variety of crustal magma types. *Earth and Planetary Science Letters*, **64**, 295-304.

Watson E. B. and Liang Y. (1995) A simple model for sector zoning in slowly grown crystals: implications for growth rate and lattice diffusion, with emphasis on accessory minerals in crustal rocks. *Amer. Min.* **80**, 1179-1187.

Watson, E.B., Wark, D.A. and Thomas, J.B. (2006) Crystallization thermometers for zircon and rutile. *Contributions to Mineralogy and Petrology,* **151**, 413-433.

*White, J.C. and Urbanczyk, K.M. (2001) Origin of a silica-oversaturated quartz trachyte-rhyolite suite through combined crustal melting, magma mixing, and fractional crystallization; the Leyva Canyon Volcano, Trans-Pecos magmatic province, Texas. *Journal of Volcanology and Geothermal Research*, **111**, 155-182.

Wiebe, R.A. and Hawkins, D.P. (2004) Multiple replenishments in an evolving silicic magma chamber: The Vinalhaven intrusive complex, Maine, USA. *Geochimica et Cosmochimica Acta*, **68**, A672-A672.

*data sources